# DIRECTION-OF-ARRIVAL ESTIMATION USING MULTIPLE SENSORS

**LIM WEI YING**
*(B.Eng. (Hons.), NUS)*

**A THESIS SUBMITTED**

**FOR THE DEGREE OF**
**DOCTOR OF PHILOSOPHY**

**NUS GRADUATE SCHOOL FOR**
**INTEGRATIVE SCIENCES AND ENGINEERING**

**NATIONAL UNIVERSITY OF SINGAPORE**

# Acknowledgements

First and foremost, I would like to express my sincere gratitude to my supervisors Prof. Lye Kin Mun, Dr. A. Rahim Leyman and Dr. See Chong Meng Samson for their professional guidance, encouragement and support throughout my graduate study. They demonstrated great freedom and patience on my research. I would also like to thank my TAC member A/Prof. Hari Garg for his helpful discussions.

I would also like to thank all my friends and colleagues who have helped and encouraged me throughout the whole course. I would like to acknowledge the Agency for Science, Technology and Research (A*STAR), the Institute for Infocomm Research ($I^2R$) and National University of Singapore (NUS) for their generous financial support and facilities.

Finally I would like to thank my family for their love, encouragement and support.

# Abstract

Sensor arrays are used in many applications where localization of sources is essential. For many applications, it is necessary to estimate the directions-of-arrival (DOAs). Although there are many DOA estimation algorithms, most of them are not able to resolve correlated signals adequately. This thesis proposes a narrowband method – the pilot-aided subarray (PAS) technique – which utilize a priori knowledge of the incident signals to overcome problems associated with signal coherence. The PAS technique performs close to the Cramer-Rao lower bound (CRLB) at low SNRs and for small array size and data samples. It is extended to include an iterative procedure to resolve correlated signals better. This technique, termed pilot-aided subarray iterative (PASI) technique, requires only a small number of iterations for accurate DOA estimates. This thesis also proposes a new coherent signal subspace method for wideband signals – the combined frequency signal subspace method (CFSSM) – which does not require the focusing stage and thus computational complexity is greatly reduced. The method is extended to the case where a priori knowledge of the impinging signals is available and is termed modified M-CFSSM (M-CFSSM). Its detection performance is robust at low SNRs for both uncorrelated and correlated signals. Moreover the estimation performance is close to the CRLB. The proposed narrowband and wideband techniques are also modified for the case of time-varying channels. Their performances are more robust to fading by the utilization of time and gain diversities.

# Contents

# List of Tables

# List of Figures

# List Of Abbreviations

| | |
|---|---|
| **AIC** | Akaike Information Criterion |
| **AM** | Alternating Maximization |
| **ARMA** | Autoregressive Moving Average |
| **AWGN** | Additive White Gaussian Noise |
| **BI-CSSM** | Beamforming Invariance Coherent Signal Subspace Method |
| **BPSK** | Binary Phase Shift Keying |
| **CS** | Conjugate Subarray |
| **CFSSM** | Combined Frequency Signal Subspace Method |
| **CSSM** | Coherent Signal Subspace Method |
| **CRLB** | Cramer-Rao Lower Bound |
| **DFT** | Discrete Fourier Transform |
| **DOA** | Direction-of-Arrival |
| **ESPRIT** | Estimation of Signal Parameters via Rotational Invariance Techniques |
| **EM** | Expectation Maximization |
| **FFT** | Fast Fourier Transform |
| **iid** | Independent and Identically Distributed |

| | |
|---|---|
| **IMUSIC** | Incoherent Multiple Signal Classification |
| **IQML** | Iterative Quadratic Maximum Likelihood |
| **ISI** | Intersymbol Interference |
| **LOS** | Line-Of-Sight |
| **MAICE** | Minimum Akaike Information Criterion Estimate |
| **M-CFSSM** | Modified Combined Frequency Signal Subspace Method |
| **MDL** | Minimum Description Length |
| **MEM** | Maximum Entropy Method |
| **ML** | Maximum Likelihood |
| **MOS** | Maximum Overlapping Subarray |
| **MSWF** | Multistage Wiener Filter |
| **MMSE** | Minimum Mean Square Error |
| **MUSIC** | Multiple Signal Classification |
| **PAS** | Pilot-Aided Subarray |
| **PASI** | Pilot-Aided Subarray Iterative |
| **RMSE** | Root-Mean-Square Error |
| **RSS** | Rotational Signal Subspace |
| **SBDOA** | Subarray Beamforming-based Direction-of-Arrival |
| **SNR** | Signal-to-Noise Ratio |
| **SST** | Subspace Transformation |
| **SVD** | Singular Value Decomposition |

| | |
|---|---|
| **TOPS** | Test of Orthogonality of Projected Subspaces |
| **UCA** | Uniform Circular Array |
| **ULA** | Uniform Linear Array |
| **WAVES** | Weighted Average Of Signal Subspaces |
| **WF** | Wiener Filter |
| **WSF** | Weighted Subspace Fitting |
| **UWB** | Ultra Wideband |

# Notations

| | |
|---|---|
| $(\cdot)^H$ | Hermitian transpose of a vector/matrix |
| $(\cdot)^T$ | Transpose of a vector/matrix |
| $(\cdot)^*$ | Complex conjugate of a vector |
| $(\cdot)^{-1}$ | Inverse of a matrix |
| $(\cdot)^\dagger$ | Moore-Penrose pseudo-inverse of a matrix |
| $\lvert\cdot\rvert$ | Magnitude of a vector |
| $\lVert\cdot\rVert_F$ | Frobenius matrix norm |
| $\mathbf{I}$ | Identity matrix |
| $\mathcal{R}(\cdot)$ | Range space of a matrix |
| $\mathrm{E}[\cdot]$ | Mathematical expectation |
| $\odot$ | Hadamard product of matrices |

# Chapter 1

# Introduction

## 1.1 Objectives & Contributions

Array signal processing is a subset of signal processing which uses independent sensors that are organized in patterns termed as arrays to detect signals from an environment of interest, and extracts as much information as possible about the signals. The array of sensors provides an interface between the environment in which it is embedded and the signal processing part of the system (see Figure 1.1). These sensors can be antennas used in radar, radio communications or radio astronomy, hydrophones used in sonar, geophones used in seismology or ultrasonic probes and X-ray detection used in medical imaging [1]. The environment of interest can be air (e.g. wireless communications applications), water (e.g. underwater sonar applications) or even solid ground (e.g. X-ray imaging). The sensors are placed judiciously at different locations to capture the signals. This is, in effect, a means of sampling the received signals in space. Array signal processing can be classified into active and passive processing. In the former, a transmitter is used to illuminate the environment and the array listens to the signals scattered by the environment and/or the object of interest(s). In the latter, the array merely listens to the environment. In either case, the objective of array signal processing is to estimate from the measurements a set of *constant* parameters upon which the received signals depend. This is achieved by fusing temporal and spatial information and exploiting prior information such as array geometry and sensor characteristics. The *constant* parameters to be estimated include:

- the number of incident sources,
- the direction(s)-of-arrival (DOAs) of incident sources,
- inter-sensor delays of incident signals impinging onto the array, and
- incident source waveforms.

The estimation of the number of incident sources is known as detection while the estimation of their DOAs is known as localization.

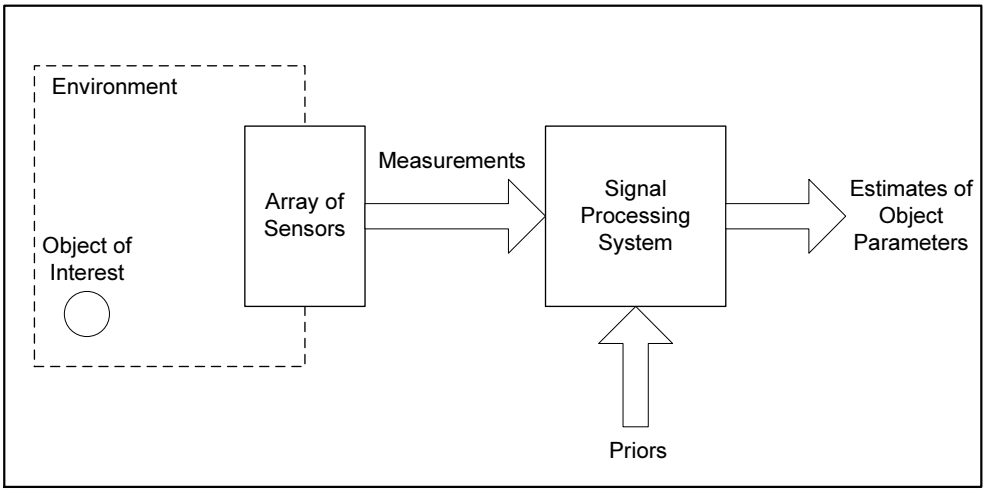


Figure 1.1: System model of array signal processing

Direction-of-arrival (DOA) is one of the most important signal parameters that needs to be estimated in most applications, e.g., radar and wireless communications. There are many existing narrowband algorithms for DOA estimation. Maximum likelihood (ML) and subspace-based methods are two of the most commonly used approaches. The former yields DOA estimates of sufficient accuracy [2]. However, ML methods are computationally intensive as they often require multidimensional search over the parameter space. The latter relies on the decomposition of the received data into signal and noise subspaces [3–7]. The subspace-based methods can provide high-resolution DOA estimates with good estimation accuracy. However, as these methods typically involve eigendecomposition of the array covariance matrix, the computational cost can be costly, especially for large arrays.

In friendly communications e.g., wireless communications and general positioning systems, some a priori knowledge of the incident signals is available to the receiver [8, 9]. This a priori knowledge may or may not be explicit. In a packet radio or mobile communications system, a known preamble may be added to the message for training purposes. On the other hand, in a digital communications system, the modulation format of the transmitted symbols is known to the receiver but the actual transmitted symbols are unknown. By exploiting the a priori knowledge of the incident signals, better DOA accuracy can be achieved. There are existing methods which utilize such information [8–12]. In [11], the ML criterion is derived under the assumption that the waveforms are known. Consequently iterative methods that use alternating maximization (AM) and expectation maximization (EM) are developed to minimize this ML criterion. In [9], a multistage Wiener filter (MSWF) uses reference signals to estimate the signal and noise subspaces without eigendecomposition of the array covariance matrix.

In [8, 10–12], it is assumed that the desired signal is uncorrelated with the interfering signals. However, in practice, either partially or perfectly correlated interference may be present, e.g., paths that are generated as a result of multipath propagation. In [9], the MSWF-based algorithm is able to resolve correlated signals by making use of the known waveforms.

In this thesis, we propose a narrowband method, termed pilot-aided subarray (PAS) technique, which makes use of preambles available to the receiver. The received signal at the array is divided into subarray outputs and correlated with the preambles. A structure similar to the conventional narrowband signal model is then obtained. A high-resolution subspace-based method, MUSIC (MUltiple SIgnal Classification), is used next to carry out the DOA estimation. The proposed PAS technique yields DOAs of sufficient accuracy with few data samples and small array size. A similar algorithm has been derived independently in [13]. An important differentiating factor from [13] is our extension of the algorithm by adding an iterative procedure to improve the accuracy of the DOAs of correlated signals. This extended algorithm is termed pilot-aided subarray iterative (PASI) technique. The proposed PASI technique is able to handle correlated

signals and resolves them adequately at low SNRs and with few iterations. Moreover, the maximum number of detectable DOAs using the proposed PAS and PASI techniques is no longer bounded by the number of antennas in the array. In the case where the channel is non-stationary, the proposed PAS and PASI techniques are modified and their performances are studied.

Wideband signals have received more attention as they are replacing narrowband signals in many applications, e.g., the ultra wideband (UWB) wireless communication can reduce channel fading effects due to multipath propagation [14]. The above narrowband algorithms cannot be applied directly to wideband signals as they have bandwidth much larger than that of narrowband signals. The narrowband algorithms can be applied to wideband signals if we first decompose the wideband signal into multiple narrowband signals. There are two main approaches of applying narrowband algorithms to the decomposed wideband signal – incoherent and coherent methods. In the former, the narrowband algorithms are applied independently to the multiple narrowband signals, e.g., the incoherent MUSIC (IMUSIC) [15]. In the latter, the multiple signals are combined coherently before the narrowband algorithms are applied, e.g., the coherent signal subspace method (CSSM) [16, 17]. Incoherent methods are computationally expensive and require high signal-to-noise ratios (SNRs) to ensure the final combination is effective [17], leading to the development of CSSM. CSSM is one of the most well-known coherent methods which carries out a pre-processing step called focusing. In this pre-processing step, the focusing matrix is used to average the correlation matrices of all frequency bins of the multiple decomposed signals. The focusing matrix requires initial DOA estimates that are as close as possible to the true DOAs. If the initial DOA estimates are too far from the true values, the estimation can be biased even if the number of data samples becomes infinite [18].

In this thesis, we also propose a wideband method, termed combined frequency signal subspace method (CFSSM), that does not require focusing matrices. The CFSSM exploits the structure of the combined correlation matrices of all the frequency bins which has a structure similar to the conventional narrowband signal model (it will be

shown in later chapters). A high-resolution subspace-based method, MUSIC, is used next to carry out the DOA estimation. The performance of CFSSM is comparable to existing methods and is computationally less intensive than the existing methods. CFSSM does not require any initial DOA estimates and can work as an initialization for existing algorithms that use focusing matrices. CFSSM is modified in the case where the preambles are known and is termed modified combined frequency signal subspace method (M-CFSSM). The detection performance is robust at low SNRs and requires only small number of data samples. The performance of M-CFSSM is also investigated in the case of time-varying channels.

The proposed PAS and PASI techniques provide new approaches to solve signal coherence problems, and the proposed CFSSM and M-CFSSM provide solutions to handle wideband signals without the use of focusing matrices which are computationally costly.

## 1.2 Organization of the Thesis

The thesis is organized as follows. In Chapter 2, the basics of array signal processing are introduced. The propagation model, wireless channels, antenna arrays are discussed briefly before the development of signal models for both narrowband and wideband signals.

In Chapter 3, we review some existing DOA algorithms for narrowband and wideband signals, highlighting their strengths and weaknesses. The narrowband estimation algorithms are classified broadly into spectral-based and parametric approaches, whereas the wideband estimation algorithms are categorized into incoherent and coherent methods.

In Chapter 4, we propose two spectral-based methods, the PAS and PASI techniques, which use pilot signals to estimate DOAs of both uncorrelated and correlated narrowband signals in time-invariant channels. The formulations of both techniques are first presented, followed by the numerical simulation to analyze their performances.

In Chapter 5, we present a coherent method, termed CFSSM, to estimate the DOAs of both uncorrelated and correlated wideband signals in time-invariant channels. The formulation is first presented and its applicability for both uncorrelated and correlated signals is next demonstrated. Simulation results are provided to illustrate its detection and estimation capabilities.

In Chapter 6, the proposed method in Chapter 5 is modified in the case where pilot signals are available. This formulation of the method, termed M-CFSSM, is first derived. Next its detection and estimation capabilities are illustrated by simulation results.

In Chapter 7, the proposed methods in Chapter 4 and 6 are extended to time-varying channels. The effects of time-varying channels on the performances of the proposed algorithms are investigated.

Finally, Chapter 8 concludes this thesis with our contributions and directions for future work.

# Chapter 2

# Mathematical Preliminaries

The basics of array signal processing are discussed in this chapter. First, the propagation model is derived from first principles in physics. Next, signal distortions experienced by signals in wireless channels are examined, followed by discussion on antenna arrays. Finally, the signal models for both narrowband and wideband signals are developed.

## 2.1 Propagating Waves

Many physical phenomena are either a result of waves propagating through a medium or exhibit a wave-like physical manifestation. A wave propagation, which may take various forms (with variations depending on the phenomenon and on the medium, e.g., an electromagnetic wave in free space or an acoustic wave in a pipe), generally follows from the homogeneous solution of the wave equation [2].

In a vacuum where there are no currents and charges, an electromagnetic wave satisfies the following Maxwell's equations [2, 19], :

$$\nabla \bullet \mathbf{E} = 0 \tag{2.1}$$

$$\nabla \bullet \mathbf{B} = 0 \tag{2.2}$$

$$\nabla \times \mathbf{E} = -\frac{\partial \mathbf{B}}{\partial t} \tag{2.3}$$

$$\nabla \times \mathbf{B} = \varepsilon_0 \mu_0 \frac{\partial \mathbf{E}}{\partial t} \tag{2.4}$$

where $\bullet$ and $\times$ denote divergence and curl respectively. $\nabla$ is the derivative of multidi-

mensional space. $\mathbf{B}$ is the magnetic field intensity and $\mathbf{E}$ is the electric field intensity, whereas $\mu_0$ and $\varepsilon_0$ are the magnetic and dielectric constants respectively. By invoking (2.1), the following curl property results:

$$\begin{aligned} \nabla \times (\nabla \times \mathbf{E}) &= \nabla (\nabla \bullet \mathbf{E}) - \nabla^2 \mathbf{E} \\ &= -\nabla^2 \mathbf{E} \end{aligned} \tag{2.5}$$

whereas by using (2.3) and (2.4) lead to:

$$\begin{aligned} \nabla \times (\nabla \times \mathbf{E}) &= -\frac{\partial}{\partial t} (\nabla \times \mathbf{B}) \\ &= -\varepsilon_0 \mu_0 \frac{\partial^2 \mathbf{E}}{\partial t^2} \end{aligned} \tag{2.6}$$

Upon combining (2.5) and (2.6), the fundamental wave equation results:

$$\nabla^2 \mathbf{E} - \frac{1}{c^2} \frac{\partial^2 \mathbf{E}}{\partial t^2} = 0 \tag{2.7}$$

where the constant $c$ is generally referred to as the speed of propagation, and it follows from the above derivation $c = 1/\sqrt{\varepsilon_0 \mu_0} = 3 \times 10^8 \mathrm{m/s}$. The homogeneous (no forcing function) wave equation (2.7) constitutes the physical motivation for the development of signal models.

Though (2.7) is a vector equation, we consider only its radial component $E(\mathbf{r}, t)$, where $\mathbf{r}$ is the position vector of any point in space. Denoting the carrier frequency by $f_c$ and a plane wave by $\tilde{x}(t)$ [2]:

$$E(\mathbf{r}, t) = \tilde{x}\left(t - \boldsymbol{r}^T \boldsymbol{\alpha}\right) e^{j2\pi f_c \left(t - \boldsymbol{r}^T \boldsymbol{\alpha}\right)} \tag{2.8}$$

satisfies the wave equation (2.7) provided $|\boldsymbol{\alpha}| = 1/c$, where $(\cdot)^T$ represents the transpose of a vector. Since the solution of the wave equation in (2.8) depends only on $\mathbf{r}^T \boldsymbol{\alpha}$, it can be interpreted as a plane wave traveling in the direction $\boldsymbol{\alpha}$ with the speed of propagation $1/|\boldsymbol{\alpha}| = c$. The vector $\boldsymbol{\alpha}$ is sometimes referred to as the slowness vector. The

solution, which carries both spatial and temporal information, is adequate for modeling signals with distinct spatio-temporal parameters [2].

Assuming the measured sensor output is proportional to $E(\mathbf{r}, t)$, the received signal at a sensor can be modeled as [2]:

$$y(t) = \alpha(t)\,\tilde{x}\left(t - \boldsymbol{r}^T\boldsymbol{\alpha}\right) e^{j2\pi f_c\left(t - \boldsymbol{r}^T\boldsymbol{\alpha}\right)} \tag{2.9}$$

where $\alpha(t)$ is the complex gain of the signal $\tilde{x}(t)$. This is the basis for the development of both narrowband and wideband signal models in Section 2.4.

## 2.2 Wireless Channels

In wireless channels, an information-bearing signal not only travels in a direct (line-of-sight (LOS)) path, but also via other non-LOS paths from the transmitter to the receiver [20–22]. The presence of reflecting objects and/or scatterers causes the signal to propagate along more than one path between the transmitter and the receiver. This phenomenon is known as multipath propagation [20–22]. The multipath waves experience random attenuation, and they arrive at the receiver from different directions-of-arrival (DOAs) at different times. These attenuated and time-delayed versions of the transmitted signal combine vectorially (either constructively or destructively) at the receiver to give a resultant signal which can vary widely in amplitude and phase [20–23]. These fluctuations in the strength of the received signal result in signal distortion due to time dispersion.

Moreover, the multipath structure of wireless channels is constantly changing with time due to moving transmitters, receivers and/or scatterers. The relative motion between transmitters, receivers and/or reflectors causes a continuous change in the propagation path lengths of each multipath and thus introduces relative phase shifts between the multipaths. The rate of change of phase, due to motion, is apparent as a frequency shift in each multipath. This results in spectral broadening in the frequency domain of

the transmitted signal at the receiver. This phenomenon is known as the Doppler effect [20–22]. The received signal experiences an apparent change in frequency (known as Doppler shift), resulting in signal distortion due to frequency dispersion.

The type of fading experienced by an information-bearing signal traveling through a wireless channel depends on the nature of the transmitted signal with respect to the characteristics of the channel. The effects of time dispersion and frequency dispersion, which are independent of one another, lead to frequency selectivity and time selectivity respectively [20–22].

### 2.2.1 Frequency Selectivity

The time dispersive nature of the channel can be characterized by delay spread $\sigma_\tau$ or coherence bandwidth $B_c$. The delay spread, which is the time difference between the arrival times of the first and last multipaths, is a natural phenomenon caused by reflection and scattering propagation paths in the channel [20–22]. Coherence bandwidth is the frequency domain dual of delay spread. It is a statistical measure of the range of frequencies over which a channel passes all spectral components with approximately equal gain and linear phase. In other words, coherence bandwidth is the range of frequencies over which two frequency components have strong amplitude correlation. A channel can thus be categorized into two types: flat fading and frequency selective fading [20–22].

A channel is considered flat fading if the channel has a constant gain and linear phase response over a bandwidth which is greater than the bandwidth of the transmitted signal, i.e., $B_c >> B$. Moreover, the delay spread of the channel is much smaller than the symbol period of the transmitted signal, i.e., $\sigma_\tau << T$. Under such conditions, the spectral characteristics of the transmitted signal are preserved at the receiver. However, the strength of the received signal varies with time, due to fluctuations of the channel gain in the multipaths. Flat fading channels are also known as amplitude-varying channels but are more commonly referred to as narrowband channels, since the bandwidth

of the signal is much smaller than that of the channel.

A channel is said to be frequency selective fading if it has a constant gain and linear phase response over a bandwidth which is smaller than the bandwidth of the transmitted signal, i.e., $B_c << B$. In addition, the delay spread of the channel is much larger than the symbol period of the transmitted signal, i.e., $\sigma_\tau >> T$. In such a channel, the received signal has multiple time-delayed versions of the attenuated transmitted signal, as multipath propagation increases the time required for the transmitted signal to reach the receiver. As a result, signal smearing occurs due to intersymbol interference (ISI). Correspondingly, the frequency components of the received signal experience different gains. Frequency selective fading channels are known as wideband channels, since the bandwidth of the signal is much larger than that of the channel.

### 2.2.2 Time Selectivity

The frequency dispersive nature of the channel can be characterized by Doppler spread $B_D$ or coherence time $T_c$. The Doppler spread, which is a measure of spectral broadening, is caused either by the relative motion between the transmitter and the receiver, or by the movement of objects in the channel [20–22]. Coherence time is the time domain dual of the Doppler spread. It is a statistical measure of the time duration over which a channel is deemed to be approximately invariant. In other words, coherence time is the time duration over which two received signals have strong amplitude correlation. A channel can thus be classified into two types: slow fading and fast fading [20–22].

A channel is slow fading if its characteristics is constant over one or several symbol periods, i.e., $T_c >> T$. In other words, the channel variations are slower than the baseband signal variations. Viewed in the frequency domain, the Doppler spread of the channel is much smaller than the bandwidth of the baseband signal, i.e., $B_D << B$.

A channel is fast fading if its characteristics changes rapidly within the symbol period, i.e., $T_c < T$. In other words, the channel variations are faster than the baseband signal variations. Correspondingly, the Doppler spread of the channel is larger than the

bandwidth of the baseband signal, i.e., $B_D > B$.

## 2.3 Antenna Arrays

An antenna is a device used for transmitting and/or receiving electromagnetic waves. Each antenna exhibits a specific radiation pattern, which is a plot of power transmitted from or received by the antenna per unit solid angle. A radiation pattern plot for a generic directional antenna is shown in Figure 2.1, illustrating the main lobe, a back lobe diametrically opposite the main lobe, and several side lobes separated by nulls where no radiation occurs. The main lobe indicates the direction of maximum radiation (sometimes called the boresight direction) [24–26]. The radiation patterns of such single antennas are unable to meet the gain or radiation requirements in some applications e.g., satellite communications. One way of overcoming this problem is to employ antenna arrays.

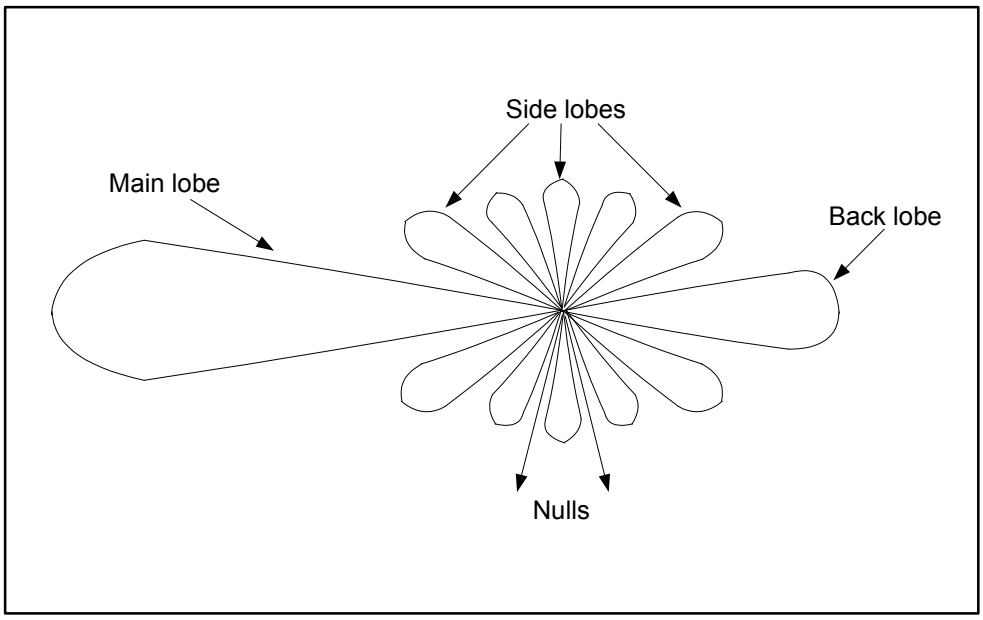


Figure 2.1: Radiation pattern of a generic directional antenna

Antenna arrays consist of single antennas, called elements, which are arranged in a specific geometry. Antenna arrays, besides providing a SNR gain proportional to the number of elements, can also separate signals from different sources transmitting at

the same frequency. Moreover, antenna arrays can combat multipath delay spread and fading fluctuations, and improve signal quality [24–26]. By using appropriate amplitude and phase weights, they are able to focus on the reception of one or more strong signals with low relative delays while signals with large excess delays can be attenuated [24–26]. The amplitude and phase weights can be controlled electronically (i.e. no physical antenna motion required) without experiencing any time delay due to mechanical constraints. These characteristics of antenna arrays enhance the capacity of wireless channels [27–29]

### 2.3.1 Array Geometries

Common array configurations include uniform linear arrays (ULAs) [3–5, 24–26, 30] and uniform circular arrays (UCAs) [24–26, 31, 32]. Before examining the array geometries in greater detail, we first examine the Cartesian coordinate system used to describe the spatial variations of electromagnetic waves.

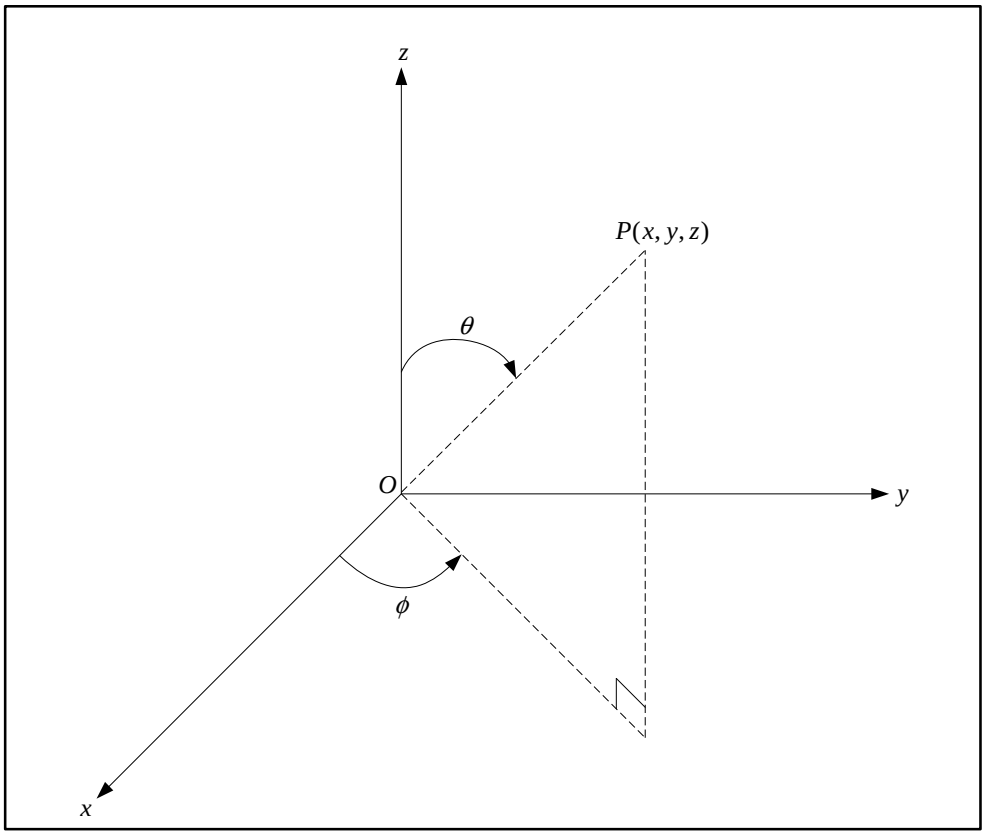


Figure 2.2: Three-dimensional coordinate system

Consider a three-dimensional coordinate system. A point $P$ can be represented as $(x, y, z)$, and is illustrated in Figure 2.2. From Figure 2.2, $\phi$ is the angle measured from the $x$-axis, and $\theta$ is the angle between the $z$-axis and the position vector of $P$. $\phi$ and $\theta$ are also known as the azimuth and elevation angles respectively. Suppose the reference antenna is at the origin, and another antenna is at point $P$ with position vector $\mathbf{r} = [x \;\; y \;\; z]^T$. The direction vector of a plane wave coming from direction $(\phi, \theta)$ is given by [19, 24–26]:

$$\boldsymbol{\alpha} = \frac{1}{c} \begin{bmatrix} \cos\phi \sin\theta & \sin\phi \sin\theta & \cos\theta \end{bmatrix}^T \tag{2.10}$$

The time delay of the plane waves between the antenna at $P$ and the reference antenna is [24–26]:

$$\begin{aligned} \kappa &= \mathbf{r}^T \boldsymbol{\alpha} \\ &= \frac{1}{c} \left( x \cos\phi \sin\theta + y \sin\phi \sin\theta + z \cos\theta \right) \end{aligned} \tag{2.11}$$

#### 2.3.1.1 Uniform Linear Arrays

The simplest array type is the ULA, which is a linear array with equal inter-element spacing $\delta$, as depicted in Figure 2.3. Suppose an ULA of $M$ elements is placed along the $y$-axis, i.e., $x = z = 0$. The position vector of the $m^{\text{th}}$ antenna is thus given by $\mathbf{r} = [0 \;\; (m-1)\,\delta \;\; 0]^T$. It is further assumed that all impinging plane waves lie in the $yz$ plane, i.e., $\phi = \pi/2$. Hence, the direction vector of a plane wave coming from direction $\theta$ is:

$$\boldsymbol{\alpha} = \frac{1}{c} \begin{bmatrix} 0 & \sin\theta & \cos\theta \end{bmatrix}^T \tag{2.12}$$

and the time delay between the $m^{\text{th}}$ antenna and the reference antenna is given by:

$$\kappa_m = \frac{(m-1)\,\delta \sin\theta}{c} \tag{2.13}$$

Note that the time delay between any two consecutive antennas is the same. In other words, there is a linear progressive phase shift across the array [24–26].

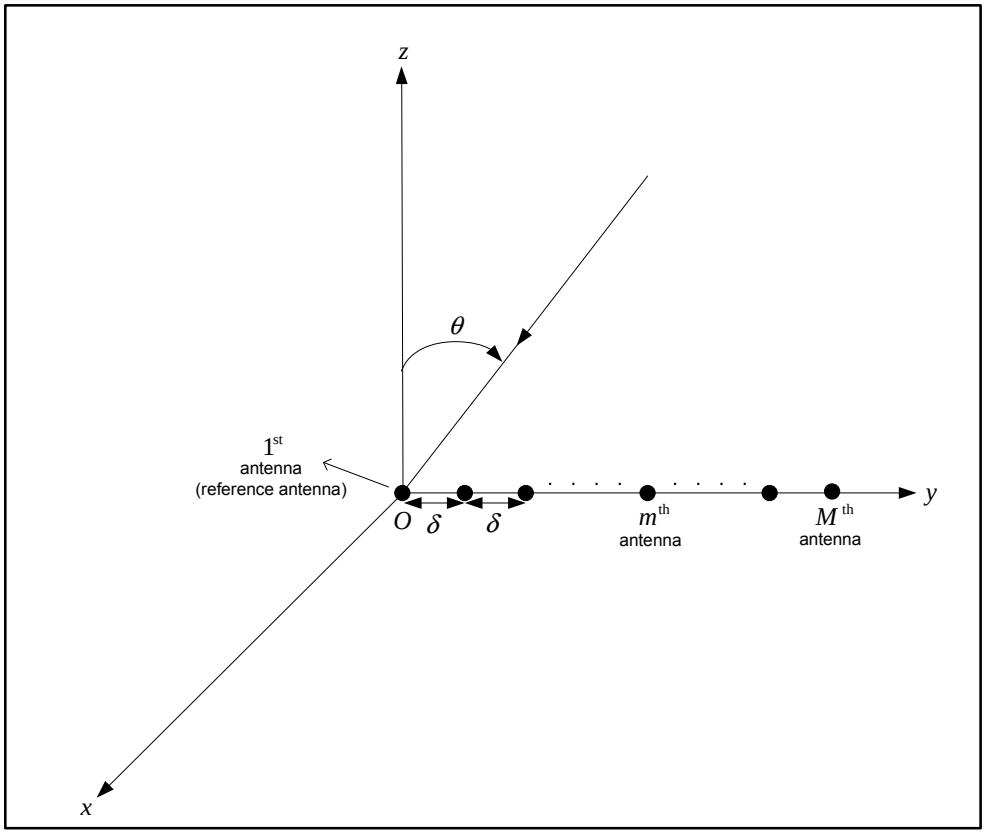


Figure 2.3: Uniform linear array geometry

Ambiguities in terms of the maximum peak in the radiation pattern are introduced when there are additional lobes having similar transmitted/radiated power compared to the main lobe. These are called the grating lobes. To avoid spatial aliasing, the phase delay between any two consecutive antennas, $2\pi f_c \kappa_2$, should be restricted to $\pm\pi$ [24–26]:

$$\begin{aligned} \left| \frac{2\pi f_c \delta \sin\theta}{c} \right| &\leq \pi \\ \left| \frac{2\pi \delta \sin\theta}{\lambda_c} \right| &\leq \pi \end{aligned} \tag{2.14}$$

where $\lambda_c = c/f_c$ is the wavelength of the carrier frequency. For $-\frac{\pi}{2} \leq \theta \leq \frac{\pi}{2}$, the inter-element spacing must thus satisfy the relation:

$$\delta \leq \frac{\lambda_c}{2} \tag{2.15}$$

If the range of $\theta$ is reduced, then it is possible to increase the inter-element spacing [24, 25].

#### 2.3.1.2 Uniform Circular Arrays

Uniform circular arrays (UCAs) are used when a $360^\circ$ field of view is required in the azimuthal plane. In applications such as surveillance and cellular communications, UCA is the natural choice [33, 34]. The elements of a UCA lie uniformly on the circumference of a circle of radius $r$, each separated by an angle $\xi$, as shown in Figure 2.4.

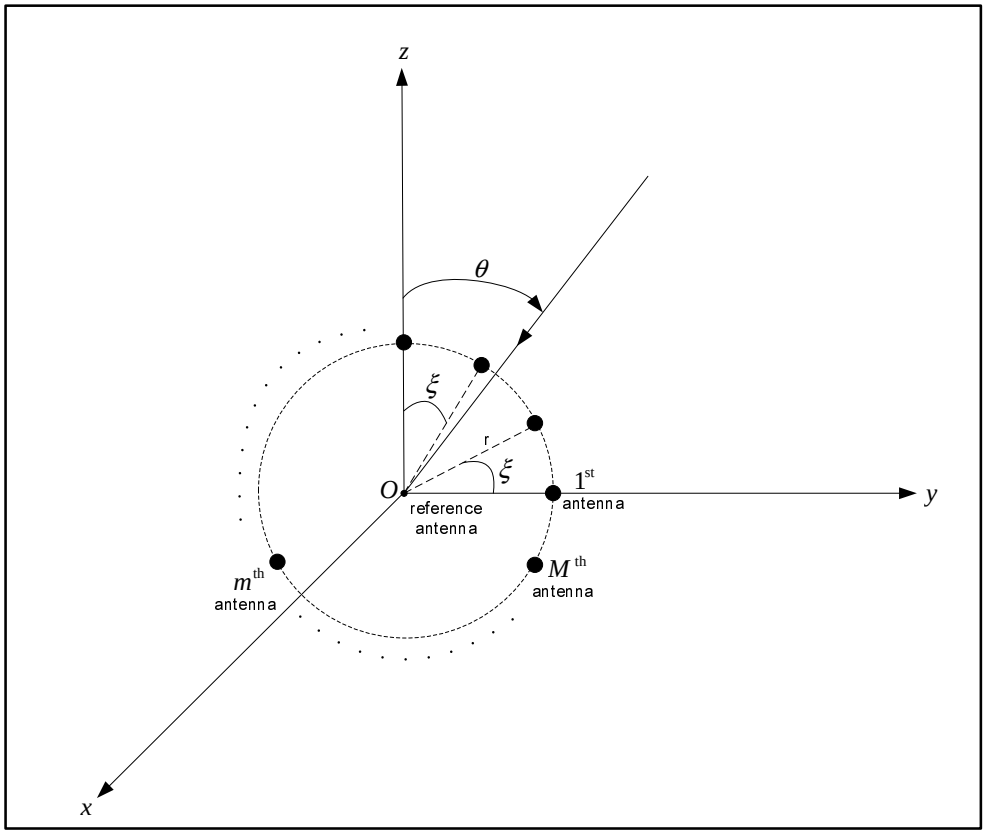


Figure 2.4: Uniform circular array geometry

Suppose we have a UCA of $M$ elements in the $yz$ plane, i.e., $x = 0$ and $\phi = \pi/2$. The

position vector of the $m^{\text{th}}$ antenna is given by $\mathbf{r} = [0 \;\; r\cos\xi_m \;\; r\sin\xi_m]^T$ where $\xi_m = 2\pi\,(m-1)\,/M$. Hence, the direction vector of a plane wave coming from direction $\theta$ is given by:

$$\boldsymbol{\alpha} = \frac{1}{c}\begin{bmatrix} 0 & \sin\theta & \cos\theta \end{bmatrix}^T \tag{2.16}$$

and the time delay between the $m^{\text{th}}$ antenna and the reference antenna is:

$$\kappa_m = \frac{r\cos\xi_m \sin\theta + r\sin\xi_m \cos\theta}{c} \tag{2.17}$$

## 2.4 Signal Models

The point source signal model is used to model the signals of interest. This model, invoking reasonable assumptions, makes the DOA estimation problem analytically tractable [6, 7]. For simplicity, we consider the signal model in a two-dimensional plane. The assumptions made in this section will apply throughout the thesis.

The point sources are assumed to be isotropic. Hence the signals propagate uniformly in all directions. These isotropic sources give rise to spherical traveling waves whose amplitudes are inversely proportional to the distance traveled [30]. All the points lying on the surface of a sphere of a certain radius share a common phase, and is referred to as a wavefront [2, 24]. The distance between the sources and the antenna array will determine whether the sphericity of the waves should be taken into account [2]. In this thesis, we assume the sources to be far-field, i.e., they lie in the Fraunhofer region [6, 7, 23–25]:

$$R \geq \frac{2D^2}{\lambda_c} \tag{2.18}$$

where $R$ is the radius of propagation, and $D$ is the diameter of the smallest sphere which completely encloses the array. Hence, signals arriving at the array have constant phase,

resulting in plane waves. Consequently, signals from each source have the same DOA at the array. Here, the DOA is defined with respect to the broadside (i.e. normal) of the array.

The signal sources are assumed to have the same bandwidth, which is common in wireless communications [22]. Note that the bandwidth and the symbol period are related by the relation: $B = 1/T$. The receiver is assumed to be equipped with an antenna array of $M$ elements in a known arbitrary geometry whereby each element is omni-directional with unity gain. The transmitters and the receiver are assumed to be perfectly synchronized. The wireless channel is assumed to be a linear medium which implies the validity of the superposition principle. It is further assumed that the wireless environment is slow-varying or stationary during the period of observation.

### 2.4.1 Narrowband Signals

We consider the general case of a wireless communication system consisting of $K$ independent narrowband sources. The fractional bandwidth, $B_f$, of these narrowband sources satisfies the condition [35]:

$$\begin{aligned} B_f &= \frac{B}{f_c} \\ &\leq \frac{1}{125} \end{aligned} \tag{2.19}$$

where $f_c$ is the carrier frequency. The complex representation of the modulated signal originating from the $k^{\text{th}}$ source is:

$$x^{(k)}(t) = \sum_{i=1}^{N_s} g\left(t - (i-1)\,T\right) s^{(k)}\left(i\right) e^{j2\pi f_c t} \tag{2.20}$$

where $N_s$ is the number of symbols, $s^{(k)}\left(i\right)$ is the $i^{\text{th}}$ symbol of the $k^{\text{th}}$ source, and $g\left(t\right)$ is the pulse-shaping waveform with finite support of length $L_g T$.

The scatterers in the vicinity of the $k^{\text{th}}$ source disperse the energy of the transmitted electromagnetic wave in each propagation path with a random amplitude and

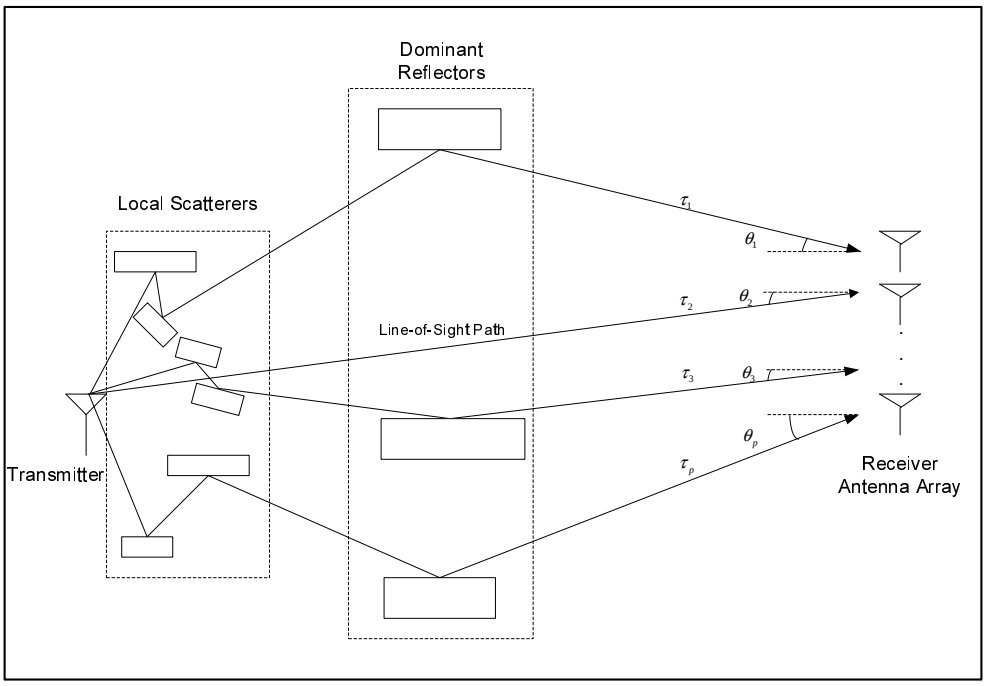


Figure 2.5: Propagation geometry for the multipath channel model

phase [23]. Each of these transmitted electromagnetic waves may encounter dominant reflectors in the far-field region of the receiver, thereby re-radiating the energy that arrives from the local scattering to the receiver [23]. Hence, each propagation path is characterized by a DOA $\theta_p^{(k)}$, an interpath delay $\tau_p^{(k)}$ (defined as the arrival time of the $p^{\text{th}}$ multipath from the $k^{\text{th}}$ source at the reference antenna relative to that of the first multipath from the same source at the same antenna), and a complex gain $\alpha_p^{(k)}$. The propagation geometry of the multipath channel model is depicted in Figure 2.5. The electromagnetic waves from each source arrive at the receiver as $P_k$ ($P_k \geq 1, k = 1, 2, \ldots, K$) plane waves. Consequently, the total number of impinging plane waves at the receiver is given by $\sum_{k=1}^{K} P_k = P$, where $P \geq K$. The received signal at the $m^{\text{th}}$ antenna can be written as a superposition of all the impinging plane waves [23, 36]:

$$\begin{aligned} y_m(t) &= \sum_{k=1}^{K}\sum_{p=1}^{P_k} \alpha_p^{(k)} x^{(k)}\left(t - \tau_p^{(k)} - \kappa_{p,m}^{(k)}\right) + w_m(t) \\ &= \sum_{k=1}^{K}\sum_{p=1}^{P_k} \alpha_p^{(k)} \left\{ \sum_{i=1}^{N_s} g\left(t - (i-1)T - \tau_p^{(k)} - \kappa_{p,m}^{(k)}\right) s^{(k)}(i) \right. \\ &\qquad \left. \times\, e^{j2\pi f_c\left(t - \tau_p^{(k)} - \kappa_{p,m}^{(k)}\right)} \right\} + w_m(t) \end{aligned} \tag{2.21}$$

where $\kappa_{p,m}^{(k)}$ is the antenna delay of the $p^{\text{th}}$ multipath from the $k^{\text{th}}$ source at $m^{\text{th}}$ antenna relative to the arrival time of the same path at the reference antenna. It can be expressed as:

$$\kappa_{p,m}^{(k)} = \frac{d_{p,m}^{(k)}}{c} \tag{2.22}$$

where $d_{p,m}^{(k)}$ is defined as the distance between the $m^{\text{th}}$ antenna and the reference antenna of the $p^{\text{th}}$ multipath from the $k^{\text{th}}$ source, and $c$ is the speed of propagation. $w_m(t)$ is the additive noise at the $m^{\text{th}}$ antenna. It is assumed to be uncorrelated with any of the impinging plane waves, and is temporally and spatially white.

Since the bandwidth of the narrowband sources is much smaller than the carrier frequency, the sources can be approximated as single-frequency sources of carrier frequency $f_c$ [30]. The wavelength of the sources is thus approximately equal to the wavelength of the carrier frequency, $\lambda_c = c/f_c$. Now it can be shown that $\kappa_{p,m}^{(k)}$ is much smaller than $T$:

$$\begin{aligned} \kappa_{p,m}^{(k)} &= \frac{d_{p,m}^{(k)}}{c} \\ &= \left(\frac{d_{p,m}^{(k)}}{\lambda_c f_c T}\right) T \\ &= \left(\frac{d_{p,m}^{(k)} B_f}{\lambda_c}\right) T \\ &<< T \end{aligned} \tag{2.23}$$

since $B_f$ is much smaller than 1 (see (2.19)). Hence, the effect of $\kappa_{p,m}^{(k)}$ is negligible on the pulse-shaping waveform, i.e., $g\left(t - \kappa_{p,m}^{(k)}\right) \approx g(t)$. However, the presence of $\kappa_{p,m}^{(k)}$ is not negligible on the carrier waveform as its phase is a linear function of $d_{p,m}^{(k)}$:

$$\begin{aligned} e^{-j2\pi f_c \kappa_{p,m}^{(k)}} &= e^{-j\frac{2\pi f_c d_{p,m}^{(k)}}{c}} \\ &= e^{-j\frac{2\pi d_{p,m}^{(k)}}{\lambda_c}} \end{aligned} \tag{2.24}$$

Now the received signal at the $m^{\text{th}}$ antenna can be simplified to:

$$\begin{aligned} y_m(t) &= \sum_{k=1}^{K}\sum_{p=1}^{P_k}\alpha_p^{(k)}\sum_{i=1}^{N_s} g\left(t-(i-1)T-\tau_p^{(k)}\right)s^{(k)}(i) \\ &\quad \times e^{j2\pi f_c t}e^{-j2\pi f_c \tau_p^{(k)}}e^{-j2\pi f_c \kappa_{p,m}^{(k)}} + w_m(t) \end{aligned} \tag{2.25}$$

The received signal is next down-converted to baseband and sampled at the Nyquist rate, i.e., at multiples of $T$ ($t = bT$):

$$\begin{aligned} y_m(bT) &= \sum_{k=1}^{K}\sum_{p=1}^{P_k}\alpha_p^{(k)}\sum_{i=1}^{N_s} g\left(bT-(i-1)T-\tau_p^{(k)}\right)s^{(k)}(i)\,e^{-j2\pi f_c \tau_p^{(k)}}e^{-j2\pi f_c \kappa_{p,m}^{(k)}} \\ &\quad + w_m(bT) \end{aligned} \tag{2.26}$$

where $b$ is a scalar.

#### 2.4.1.1 Flat Fading Channels

Consider the case when the channel is flat fading, i.e., $\tau_p^{(k)} << T$. The baseband received signal at the $m^{\text{th}}$ antenna can be further reduced to:

$$y_m(bT) = \sum_{k=1}^{K}\sum_{p=1}^{P_k}\alpha_p^{(k)}\sum_{i=1}^{N_s} g\left(bT-(i-1)T\right)s^{(k)}(i)\,e^{-j2\pi f_c \kappa_{p,m}^{(k)}} + w_m(bT) \tag{2.27}$$

Thus the effect of an antenna delay $\kappa_{p,m}^{(k)}$ on the narrowband signals is simply a phase shift.

To avoid ISI, an appropriate pulse-shaping waveform such as the raised cosine waveform with a roll-off factor $\beta$ (see Figure 2.6) can be used [21]:

$$g(t) = \frac{\sin\left(\frac{\pi t}{T}\right)}{\frac{\pi t}{T}}\frac{\cos\left(\frac{\pi \beta t}{T}\right)}{1-\frac{4\beta^2 t^2}{T^2}} \tag{2.28}$$

where it exhibits the following property:

$$g\left(bT-\left(i-1\right)T\right)=\begin{cases}1, & b-i+1=L_g/2\\ 0, & \text{otherwise}\end{cases} \tag{2.29}$$

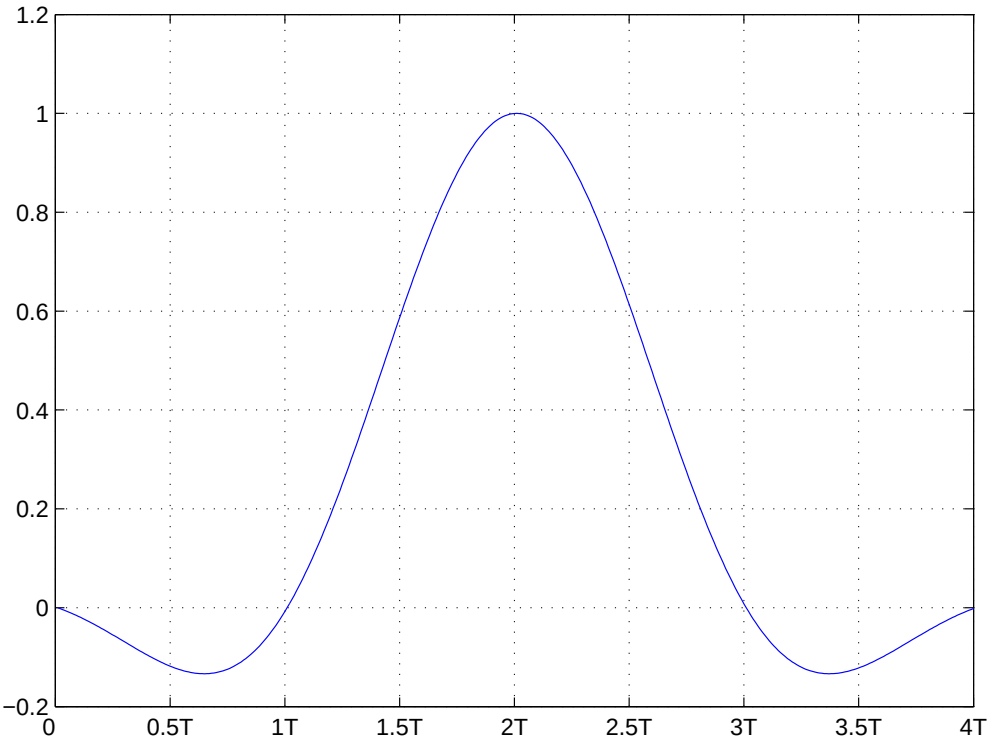


Figure 2.6: Raised cosine waveform of length $4T$ with roll-off factor $\beta=0.5$

Considering only non-zero antenna outputs, the $n^{\text{th}}$ sample of the baseband received signal at the $m^{\text{th}}$ antenna is thus as follows:

$$y_m\left(n\right)=\sum_{k=1}^{K}\sum_{p=1}^{P_k}\alpha_p^{(k)}s^{(k)}\left(n\right)e^{-j2\pi f_c\kappa_{p,m}^{(k)}}+w_m\left(n\right) \tag{2.30}$$

for $n=1,2,\ldots,N$. Note that the number of snapshots is equal to the number of transmitted symbols, i.e., $N=N_s$.

For each snapshot, the noisy signals received by the array can be cast into a vector form [3–7, 26]:

$$\mathbf{y}\left(n\right)=\mathbf{A}\left(\boldsymbol{\theta}\right)\boldsymbol{\Lambda}\mathbf{s}\left(n\right)+\mathbf{w}\left(n\right) \tag{2.31}$$

where

$$\mathbf{y}(n) = \left[ \begin{array}{cccc} y_1(n) & y_2(n) & \cdots & y_M(n) \end{array} \right]^T \tag{2.32}$$

$$\mathbf{w}(n) = \left[ \begin{array}{cccc} w_1(n) & w_2(n) & \cdots & w_M(n) \end{array} \right]^T \tag{2.33}$$

$$\mathbf{s}(n) = \left[ \begin{array}{ccccccccc} s^{(1)}(n) & \cdots & s^{(1)}(n) & \cdots & s^{(k)}(n) & \cdots & s^{(K)}(n) & \cdots & s^{(K)}(n) \end{array} \right]^T \tag{2.34}$$

$$\mathbf{\Lambda} = \mathrm{diag} \left\{ \begin{array}{ccccccccc} \alpha_1^{(1)}, & \cdots & \alpha_{P_1}^{(1)}, & \cdots & \alpha_p^{(k)}, & \cdots & \alpha_1^{(K)}, & \cdots & \alpha_{P_K}^{(K)} \end{array} \right\} \tag{2.35}$$

$$\boldsymbol{\theta} = \left[ \begin{array}{cccccccc} \theta_1^{(1)} & \cdots & \theta_{P_1}^{(1)} & \cdots & \theta_p^{(k)} & \cdots & \theta_1^{(K)} & \cdots & \theta_{P_K}^{(K)} \end{array} \right]^T \tag{2.36}$$

$\mathbf{y}(n)$ is the $M \times 1$ noisy received signal at the array whereas $\mathbf{w}(n)$ is the $M \times 1$ additive white noise at the array. $\mathbf{s}(n)$ is the $P \times 1$ vector comprising of the repetitions of the $K$ signal sources according to the number of impinging plane waves for each source (i.e. $P_k$ repetitions for the $k^{\mathrm{th}}$ source). $\mathbf{\Lambda}$ is the $P \times P$ diagonal matrix of the complex gains with entries equal to $\alpha_p^{(k)}$. $\boldsymbol{\theta}$ is the $P \times 1$ vector containing the DOAs of all impinging plane waves and the $M \times P$ array response matrix $\mathbf{A}(\boldsymbol{\theta})$ is defined as:

$$\mathbf{A}(\boldsymbol{\theta}) = \left[ \begin{array}{ccccccccc} \mathbf{a}\left(\theta_1^{(1)}\right) & \cdots & \mathbf{a}\left(\theta_{P_1}^{(1)}\right) & \cdots & \mathbf{a}\left(\theta_p^{(k)}\right) & \cdots & \mathbf{a}\left(\theta_1^{(K)}\right) & \cdots & \mathbf{a}\left(\theta_{P_K}^{(K)}\right) \end{array} \right] \tag{2.37}$$

where each $M \times 1$ steering vector is given by:

$$\mathbf{a}\left(\theta_p^{(k)}\right) = \left[ \begin{array}{cccc} e^{-j2\pi f_c \kappa_{p,1}^{(k)}} & e^{-j2\pi f_c \kappa_{p,2}^{(k)}} & \cdots & e^{-j2\pi f_c \kappa_{p,M}^{(k)}} \end{array} \right]^T \tag{2.38}$$

By concatenating the array outputs at different snapshots, the received signals can be written compactly in the following matrix structure [3–5]:

$$\mathbf{Y} = \mathbf{A}(\boldsymbol{\theta}) \mathbf{\Lambda} \mathbf{S} + \mathbf{W} \tag{2.39}$$

where

$$\mathbf{Y} = \left[ \begin{array}{cccc} \mathbf{y}(1) & \mathbf{y}(2) & \cdots & \mathbf{y}(N) \end{array} \right] \tag{2.40}$$

$$\mathbf{S} = \left[ \begin{array}{cccc} \mathbf{s}(1) & \mathbf{s}(2) & \cdots & \mathbf{s}(N) \end{array} \right] \tag{2.41}$$

$$\mathbf{W} = \left[ \begin{array}{cccc} \mathbf{w}(1) & \mathbf{w}(2) & \cdots & \mathbf{w}(N) \end{array} \right] \tag{2.42}$$

The aim is to estimate all the DOAs $\boldsymbol{\theta} = \left[\theta_1^{(1)} \ \cdots \ \theta_{P_1}^{(1)} \ \cdots \ \theta_p^{(k)} \ \cdots \ \theta_1^{(K)} \ \cdots \ \theta_{P_K}^{(K)}\right]^T$ from the $N$ snapshots.

#### 2.4.1.2 Frequency Selective Channels

Consider the case of a frequency selective channel, i.e., $\tau_p^{(k)} >> T$. In this case, the effect of interpath delay $\tau_p^{(k)}$ cannot be disregarded on the pulse-shaping waveform $g(t)$ [37]. Thus the baseband received signal at the $m^{\text{th}}$ antenna from (2.25) is given by:

$$y_m(bT) = \sum_{k=1}^{K} \sum_{p=1}^{P_k} \alpha_p^{(k)} \sum_{i=1}^{N_s} g\left(bT - (i-1)T - \tau_p^{(k)}\right) s^{(k)}(i) \, e^{-j2\pi f_c \tau_p^{(k)}} e^{-j2\pi f_c \kappa_{p,m}^{(k)}} + w_m(bT) \tag{2.43}$$

The presence of the interpath delay $\tau_p^{(k)}$ causes manifestation of the $i^{\text{th}}$ symbol from the $k^{\text{th}}$ source for a duration as long as $L_c T$ seconds, where $L_c T = L_g T + \lceil \Delta\tau \rceil$ is the length of the channel, and the temporal spread $\Delta\tau$ is the time difference of the arrival times between the first and the last multipaths. The exponential term containing the interpath delay $\tau_p^{(k)}$ can be absorbed into the complex gain $\alpha_p^{(k)}$. Hence, the $n^{\text{th}}$ sample of the baseband received signal at the $m^{\text{th}}$ antenna can be re-written as:

$$y_m(n) = \sum_{k=1}^{K} \sum_{p=1}^{P_k} \tilde{\alpha}_p^{(k)} \sum_{l=1}^{L_c} g\left((l-1)T - \tau_p^{(k)}\right) s^{(k)}(n + L_c - l) \, e^{-j2\pi f_c \kappa_{p,m}^{(k)}} + w_m(n) \tag{2.44}$$

where $n = 1, 2, \ldots, N$. Note that the number of snapshots $N$ is equal to $N_s + L_c - 1$.

For each sample, the received signal at the array can be cast into the following form:

$$\mathbf{y}(n) = \mathbf{A}(\boldsymbol{\theta})\,\boldsymbol{\Lambda}\mathbf{G}^T(\boldsymbol{\tau})\,\mathbf{S}(n) + \mathbf{w}(n) \tag{2.45}$$

where

$$\mathbf{y}(n) = \begin{bmatrix} y_1(n) & y_2(n) & \cdots & y_M(n) \end{bmatrix}^T \tag{2.46}$$

$$\mathbf{w}(n) = \begin{bmatrix} w_1(n) & w_2(n) & \cdots & w_M(n) \end{bmatrix}^T \tag{2.47}$$

$$\boldsymbol{\Lambda} = \operatorname{diag}\left\{ \alpha_1^{(1)}, \ \cdots \ \alpha_{P_1}^{(1)}, \ \cdots \ \alpha_p^{(k)}, \ \cdots \ \alpha_1^{(K)}, \ \cdots \ \alpha_{P_K}^{(K)} \right\} \tag{2.48}$$

$$\boldsymbol{\theta} = \begin{bmatrix} \theta_1^{(1)} & \cdots & \theta_{P_1}^{(1)} & \cdots & \theta_p^{(k)} & \cdots & \theta_1^{(K)} & \cdots & \theta_{P_K}^{(K)} \end{bmatrix}^T \tag{2.49}$$

$$\boldsymbol{\tau} = \begin{bmatrix} \tau_1^{(1)} & \cdots & \tau_{P_1}^{(1)} & \cdots & \tau_p^{(k)} & \cdots & \tau_1^{(K)} & \cdots & \tau_{P_K}^{(K)} \end{bmatrix}^T \tag{2.50}$$

$\mathbf{y}(n)$ is the $M \times 1$ noisy received signal at the array, whereas $\mathbf{w}(n)$ is the $M \times 1$ additive white noise at the array. $\boldsymbol{\Lambda}$ is the $P \times P$ diagonal matrix of the complex gains with entries equal to $\tilde{\alpha}_p^{(k)}$. $\boldsymbol{\theta}$ and $\boldsymbol{\tau}$ are the $P \times 1$ vectors containing the DOAs and interpath delays of all impinging plane waves respectively. $\mathbf{S}(n)$ is the $KL_c \times 1$ vector containing the transmitted symbols from all sources, which is defined as follows:

$$\mathbf{S}(n) = \begin{bmatrix} \mathbf{s}^{(1)}(n) & \mathbf{s}^{(2)}(n) & \cdots & \mathbf{s}^{(K)}(n) \end{bmatrix}^T \tag{2.51}$$

where

$$\mathbf{s}^{(k)}(n) = \begin{bmatrix} s^{(k)}(n + L_c - 1) & s^{(k)}(n + L_c - 2) & \cdots & s^{(k)}(n) \end{bmatrix}^T \tag{2.52}$$

The $\mathbf{G}(\boldsymbol{\tau})$ is the $KL_c \times P$ diagonal block matrix with the following structure:

$$\mathbf{G}(\boldsymbol{\tau}) = \begin{bmatrix} \mathbf{G}\left(\boldsymbol{\tau}^{(1)}\right) & 0 & \cdots & 0 \\ 0 & \mathbf{G}\left(\boldsymbol{\tau}^{(2)}\right) & \cdots & 0 \\ \vdots & \vdots & \ddots & \vdots \\ 0 & 0 & \cdots & \mathbf{G}\left(\boldsymbol{\tau}^{(K)}\right) \end{bmatrix} \tag{2.53}$$

where

$$\boldsymbol{\tau}^{(k)} = \begin{bmatrix} \tau_1^{(k)} & \tau_2^{(k)} & \cdots & \tau_{P_k}^{(k)} \end{bmatrix}^T \tag{2.54}$$

$$\mathbf{G}\left(\boldsymbol{\tau}^{(k)}\right) = \begin{bmatrix} \mathbf{g}\left(\tau_1^{(k)}\right) & \mathbf{g}\left(\tau_2^{(k)}\right) & \cdots & \mathbf{g}\left(\tau_{P_k}^{(k)}\right) \end{bmatrix} \tag{2.55}$$

$$\mathbf{g}\left(\tau_p^{(k)}\right) = \begin{bmatrix} g\left(-\tau_p^{(k)}\right) & g\left(T - \tau_p^{(k)}\right) & \cdots & g\left((L_c - 1)T - \tau_p^{(k)}\right) \end{bmatrix}^T \tag{2.56}$$

The $M \times P$ array response matrix $\mathbf{A}(\boldsymbol{\theta})$ is defined as:

$$\mathbf{A}(\boldsymbol{\theta}) = \begin{bmatrix} \mathbf{a}\left(\theta_1^{(1)}\right) & \cdots & \mathbf{a}\left(\theta_{P_1}^{(1)}\right) & \cdots & \mathbf{a}\left(\theta_p^{(k)}\right) & \cdots & \mathbf{a}\left(\theta_1^{(K)}\right) & \cdots & \mathbf{a}\left(\theta_{P_K}^{(K)}\right) \end{bmatrix} \tag{2.57}$$

where each $M \times 1$ steering vector is given by:

$$\mathbf{a}\left(\theta_p^{(k)}\right) = \begin{bmatrix} e^{-j2\pi f_c \kappa_{p,1}^{(k)}} & e^{-j2\pi f_c \kappa_{p,2}^{(k)}} & \cdots & e^{-j2\pi f_c \kappa_{p,M}^{(k)}} \end{bmatrix}^T \tag{2.58}$$

By concatenating the array outputs at different snapshots, the received signals can be written compactly in the following matrix structure:

$$\mathbf{Y} = \mathbf{A}(\boldsymbol{\theta})\,\boldsymbol{\Lambda}\mathbf{G}^T(\boldsymbol{\tau})\,\mathbf{S} + \mathbf{W} \tag{2.59}$$

where

$$\mathbf{Y} = \begin{bmatrix} \mathbf{y}(1) & \mathbf{y}(2) & \cdots & \mathbf{y}(N) \end{bmatrix} \tag{2.60}$$

$$\mathbf{S} = \begin{bmatrix} \mathbf{S}(1) & \mathbf{S}(2) & \cdots & \mathbf{S}(N) \end{bmatrix} \tag{2.61}$$

$$\mathbf{W} = \begin{bmatrix} \mathbf{w}(1) & \mathbf{w}(2) & \cdots & \mathbf{w}(N) \end{bmatrix} \tag{2.62}$$

The aim is to estimate all the DOAs $\boldsymbol{\theta} = \begin{bmatrix} \theta_1^{(1)} & \cdots & \theta_{P_1}^{(1)} & \cdots & \theta_p^{(k)} & \cdots & \theta_1^{(K)} & \cdots & \theta_{P_K}^{(K)} \end{bmatrix}^T$ from the $N$ snapshots.

### 2.4.2 Wideband Signals

We consider the general case of a system consisting of $K$ independent wideband sources. The fractional bandwidth, $B_f$, of these wideband sources satisfies the condition [35]:

$$\begin{aligned} B_f &= \frac{B}{f_c} \\ &> \frac{1}{125} \end{aligned} \tag{2.63}$$

where $f_c$ is the carrier frequency.

Keeping to the same notations in Section 2.4.1, the received wideband signal at the $m^{\text{th}}$ antenna can be written as a superposition of all the impinging plane waves [23,36]:

$$y_m(t) = \sum_{k=1}^{K} \sum_{p=1}^{P_k} \alpha_p^{(k)} x^{(k)} \left(t - \tau_p^{(k)} - \kappa_{p,m}^{(k)}\right) + w_m(t) \tag{2.64}$$

Unlike the case for narrowband signals, where the bandwidth is small relative to the carrier frequency, the time delay cannot be modeled as a simple phase shift [35]. The most common approach to wideband signal formulation, which is used in this thesis, is to decompose the wide frequency band into non-overlapping narrow bands through a bank of bandpass filters [17, 18, 38, 39]. An alternative approach is to make use of interpolating sequence in the time domain to model the wideband sources [40, 41].

In this thesis, we consider Discrete Fourier Transform (DFT) bandpass filters which can be efficiently implemented by Fast Fourier Transform (FFT). However, the resolution of the filter bank (i.e. the bandwidth of each frequency bin) is dependent on the length of the kernel. The higher the resolution, and hence more accurate representation of the frequency spectrum can only be obtained by using long kernels. Moreover, there is no flexibility given in shaping the transfer function of the filter bank. Despite these limitations, DFT bandpass filters are adopted due to its design simplicity and its high-speed implementation.

We assume that the observation time is much larger than the correlation time of sources so that the Fourier Transform of the antenna outputs have good resolution, and the sub-bands are independent of one another with respect to both time and frequency [18, 38, 39]. The Fourier Transform of the received signal at the $m^{\text{th}}$ antenna from (2.64) can be written as:

$$\begin{aligned} Y_m(f_q) &= \int_{-\infty}^{\infty} y_m(t)\, e^{-j2\pi f_q t}\mathrm{d}t \\ &= \sum_{k=1}^{K}\sum_{p=1}^{P_k} \alpha_p^{(k)} \int_{-\infty}^{\infty} x^{(k)}\left(t-\tau_p^{(k)}-\kappa_{p,m}^{(k)}\right) e^{-j2\pi f_q t}\mathrm{d}t + \int_{-\infty}^{\infty} w_m(t)\, e^{-j2\pi f_q t}\mathrm{d}t \\ &= \sum_{k=1}^{K}\sum_{p=1}^{P_k} \alpha_p^{(k)} X^{(k)}(f_q)\, e^{-j2\pi f_q \tau_p^{(k)}} e^{-j2\pi f_q \kappa_{p,m}^{(k)}} + W_m(f_q) \end{aligned} \tag{2.65}$$

The antenna array output is observed over a total duration of $T_0$ seconds. The observation window is divided into $N$ intervals each with duration $\Delta T = T_0/N$ seconds. The received signal is sampled at the Nyquist rate, and a $Q$-point DFT is applied to the samples to obtain the $Q$ frequencies output for each interval. In other words, we have $N$ snapshots of the $Q$ frequency bins. The aim is to estimate all the $P$ DOAs $\theta_p^{(k)}$ from these data.

For each decomposed narrowband frequency $f_q$, the signals at the array can be written in the conventional narrowband structure [26]:

$$\boldsymbol{Y}(f_q) = \mathbf{A}(f_q)\,\boldsymbol{\Lambda}\boldsymbol{X}(f_q) + \boldsymbol{W}(f_q) \tag{2.66}$$

where

$$\boldsymbol{Y}(f_q) = \left[ \begin{array}{cccc} Y_1(f_q) & Y_2(f_q) & \cdots & Y_M(f_q) \end{array} \right]^T \tag{2.67}$$

$$\boldsymbol{W}(f_q) = \left[ \begin{array}{cccc} W_1(f_q) & W_2(f_q) & \cdots & W_M(f_q) \end{array} \right]^T \tag{2.68}$$

$$\boldsymbol{X}(f_q) = \left[ \begin{array}{cccccccc} X^{(1)}(f_q) & \cdots & X^{(1)}(f_q) & \cdots & X^{(k)}(f_q) & \cdots & & \\ & & & & \cdots & X^{(K)}(f_q) & \cdots & X^{(K)}(f_q) \end{array} \right]^T \tag{2.69}$$

$$\boldsymbol{\Lambda} = \operatorname{diag}\left\{ \begin{array}{cccccccccc} \alpha_1^{(1)}, & \cdots & \alpha_{P_1}^{(1)}, & \cdots & \alpha_p^{(k)}, & \cdots & \alpha_1^{(K)}, & \cdots & \alpha_{P_K}^{(K)} \end{array} \right\} \tag{2.70}$$

$$\boldsymbol{\theta} = \left[ \begin{array}{cccccccc} \theta_1^{(1)} & \cdots & \theta_{P_1}^{(1)} & \cdots & \theta_p^{(k)} & \cdots & \theta_1^{(K)} & \cdots & \theta_{P_K}^{(K)} \end{array} \right]^T \tag{2.71}$$

$\boldsymbol{Y}(f_q)$ is the $M \times 1$ noisy received signal at the array whereas $\boldsymbol{W}(f_q)$ is $M \times 1$ frequency domain additive white noise at the array. $\boldsymbol{X}(f_q)$ is the $P \times 1$ vector comprising of the repetitions of the $K$ signal sources according to the number of arrival paths for each source (i.e. $P_k$ repetitions for the $k^{\text{th}}$ source). $\boldsymbol{\Lambda}$ is the $P \times P$ diagonal matrix of the complex gains with entries equal to $\alpha_p^{(k)}$. $\boldsymbol{\theta}$ is the $P \times 1$ vector containing the DOAs of all impinging plane waves and the $M \times P$ frequency-dependent array response matrix $\mathbf{A}(f_q, \boldsymbol{\theta})$ is defined as:

$$\mathbf{A}(f_q, \boldsymbol{\theta}) = \left[ \begin{array}{cccccccc} \mathbf{a}\left(f_q, \theta_1^{(1)}\right) & \cdots & \mathbf{a}\left(f_q, \theta_{P_1}^{(1)}\right) & \cdots & \mathbf{a}\left(f_q, \theta_p^{(k)}\right) & \cdots & & \\ & & & & \cdots & \mathbf{a}\left(f_q, \theta_1^{(K)}\right) & \cdots & \mathbf{a}\left(f_q, \theta_{P_K}^{(K)}\right) \end{array} \right] \tag{2.72}$$

with each $M \times 1$ frequency-dependent steering vector given by:

$$\mathbf{a}\left(f_q, \theta_p^{(k)}\right) = \left[ \begin{array}{cccc} e^{-j2\pi f_q\left(\tau_p^{(k)} + \kappa_{p,1}^{(k)}\right)} & e^{-j2\pi f_q\left(\tau_p^{(k)} + \kappa_{p,2}^{(k)}\right)} & \cdots & e^{-j2\pi f_q\left(\tau_p^{(k)} + \kappa_{p,M}^{(k)}\right)} \end{array} \right]^T \tag{2.73}$$

# Chapter 3

# DOA Estimation – Existing Techniques

In this chapter, we review the existing DOA algorithms for both narrowband and wideband signals. We discuss each algorithm briefly and identify their strengths and weaknesses.

## 3.1 Narrowband Algorithms

Narrowband DOA estimation methods can be broadly categorized into two types, namely spectral-based and parametric methods. In the former, a spectrum-like function of the DOAs is formed and the estimates are given by the locations of the highest (resolvable) peaks of the function. The latter often requires a simultaneous search for all parameters of interest, e.g., the DOAs and the complex gains.

### 3.1.1 Spectral-Based Methods

Spectral-based methods can be further classified into two groups – beamforming and subspace-based techniques. In beamforming, the array is steered (either manually or electronically) in one direction at a time and the output power is measured. The maximum output power yields the directions of the signals. For subspace-based techniques, a well-known method is the MUSIC algorithm [3–5]. It is a superresolution algorithm as it has the ability to resolve sources separated by $0.1$ beamwidth [42]. With its high resolution detection capability, we utilize the MUSIC algorithm together with our pro-

posed techniques in later chapters. Hence the MUSIC algorithm is examined in details in the following section. However, the DOAs estimated from the MUSIC algorithm are not associated with the sources, making their localization impossible. To overcome this and to improve the accuracy of DOA estimation, reference signals (either pilot signals or decision-directed signals) are used in the development of some algorithms. Two relatively new techniques – subarray beamforming-based DOA (SBDOA) and MSWF-based – assume some a priori knowledge about the sources were proposed in [43] and [9] respectively.

#### 3.1.1.1 MUSIC

A significant breakthrough in spectral-based methods came when Schmidt developed the MUSIC algorithm [3–5]. Similar approaches have also been reported in [44–48]. Unlike previous works which were mostly derived in the context of time series analysis and later applied to sensor array problems, Schmidt developed MUSIC in the context of array signal processing. Till mid-1970s, direction finding techniques required the knowledge of the array directional sensitivity pattern in analytical form. With the introduction of MUSIC, it relieved the designers from designing an array of elements with a pre-specified sensitivity pattern [45, 49]. The reduction in analytical complexity was achieved by calibrating the array. In other words, the highly non-linear problem of calculating the array response to a signal from a given direction was reduced to that of measuring and storing the array response [3–5]. Moreover, the MUSIC algorithm is applicable to any configuration of the array. In addition, the MUSIC algorithm asymptotically yields unbiased parameter estimates [7]. As the number of available samples tends to infinity, the estimated signal and noise subspaces converge to the true signal and noise subspaces, and the parameter estimates converge to the true values as well [7].

**The Geometric Approach**

Schmidt developed the MUSIC algorithm by taking a geometric view of the signal parameter estimation problem [3–5]. Consider a noiseless environment and that there

is an array of $M$ elements. Thus the complex signal at the array can be visualized and characterized by a vector in $\mathbb{C}^M$. In the case of one impinging plane wave, the received signal vector:

$$\mathbf{y}(n) = \alpha \mathbf{a}(\theta) s(n) \tag{3.1}$$

is confined to a 1-dimensional subspace of $\mathbb{C}^M$ characterized by $\mathbf{a}(\theta)$. Generalizing this key observation to the case of $P$ $(P \leq M)$ impinging wavefronts, the received signal vector:

$$\mathbf{y}(n) = \mathbf{A}(\boldsymbol{\theta}) \boldsymbol{\Lambda} \mathbf{s}(n) \tag{3.2}$$

is confined to a $P$-dimensional subspace of $\mathbb{C}^M$, termed the signal subspace $\mathcal{S}_Y$. It is spanned by the $P$ steering vectors $\mathbf{a}(\theta)$, the column vectors of $\mathbf{A}(\boldsymbol{\theta})$, i.e., $\mathcal{S}_Y = \mathcal{R}(\mathbf{A}(\boldsymbol{\theta}))$. These steering vectors are elements of a set, termed array manifold $\mathcal{A}$, consisting of all the possible steering vectors in the $M$-dimensional space. The array manifold $\mathcal{A}$ is completely determined by the array directional sensitivity patterns and the array geometry. It can be computed analytically for simple arrays, but it is generally obtained by calibration of the array [3–7]. Hence the estimates of signal parameters can be obtained by finding the intersections of the array manifold $\mathcal{A}$ with the signal subspace $\mathcal{S}_Y$.

**Estimation of the Signal Subspace**

In order to locate the intersections between the array manifold $\mathcal{A}$ and the signal subspace $\mathcal{S}_Y$, the latter has to be estimated from the noisy measurements $\mathbf{y}(n)$:

$$\mathbf{y}(n) = \mathbf{A}(\boldsymbol{\theta}) \boldsymbol{\Lambda} \mathbf{s}(n) + \mathbf{n}(n) \tag{3.3}$$

In other words, it is to estimate the set of vectors that spans the signal subspace [49].

To obtain such a set, first consider the $M \times M$ covariance matrix of $\mathbf{y}(n)$:

$$\begin{aligned} \mathbf{R}_y &= \mathrm{E}\left[\mathbf{y}(n)\,\mathbf{y}^H(n)\right] \\ &= \mathbf{A}(\boldsymbol{\theta})\,\mathbf{R}_x\mathbf{A}^H(\boldsymbol{\theta}) + \mathbf{R}_w \end{aligned} \tag{3.4}$$

where

$$\mathbf{R}_x = \boldsymbol{\Lambda}\mathrm{E}\left[\mathbf{s}(n)\,\mathbf{s}^H(n)\right]\boldsymbol{\Lambda}^H \tag{3.5}$$

$$\mathbf{R}_w = \mathrm{E}\left[\mathbf{w}(n)\,\mathbf{w}^H(n)\right] \tag{3.6}$$

For spatially and temporally white noise, the noise covariance matrix is diagonal, i.e., $\mathbf{R}_w = \sigma^2\mathbf{I}$. Next, consider the eigendecomposition of $\mathbf{R}_y$ [50, 51]:

$$\begin{aligned} \mathbf{R}_y\mathbf{E} &= \mathbf{E}\boldsymbol{\Phi} \\ \mathbf{A}(\boldsymbol{\theta})\,\mathbf{R}_x\mathbf{A}^H(\boldsymbol{\theta}) &= \mathbf{E}\left[\boldsymbol{\Phi} - \sigma^2\mathbf{I}\right]\mathbf{E}^H \end{aligned} \tag{3.7}$$

where

$$\mathbf{E} = \begin{bmatrix} \mathbf{e}_1 & \mathbf{e}_2 & \cdots & \mathbf{e}_M \end{bmatrix} \tag{3.8}$$

$$\boldsymbol{\Phi} = \begin{bmatrix} \lambda_1 & 0 & \cdots & 0 \\ 0 & \lambda_2 & \cdots & 0 \\ \vdots & \vdots & \ddots & \vdots \\ 0 & 0 & \cdots & \lambda_M \end{bmatrix} \tag{3.9}$$

The columns of $\mathbf{E}$ are eigenvectors of $\mathbf{R}_y$ and $\boldsymbol{\Phi}$ contains the corresponding eigenvalues. Note that $\mathbf{E}$ is a unitary matrix, i.e., $\mathbf{E}\mathbf{E}^H = \mathbf{E}^H\mathbf{E} = \mathbf{I}$.

Since $\mathbf{A}(\boldsymbol{\theta})$ is a full column rank matrix and $\mathbf{R}_x$ is positive definite, the matrix $\mathbf{A}(\boldsymbol{\theta})\,\mathbf{R}_x\mathbf{A}^H(\boldsymbol{\theta})$ has a rank of $P$ and is non-negative definite. Therefore the eigenvectors $\{\mathbf{e}_i,\ i = 1, 2,\ \ldots, P\}$ corresponding to the $P$ largest eigenvalues span the signal subspace, and the remaining eigenvectors $\{\mathbf{e}_i,\ i = P+1, P+2, \ldots, M\}$ correspond-

ing to the $(M-P)$ remaining eigenvalues span the noise subspace. As the measurements are noisy, the estimated signal and noise subspaces are given by:

$$\hat{\mathcal{S}}_Y = \mathcal{R}(\mathbf{E}_S) \qquad \text{where} \qquad \mathbf{E}_S = \begin{bmatrix} \mathbf{e}_1 & \mathbf{e}_2 & \cdots & \mathbf{e}_P \end{bmatrix} \tag{3.10}$$

$$\hat{\mathcal{S}}_Y^{\perp} = \mathcal{R}(\mathbf{E}_W) \qquad \text{where} \qquad \mathbf{E}_W = \begin{bmatrix} \mathbf{e}_{P+1} & \mathbf{e}_{P+2} & \cdots & \mathbf{e}_M \end{bmatrix} \tag{3.11}$$

where $\mathcal{R}(\cdot)$ denotes the range/column space.

In practical situations, the covariance matrices are usually unknown. Thus the covariance matrix $\mathbf{R}_y$ has to be estimated from the finite samples of the received signals. A natural estimate of $\mathbf{R}_y$ is the sample covariance matrix [2]:

$$\hat{\mathbf{R}}_y = \frac{1}{N}\sum_{n=1}^{N} \mathbf{y}(n)\,\mathbf{y}^H(n) \tag{3.12}$$

The noise covariance matrix $\mathbf{R}_w$ can be estimated from measurements without the presence of desired signals.

**Estimation of the Signal Parameters**

The DOA estimates can be obtained by the intersections of the array manifold $\mathcal{A}$ and the signal subspace $\mathcal{S}_Y$, or equivalently, finding vectors from the array manifold $\mathcal{A}$ that are orthogonal to the noise subspace $\mathcal{S}_Y^{\perp}$. However, the computational effort in locating the intersections is costly, especially for multidimensional parameters (e.g. elevation, azimuth and range). The problem is further complicated by noise. In the presence of noise, with probability one, the array manifold $\mathcal{A}$ does not intersect with the signal subspace $\mathcal{S}_Y$. Consequently there are no vectors that are orthogonal to the noise subspace $\mathcal{S}_Y^{\perp}$. Clearly, vectors from the array manifold $\mathcal{A}$ that are closest to the signal subspace $\mathcal{S}_Y$ should be potential solutions. Schmidt proposed the following cost function as a measure of closeness [3–5]:

$$P(\theta) = \frac{\mathbf{a}^H(\theta)\,\mathbf{a}(\theta)}{\mathbf{a}^H(\theta)\,\mathbf{E}_W\mathbf{E}_W^H\mathbf{a}(\theta)} \tag{3.13}$$

The measure is termed the MUSIC spectrum. In the absence of noise, the MUSIC spectrum is infinite for vectors which span the signal subspace $\mathcal{S}_Y$. In the presence of noise, the MUSIC spectrum shows peaks for vectors that are closest to the signal subspace $\mathcal{S}_Y$, i.e., vectors that are almost orthogonal to the noise subspace $\mathcal{S}_Y^{\perp}$.

MUSIC is computationally prohibitive as it requires multidimensional search over the parameter space [7]. Even though the MUSIC spectrum is used, thereby reducing the search to 1-dimensional, the process of estimating the signal parameters is not optimal. The parameter estimates are not sought simultaneously; instead they are found one at a time. Furthermore, the capacity of detection of MUSIC is bounded by the number of antennas. The maximum number of detectable DOAs is no more than $M - 1$. Moreover, MUSIC fails to resolve correlated signals. Correlatedness is defined as follows: two signals $x_i(n)$ and $x_j(n)$ are correlated when:

$$\mathrm{E}\left[x_i(n)\, x_j^*(n)\right] \neq 0, \quad i \neq j \tag{3.14}$$

In cases of fully correlated signals, they are known as coherent signals, i.e.,

$$x_i(n) = \alpha x_j(n) \tag{3.15}$$

Despite these drawbacks, MUSIC is a superresolution algorithm (defined as the ability to resolve sources separated by only $0.1$ beamwidth) and has been shown to outperform other techniques such as maximum entropy method (MEM) [42].

#### 3.1.1.2 SBDOA

A relatively recent technique that uses reference signals known as SBDOA was developed [43]. It uses similar array geometry as ESPRIT (Estimation of Signal Parameters via Rotational Invariance Technique) [6, 7]. ESPRIT retains most of the essential features of arbitrary arrays, but achieves a significant reduction in computational complexity by employing two arrays where the elements in each array are separated by a fixed

translational distance. SBDOA differs from ESPRIT in that it utilizes *virtual* subarrays to obtain the doublets. The array is divided into two virtual subarrays of equal elements, through the use of either maximum overlapping subarrays (MOSs) [43,52] or conjugate subarrays (CSs) [43, 53]. For each element in the subarray, there is a corresponding element in the other subarray displaced by a fixed translational distance. Thus, the phase shift between the two subarray signals is a function of the DOA [43].

The two subarray signals $\mathbf{y}_A(n)$ and $\mathbf{y}_B(n)$ are fed into beamformers $A$ and $B$ separately. For the $k^{\text{th}}$ source, the weight vector $\mathbf{w}_A^{(k)}$ of beamformer $A$ is obtained by minimizing the mean-square error between its output signal $\mathbf{y}_A(n)$ and the reference signal $r^{(k)}(n)$:

$$\arg\min_{\mathbf{w}_A^{(k)}} \mathrm{E}\left[\left|\left(\mathbf{w}_A^{(k)}\right)^H \mathbf{y}_A(n) - r^{(k)}(n)\right|^2\right] \tag{3.16}$$

and it is given in a closed form:

$$\mathbf{w}_A^{(k)} = \mathbf{R}_A^{-1}\mathbf{h}_A^{(k)} \tag{3.17}$$

where

$$\mathbf{R}_A = \mathrm{E}\left[\mathbf{y}_A(n)\,\mathbf{y}_A^H(n)\right] \tag{3.18}$$

$$\mathbf{h}_A^{(k)} = \mathrm{E}\left[\left(r^{(k)(n)}\right)^* \mathbf{y}_A(n)\right] \tag{3.19}$$

The weight vector $\mathbf{w}_A^{(k)}$ obtained from beamformer $A$ is the same weight vector that minimizes the mean-square error between the output signal of beamformer $B$ $\mathbf{y}_B(n)$ and the reference signal $r^{(k)}(n)$ [43]:

$$\arg\min_{\mathbf{w}_B^{(k)}} \mathrm{E}\left[\left|\left(\mathbf{w}_B^{(k)}\right)^H \mathbf{y}_B(n) - e^{j\phi^{(k)}} r^{(k)}(n)\right|^2\right] \tag{3.20}$$

and the weight vector $\mathbf{w}_B^{(k)}$ is thus given by:

$$\mathbf{w}_B^{(k)} = \mathbf{w}_A^{(k)} \tag{3.21}$$

It has been proven that the output signal of beamformer $B$ is an optimum estimation of the phase-shifted reference signal $\hat{r}^{(k)}(n)$, and its phase relative to that of the reference signal is a function of the DOA [43]. Let:

$$\mathbf{r}^{(k)} = \left[ \begin{array}{cccc} r^{(k)}(1) & r^{(k)}(2) & \cdots & r^{(k)}(N) \end{array} \right]^T \tag{3.22}$$

$$\hat{\mathbf{r}}^{(k)} = \left[ \begin{array}{cccc} \hat{r}^{(k)}(1) & \hat{r}^{(k)}(2) & \cdots & \hat{r}^{(k)}(N) \end{array} \right]^T \tag{3.23}$$

denote vectors with $N$ snapshots of the reference signal and the estimated phase-shifted reference signal respectively. The estimation of the DOA is then obtained based on the computation of the phase shift between the phase-shifted reference signal and the reference signal [43], i.e.,

$$\hat{\phi}^{(k)} = \arg\left( \left( \mathbf{r}^{(k)} \right)^H \hat{\mathbf{r}}^{(k)} \right) \tag{3.24}$$

Subspace estimation, eigendecomposition and multidimensional optimization are not required in the SBDOA technique. Hence, it is computationally simpler and can be easily implemented in terms of hardware [43]. Moreover, its capacity of DOA estimation is larger than the number of antennas in the array [43]. More significantly, the effect of co-channel interference on DOA estimation is reduced as the DOAs are estimated after interference rejection through subarray beamforming [43]. This is not the case for subspace-based methods using eigendecomposition of array covariance matrix. Steering vectors or the signal subspace spanned by the steering vectors have to be computed for DOA estimation [54], and information pertaining to such steering vectors exists only before interference rejection. As a result, the performance of such methods is significantly degraded by the interference. Hence, the estimation resolution and accuracy of SBDOA technique are better than those of methods using eigendecomposition of array

covariance matrix [43].

However, the SBDOA technique is not able to handle correlated signals due to the limited capability of optimum beamformers [26, 55–57]. The conventional beamformers not only fail to form nulls in the direction of correlated interferences, but they also tend to cancel desired signal in their outputs [26, 55–57].

#### 3.1.1.3 MSWF-based Algorithm

A computationally efficient method for DOA estimation, based on partial a priori knowledge of signal sources, was proposed in [9]. Unlike other subspace-based techniques which use eigendecomposition to obtain the signal and noise subspaces [3–5], this technique estimates these subspaces by forward recursion of the MSWF.

It is well-known that the Wiener filter (WF) can be used to estimate the desired signal from the received signals in the minimum mean-square error (MMSE) sense [25, 26, 58, 59]:

$$\mathbf{w}_{wf} = \arg\min_{\mathbf{w}_{wf}} \mathrm{E}\left\{\left|\mathbf{w}_{wf}^{H}\mathbf{y}\left(n\right) - r\left(n\right)\right|^{2}\right\} \tag{3.25}$$

where $r\left(n\right)$ is the pilot signal. The solution to (3.25) leads to the Wiener-Hopf equation [25, 26, 58, 59]:

$$\mathbf{R}_{y}\mathbf{w}_{wf} = \mathbf{R}_{yr} \tag{3.26}$$

where $\mathbf{R}_{y} = \mathrm{E}\left[\mathbf{y}\left(n\right)\mathbf{y}^{H}\left(n\right)\right]$ and $\mathbf{R}_{yr} = \mathrm{E}\left[\mathbf{y}\left(n\right)r^{*}\left(n\right)\right]$. The solution to the Wiener-Hopf equation is given by [25, 26, 58, 59]:

$$\mathbf{w}_{wf} = \mathbf{R}_{y}^{-1}\mathbf{R}_{yr} \tag{3.27}$$

where it is computationally intensive for large arrays as the inverse of the array covariance matrix $\mathbf{R}_{y}$ has to be computed. The authors overcame this difficultly by employing the MSWF developed in [60]. The MSWF approximates the solution to the Wiener-

Hopf equation, thereby eliminating the need to find the inverse of the array covariance matrix. Furthermore, by exploiting the orthogonal property of the matched filters of the MSWF, the signal and noise subspaces can be spanned by the matched filters [61]. Hence the computational complexity in estimating the noise subspace is reduced compared to that of eigendecomposition of the array covariance matrix. The estimated noise subspace is then used in the cost function of MUSIC to locate the DOA peaks. Alternatively, the DOA estimates can be estimated using root-MUSIC algorithm [62]. In the case of correlated signals, spatial smoothing technique is used to decorrelate them. Since the array covariance matrix is not estimated to obtain the noise subspace, spatial smoothing technique is applied to the array data matrix and the reference signal vector instead of the array covariance matrix. The MSWF-based technique can be used for small number of snapshots where the array covariance matrix cannot be estimated accurately and efficiently.

### 3.1.2 Parametric Methods

While the spectral-based methods are computationally attractive, they are suboptimal and do not always yield sufficient accuracy, especially in the case of correlated signals [2]. An alternative is to more fully exploit the underlying signal model, leading to the so-called parametric methods. The price to pay for is increased computational load as it requires a multidimensional search over the parameter space [2].

The most common model-based technique is the ML. There are two types of approaches depending on the assumption of incident signals. If the transmitted signals are deterministic (i.e. signal waveforms are known), deterministic ML results; if the transmitted signals are random, stochastic ML results. Since the proposed algorithms utilize reference signals, we concentrate our reviews on deterministic signals.

Under the additive white Gaussian noise (AWGN) assumption, the ML estimate of the DOAs and complex gains are obtained by solving the non-linear least squares

problem [2, 11, 63]:

$$\arg\min_{\theta,\alpha} \sum_{n=1}^{N} \left\| \mathbf{y}\left(n\right) - \mathbf{A}\left(\boldsymbol{\theta}\right) \boldsymbol{\Lambda} \mathbf{s}\left(n\right) \right\|^2 \tag{3.28}$$

The ML function is highly non-linear in the unknown signal parameters. Hence direct maximization of the ML function requires a computationally expensive multidimensional search. Computational savings are achieved by applying the result in [64] and the least squares problem can be re-expressed as:

$$\arg\min_{\theta} \operatorname{tr}\left[ \mathbf{P}_A^{\perp}\left(\boldsymbol{\theta}\right) \hat{\mathbf{R}}_y \right] \tag{3.29}$$

where $\mathbf{P}_A^{\perp}\left(\boldsymbol{\theta}\right)$ is the projection matrix onto the orthogonal complement of the range space of $\mathbf{A}\left(\boldsymbol{\theta}\right)$, $\hat{\mathbf{R}}_y$ is the sample covariance matrix, and $\operatorname{tr}\left(\cdot\right)$ is the trace of a matrix. As the ML criterion in (3.29) is multimodal, it still requires a computationally expensive multidimensional search for a global minimum. Thus the authors in [65] and [11] proposed iterative algorithms to reduce the computational load in estimating the ML solution.

#### 3.1.2.1 IQML

In [65], the authors expressed the ML criterion in (3.29) in terms of the prediction polynomial of the noiseless signal before developing an iterative algorithm that solves for the minimization of the ML criterion.

The signal components $y_m\left(n\right)$ in $\mathbf{y}\left(n\right)$ obey the special autoregressive moving average (ARMA) [66]:

$$\begin{aligned} &b_0 y_m\left(n\right) + b_1 y_{m-1}\left(n\right) + \cdots + b_P y_{m-P}\left(n\right) = \\ &\quad b_0 n_m\left(n\right) + b_1 n_{m-1}\left(n\right) + \cdots + b_P n_{m-P}\left(n\right) \end{aligned} \tag{3.30}$$

where

$$b(z) = b_0 z^P + b_1 z^{P-1} + \cdots + b_P \tag{3.31}$$

is the linear prediction polynomial for the noiseless signal. By the invariance principle of the ML estimate, the roots of the polynomial are the ML estimates of the signal exponential parameters [65]. Thus the ML criterion can be re-written in terms of the polynomial coefficients:

$$\min_{\mathbf{b}} \mathbf{b}^H \left[ \sum_{n=1}^{N} \mathbf{Y}_1^H(n) \left( \mathbf{B}^H \mathbf{B} \right)^{-1} \mathbf{Y}_1(n) \right] \mathbf{b} \tag{3.32}$$

where

$$\mathbf{b} = \begin{bmatrix} b_0 & b_1 & \cdots & b_P \end{bmatrix}^T \tag{3.33}$$

$$\mathbf{B} = \begin{bmatrix} b_P^* & 0 & \cdots & 0 & 0 \\ \vdots & \vdots & \ddots & \vdots & \vdots \\ b_0^* & b_1^* & \cdots & b_P^* & 0 \\ 0 & b_0^* & \cdots & b_{P-1}^* & b_P^* \\ \vdots & \vdots & \ddots & \vdots & \vdots \\ 0 & 0 & \cdots & 0 & b_0^* \end{bmatrix} \tag{3.34}$$

$$\mathbf{Y}_1(n) = \begin{bmatrix} y_{P+1}(n) & y_P(n) & \cdots & y_1(n) \\ y_{P+2}(n) & y_{P+1}(n) & \cdots & y_2(n) \\ \vdots & \vdots & \ddots & \vdots \\ y_M(n) & y_{M-1}(n) & \cdots & y_{M-P}(n) \end{bmatrix} \tag{3.35}$$

To avoid direct minimization of the ML criterion in (3.32), an iterative quadratic maximum likelihood (IQML) algorithm was developed. The algorithm requires only the solution of a quadratic minimization problem at each step and usually converges in a small number of steps. However, it is not guaranteed that the ML estimate will always converge to the global minimum, especially so at low SNRs. A noteworthy point is that

IQML is able to perform even in the case of multipath propagation.

#### 3.1.2.2 Modified AM & EM

As direct minimization of the ML function in (3.28) involves large dimensional search, iterative procedures were developed using the AM [67] and EM [68] algorithms. Initial estimates are necessary and they are provided by the IQML algorithm. Instead of searching over the parameter space, the angle estimates are obtained by polynomial roots [62]. The AM algorithm estimates the DOAs and complex gains serially at each iteration, whereas the EM algorithm splits up the search for the ML estimate into a set of parallel searches. However, there is no guarantee of convergence to the global minimum of the ML criterion.

The authors consider two possible scenarios of the signal waveforms. In the case of multiple signals with known waveforms, when the two waveforms are perfectly correlated, it is assumed they are identical. In the case of a signal with known waveform in the presence of interfering signals, the desired signal is assumed to be uncorrelated with the interfering signals and there is no knowledge of the waveforms for these interfering signals. Hence, the iterative procedures employing AM and EM algorithms are not able to resolve the correlated signals.

### 3.1.3 Computational Complexity

In this section, we give a comparative view of the computational complexity of the various algorithms. Here, we are primarily concerned about the computational cost of the algorithms in relation to the number of elements in the antenna array $M$ and the number of snapshots used $N$ as they invariably affect the estimation accuracy. For ease of comparison, the complexity of each algorithm is presented by the number of matrix operations required and their corresponding complexity order.

#### 3.1.3.1 MUSIC

To use MUSIC algorithm to estimate $P$ angles using an antenna array of $M$ elements and $N$ snapshots of observed data, we first need to obtain the sample covariance matrix $\hat{\mathbf{R}}_y$ which requires $N$ operations of order $O\left(M^2\right)$. Next, we need to estimate the noise subspace through SVD of $\hat{\mathbf{R}}_y$ which is followed by the matrix multiplication $\mathbf{E}_W\mathbf{E}_W^H$. Each of the two operations requires a computational complexity of order $O\left(M^3\right)$. Finally, the search process requires an operation with $O(M^2)$ computation cost for each hypothesized angle.

#### 3.1.3.2 SBDOA

SBDOA is a relatively less complex algorithm compared to MUSIC as it eliminates the need of the estimation of noise subspace and the subsequent computationally expensive search process. Instead, it only requires an inverse operation of order $O\left(M^3\right)$ and an additional matrix multiplication of order $O\left(M\right)$ to compute the cross-correlation vector between the output signal and the reference signal, the weight vectors $\mathbf{w}_A^{(k)}$ and $\mathbf{w}_B^{(k)}$ from the estimated covariance matrix $\hat{\mathbf{R}}_y$. Subsequently, the phase-shifted reference signal for each of the $N$ snapshots can be computed using a matrix multiplication of complexity order $O\left(M\right)$. Finally, the phase shift which carries the DOA information can be estimated using a matrix multiplication of order $O(N)$.

#### 3.1.3.3 MSWF-based Algorithm

The MSWF-based algorithm uses a multistage filter bank with a lattice structure to estimate the noise subspace in place of the SVD operation used by MUSIC algorithm to reduce the computational cost required. The estimation of each noise eigenvector only requires a vector-vector product with the complexity order of $O\left(MN\right)$. Hence to calculate all $M$ eigenvectors (including those for signal subspace as the vectors are obtained recursively), only $M$ operation of order $O\left(MN\right)$ is required. This compares favorably to MUSIC where the noise subspace is estimated through SVD with complexity order

of $O(M^3)$.

#### 3.1.3.4 IQML

To perform the iterative minimization required in IQML, the coefficient matrix in (3.33) needs to be updated in each iteration. This requires $N$ matrix multiplication of complexity order $O\left(M^3\right)$. The minimization itself requires an inverse of a $(P+1) \times (P+1)$ matrix with a complexity cost of order $O\left(P^3\right)$. Note that these computational costs are for a single iteration. The total computational cost will be determined by the number of iterations required for the termination of the minimization. After the iterative minimization has reached the terminating condition, the DOAs are estimated by solving for the roots of the polynomial with coefficients given in the final estimated vector $\mathbf{b}$. To solve for these roots, an eigenvalue decomposition of a $(P+1) \times (P+1)$ matrix can be used with a computational cost of order $O\left(P^3\right)$.

#### 3.1.3.5 Modified AM & EM

Both AM and EM algorithms use IQML to obtain the initial DOA estimates and hence the computational complexity listed here need to be compounded with the computational cost of IQML to form the total computational cost of these algorithms. In each iteration of the minimization procedure after the initial IQML estimation, a matrix multiplication of complexity order $O\left(MN\right)$ is used to derive the coefficients of the polynomial function used for DOA estimation. Each of the $P$ DOAs is estimated from the roots of the polynomial which can be solved by eigendecomposition of a $2\left(M-1\right) \times 2\left(M-1\right)$ matrix with a computational cost of order $O\left(M^3\right)$. Each of the $P$ complex gains can be solved for using an matrix multiplications with complexity order of $O\left(M\right)$.

## 3.2 Wideband Algorithms

Subspace-based estimation approach has been used extensively for DOA estimation of wideband sources [15, 16, 18, 38–40, 69, 70]. There are also ML estimation techniques using decomposed narrowband frequency data [71–73]. Algorithms, which utilize this subspace-based estimation approach, can be further classified into two main categories using narrowband decomposition as the classification criterion. Methods developed in [40, 41, 69, 74] do not decompose the wide bandwidth of the sources into narrowband frequency bins, whereas methods in [17, 18, 38, 39, 75] use narrowband decomposition and are built upon the foundation of well-established narrowband subspace-based estimation methods. As the newly proposed DOA estimation method in this thesis belongs to the latter group, we concentrate our reviews on the methods involved therein.

The corresponding correlation matrix used for signal subspace estimation for the received data in (2.66) is given by:

$$\mathbf{R}_y\left(f_q\right) = \mathbf{A}(f_q, \boldsymbol{\theta})\boldsymbol{\Lambda}\mathbf{R}_x\left(f_q\right)\boldsymbol{\Lambda}^H\mathbf{A}^H(f_q, \boldsymbol{\theta}) + \boldsymbol{\Sigma}\left(f_q\right) \tag{3.36}$$

where

$$\mathbf{R}_x\left(f_q\right) = \mathrm{E}\left[\mathbf{X}(f_q)\mathbf{X}^H(f_q)\right] \tag{3.37}$$

and $\boldsymbol{\Sigma}\left(f_q\right)$ is the noise spectral density matrix. For spatially and temporally white noise, the matrix is diagonal, i.e., $\boldsymbol{\Sigma}\left(f_q\right) = \sigma^2(f_q)\mathbf{I}$.

Note that there are $Q$ correlation matrices, one for each of the $Q$ decomposed narrowband frequencies. The various methods make use of these $Q$ matrices to perform DOA estimation. The methods are further categorized into two subgroups based on whether the decomposed signals are used independently or combined coherently in some ways to generate new statistics.

### 3.2.1 Incoherent Estimation Methods

A rather direct and brute force way to apply narrowband signal subspace estimation technique to wideband sources is to estimate the DOAs using each narrowband frequency bin independently, and then combine the estimates into an average final result [15, 76–78]. In [15], the IMUSIC algorithm was introduced which performs signal subspace estimation at each frequency bin and the final estimates of the DOAs are obtained from the combination of the search in the array manifolds for different frequency bins. Mathematically, the DOA estimates using IMUSIC are given by [18, 39]:

$$\hat{\theta} = \arg\min_{\theta} \sum_{q=0}^{Q-1} \mathbf{a}^H (f_q, \theta) \mathbf{E}_W (f_q) \mathbf{E}_W^H (f_q) \mathbf{a} (f_q, \theta) \tag{3.38}$$

where $\mathbf{E}_W (f_q)$ is the noise subspace at frequency $f_q$. Other narrowband techniques such as the ESPRIT technique as described in [77, 78] can be used in place of IMUSIC for the DOA estimation.

These incoherent methods have been shown to perform well under high SNR conditions and for uncorrelated signal sources [15, 18, 39, 78]. However, they are unable to separate correlated signal sources completely [17], and require singular value decomposition (SVD) of $M \times M$ matrix for each individual frequency bin, resulting in significant increase in computational complexity [18, 39]. Moreover, in low SNR environments, the combination of the estimates becomes ineffective due to the threshold effect [17] as a single outlier in one of the frequency bins can degrade the final estimates in the averaging process [18,39]. Thus at low SNRs, the increase in complexity due to the processing of more frequency bins not only does not guarantee better performance of the estimator, it may even degrade it. To address these problems, a coherent estimation method using focusing matrices was proposed in [16]. In addition, a series of subsequent coherent methods which uses different focusing matrices were proposed [18, 38, 39, 75, 79].

### 3.2.2 Coherent Estimation Methods

Wang and Kaveh proposed the first coherent estimation method for wideband sources in 1984 [16] and showed that it can be used to detect and estimate the DOAs for both uncorrelated and correlated signal sources [17, 80]. They introduced the use of focusing matrices in their CSSM to average the correlation matrices of various frequency bins coherently and estimate the DOAs from the resulting signal subspace. The authors of [81] later extended CSSM to the use of ESPRIT instead of MUSIC considered in [16]. Considerable works have been done on designing the focusing matrices used in CSSM to improve the estimator's performance in terms of minimizing bias and focusing error [75, 82–84]. Variations of CSSM have also been proposed [79, 85–88]. The simplified implementation of CSSM for linear arrays through the use of spatial sampling have also been proposed in [89–91]. More recently, the weighted average of signal subspace (WAVES) [38] method based on the weighted subspace fitting (WSF) [30, 92] approach and the test of orthogonality of projected subspaces (TOPS) [18, 39] method were proposed.

#### 3.2.2.1 CSSM

CSSM was the first method to introduce a processing step, known as focusing, to combine the correlation matrices from different frequency bins coherently to form a single signal subspace [16, 17]. Focusing is achieved by first transforming the correlation matrices $\mathbf{R}_y(f_q)$ using transformation matrices known as focusing matrices $\mathbf{T}_q$ to transform the signal subspace of a certain frequency to that of a pre-determined frequency (usually the carrier frequency), and then averaging them into a single combined correlation matrix $\mathbf{R}_{com}$. The combined correlation matrix is thus as follows:

$$\mathbf{R}_{com} = \sum_{q=0}^{Q-1} \gamma_q \mathbf{T}_q \mathbf{R}_y(f_q) \mathbf{T}_q^H \tag{3.39}$$

where $\gamma_q$ is a normalized weight proportional to the SNR in $q^{\text{th}}$ frequency bin and $Q$ is

the number of frequency bins. Without loss of generality, we can assume $\gamma_q = 1$ (i.e. identical SNR for all frequency bins).

Perfect focusing is achieved when focusing matrices for each frequency bin can be found which satisfy [17]:

$$\mathbf{A}(f_c, \boldsymbol{\theta}) = \mathbf{T}_q \mathbf{A}(f_q, \boldsymbol{\theta}) \tag{3.40}$$

However, perfect focusing has been shown to be unattainable due to finite dimension of the transformation matrix [93, 94] and an irreducible focusing error is introduced [38]. A practical approach to design the focusing matrices is hence [75]:

$$\arg\min_{\mathbf{T}_q} \|\mathbf{A}(f_c, \boldsymbol{\theta}_f) - \mathbf{T}_q \mathbf{A}(f_q, \boldsymbol{\theta}_f)\|_F \tag{3.41}$$

where $\|\cdot\|_F$ is the Frobenius matrix norm [50], $f_c$ is the carrier frequency and $\boldsymbol{\theta}_f$ is the set of focusing angles which could be preliminary angle estimates or strategically chosen anchor points [17].

For $\boldsymbol{\theta}_f = \boldsymbol{\theta}$ and $\mathbf{T}_q$ that satisfies $\|\mathbf{A}(f_q, \boldsymbol{\theta}_f) - \mathbf{T}_q \mathbf{A}(f_q, \boldsymbol{\theta}_f)\|_F \simeq 0$, the combined correlation matrix in (3.39) can be rewritten into:

$$\begin{aligned}
\mathbf{R}_{com} &= \sum_{q=0}^{Q-1} \mathbf{T}_q \mathbf{R}_y(f_q) \mathbf{T}_q^H \\
&= \sum_{q=0}^{Q-1} \mathbf{T}_q \left\{ \mathbf{A}(f_q, \boldsymbol{\theta}) \mathbf{R}_x(f_q) \mathbf{A}^H(f_q, \boldsymbol{\theta}) + \boldsymbol{\Sigma}(f_q) \right\} \mathbf{T}_q^H \\
&\simeq \mathbf{A}(f_c, \boldsymbol{\theta}) \sum_{q=0}^{Q-1} \mathbf{R}_x(f_q) \mathbf{A}^H(f_c, \boldsymbol{\theta}) + \mathbf{T}_q \sum_{q=0}^{Q-1} \boldsymbol{\Sigma}(f_q) \mathbf{T}_q^H
\end{aligned} \tag{3.42}$$

From (3.42), we can see that the noiseless combined correlation matrix has exactly the same matrix structure as that of narrowband signals at the carrier frequency $f_c$. Hence, any narrowband signal subspace method can be readily applied to $\mathbf{R}_{com}$ to estimate the DOAs. Note that even if the noise is spatially white for each frequency bin, the noise covariance matrix in (3.42) is not a diagonal matrix unless $\mathbf{T}_q \mathbf{T}_q^H = \mathbf{I}$.

The performance of CSSM is greatly dependent on the choice of the focusing angles $\boldsymbol{\theta}_f$ and the design of focusing matrices $\mathbf{T}_q$. For spatially white noise (i.e. $\boldsymbol{\Sigma}(f_q) =$

$\sigma^2(f_q)\mathbf{I}$), the focusing loss, $g_{focus}$, defined in [75] as the ratio of the array SNR after and before focusing operation, is given by:

$$g_{focus} = \frac{\mathrm{tr}\left\{\mathbf{R}_w^{-1}\sum_{q=0}^{Q-1}\mathbf{T}_q\mathbf{A}(f_q,\boldsymbol{\theta})\mathbf{R}_x\left(f_q\right)\mathbf{A}^H(f_q,\boldsymbol{\theta})\mathbf{T}_q^H\right\}}{\mathrm{tr}\left\{\sum_{q=0}^{Q-1}\mathbf{A}(f_q,\boldsymbol{\theta})\mathbf{R}_x\left(f_q\right)\mathbf{A}^H(f_q,\boldsymbol{\theta})\right\}} \tag{3.43}$$

where

$$\mathbf{R}_w = \frac{\sum_{q=0}^{Q-1}\sigma^2\left(f_q\right)\mathbf{T}_q\mathbf{T}_q^H}{\sum_{q=0}^{Q-1}\sigma^2\left(f_q\right)} \tag{3.44}$$

A class of focusing matrices that minimizes the focusing loss is the subspace transformation (SST) matrix [82]. Rotational signal subspace (RSS) focusing matrix which was proposed in [75] adds the constraint $\mathbf{T}_q\mathbf{T}_q^H = \mathbf{I}$ to the minimization problem in (3.41). Since $g_{focus} = 1$ when $\mathbf{T}_q\mathbf{T}_q^H$ is independent of $f_q$ [82], RSS focusing matrices can be considered as a type of SST matrices.

A solution to the constrained minimization problem of (3.41) which uses the RSS focusing matrix is given by [75]:

$$\mathbf{T}_q = \mathbf{V}\left(f_q\right)\mathbf{U}^H\left(f_q\right) \tag{3.45}$$

where the columns of $\mathbf{V}\left(f_q\right)$ and $\mathbf{U}\left(f_q\right)$ are the left and right singular vectors of $\mathbf{A}(f_q,\boldsymbol{\theta}_f)\mathbf{A}^H(f_c,\boldsymbol{\theta}_f)$.

Therefore, by using the RSS focusing matrices, the twin problem of finding appropriate focusing matrices and focusing angles reduces to that of finding accurate focusing angles, $\boldsymbol{\theta}_f$ which is exactly the problem we set out to solve, that is to estimate the DOAs, $\boldsymbol{\theta}$. Low-resolution DOA estimation techniques such as the Capon's ML estimator [95] have been proposed to obtain the initial DOA estimates [18, 39, 75] that would be close enough to the actual DOAs for the subsequent focusing step. However, these methods has been shown to have poor resolution [17] and poor initial DOAs estimates can lead to biased estimates [96]. Moreover, focusing error cannot be completely eliminated [38] even if the focusing process is applied iteratively.

In [88], beamforming invariance CSSM (BI-CSSM) was proposed that uses beam-

forming matrices that align the beams of multiple frequency bins instead of the signal subspace. Therefore, there is no requirement of initial focusing angles. However, BI-CSSM requires a robust design of reference beamformer applied to the carrier frequency. Practical reference beamformers requires high directional gain in the interested spatial band while having uniformly low sidelobes. The beam pattern must also be invariant across the different frequency bins.

#### 3.2.2.2 WAVES

A relatively recent coherent signal subspace estimation method, WAVES, was proposed in [38]. The method applies WSF algorithm [30, 92] in the coherent combining of the signal subspace of the different frequency bins. WAVES uses the same focusing matrices as that of CSSM but unlike CSSM, the matrices are not applied directly to the correlation matrices of the different narrowband frequencies. Instead they are applied to the estimated signal subspace of each frequency to form the pseudodata matrix given by [38]:

$$\mathbf{Z} = \left[ \begin{array}{cccc} \mathbf{T}_0\mathbf{E}_S\left(f_0\right)\mathbf{P}_0 & \mathbf{T}_1\mathbf{E}_S\left(f_1\right)\mathbf{P}_1 & \cdots & \mathbf{T}_{Q-1}\mathbf{E}_S\left(f_{Q-1}\right)\mathbf{P}_{Q-1} \end{array} \right] \tag{3.46}$$

where $\mathbf{E}_S\left(f_q\right)$ and $\mathbf{P}_q$ is the signal subspace and weighting matrix for the $q^{\text{th}}$ frequency bin respectively. If the signal and noise are Gaussian distributed, $\mathbf{P}_q$ is diagonal with elements given by [38, 92]:

$$\mathbf{P}_q[i,i] = \frac{\lambda_i\left(f_q\right) - \sigma_w^2}{\sqrt{\lambda_i\left(f_q\right) - \sigma_w}} \tag{3.47}$$

where $\lambda_i\left(f_q\right)$ is the $i^{\text{th}}$ largest eigenvalue of $\mathbf{E}_S\left(f_q\right)$ and $\sigma_w^2$ is the noise power which is assumed to be constant over all frequency bins. The noise subspace $\mathbf{E}_W$ for WAVES is

obtained by the reduced-size SVD [50] of $\mathbf{Z}$ which is given by:

$$\mathbf{Z} = \begin{bmatrix} \tilde{\mathbf{U}}_S & \tilde{\mathbf{U}}_W \end{bmatrix} \begin{bmatrix} \tilde{\mathbf{\Sigma}}_S & 0 \\ 0 & \tilde{\mathbf{\Sigma}}_W \end{bmatrix} \begin{bmatrix} \tilde{\mathbf{V}}_S & \tilde{\mathbf{V}}_W \end{bmatrix}^H \tag{3.48}$$

The eigenvectors $\tilde{\mathbf{U}}_W$ is used in place of the CSSM noise subspace in any narrowband subspace-based estimation algorithm such as MUSIC. WAVES has been shown to perform better than CSSM [38] but the explicit use of all of the narrowband signal subspace eigenvalues requires $Q$ SVD of $M \times M$ matrix which can be computationally costly.

#### 3.2.2.3 TOPS

Another recent coherent signal subspace estimation method known as TOPS was proposed in [18, 39]. Like WAVES, the method applies the focusing matrix on the signal subspace of individual narrowband frequency bins instead of their correlation matrices. However, unlike WAVES which uses a final combined noise subspace for DOA estimation, TOPS uses an orthogonality test between the transformed signal and noise subspaces to determine the true DOAs in a one-dimensional search through the field of hypothesized angles.

SVD is performed on the individual narrowband frequency bins to obtain the signal subspace $\mathbf{E}_S(f_q)$ and noise subspace $\mathbf{E}_W(f_q)$ for $q = 0, 1, \ldots, Q-1$. Similar to CSSM, a reference frequency bin (i.e. $q = 0$) is chosen. The signal subspace eigenvectors matrix $\mathbf{E}_S(f_0)$ of the reference frequency bin is used as the converging point for the testing statistic. For a hypothesized angle $\phi$, a decision $P \times (Q-1)(M-P)$ matrix, $\mathbf{D}(\phi)$, is formed as:

$$\mathbf{D}(\phi) = \begin{bmatrix} \mathbf{F}_1^H \mathbf{E}_W(f_1) & \mathbf{F}_2^H \mathbf{E}_W(f_2) & \cdots & \mathbf{F}_{Q-1}^H \mathbf{E}_W(f_{Q-1}) \end{bmatrix}^H \tag{3.49}$$

where

$$\mathbf{F}_q = \mathbf{P}_q(\phi)\mathbf{\Phi}\left(\Delta f_q, \phi\right)\mathbf{E}_S\left(f_0\right) \tag{3.50}$$

$$\mathbf{\Phi}\left(\Delta f_q, \phi\right) = \mathrm{diag}\left\{ e^{-j2\pi\Delta f_q \frac{d_1}{c} sin\phi}, \quad e^{-j2\pi\Delta f_q \frac{d_2}{c} sin\phi}, \quad \ldots \quad e^{-j2\pi\Delta f_q \frac{d_M}{c} sin\phi} \right\} \tag{3.51}$$

$$\mathbf{P}_q(\phi) = \mathbf{I} - \left[\mathbf{a}^H\left(f_q, \phi\right)\mathbf{a}\left(f_q, \phi\right)\right]^{-1}\mathbf{a}\left(f_q, \phi\right)\mathbf{a}^H\left(f_q, \phi\right) \tag{3.52}$$

with $\Delta f_q = f_q - f_0$ and $d_m$ is the distance between the $m^{\mathrm{th}}$ antenna and the reference antenna. $\mathbf{\Phi}\left(\Delta f_q, \phi\right)$ is a RSS focusing matrix [75] with a single focusing angle and $\mathbf{P}_q(\phi)$ is the projection matrix [18, 39]. The latter is used to reduce the error terms in the decision matrix due to error in estimating the correlation matrix from limited snapshots. The DOAs are then estimated as:

$$\hat{\theta} = \arg\max_{\phi} \frac{1}{\sigma_{min}(\phi)} \tag{3.53}$$

where $\sigma_{min}(\phi)$ is the smallest singular value of $\mathbf{D}(\phi)$.

TOPS is a computationally expensive algorithm with the search process of each hypothesized angle requiring a SVD of $P \times P$ matrix. The performance of TOPS sits between the conventional incoherent and coherent estimation methods [18, 39]. However, the use of both signal and noise subspaces make the TOPS method more robust against degradation of the range space spanned by the steering vectors due to bandpass filtering compared to CSSM [18, 39].

# Chapter 4

# Pilot-Aided Narrowband DOA Estimator

In this chapter, we propose a high-resolution DOA estimation method for narrowband sources by utilization of pilot signals, which we term the PAS technique. In the case of correlated signals, we incorporate an iterative procedure to the proposed PAS technique, which is termed the PASI technique. We first derive the formulation of the methods and then discuss the parameters that affect their performance. Numerical results are provided at the end of the chapter to illustrate the estimation capability of both techniques.

## 4.1 Formulation of Proposed Method

In this section, we derive the formulation of the proposed PAS technique used for DOA estimation of narrowband signals. Recall from Section 2.4.1.1 that for the general case of a wireless communication system consisting of $K$ independent narrowband sources, the received signal at the array in a flat fading channel is:

$$\mathbf{y}(n) = \mathbf{A}(\boldsymbol{\theta})\,\boldsymbol{\Lambda}\mathbf{s}(n) + \mathbf{w}(n) \tag{4.1}$$

where

$$\mathbf{y}(n) = \left[ \begin{array}{cccc} y_1(n) & y_2(n) & \cdots & y_M(n) \end{array} \right]^T \tag{4.2}$$

$$\mathbf{w}(n) = \left[ \begin{array}{cccc} w_1(n) & w_2(n) & \cdots & w_M(n) \end{array} \right]^T \tag{4.3}$$

$$\mathbf{s}(n) = \left[ \begin{array}{ccccccccc} s^{(1)}(n) & \cdots & s^{(1)}(n) & \cdots & s^{(k)}(n) & \cdots & s^{(K)}(n) & \cdots & s^{(K)}(n) \end{array} \right]^T \tag{4.4}$$

$$\mathbf{\Lambda} = \operatorname{diag}\left\{ \begin{array}{ccccccccc} \alpha_1^{(1)}, & \cdots & \alpha_{P_1}^{(1)}, & \cdots & \alpha_p^{(k)}, & \cdots & \alpha_1^{(K)}, & \cdots & \alpha_{P_K}^{(K)} \end{array} \right\} \tag{4.5}$$

$$\boldsymbol{\theta} = \left[ \begin{array}{ccccccccc} \theta_1^{(1)} & \cdots & \theta_{P_1}^{(1)} & \cdots & \theta_p^{(k)} & \cdots & \theta_1^{(K)} & \cdots & \theta_{P_K}^{(K)} \end{array} \right]^T \tag{4.6}$$

$\mathbf{y}(n)$ is the $M \times 1$ noisy received signal at the array, whereas $\mathbf{w}(n)$ is the $M \times 1$ additive white noise at the array. $\mathbf{s}(n)$ is the $P \times 1$ vector comprising of the repetitions of the $K$ signal sources according to the number of impinging plane waves for each source (i.e. $P_k$ repetitions for the $k^{\text{th}}$ source). $\mathbf{\Lambda}$ is the $P \times P$ diagonal matrix of the complex gains with entries equal to $\alpha_p^{(k)}$. $\boldsymbol{\theta}$ is the $P \times 1$ vector containing the DOAs of all impinging plane waves, and the $M \times P$ array response matrix $\mathbf{A}(\boldsymbol{\theta})$ is defined as:

$$\mathbf{A}(\boldsymbol{\theta}) = \left[ \begin{array}{cccccccc} \mathbf{a}\left(\theta_1^{(1)}\right) & \cdots & \mathbf{a}\left(\theta_{P_1}^{(1)}\right) & \cdots & \mathbf{a}\left(\theta_p^{(k)}\right) & \cdots & \mathbf{a}\left(\theta_1^{(K)}\right) & \cdots & \mathbf{a}\left(\theta_{P_K}^{(K)}\right) \end{array} \right] \tag{4.7}$$

where each $M \times 1$ steering vector is given by:

$$\mathbf{a}\left(\theta_p^{(k)}\right) = \left[ \begin{array}{cccc} e^{-j2\pi f_c \kappa_{p,1}^{(k)}} & e^{-j2\pi f_c \kappa_{p,2}^{(k)}} & \cdots & e^{-j2\pi f_c \kappa_{p,M}^{(k)}} \end{array} \right]^T \tag{4.8}$$

From this point onwards, we consider a ULA with an inter-element spacing $\delta$. Note that the formulation can be adapted accordingly for other array geometries. Thus, the antenna delay of the $p^{\text{th}}$ multipath from the $k^{\text{th}}$ source between the $m^{\text{th}}$ antenna and the reference antenna from (2.13) is:

$$\kappa_{p,m}^{(k)} = \frac{(m-1)\,\delta}{c} \sin\theta_p^{(k)} \tag{4.9}$$

Correspondingly, the steering vector in (4.8) is simplified to:

$$\mathbf{a}\left(\theta_p^{(k)}\right) = \left[\begin{array}{cccc} 1 & e^{-j\frac{2\pi\delta}{\lambda_c}\sin\theta_p^{(k)}} & \cdots & e^{-j\frac{2\pi\delta}{\lambda_c}(M-1)\sin\theta_p^{(k)}} \end{array}\right]^T \tag{4.10}$$

where $\lambda_c$ is the wavelength of the carrier frequency.

We divide the $M$-element ULA into $L$ overlapping subarrays of size $M_0$, where $M_0 = M - L + 1$. The first subarray consists of $1^{\text{st}}$ to $M_0^{\text{th}}$ antennas, the second subarray consists of $2^{\text{nd}}$ to $(M_0+1)^{\text{th}}$ antennas, and so on. Hence, the $l^{\text{th}}$ subarray output $\mathbf{y}_l(n)$, which are the $l^{\text{th}}$ to $(M_0+l-1)^{\text{th}}$ antenna outputs, can be written as:

$$\mathbf{y}_l(n) = \mathbf{A}_1(\boldsymbol{\theta})\,\mathbf{D}^{l-1}\boldsymbol{\Lambda}\mathbf{s}(n) + \mathbf{w}_l(n) \tag{4.11}$$

where $\mathbf{w}_l(n)$ is $M_0 \times 1$ additive white noise at the $l^{\text{th}}$ subarray, $\mathbf{D}$ is the $P \times P$ diagonal matrix with entries equal to $e^{-j\frac{2\pi\delta}{\lambda_c}\sin\theta_p^{(k)}}$ and $\mathbf{A}_1(\boldsymbol{\theta})$ is the $M_0 \times P$ submatrix consisting of the first $M_0$ rows of $\mathbf{A}(\boldsymbol{\theta})$:

$$\begin{aligned}\mathbf{A}_1(\boldsymbol{\theta}) \;=\; \Bigg[\; & \mathbf{a}_1\left(\theta_1^{(1)}\right) \;\cdots\; \mathbf{a}_1\left(\theta_{P_1}^{(1)}\right) \;\cdots\; \mathbf{a}_1\left(\theta_p^{(k)}\right) \;\cdots \\ & \cdots\; \mathbf{a}_1\left(\theta_1^{(K)}\right) \;\cdots\; \mathbf{a}_1\left(\theta_{P_K}^{(K)}\right) \;\Bigg]\end{aligned} \tag{4.12}$$

where

$$\mathbf{a}_1\left(\theta_p^{(k)}\right) = \left[\begin{array}{cccc} 1 & e^{-j\frac{2\pi\delta}{\lambda_c}\sin\theta_p^{(k)}} & \cdots & e^{-j\frac{2\pi\delta}{\lambda_c}(M_0-1)\sin\theta_p^{(k)}} \end{array}\right]^T \tag{4.13}$$

Suppose there are $N$ snapshots. By concatenating the $l^{\text{th}}$ subarray outputs at different snapshots, the received signal can be written compactly as:

$$\mathbf{Y}_l = \mathbf{A}_1(\boldsymbol{\theta})\,\mathbf{D}^{l-1}\boldsymbol{\Lambda}\mathbf{S} + \mathbf{W}_l \tag{4.14}$$

where

$$\mathbf{Y}_l = \left[ \begin{array}{cccc} \mathbf{y}_l(1) & \mathbf{y}_l(2) & \cdots & \mathbf{y}_l(N) \end{array} \right] \tag{4.15}$$

$$\mathbf{S} = \left[ \begin{array}{cccc} \mathbf{s}(1) & \mathbf{s}(2) & \cdots & \mathbf{s}(N) \end{array} \right] \tag{4.16}$$

$$\mathbf{W}_l = \left[ \begin{array}{cccc} \mathbf{w}_l(1) & \mathbf{w}_l(2) & \cdots & \mathbf{w}_l(N) \end{array} \right] \tag{4.17}$$

We consider the case where the transmitted signals are known at the receiver. Note that the receiver only has the knowledge of transmitted symbols, but not other parameters that characterize each signal path from each source. In other words, the receiver only has the knowledge of transmitted symbols $s^{(k)}(n)$ from the $k^{\text{th}}$ source, while the DOA $\theta_p^{(k)}$, the interpath delay $\tau_p^{(k)}$, and the complex gain $\alpha_p^{(k)}$ are unknown parameters at the receiver. We can ensure that the transmitted symbols from different sources are designed such that they are uncorrelated within the period while the DOAs are being estimated, i.e.,the pilot symbols from the different sources are designed ideally such that:

$$\frac{1}{N}\sum_{n=1}^{N} s^{(k_1)}(n)\left[s^{(k_2)}(n)\right]^* = \begin{cases} 1, & k_1 = k_2 \\ 0, & k_1 \neq k_2 \end{cases} \tag{4.18}$$

where $(\cdot)^*$ denotes the complex conjugate.

As pilot symbols are used, the DOAs of each source can be estimated separately, i.e., parallel processing. Now we consider the pilot symbols of the $k^{\text{th}}$ source:

$$\mathbf{s}^{(k)} = \left[ \begin{array}{cccc} s^{(k)}(1) & s^{(k)}(2) & \cdots & s^{(k)}(N) \end{array} \right]^T \tag{4.19}$$

We correlate the noiseless received signals at the $l^{\text{th}}$ subarray with the pilot symbols:

$$\begin{aligned} \mathbf{z}_l^{(k)} &= \frac{1}{N}\mathbf{Y}_l\left[\mathbf{s}^{(k)}\right]^* \\ &= \mathbf{A}_2\left(\boldsymbol{\theta}^{(k)}\right)\boldsymbol{\Lambda}^{(k)}\mathbf{b}_l\left(\boldsymbol{\theta}^{(k)}\right) \end{aligned} \tag{4.20}$$

where

$$\boldsymbol{\theta}^{(k)} = \left[ \begin{array}{cccc} \theta_1^{(k)} & \theta_2^{(k)} & \cdots & \theta_{P_k}^{(k)} \end{array} \right]^T \tag{4.21}$$

$$\mathbf{A}_2\left(\boldsymbol{\theta}^{(k)}\right) = \left[ \begin{array}{cccc} \mathbf{a}_1\left(\theta_1^{(k)}\right) & \mathbf{a}_1\left(\theta_2^{(k)}\right) & \cdots & \mathbf{a}_1\left(\theta_{P_k}^{(k)}\right) \end{array} \right] \tag{4.22}$$

$$\boldsymbol{\Lambda}^{(k)} = \mathrm{diag}\left\{ \begin{array}{cccc} \alpha_1^{(k)}, & \alpha_2^{(k)}, & \cdots & \alpha_{P_k}^{(k)} \end{array} \right\} \tag{4.23}$$

$$\mathbf{b}_l\left(\boldsymbol{\theta}^{(k)}\right) = \left[ \begin{array}{cccc} e^{-j\frac{2\pi\delta}{\lambda_c}(l-1)\sin\theta_1^{(k)}} & e^{-j\frac{2\pi\delta}{\lambda_c}(l-1)\sin\theta_2^{(k)}} & \cdots & e^{-j\frac{2\pi\delta}{\lambda_c}(l-1)\sin\theta_{P_k}^{(k)}} \end{array} \right]^T \tag{4.24}$$

$\boldsymbol{\theta}^{(k)}$ is the $P_k \times 1$ vector containing all the DOAs of the $k^{\mathrm{th}}$ source, and $\mathbf{A}_2\left(\boldsymbol{\theta}^{(k)}\right)$ is the $M_0 \times P_k$ submatrix of $\mathbf{A}_1(\boldsymbol{\theta})$ which consists of the $P_k$ steering vectors of the $k^{\mathrm{th}}$ source. $\boldsymbol{\Lambda}^{(k)}$ is the $P_k \times P_k$ diagonal matrix of the complex gains of the signal paths from the $k^{\mathrm{th}}$ source and $\mathbf{b}_l\left(\boldsymbol{\theta}^{(k)}\right)$ is as defined in (4.24).

By concatenating $\mathbf{Z}_l^{(k)}$ at different subarrays, we arrive at the following matrix:

$$\begin{aligned} \mathbf{Z}^{(k)} &= \left[ \begin{array}{cccc} \mathbf{z}_1^{(k)} & \mathbf{z}_2^{(k)} & \cdots & \mathbf{z}_L^{(k)} \end{array} \right] \\ &= \mathbf{A}_2\left(\boldsymbol{\theta}^{(k)}\right)\boldsymbol{\Lambda}^{(k)}\mathbf{B}\left(\boldsymbol{\theta}^{(k)}\right) \end{aligned} \tag{4.25}$$

where $\mathbf{B}\left(\boldsymbol{\theta}^{(k)}\right)$ is a $P_k \times L$ Vandermonde matrix expressed as:

$$\begin{aligned} \mathbf{B}\left(\boldsymbol{\theta}^{(k)}\right) &= \left[ \begin{array}{cccc} \mathbf{b}_1\left(\boldsymbol{\theta}^{(k)}\right) & \mathbf{b}_2\left(\boldsymbol{\theta}^{(k)}\right) & \cdots & \mathbf{b}_L\left(\boldsymbol{\theta}^{(k)}\right) \end{array} \right] \\ &= \left[ \begin{array}{cccc} 1 & e^{-j\frac{2\pi\delta}{\lambda_c}\sin\theta_1^{(k)}} & \cdots & e^{-j\frac{2\pi\delta}{\lambda_c}(L-1)\sin\theta_1^{(k)}} \\ 1 & e^{-j\frac{2\pi\delta}{\lambda_c}\sin\theta_2^{(k)}} & \cdots & e^{-j\frac{2\pi\delta}{\lambda_c}(L-1)\sin\theta_2^{(k)}} \\ \vdots & \vdots & \ddots & \vdots \\ 1 & e^{-j\frac{2\pi\delta}{\lambda_c}\sin\theta_{P_k}^{(k)}} & \cdots & e^{-j\frac{2\pi\delta}{\lambda_c}(L-1)\sin\theta_{P_k}^{(k)}} \end{array} \right] \end{aligned} \tag{4.26}$$

Note that $\mathbf{B}\left(\boldsymbol{\theta}^{(k)}\right)$ is a submatrix of $\mathbf{A}^T(\boldsymbol{\theta})$, which consists of the first $L$ rows of the

$P_k$ steering vectors of the $k^{\text{th}}$ source:

$$\mathbf{B}\left(\boldsymbol{\theta}^{(k)}\right) = \left[\begin{array}{cccc} \mathbf{a}_2\left(\theta_1^{(k)}\right) & \mathbf{a}_2\left(\theta_2^{(k)}\right) & \cdots & \mathbf{a}_2\left(\theta_{P_k}^{(k)}\right) \end{array}\right]^T \tag{4.27}$$

where

$$\mathbf{a}_2\left(\theta_p^{(k)}\right) = \left[\begin{array}{cccc} 1 & e^{-j\frac{2\pi\delta}{\lambda_c}\sin\theta_p^{(k)}} & \cdots & e^{-j\frac{2\pi\delta}{\lambda_c}(L-1)\sin\theta_p^{(k)}} \end{array}\right]^T \tag{4.28}$$

$\mathbf{A}_2\left(\boldsymbol{\theta}^{(k)}\right)$ is a full column matrix for $M_0 > P_k$, while $\mathbf{B}\left(\boldsymbol{\theta}^{(k)}\right)$ is a full row matrix for $L \geq P_k$. Therefore, under these two conditions, the DOAs associated with the $k^{\text{th}}$ source can be estimated from the left null space of $\mathbf{Z}^{(k)}$ since $\mathcal{R}\left(\mathbf{Z}^{(k)}\right) = \mathcal{R}\left(\mathbf{A}_2\left(\boldsymbol{\theta}^{(k)}\right)\right)$, where $\mathcal{R}(\cdot)$ denotes the range/column space. The left null space of $\mathbf{Z}^{(k)}$ can be estimated by existing techniques such as the high-resolution MUSIC algorithm. MUSIC estimates the DOAs by exploiting the orthogonality between signal and noise subspaces [3–5]:

$$\left[\mathbf{Z}^{(k)}\right]^H \mathbf{e}_i = 0, \quad i = P_k + 1, \ldots, M \tag{4.29}$$

where $\mathbf{e}_i$ is the noise eigenvector. The DOA estimates obtained are denoted by $\hat{\boldsymbol{\theta}}^{(k)} = \left[\hat{\theta}_1^{(k)} \;\; \hat{\theta}_2^{(k)} \;\; \cdots \;\; \hat{\theta}_{P_k}^{(k)}\right]^T$.

In cases of signal coherence, i.e., $P_k > 1$, an iterative procedure is carried out to refine the DOA estimates. This method, termed the PASI technique, does so by exploiting the structure of $\mathbf{B}\left(\boldsymbol{\theta}^{(k)}\right)$. First, the estimates of the matrices $\mathbf{A}_2\left(\boldsymbol{\theta}^{(k)}\right)$ and $\mathbf{B}\left(\boldsymbol{\theta}^{(k)}\right)$, denoted by $\hat{\mathbf{A}}_2\left(\hat{\boldsymbol{\theta}}^{(k)}\right)$ and $\hat{\mathbf{B}}\left(\hat{\boldsymbol{\theta}}^{(k)}\right)$ respectively, are formed accordingly to (4.22) and (4.26) respectively. Next, the complex gains $\hat{\boldsymbol{\Lambda}}^{(k)}$ are estimated from (4.25):

$$\hat{\boldsymbol{\Lambda}}^{(k)} = \left[\hat{\mathbf{A}}_2\left(\hat{\boldsymbol{\theta}}^{(k)}\right)\right]^{\dagger} \boldsymbol{Z}^{(k)} \left[\hat{\mathbf{B}}\left(\hat{\boldsymbol{\theta}}^{(k)}\right)\right]^{\dagger} \tag{4.30}$$

where $(\cdot)^{\dagger}$ denotes the Moore-Penrose pseudo-inverse of a matrix. We define the interference-

nulled array response matrix $\mathbf{H}_p$ as follows:

$$\mathbf{H}_p = \mathbf{Z}^{(k)} - \sum_{i \neq p, i=1}^{P_k} \mathbf{a}_1 \left( \hat{\theta}_i^{(k)} \right) \hat{\mathbf{\Lambda}}^{(k)} (i,i) \, \mathbf{a}_2^T \left( \hat{\theta}_i^{(k)} \right) \tag{4.31}$$

where $\boldsymbol{a}_1 \left( \hat{\theta}_i^{(k)} \right)$ and $\boldsymbol{a}_2 \left( \hat{\theta}_i^{(k)} \right)$ are as defined in (4.13) and (4.28) respectively. The $p^{\text{th}}$ DOA is then estimated from the left null space of $\boldsymbol{H}_p$ using MUSIC. For only a small number of iterations, the accuracy of DOA estimates improves significantly, as seen in the later section.

## 4.2 Proposed DOA Estimation Algorithm

From the discussion in Section 4.1, we can now list in details the steps of the basic algorithm for DOA estimation using the proposed PAS technique, together with the narrowband signal subspace estimation method, MUSIC. The proposed PASI technique, the extension of the proposed PAS technique, is carried in the case of correlated signals. To estimate the DOAs of the $k^{\text{th}}$ source:

1. Down-convert the received signal at the array to baseband and sample the baseband signal at the Nyquist rate, $T$ seconds.

2. Divide the $M$-element ULA into $L^{(k)}$ overlapping subarrays of size $M_0^{(k)}$, where $M_0^{(k)} = M - L^{(k)} + 1$.

3. For each snapshot ($n = 1, 2, \ldots, N$), form the $l^{\text{th}}$ subarray output $\mathbf{y}_l(n)$ in (4.11) for $l = 1, 2, \ldots, L^{(k)}$.

4. Concatenate all the $l^{\text{th}}$ subarray outputs at different snapshots to form $\mathbf{Y}_l$ in (4.14) for $l = 1, 2, \ldots, L^{(k)}$.

5. Correlate each $\mathbf{Y}_l$ with the pilot signals to form $\mathbf{z}_l^{(k)}$ in (4.20) for $l = 1, 2, \ldots, L^{(k)}$.

6. Concatenate all the vectors $\mathbf{z}_l^{(k)}$ to form the matrix $\mathbf{Z}^{(k)}$ in (4.25).

7. Obtain the initial DOA estimates $\hat{\boldsymbol{\theta}}^{(k)}$ from the left null space of $\mathbf{Z}^{(k)}$ using MUSIC.

8. Refine the DOA estimates by the iterative procedure:

   For $i = 1, 2, \ldots, L_{iter}$ (where $L_{iter}$ is the maximum number of iterations)

   For $p = 1, 2, \ldots, P_k$

   (a) Form the estimates of

   - $\mathbf{A}_2\left(\hat{\boldsymbol{\theta}}^{(k)}\right)$ using (4.22)
   - $\mathbf{B}\left(\hat{\boldsymbol{\theta}}^{(k)}\right)$ using (4.26)
   - $\boldsymbol{\Lambda}^{(k)}$ using (4.30)

   (b) Form the interference-nulled array response matrix $\mathbf{H}_p$ in (4.31).

   (c) Obtain the new $p^{\text{th}}$ DOA estimate from the left null space of $\mathbf{H}_p$ using MUSIC.

   (d) Update the $p^{\text{th}}$ DOA estimate in $\hat{\boldsymbol{\theta}}^{(k)}$.

   End

   End

Note that the iterative procedure in Step 8 is carried out in cases of signal coherence. In other words, the proposed PASI technique is used only in the presence of correlated signals.

The inclusion of the iterative procedure does not increase the time taken to estimate DOAs significantly. The search process in the MUSIC algorithm is greatly reduced since the searching range is carried out over a much smaller interval due to the knowledge of initial DOA estimates.

The maximum number of iterations is arbitrarily set in the iterative procedure. As shown in later sections, only a small number of iterations is required to achieve good performance. Alternatively, the stopping condition for the iterative procedure can be determined by the absolute difference between the current estimated DOA and the pre-

vious DOA estimate lesser than a pre-determined threshold whereby this threshold determines the resolution of the detected DOAs.

## 4.3 Effect of Subarrays

From Section 4.1, the signal subspace of the $k^{\text{th}}$ source is estimated from the left null space of $\mathbf{Z}^{(k)}$ under two conditions:

$$M_0^{(k)} > P_k \tag{4.32}$$

$$L^{(k)} \geq P_k \tag{4.33}$$

The number of antennas must thus satisfy:

$$M \geq \max_k \{2P_k\} \tag{4.34}$$

which is independent of the total number of impinging plane waves. In other words, the maximum detectable DOAs using the proposed PAS and PASI techniques is no longer bounded by the number of antennas in the array. Hence the capacity of DOA estimation is increased. In addition, the antenna array can be partitioned into subarrays of different sizes for each source since the proposed PAS and PASI techniques estimate the DOAs of each source separately. This results in an optimal usage of antennas for each source. It follows that for the $k^{\text{th}}$ source, the antenna is divided into $L^{(k)}$ overlapping subarrays of size $M_0^{(k)} = M - L^{(k)} + 1$, where $M_0^{(k)}$ and $L^{(k)}$ satisfy the conditions in (4.32).

Consider two independent signals arising from two uncorrelated sources, i.e., $P_k = 1$, arrive at an array of $M = 4$ elements. In order to resolve these signals, $L^{(k)} = 2$ subarrays of size $M_0^{(k)} = 3$ are deployed, satisfying the conditions in (4.32). Consider another example where a signal arrives at an array of $M = 10$ antennas via $P_k = 4$ multipaths. To resolve these multipaths, $L^{(k)} = 7$ subarrays are chosen accordingly to (4.32) and hence the number of elements in each subarray will be $M_0^{(k)} = 4$.

We now investigate the effect of subarray size on the performance of both proposed

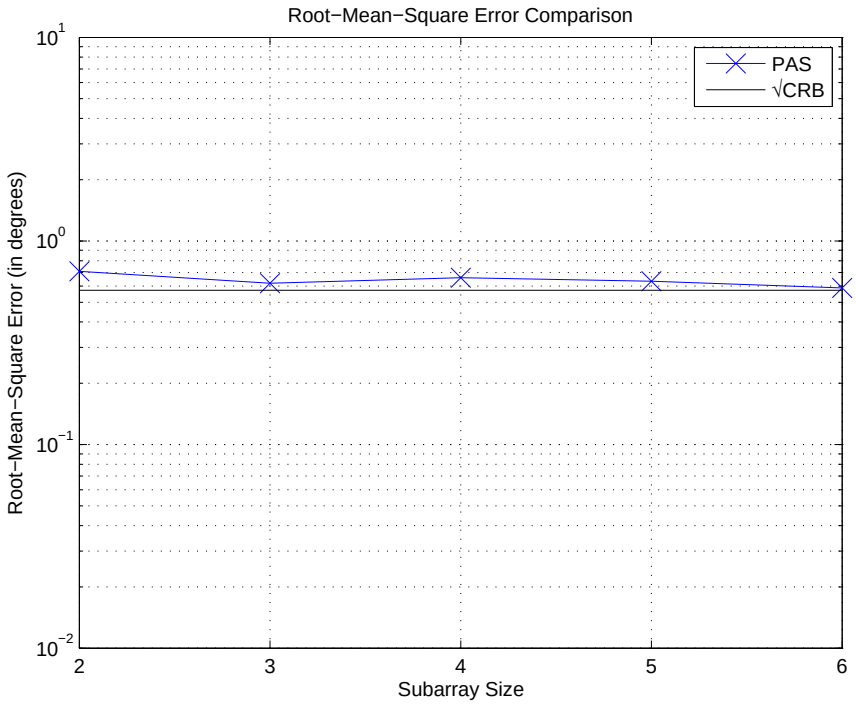


Figure 4.1: RMSE performance against subarray size for uncorrelated signals

techniques. Firstly, two uncorrelated sources, each having a single path, are considered. The two independent sources transmit binary phase shift keying (BPSK) sequences which are known to the receiver. The DOAs of the two paths are randomly generated with a fixed angle separation of $10^\circ$. The magnitudes of their complex gains are set to 2, i.e., $\left|\alpha_1^{(1)}\right| = \left|\alpha_1^{(2)}\right| = 2$; the phases of their complex gains are randomly generated with uniform distribution between $0$ and $2\pi$. The size of each subarray is varied from $2$ to $6$. Correspondingly, the number of subarrays is varied from $1$ to $5$. The subarray size and the number of subarrays are chosen such that they satisfy the conditions in (4.32). The receiver has a $6$-element ULA with inter-element spacing $\delta = \frac{1}{2}\lambda_c$ where $\lambda_c$ is the wavelength of the carrier frequency. The noise at the array is assumed to be AWGN. The number of snapshots is set to $30$ and the SNR is fixed at $0$ dB. The results are obtained through Monte Carlo simulation of $2000$ independent trials (for which the statistical performance converges). From Figure 4.1, it is seen that the performance of the proposed PAS technique is very close to the Cramer-Rao lower bound (CRLB), regardless of subarray size. Hence, the subarray size of uncorrelated signals will be

chosen to be $5$ with negligible impact on the performance analysis of the proposed algorithm in later sections.

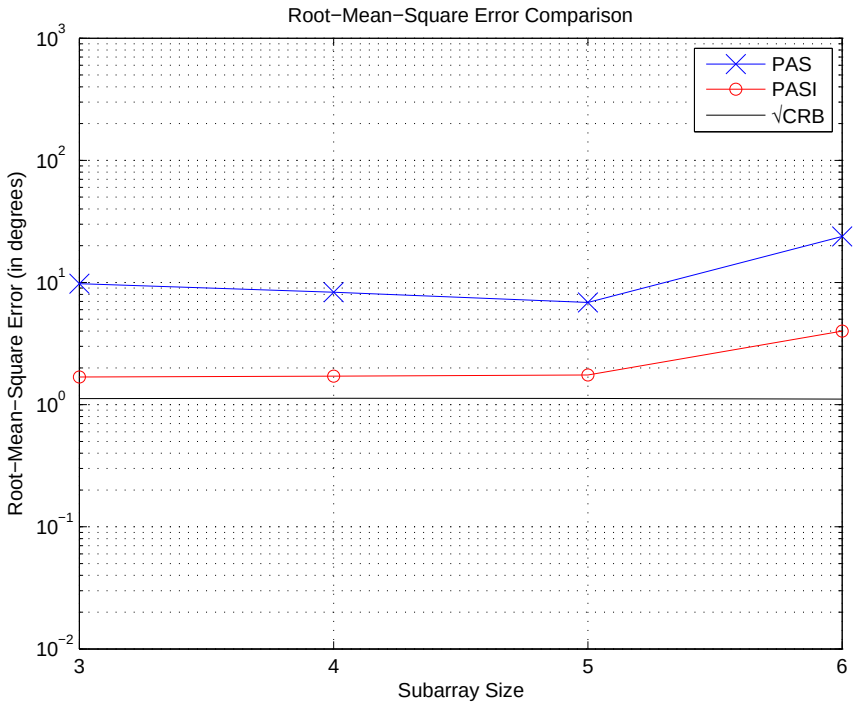


Figure 4.2: RMSE performance against subarray size for correlated signals

Next consider the case of two perfectly correlated signals which arrive at the receiver simultaneously. The correlated signals are as a result of two impinging plane waves from the same source that arrive at the receiver through two independent multipaths. The two DOAs are randomly generated with a fixed angle separation of $20°$. The size of each subarray is varied from $3$ to $6$. Correspondingly, the number of subarrays is varied from $1$ to $4$. The subarray size and the number of subarrays are chosen such that they satisfy the conditions in (4.32). The rest of the parameters are unchanged. From Figure 4.2, the performance of the proposed PASI is better than that of the proposed PAS as the former is able to decorrelate the correlated signals through the use of subarrays. It is observed that the proposed PASI technique exhibits performance close to the CRLB of subarray size ranging from $3$ to $5$. Hence, the subarray size will be set to $5$ for correlated signals in later sections.

## 4.4 Detection of The Number of Multipaths Per Source

The number of sources is known since we utilize their pilot signals. However, the derivation in Section 4.1 assumes the number of multipaths per source $P_k$ is known so as to estimate the signal subspace. We can estimate the value of $P_k$ from the test profile of how the rank of $\mathbf{Z}^{(k)}$ in (4.25) varies with the number of subarrays $L^{(k)}$. The value of $P_k$ corresponds to the smallest value of $L^{(k)}$ where the rank of $\mathbf{Z}^{(k)}$ stays constant. The rank of $\mathbf{Z}^{(k)}$ is estimated from the number of dominant eigenvalues.

We consider the case of two perfectly correlated signals which arrive at the receiver simultaneously. The correlated signals are the result of two impinging plane waves from the same source that arrive at the receiver through two independent multipaths. The signal source transmits BPSK sequences which are known to the receiver. The DOAs of the two multipaths are set to $\theta_1^{(1)} = 20^\circ$ and $\theta_2^{(1)} = 40^\circ$ respectively. The magnitudes of their complex gains are set to 2, i.e., $\left|\alpha_1^{(1)}\right| = \left|\alpha_2^{(1)}\right| = 2$; the phases of their complex gains are randomly generated with uniform distribution between $0$ and $2\pi$. The receiver has a 6-element ULA with inter-element spacing $\delta = \frac{1}{2}\lambda_c$ where $\lambda_c$ is the wavelength of the carrier frequency. The noise at the array is assumed to be AWGN. The number of snapshots is set to $30$ and the SNR is fixed at $20$ dB.

From Figure 4.3, the rank of $\mathbf{Z}^{(1)}$ stays constant at $2$ when the number of subarrays is varied from $2$ to $5$. We conclude that the number of multipaths for the first source is $2$, which verifies our simulation. When there is only $1$ subarray, the rank of $\mathbf{Z}^{(1)}$ is $1$ as the correlated signals are not resolved. The rank of $\mathbf{Z}^{(1)}$ is also $1$ when there are $6$ subarrays (i.e. $1$ element in the subarray) as the condition $M_0^{(1)} > P_k$ is not satisfied.

Next, the performance of the detection algorithm is investigated against SNR. The results are obtained through Monte Carlo simulation of $2000$ independent trials (for which the statistical performance converges). From Figure 4.4, the detection algorithm is able to detect with $100\%$ correct rank detection from $1$ dB onwards.

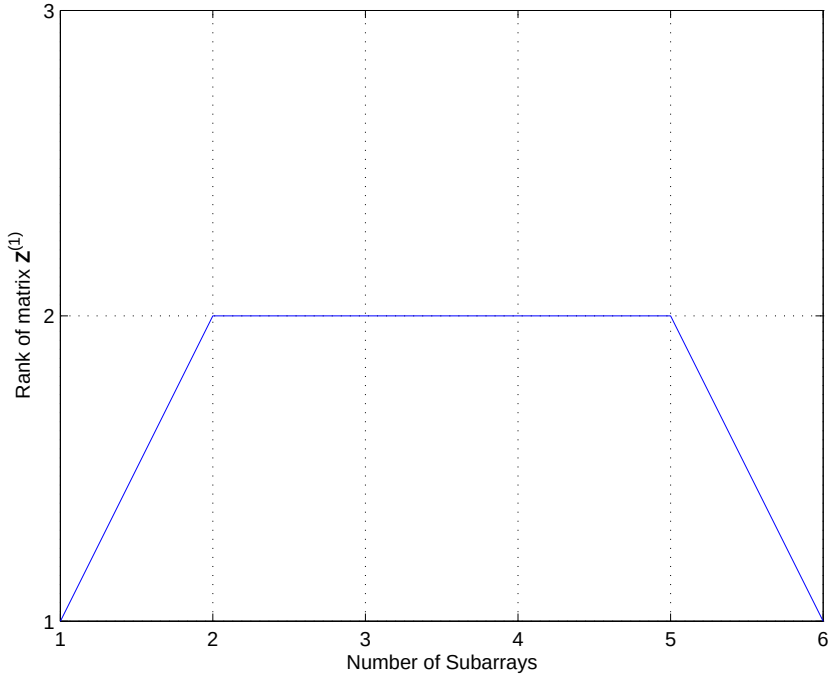


Figure 4.3: Rank of $\mathbf{Z}^{(1)}$ against number of subarrays

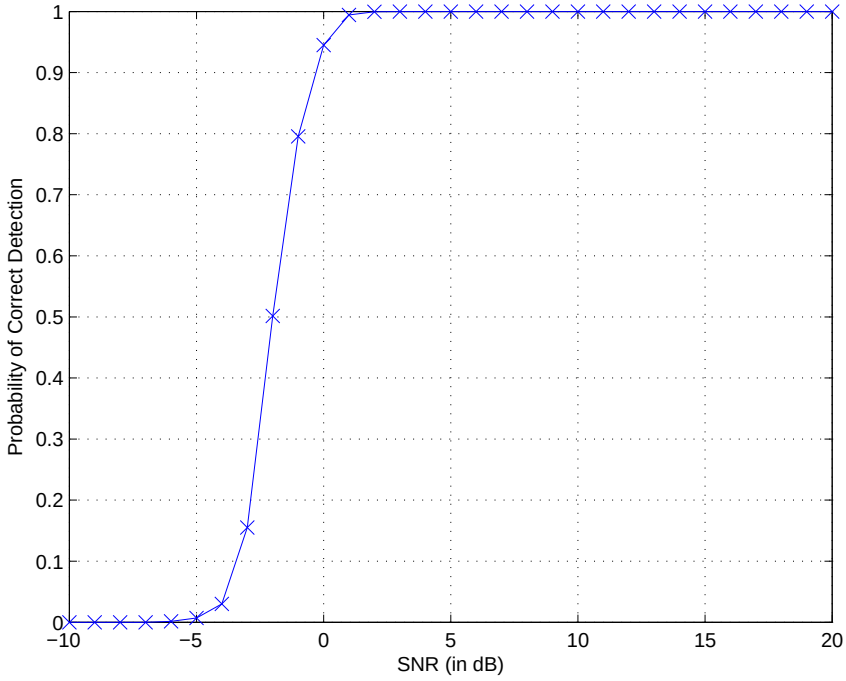


Figure 4.4: Probability of correct rank detection against SNR for correlated signals

## 4.5 Simulation Results

In this section, we provide some numerical results to compare the performance of the proposed PAS and the PASI techniques with other algorithms available in the literature.

We first investigate the performance of the proposed PAS technique for uncorrelated signals from independent sources. We next demonstrate the robustness of both proposed techniques for correlated signals from the same source that arrive at the receiver through different multipaths. We establish, through a series of simulations, the robustness of both proposed algorithms in testing conditions such as low SNRs, small array size and closely-spaced DOAs.

### 4.5.1 Uncorrelated Signals

For uncorrelated signals, the performance of the proposed PAS technique is compared with the existing algorithms: IQML estimator, the modified AM estimator, the modified EM estimator, the SBDOA estimator as well as the MSWF-based estimator. We compare the performance of the various algorithms with the CRLB derived for known waveforms given in [11]. Monte Carlo simulation of $2000$ independent trials are conducted to obtain the statistical performance. Note that the CRLB is a tight bound derived for Gaussian signals. Hence in the simulation plots that follow, some of the points may appear to be lower than that of the CRLB as BPSK signals are considered.

We consider the case where there are two uncorrelated sources, each having a single impinging wavefront at the receiver. The two independent sources transmit BPSK sequences which are known to the receiver. The DOAs of the first and second sources are randomly generated with a fixed angle separation of $10^\circ$. The magnitudes of their complex gains are set to 2, i.e., $\left|\alpha_1^{(1)}\right| = \left|\alpha_1^{(2)}\right| = 2$; the phases of their complex gains are randomly generated with uniform distribution between $0$ and $2\pi$. We set the number of subarrays to $L = 2$ (this is for fair comparison with the SBDOA algorithm which uses $2$ subarrays) and thus the size of each subarray is $M_0 = 5$. The number of snapshots is set to $N = 30$. We consider a 6-element ULA with inter-element spacing $\delta = \frac{1}{2}\lambda_c$ where $\lambda_c$ is the wavelength of the carrier frequency. The noise at the array is assumed to be AWGN.

The effect of SNR on the performance of all algorithms is first investigated. From

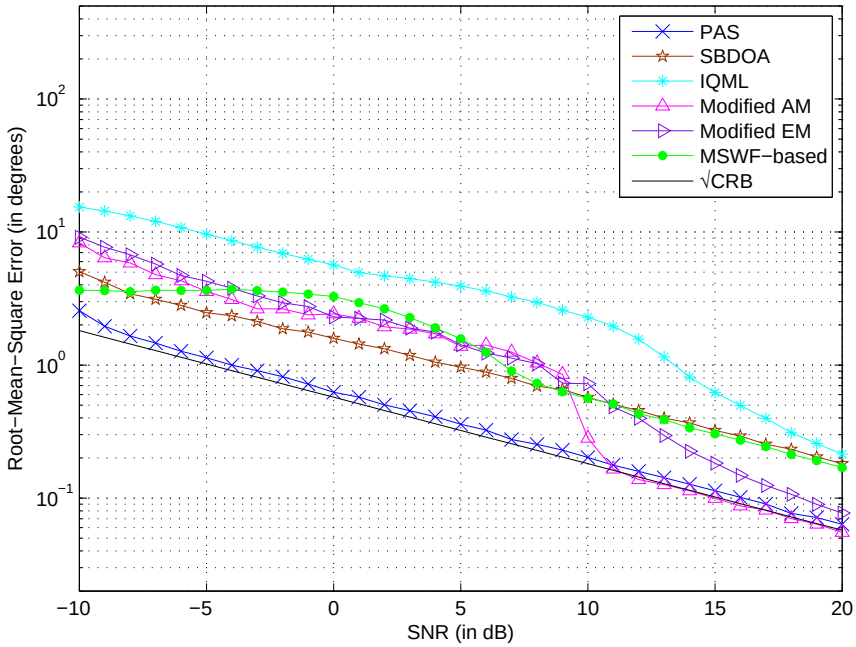


Figure 4.5: RMSE performance against SNR for uncorrelated signals

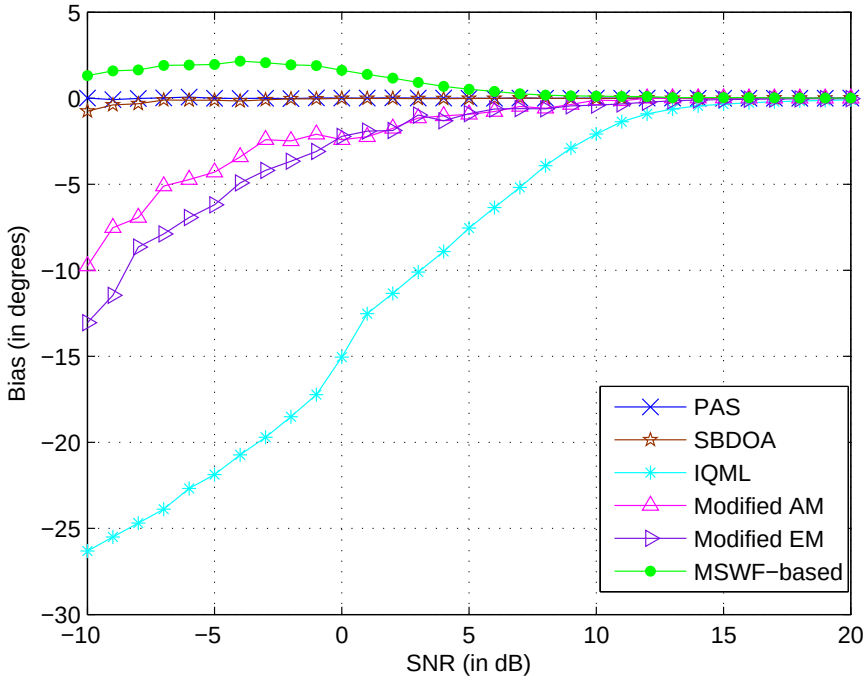


Figure 4.6: Bias performance against SNR for uncorrelated signals

Figure 4.5, the proposed PAS technique performs the best among all the algorithms. It is the only algorithm that approaches the CRLB in the low SNR region. The modified AM and modified EM algorithms converge to the CRLB after a SNR threshold of 11

dB and $20$ dB respectively. The performance of the SBDOA algorithm is displaced from the CRLB by approximately $10$ dB across all SNRs. Both the IQML and MSWF-based algorithms are not close to the CRLB from $-10$ dB to $20$ dB. However, they may converge to the CRLB at much higher SNRs.

The bias performance against SNR of these algorithms is also plotted. From Figure 4.6, the proposed PAS technique exhibits the lowest bias across all SNRs. The SBDOA algorithm has the next best bias performance, followed by the MSWF-based algorithm. The remaining three algorithms have almost zero bias after a threshold of approximately $15$ dB.

Next, we fix the SNR to $20$ dB and investigate the performance of the algorithms with array size varying from $3$ to $20$. The number of subarrays is kept constant at $L = 2$. The rest of the parameters are unchanged. From Figure 4.7, the proposed PAS technique and modified AM algorithm exhibit performance close to the CRLB regardless of the array size. The modified EM algorithm is also close to the CRLB from approximately $9$ dB onwards. However, as shown from Figure 4.5, these two algorithm perform close to the CRLB when the operating SNRs are larger than $11$ dB and $20$ dB respectively so that their iterative processes can converge [11]. The performance of the IQML and the MSWF-based algorithms approach the CRLB when the array size is larger than $14$ while the performance of the SBDOA algorithm saturates when the array size is larger than $10$, with a significant performance gap compared to other algorithms.

The correspondingly bias performance against array size is plotted in Figure 4.8. The performance of the proposed PAS technique has the lowest bias, closely followed by the SBDOA and the modified AM algorithms. The MSWF-based algorithm has a slightly worse bias performance below $7$ dB compared to the proposed PAS, the SBDOA and the modified AM algorithms. The remaining algorithms – modified EM and IQML – have almost zero bias only from approximately $12$ dB onwards.

Lastly, we demonstrate the resolution capability of the proposed PAS algorithm. We fix array size at $M = 6$ and set the number of subarrays to $L = 2$ with the elements in each subarray to $M_0 = 5$. The number of snapshots is set to $N = 30$ and the SNR

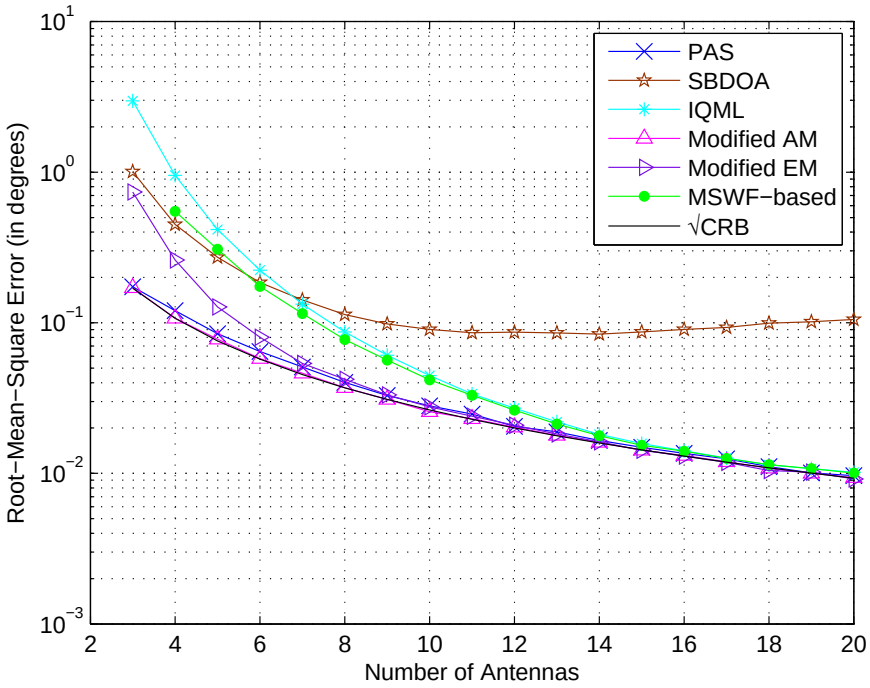


Figure 4.7: RMSE performance against number of antennas for uncorrelated signals

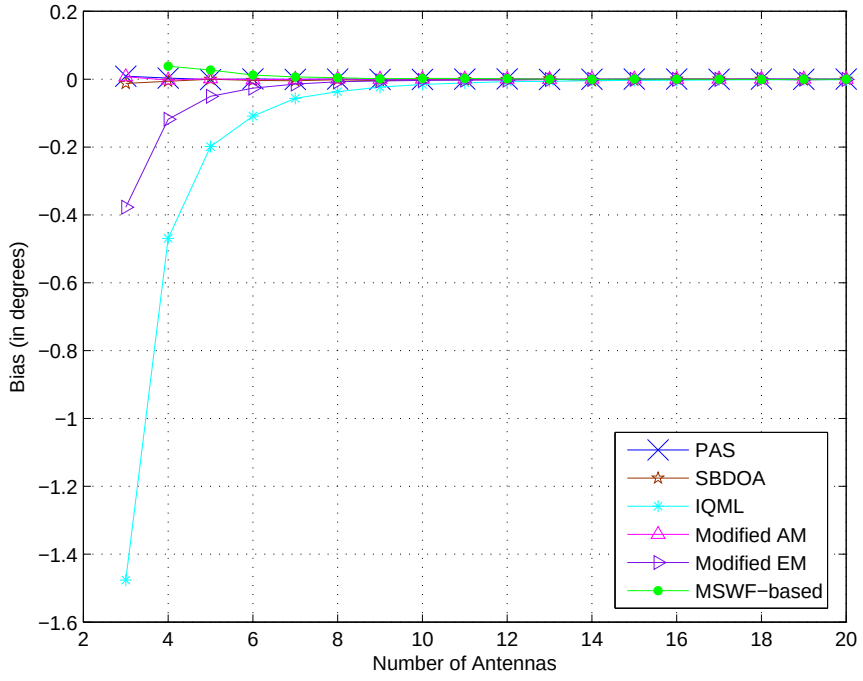


Figure 4.8: Bias performance against number of antennas for uncorrelated signals

is kept at 20 dB. The DOA for first path is randomly generated while the DOA for the second path is varied from the first DOA by an angle separation of 1° to 20°.

From Figure 4.9, the proposed PAS technique proves to be the algorithm with the best resolution performance. Even at an angle separation of $1^\circ$, the performance of the proposed PAS technique is comparable to the CRLB. The modified AM algorithm also exhibits good performance as it is able to resolve the two signals accurately when they are separated by more than $3^\circ$. The modified EM algorithm is able to resolve the signals accurately from an angle separation of approximately $15^\circ$ onwards. The MSWF-based, SBDOA and IQML algorithms do not approach the CRLB for the SNR under consideration. The ability of the IQML and MSWF-based estimators to resolve closely-spaced angles is dependent on the number of antennas as illustrated in Figure 4.7. Using a small array size, they are not able to resolve the signals.

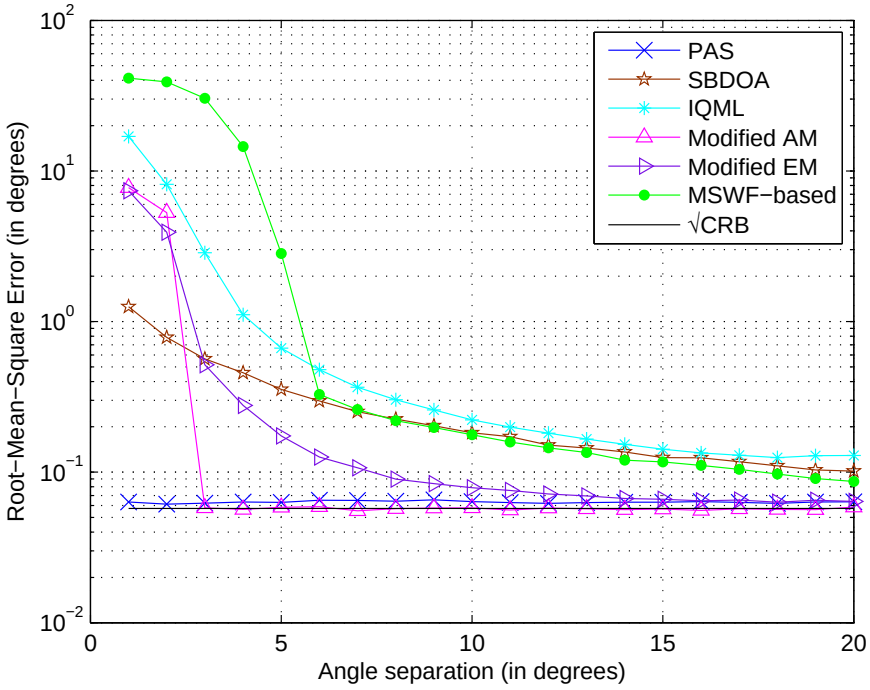


Figure 4.9: RMSE performance against angle separation for uncorrelated signals

The bias performance against angle separation is plotted in Figure 4.10. The proposed PAS technique displays the best bias performance. It is closely followed by the SBDOA, the modified AM and EM algorithms. The MSWF-based and IQML algorithms exhibit bias close to zero from an angle separation of $5^\circ$ onwards.

Summarizing the insights we gain from the three different simulation configurations, we come to the conclusion that the proposed PAS technique has significant ad-

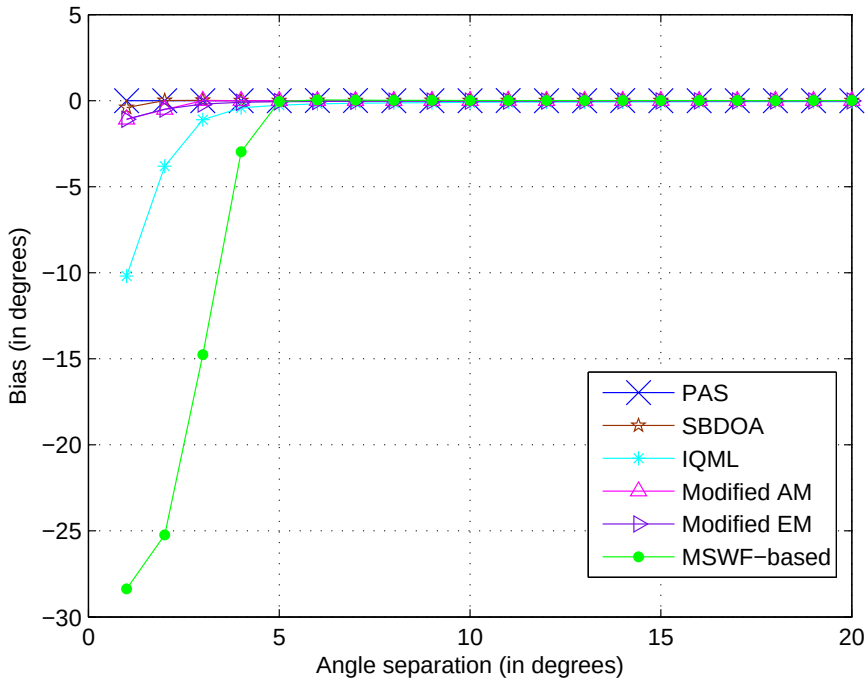


Figure 4.10: Bias performance against angle separation for uncorrelated signals

vantages over existing algorithms in terms of performance. It is able to achieve performance close to the CRLB as it makes use of a priori knowledge of the transmitted symbols. It is robust at low SNRs and has the ability to resolve closely-spaced angles. Moreover, the proposed PAS algorithm does not require a large number of antenna at the receiver to achieve good performance, hence relaxing the implementation constraints. The proposed PAS technique is able to achieve such excellent performance as the signal subspace used in the DOA estimation contains negligible interference from other sources after the received signals are correlated with the pilot signals of the desired source.

### 4.5.2 Correlated Signals

We now investigate the performance of the proposed algorithms in the context of correlated signals. We compare the performance of the proposed PAS and PASI techniques with existing algorithms that are able to handle correlated signals, namely the IQML algorithm and the MSWF-based algorithm. Note that the best performing algorithms

among the existing algorithms in Section 4.5.1, the modified AM and modified EM algorithms, cannot handle correlated signals [11] and are not be used for comparison. Similarly, the SBDOA algorithm is not used for comparison [43]. We compare the performance of the remaining algorithms with the CRLB given in [11]. Monte Carlo simulation of $2000$ independent trials are conducted to obtain the statistical performance.

We consider the most demanding but common operating scenario where two perfectly correlated signals arrive at the receiver simultaneously. The correlated signals are the result of two impinging wavefronts from the same source that arrive at the receiver through two independent multipaths. The signal source transmits BPSK sequences which are known to the receiver. The DOAs of the two multipaths are randomly generated with a fixed angle separation of $20^\circ$. The magnitudes of their complex gains are set to 2, i.e., $\left|\alpha_1^{(1)}\right| = \left|\alpha_2^{(1)}\right| = 2$; the phases of their complex gains are randomly generated with uniform distribution between $0$ and $2\pi$. The receiver has a $6$-element ULA with inter-element spacing $\delta = \frac{1}{2}\lambda_c$ where $\lambda_c$ is the wavelength of the carrier frequency. The noise at the array is assumed to be AWGN. We set the number of subarrays to $L = 2$ and hence the size of each subarray is $M_0 = 5$. The number of snapshots is set to $N = 30$. The number of iterations used in the proposed PASI technique is set to $2$.

We first investigate the performance of the algorithms against SNR. Here the root-mean-square error (RMSE) is averaged over the two paths. From Figure 4.11, we see that the proposed PAS technique has performance nearer to the CRLB from $4$ dB onwards. However, the proposed PASI technique has better performance, which approaches the CRLB across all SNRs. The proposed iterative process is able to decorrelate the two correlated signals even at low SNRs. This improves the estimation accuracy and results in consistent performance of the proposed PASI technique. The MSWF-based algorithm is nearer to the CRLB from $8$ dB onwards. The IQML algorithm may converge to the CRLB from $20$ dB onwards which is not plotted here.

The bias performance against SNR is plotted in Figure 4.12. The proposed PASI technique has almost zero bias across all SNRs. The proposed PAS technique has the

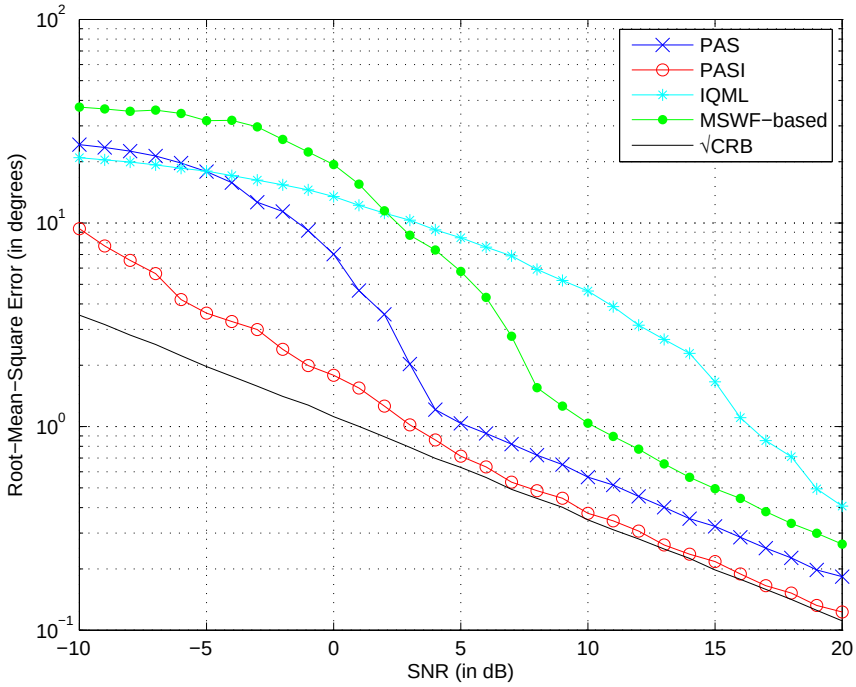


Figure 4.11: RMSE performance against SNR for correlated signals

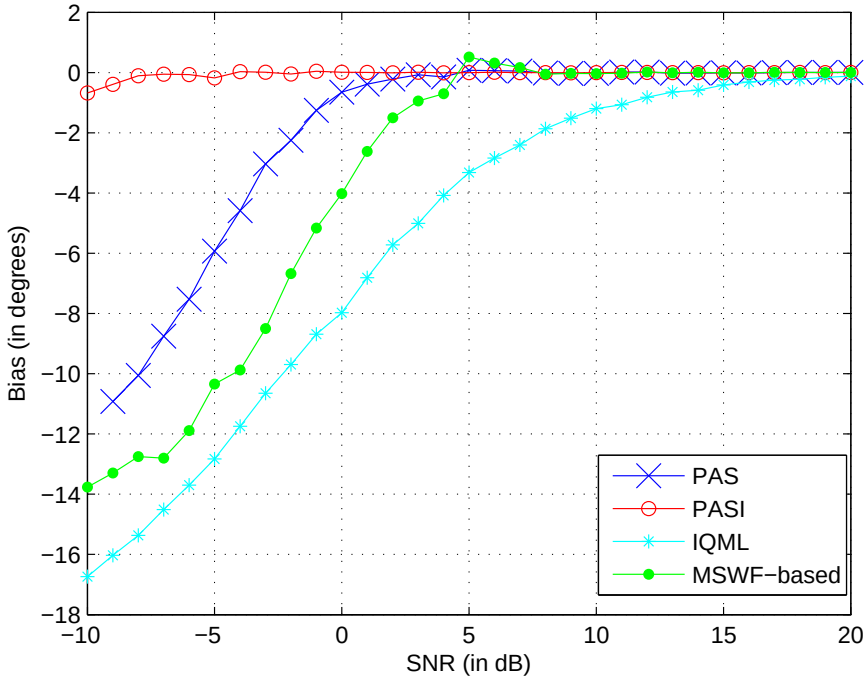


Figure 4.12: Bias performance against SNR for correlated signals

next best bias performance which exhibits zero bias from 5 dB onwards. The IQML has the worse bias among all the algorithms and exhibits zero bias only from 20 dB

onwards.

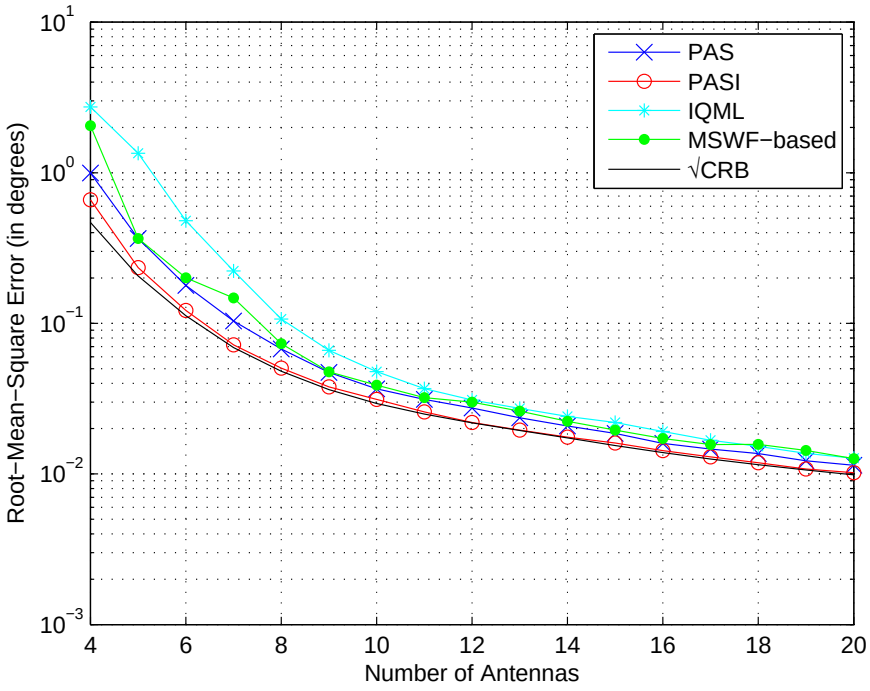


Figure 4.13: RMSE performance against number of antennas for correlated signals

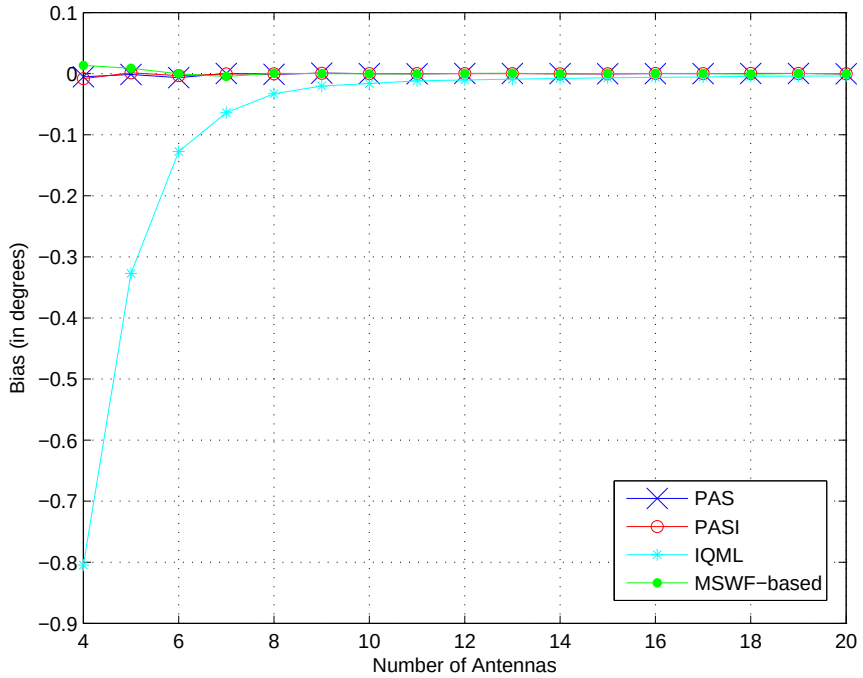


Figure 4.14: Bias performance against number of antennas for correlated signals

Next, we investigate the effect of array size on the estimation performance of the

various algorithms. We set the SNR to $20$ dB. The rest of the parameters are unchanged. The estimation performance of all algorithms is plotted in Figure 4.13 together with the CRLB. From Figure 4.13, we see that the proposed PASI technique achieves the best performance and approaches the CRLB even with $4$ antennas. This is closely followed by the proposed PAS technique and the MSWF-based algorithm. They have similar performances as both correlate received signals with pilot signals and hence the corresponding signal subspaces contain limited interference from undesired sources which thus results in more accurate DOA estimation. The IQML algorithm has much poorer performance compared to the MSWF-based algorithm for array size less than $12$.

The corresponding bias performance against array size is plotted in Figure 4.14. The proposed PAS, the proposed PASI and the MSWF-based algorithms have almost zero bias across all array sizes. The IQML has bias close to zero from $14$ dB onwards.

Lastly, we illustrate the ability of the proposed algorithms to resolve the closely-spaced multipaths impinging at the array. We keep the SNR at $20$ dB and set the array size and the number of subarrays to $M = 6$ and $L = 2$ respectively. The DOA for the first path is randomly generated while the DOA for the second path is varied from the first DOA by an angle separation of $1^\circ$ to $20^\circ$. The rest of the parameters are unchanged.

In Figure 4.15, the performance of various algorithms is plotted against angle separation. Comparing Figure 4.15 to Figure 4.9, we see that for correlated signals, a minimum angle separation of $11^\circ$ is required even for the best performing PASI technique. The proposed PASI technique is the best performing algorithm in terms of RMSE as well as minimum angle separation. The proposed PAS and MSWF-based algorithms have reasonable performance as they approach the CRLB for large angle separation. The RMSE performance of the IQML algorithm does not approach the CRLB across the angle separation under consideration.

The bias performance against angle separation is shown in Figure 4.16. The proposed PASI technique exhibits zero bias for all angle separation. The IQML has the next best bias performance. It only displays non-zero bias when the angle separation is

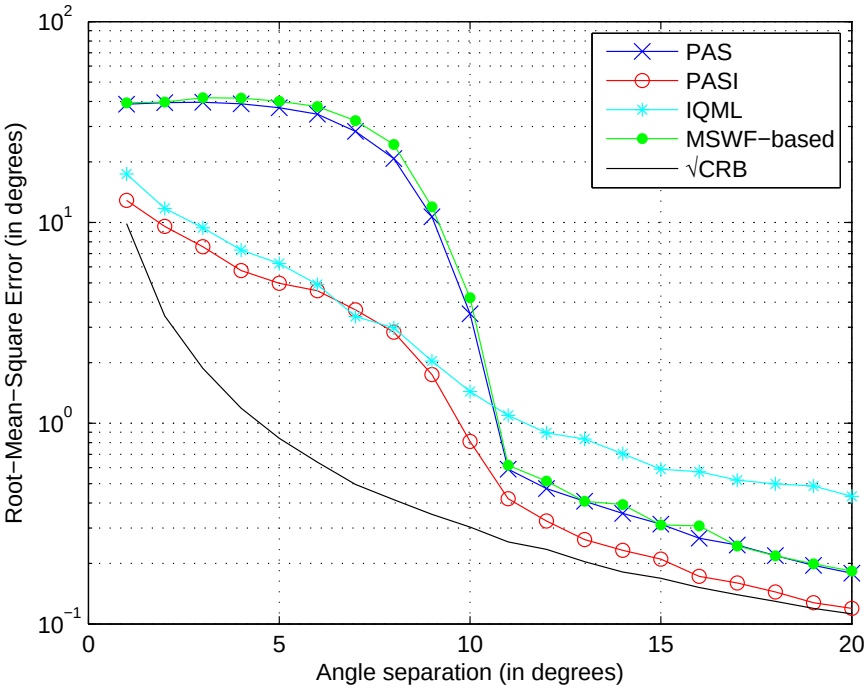


Figure 4.15: RMSE performance against angle separation for correlated signals

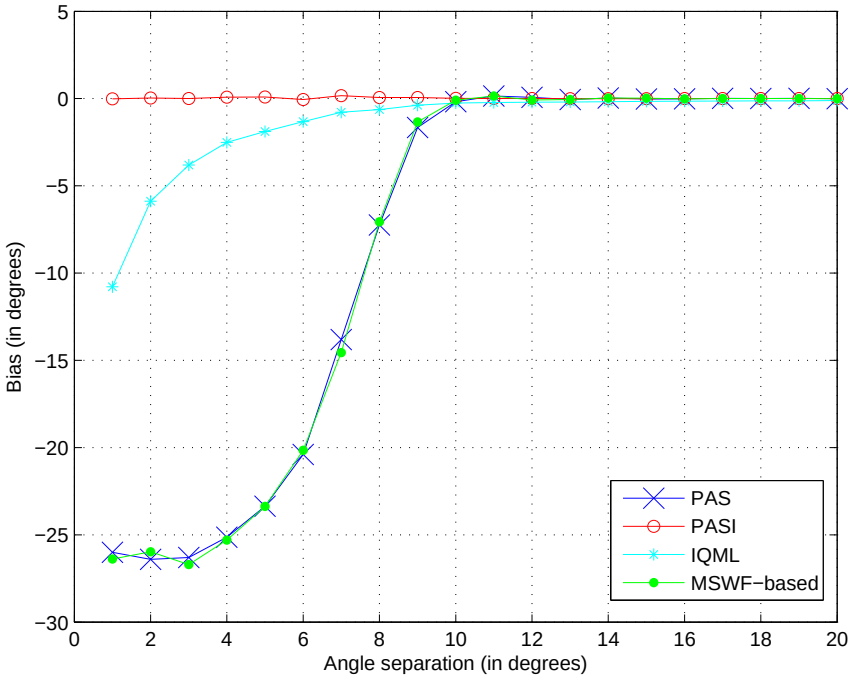


Figure 4.16: Bias performance against angle separation for correlated signals

less than $10^{\circ}$. Moreover, its deviation is much smaller compared to that of the proposed PAS technique and the MSWF-based algorithm.

We have shown through various simulation that by using the proposed PASI technique, we can achieve the CRLB at low SNRs which none of the existing algorithms being compared is able to achieve. Moreover, the proposed PASI technique is able to resolve correlated signals adequately provided that the angle separation of the multipaths paths is greater than $10^{\circ}$. The required array size can be small as long as it satisfies the criteria $M_0^{(k)} > P_k$ and $L^{(k)} \geq P_k$. The total number of antennas is independent of the total number of impinging plane waves $P$ and thus relaxes the hardware requirement of the proposed algorithms.

## 4.6 Conclusion

We introduced two new DOA estimation methods for narrowband sources. The first method, termed PAS technique, shows good performance in the low SNR region for uncorrelated signals. It is able to separate uncorrelated paths that are as close as $1^{\circ}$ apart. To further improve the performance of the proposed PAS technique in the case of correlated signals, the technique is extended to include an iterative procedure which is termed the PASI technique. Both the proposed PAS and PASI techniques perform close to the CRLB, even at low SNRs and with small number of antennas. We also showed through simulation that there is negligible effect of subarray size and number on the performance of the proposed PAS and PASI techniques provided the conditions $M_0^{(k)} > P_k$ and $L^{(k)} \geq P_k$ are satisfied for each source.

# Chapter 5

# CFSSM: New Wideband DOA Estimator

In this chapter, we introduce a computationally attractive, coherent DOA estimation method for wideband sources which we term combined frequency signal subspace method (CFSSM). We first discuss the formulation of the DOA estimation method and demonstrate the applicability of the proposed method for both uncorrelated and correlated wideband signals. We then quantify the computational efficiency of CFSSM over existing methods [17, 38, 39]. Numerical results are provided at the end of the chapter to exemplify the detection and estimation capabilities of the proposed method.

## 5.1 Formulation of Proposed Method

In this section, we derive the theoretical formulation of the proposed CFSSM used for DOA estimation of wideband signals. Recall from Section 2.4.2 that for the general case of a wireless communication system consisting of $K$ independent wideband sources, the received signal at the $m^{\text{th}}$ antenna can be written compactly as:

$$y_m(t) = \sum_{k=1}^{K} \sum_{p=1}^{P_k} \alpha_p^{(k)} x^{(k)} \left(t - \tau_p^{(k)} - \kappa_{p,m}^{(k)}\right) + w_m(t) \tag{5.1}$$

where $x^{(k)}(t)$ is the modulated signal from the $k^{\text{th}}$ source. $\tau_p^{(k)}$ and $\alpha_p^{(k)}$ denote the interpath delay and the complex gain of the $p^{\text{th}}$ multipath from the $k^{\text{th}}$ source respectively. $\kappa_{p,m}^{(k)}$ is the antenna delay of the $p^{\text{th}}$ multipath from the $k^{\text{th}}$ source at $m^{\text{th}}$ antenna

relative to the arrival time of the same path at the reference antenna. It can be expressed as:

$$\kappa_{p,m}^{(k)} = \frac{d_{p,m}^{(k)}}{c} \tag{5.2}$$

where $d_{p,m}^{(k)}$ is defined as the distance between the $m^{\text{th}}$ antenna and the reference antenna of the $p^{\text{th}}$ multipath from the $k^{\text{th}}$ source, and $c$ is the speed of propagation. $w_m(t)$ is the additive noise at the $m^{\text{th}}$ antenna which is assumed to be uncorrelated with any of the impinging plane waves, and is temporally and spatially white.

At the receiver, the signal is down-converted to baseband and sampled at the Nyquist rate, $B$ Hz. The antenna array output is observed over a total duration of $T_0$ seconds. The observation window is divided into $N$ intervals whereby each interval has a duration of $\Delta T = T_0/N$ seconds. For each interval, a $Q$-point DFT is applied to the $Q$ samples to obtain $Q$ frequency bins. Hence, the bandwidth of the signal sources $B$ is given by $Q/\Delta T$ Hz. The $i^{\text{th}}$ sample within each interval at the $m^{\text{th}}$ antenna for $i = 0, 1, \ldots, Q-1$ is given by:

$$y_m(i) = \sum_{k=1}^{K} \sum_{p=1}^{P_k} \alpha_p^{(k)} \tilde{x}^{(k)} \left( \frac{i}{B} - \tilde{\tau}_{p,m}^{(k)} \right) e^{-j2\pi f_c \tilde{\tau}_{p,m}^{(k)}} + w_m(i) \tag{5.3}$$

where $\tilde{\tau}_{p,m}^{(k)} = \tau_p^{(k)} + \kappa_{p,m}^{(k)}$ and $\tilde{x}^{(k)}(t)$ is the baseband signal of the $k^{\text{th}}$ source. The $Q$-point DFT output at the $m^{\text{th}}$ antenna for $q = 0, 1, \ldots, Q-1$ is thus [26]:

$$\begin{aligned} Y_m(q) &= \sum_{i=0}^{Q-1} \sum_{k=1}^{K} \sum_{p=1}^{P_k} \alpha_p^{(k)} \tilde{x}^{(k)} \left( \frac{i}{B} - \tilde{\tau}_{p,m}^{(k)} \right) e^{-j2\pi f_c \tilde{\tau}_{p,m}^{(k)}} e^{-j2\pi \frac{iq}{Q}} + W_m(q) \\ &= \sum_{k=1}^{K} \sum_{p=1}^{P_k} \alpha_p^{(k)} \tilde{X}^{(k)}(q) e^{-j2\pi \frac{q}{Q} B \tilde{\tau}_{p,m}^{(k)}} e^{-j2\pi f_c \tilde{\tau}_{p,m}^{(k)}} + W_m(q) \\ &= \sum_{k=1}^{K} \sum_{p=1}^{P_k} \alpha_p^{(k)} \tilde{X}^{(k)}(q) e^{-j2\pi \left( f_c + \frac{q}{Q} B \right) \tilde{\tau}_{p,m}^{(k)}} + W_m(q) \end{aligned} \tag{5.4}$$

where $\tilde{X}^{(k)}(q)$ and $W_m(q)$ are the baseband signal of the $k^{\text{th}}$ source and the additive white noise in the frequency domain respectively.

Note that there exists a linear relationship between the array manifolds of the different frequency bins regardless of the array geometry. We exploit this fact for our proposed estimation method. To simplify the derivations and illuminate the formulation of the proposed method clearly, we shall consider from this point onwards that the antenna array at the receiver is a ULA with inter-element spacing $\delta$. Note that the proposed method is equally applicable to other array geometries and can be easily derived accordingly.

Hence, taking into account of a ULA array configuration, (5.2) becomes:

$$\kappa_{p,m}^{(k)} = \frac{(m-1)\,\delta}{c} \sin\theta_p^{(k)} \tag{5.5}$$

We also rewrite the frequency-dependent steering vector from (2.73) as:

$$\begin{aligned} \boldsymbol{a}\left(q, \theta_p^{(k)}\right) = \Bigg[ & e^{-j2\pi\left(f_c + \frac{q}{Q}B\right)\left(\tau_p^{(k)}\right)} \quad e^{-j2\pi\left(f_c + \frac{q}{Q}B\right)\left(\tau_p^{(k)} + \frac{\delta}{c}\sin\theta_p^{(k)}\right)} \quad \dots \\ & \dots \quad e^{-j2\pi\left(f_c + \frac{q}{Q}B\right)\left(\tau_p^{(k)} + \frac{(M-1)\delta}{c}\sin\theta_p^{(k)}\right)} \Bigg]^T \end{aligned} \tag{5.6}$$

We can separate each entry in (5.6) into a frequency-independent portion given by:

$$C_m\left(k,p\right) = e^{-j2\pi f_c \tau_p^{(k)}} e^{-j2\pi\frac{\delta}{\lambda_c}(m-1)\sin\theta_p^{(k)}} \tag{5.7}$$

and a frequency-dependent portion given by:

$$D_m^{(q)}\left(k,p\right) = e^{-j2\pi\frac{q}{Q}B\tau_p^{(k)}} e^{-j2\pi\frac{\delta}{\lambda_c}(m-1)\frac{q}{Q}B_f\sin\theta_p^{(k)}} \tag{5.8}$$

where $B_f = B/f_c$ is the fractional bandwidth of the signals and $\lambda_c$ is the wavelength of the carrier frequency.

Using top-down approach, we first split the general problem stated in Section 2.4.2 into two classes: uncorrelated signals and correlated signals. The case of uncorrelated signals arises if all the signal sources have one and only one impinging wave at the receiver (i.e. $P_k = 1$ for all $k$). The scenario of correlated signals occurs when the

signal from a source arrives at the receiver through multiple paths. Obviously, the general problem is simply an amalgamation of the two classes.

### 5.1.1 Uncorrelated Signals

For uncorrelated signals, the correlation matrix of the signals in (3.37) is simply a diagonal matrix of the complex gains for each source [16] (assuming unity power for each source):

$$\mathbf{R}_x(q) = \begin{bmatrix} \left|\alpha^{(1)}\right|^2 & 0 & \cdots & 0 \\ 0 & \left|\alpha^{(2)}\right|^2 & \cdots & 0 \\ \vdots & \vdots & \ddots & \vdots \\ 0 & 0 & \cdots & \left|\alpha^{(k)}\right|^2 \end{bmatrix} \tag{5.9}$$

For clarity, the subscripts have been removed from all descriptions of angles, interpath delays and complex gains since each source has only one impinging wave.

The element in the $i^{\text{th}}$ row and $l^{\text{th}}$ column of the noiseless correlation matrix of the $q^{\text{th}}$ frequency bin is given as:

$$[\mathbf{R}_y(q)]_{il} = \sum_{k=1}^{K} \left|\alpha^{(k)}\right|^2 e^{-j2\pi\frac{\delta}{\lambda_c}(i-l)\left(1+\frac{q}{Q}B_f\right)\sin\theta^{(k)}} \tag{5.10}$$

Note that the above noiseless correlation matrix of the received data is a Hermitian matrix, i.e., $\mathbf{R}_y(q) = \mathbf{R}_y^H(q)$. Consequentially, if we are to sum each element in $\mathbf{R}_y(q)$ across $q$, we have:

$$\begin{aligned} \sum_{q=0}^{Q-1}[\mathbf{R}_y(q)]_{il} &= \sum_{q=0}^{Q-1}\sum_{k=1}^{K}\left|\alpha^{(k)}\right|^2 e^{-j2\pi\frac{\delta}{\lambda_c}(i-l)\left(1+\frac{q}{Q}B_f\right)\sin\theta^{(k)}} \\ &= \sum_{k=1}^{K}\left|\alpha^{(k)}\right|^2 e^{-j2\pi\frac{\delta}{\lambda_c}(i-l)\sin\theta^{(k)}}\sum_{q=0}^{Q-1} e^{-j2\pi\frac{\delta}{\lambda_c}(i-l)\frac{q}{Q}B_f\sin\theta^{(k)}} \\ &= \sum_{k=1}^{K}\left|\alpha^{(k)}\right|^2 e^{-j2\pi\frac{\delta}{\lambda_c}(i-l)\sin\theta^{(k)}}\mathrm{GP}_{sum} \end{aligned} \tag{5.11}$$

where $\mathrm{GP}_{sum}$ is the summation of a geometric series given by:

$$\mathrm{GP}_{sum} = F_1\left(i-l,\theta^{(k)}\right)\exp\left\{-j2\pi\frac{\delta}{\lambda_c}\left(i-l\right)\left(\frac{Q-1}{2Q}B_f\right)\sin\theta^{(k)}\right\} \tag{5.12}$$

where

$$F_1\left(i-l,\theta^{(k)}\right) = \frac{\sin\left(\frac{\pi\delta}{\lambda_c}\left(i-l\right)B_f\sin\theta^{(k)}\right)}{\sin\left(\frac{\pi\delta}{Q\lambda_c}\left(i-l\right)B_f\sin\theta^{(k)}\right)} \tag{5.13}$$

To avoid grating lobes, $\delta \leq \lambda_c/2$ and hence $\left(\delta/\lambda_c\right)B_f\sin\theta^{(k)} << 1$. This leads to the following approximation: $F_1\left(i-l,\theta^{(k)}\right) \approx 1$ for $i,l = 1,2,\ldots,M$, thus the element in the $i^{\mathrm{th}}$ row and $l^{\mathrm{th}}$ column simplifies to:

$$\left[\mathbf{R}_y\right]_{il} = \sum_{k=1}^{K}\left|\alpha^{(k)}\right|^2 e^{-j2\pi\frac{\delta}{\lambda_c}(i-l)\left(1+\frac{Q-1}{2Q}B_f\right)\sin\theta^{(k)}} \tag{5.14}$$

The combined correlation matrix $\mathbf{R}_y$ is thus:

$$\mathbf{R}_y = \mathbf{A}\left(\boldsymbol{\theta}\right)\mathbf{R}_x\mathbf{A}^H\left(\boldsymbol{\theta}\right) + \boldsymbol{\Sigma} \tag{5.15}$$

where

$$\mathbf{A}\left(\boldsymbol{\theta}\right) = \left[\begin{array}{cccc}\mathbf{a}\left(\theta^{(1)}\right) & \mathbf{a}\left(\theta^{(2)}\right) & \cdots & \mathbf{a}\left(\theta^{(K)}\right)\end{array}\right] \tag{5.16}$$

with each column of (5.16) given by:

$$\mathbf{a}\left(\theta^{(k)}\right) = \left[\begin{array}{cccc}1 & e^{-j\phi^{(k)}} & \cdots & e^{-j(M-1)\phi^{(k)}}\end{array}\right]^T \tag{5.17}$$

and

$$\phi^{(k)} = 2\pi\frac{\delta}{\lambda_c}\left(1+\frac{Q-1}{2Q}B_f\right)\sin\theta^{(k)} \tag{5.18}$$

The details of the derivation for the structure in (5.15) can be found in Appendix A.

Since (5.15) has an identical structure to that of narrowband signal model, we can apply any of the signal subspace estimation methods developed for narrowband signals, e.g. MUSIC, to estimate the DOAs. Note that the array response matrix given by (5.16) is different from the array response matrix of any of the individual frequency bin. So unlike CSSM [17], we do not convert the signal subspace of different frequency bins into a pre-determined one. Instead, we establish a new signal subspace which can be viewed as the combined frequency signal subspace, hence the name of the proposed method. Once a set of preliminary DOA estimates, $\hat{\boldsymbol{\theta}} = \begin{bmatrix} \hat{\theta}^{(1)} & \hat{\theta}^{(2)} & \dots & \hat{\theta}^{(K)} \end{bmatrix}^T$ is obtained, we can use them to form a weighting matrix $\mathbf{F}$ that can be used to create a refined combined frequency correlation matrix $\tilde{\mathbf{R}}_y$ to estimate the DOAs iteratively:

$$\tilde{\mathbf{R}}_y = \mathbf{F} \odot \mathbf{R}_y \tag{5.19}$$

where $\odot$ is the Hadamard (element-by-element) product of matrices.

For example, if the complex gains are known, the element in the $i^{\text{th}}$ row and $l^{\text{th}}$ column of the weighting matrix $\mathbf{F}$ denoted by $[\mathbf{F}]_{il}$ is given by:

$$[\mathbf{F}]_{il} = \frac{\sum_{k=1}^{K} \left|\alpha^{(k)}\right|^2 e^{j(l-i)\phi^{(k)}}}{\sum_{k=1}^{K} F_1\left(l-i, \theta^{(k)}\right) \left|\alpha^{(k)}\right|^2 e^{j(l-i)\phi^{(k)}}} \tag{5.20}$$

Note that the diagonal elements of $\mathbf{F}$ are always unity as $F_1\left(0, \theta^{(k)}\right) = 1$ for all $\theta^{(k)}$. Since the noise correlation matrix $\boldsymbol{\Sigma}$ is a diagonal matrix for spatially uncorrelated noise, the application of the weighting matrix will not result in noise amplification. Subspace estimation methods can be applied to the new combined correlation matrix $\tilde{\mathbf{R}}_y$ to get the refined DOA estimates. Note that this process can be applied iteratively.

### 5.1.2 Correlated Signals

In the preceding section, we showed that CFSSM can be used for uncorrelated signals. In this section, we show that a similar structure for the combined correlation matrix of received signals exists for correlated signals. For clarity, we consider the case of

a single source with two impinging waves at the receiver after passing through two independent multipaths. Though we only consider two paths, the derived expression is equally valid for three or more paths, and can be easily extended to the general case. As we are considering only a single source, we drop the superscripts of the source index in all descriptions of angles, time delays and complex gains in this section.

For the case of two multipaths, the correlation matrix of the signals in (3.37) becomes:

$$\mathbf{R}_x\left(q\right) = \begin{bmatrix} \left|\alpha_1\right|^2 & \alpha_1\alpha_2^* \\ \alpha_2\alpha_1^* & \left|\alpha_2\right|^2 \end{bmatrix} \tag{5.21}$$

The element in the $i^{\text{th}}$ row and $l^{\text{th}}$ column of the noiseless correlation matrix of the $q^{\text{th}}$ frequency bin is then given as:

$$\begin{aligned} \left[\mathbf{R}_y\left(q\right)\right]_{il} &= \left|\alpha_1\right|^2 e^{-j(i-l)\psi_1(q)} + \left|\alpha_2\right|^2 e^{-j(i-l)\psi_2(q)} \\ &\quad + \alpha_1^*\alpha_2 e^{-j2\pi\left(f_c+\frac{q}{Q}B\right)\Delta\tau} e^{-j2\pi\frac{\delta}{\lambda_c}\left(1+\frac{q}{Q}B_f\right)[(i-1)\sin\theta_2-(l-1)\sin\theta_1]} \\ &\quad + \alpha_1\alpha_2^* e^{j2\pi\left(f_c+\frac{q}{Q}B\right)\Delta\tau} e^{j2\pi\frac{\delta}{\lambda_c}\left(1+\frac{q}{Q}B_f\right)[(l-1)\sin\theta_2-(i-1)\sin\theta_1]} \end{aligned} \tag{5.22}$$

where $\Delta\tau = \tau_2 - \tau_1$ and

$$\psi_p\left(q\right) = 2\pi\frac{\delta}{\lambda_c}\left(1+\frac{q}{Q}B_f\right)\sin\theta_p \tag{5.23}$$

Summing the various correlation matrices together as in (5.11), we get the elements of the combined correlation matrix:

$$\begin{aligned} \left[\mathbf{R}_y\right]_{il} &= \left|\alpha_1\right|^2 F_1\left(i-l,\theta_1\right) e^{-j(i-l)\tilde{\psi}_1} + \left|\alpha_2\right|^2 F_1\left(i-l,\theta_2\right) e^{-j(i-l)\tilde{\psi}_2} \\ &\quad + \alpha_1^*\alpha_2 F_2\left(i,l,\theta_2,\theta_1\right) e^{-j2\pi\left[f_c\Delta\tau+\frac{\delta}{\lambda_c}\varphi_1\right]} e^{-j\pi\left(\frac{Q-1}{Q}\right)\left[B\Delta\tau+\frac{\delta}{\lambda_c}B_f\varphi_1\right]} \\ &\quad + \alpha_2^*\alpha_1 F_2\left(l,i,\theta_2,\theta_1\right) e^{j2\pi\left[f_c\Delta\tau+\frac{\delta}{\lambda_c}\varphi_2\right]} e^{j\pi\left(\frac{Q-1}{Q}\right)\left[B\Delta\tau+\frac{\delta}{\lambda_c}B_f\varphi_2\right]} \end{aligned} \tag{5.24}$$

where $\varphi_1 = (i-1)\sin\theta_2 - (l-1)\sin\theta_1$, $\varphi_2 = (l-1)\sin\theta_2 - (i-1)\sin\theta_1$, and $\tilde{\psi}_p$

is given by the following:

$$\tilde{\psi}_p = 2\pi \frac{\delta}{\lambda_c} \left(1 + \frac{Q-1}{2Q} B_f\right) \sin\theta_p \tag{5.25}$$

$F_1(i-l,\theta)$ is as defined in (5.13), and $F_2(i,l,\theta_{p_1},\theta_{p_2})$ is defined as follows:

$$F_2(i,l,\theta_{p_1},\theta_{p_2}) = \frac{\sin\left[\pi\left\{B\Delta\tau + \frac{\delta}{\lambda_c} B_f\left((i-1)\sin\theta_{p_1} - (l-1)\sin\theta_{p_2}\right)\right\}\right]}{\sin\left[\frac{\pi}{Q}\left\{B\Delta\tau + \frac{\delta}{\lambda_c} B_f\left((i-1)\sin\theta_{p_1} - (l-1)\sin\theta_{p_2}\right)\right\}\right]} \tag{5.26}$$

For multipaths that are well separated in their arrival times at the receiver (i.e. $B\Delta\tau > 1$), $F_2(i,l,\theta_2,\theta_1)$ and $F_2(l,i,\theta_2,\theta_1)$ are approximately zero. Hence the combined correlation matrix reduces to the same structure as that of uncorrelated signals given in (5.15). The details of the derivation for the structure can be found in Appendix A. Narrowband subspace estimation can be carried out using the combined correlation matrix to estimate the DOAs like in the case of uncorrelated signals.

## 5.2 Proposed DOA Estimation Algorithm

From the discussion in Section 5.1, we can now list in details the steps of the algorithm for DOA estimation using CFSSM together with the narrowband signal subspace estimation method, MUSIC:

1. Down-convert the received signal at the array to baseband and sample the baseband signal at the Nyquist rate, $B$ Hz.

2. Divide the total number of sampled data into $N$ snapshots of $Q$ samples each.

3. For each snapshot, convert the sampled time domain data into frequency domain data of $Q$ frequency bins using $Q$-point DFT.

4. For each frequency bin, estimate the correlation matrix $\mathbf{R}_y(q)$ by averaging the

cross-product of $\mathbf{Y}^{(n)}(q)$ of each snapshot, $n = 1, 2, \ldots, N$:

$$\hat{\mathbf{R}}_y(q) = \frac{1}{N}\sum_{n=1}^{N}\mathbf{Y}^{(n)}(q)\left[\mathbf{Y}^{(n)}(q)\right]^H \tag{5.27}$$

where $\mathbf{Y}^{(n)}(q) = \begin{bmatrix} Y_1^{(n)}(q) & Y_2^{(n)}(q) & \cdots & Y_M^{(n)}(q) \end{bmatrix}^T$ with $Y_m^{(n)}(q)$ as defined in (5.4).

5. Form the combined correlation matrix $\hat{\mathbf{R}}_y$ by averaging the different $\hat{\mathbf{R}}_y(q)$ across $q$:

$$\hat{\mathbf{R}}_y = \frac{1}{Q}\sum_{q=0}^{Q-1}\hat{\mathbf{R}}_y(q) \tag{5.28}$$

6. Estimate the combined frequency signal subspace $\hat{\mathbf{E}}_S$ and noise subspace $\hat{\mathbf{E}}_W$ by SVD of the estimated combined correlation matrix $\hat{\mathbf{R}}_y$.

7. Estimate the DOAs $\hat{\theta}_p^{(k)}$ using the MUSIC algorithm which is given by:

$$\hat{\theta}_p^{(k)} = \arg\min_{\theta}\mathbf{a}^H(\theta)\hat{\mathbf{E}}_W\hat{\mathbf{E}}_W^H\mathbf{a}(\theta) \tag{5.29}$$

where

$$\mathbf{a}(\theta) = \begin{bmatrix} 1 & e^{-j2\pi\frac{\delta}{\lambda_c}\left(1+\frac{Q-1}{2Q}B_f\right)\sin\theta} & \cdots & e^{-j2\pi\frac{\delta}{\lambda_c}(M-1)\left(1+\frac{Q-1}{2Q}B_f\right)\sin\theta} \end{bmatrix}^T \tag{5.30}$$

Note that unlike CSSM [17] and WAVES [38], CFSSM does not require any preliminary DOA estimates, and it can actually be used in combination with these methods. In other words, the preliminary estimates can first be obtained using the proposed estimation algorithm, and then these estimates can be used to form the required transformation matrix $\mathbf{T}(q)$ [17, 38].

## 5.3 Computational Complexity

The exact computational complexity of the proposed method is dependent on the actual implementation and is difficult to be determined without the implementation details. Our objective in this section is to provide an estimation of computational complexity in terms of the number of arithmetic operations required [50] to illustrate the comparatively computational simplicity of our proposed algorithm to existing algorithms. We compare the computational complexity of our proposed algorithm with the traditional CSSM [17, 75], WAVES [38] and TOPS [39]. We assume that the Capon's algorithm is used as the initial estimator of the DOAs to construct the required transformation matrix in CSSM and WAVES. Since Steps 1 to 4 of the algorithm are common to all the considered algorithms, we shall disregard their computational complexity in our discussion.

### 5.3.1 CSSM

The computational cost of CSSM can be divided into two parts: pre-processing and actual estimation [39]. We assume that the Capon estimator [95] is used in the pre-processing stage to obtain the initial DOA estimates for a chosen frequency bin. The overhead in forming the Capon estimator [97] includes the inversion of the estimated correlation matrix which requires $O(M^3)$ [50] arithmetic operations. The search process using the Capon estimator requires a computational cost of order $O(M^2)$ for each hypothesized angle.

In the formation of RSS transformation matrix [75], we consider the simplest case where there is only one preliminary angle estimate so as to avoid the use of SVD for each frequency bin. The total computational cost of transforming the signal subspace of each frequency bin to the signal subspace of a pre-determined frequency, resulting from matrix multiplications, is thus $Q$ operations of order $O(M^2)$. The overhead in using the MUSIC algorithm, consisting of two operations (i.e. SVD of correlation matrix and matrix multiplication $\mathbf{E}_W \mathbf{E}_W^H$), is a computational cost of order $O(M^3)$ each while the

search process requires a computational cost of order $O(M^2)$ for each hypothesized angle.

### 5.3.2 WAVES

The pre-processing stage of WAVES is similar to CSSM and thus it has similar computational complexity. However, in the formation of the pseduodata matrix $\mathbf{Z}$ [38], $Q$ additional SVD operations (one for each frequency bin) of the correlation matrix are required. This results in a drastic increase in computational cost since each SVD operation requires $O(M^3)$ arithmetic operations. The computational costs of forming the noise subspace and search process for WAVES are similar to CSSM when both use the MUSIC algorithm.

### 5.3.3 TOPS

The TOPS algorithm does not require an initial estimate of the focusing angles unlike the CSSM and WAVES [39]. However, the computation of each hypothesized angle matrix $\mathbf{D}(\phi)$ requires the knowledge of the signal and noise subspaces at each frequency bin. Hence, the computational cost arising from $Q$ SVD operations cannot be eliminated. Moreover, the search process requires a SVD of $P \times P$ matrix [39] with a computational cost of $O(P^3)$ operations. For large values of $P$, the search process may become much more computational costly than WAVES and CSSM.

### 5.3.4 Proposed CFSSM

The averaging of the correlation matrices of the different frequency bins to form the combined correlation matrix requires only $(M^2+1)$ arithmetic operations. The SVD of $\hat{\mathbf{R}}_y$ requires $12M^3$ operations while the construction of $\mathbf{E}_W\mathbf{E}_W^H$ requires $2(M-P)M^2$ operations [50]. The one-dimensional search process in Step 7 of the proposed algorithm requires $(2M^2+3M)$ operations for each hypothesized angle. Equivalently, we

can regard the overhead computational cost of forming the DOA cost function consisting of an operation with complexity order of $O\left(M^2\right)$ and another two operations with complexity order of $O(M^3)$ each, while the search process requires an operation with $O\left(M^2\right)$ computation cost for each hypothesized angle.

The computational complexity of the existing methods and the proposed CFSSM is summarized in Table 5.1. From our discussions, we can see that the proposed method has the least computational cost, and is much more efficient in terms of computational complexity. The savings in the computational load become crucial when real-time processing is required. In fact, the proposed algorithm has about the same computational cost as that of CSSM and WAVES in the pre-processing stage. Coupled with the fact that CFSSM does not require any preliminary DOAs estimation, the proposed algorithm can be implemented in place of the Capon estimator and be used in tandem with CSSM or WAVES.

| **Algorithm** | **Computational Complexity** | | |
|---|---|---|---|
| | **Stage** | **Description** | **Order** |
| Proposed CFSSM | Estimation of combined correlation matrix | Averaging of correlation matrices from all frequency bins | $O\left(M^2\right)$ |
| | DOA Estimation (by MUSIC) | Formation of noise subspace | $O\left(M^3\right)$ |
| | | Construction of $\mathbf{E}_W\mathbf{E}_W^H$ | $O\left(M^3\right)$ |
| | | Search process for each hypothesized angle | $O\left(M^2\right)$ |
| CSSM | Initial DOA Estimation (by Capon Beamformer) | Inversion of estimated correlation matrix | $O\left(M^3\right)$ |
| | | Search process for each hypothesized angle | $O\left(M^2\right)$ |
| | Focusing (by RSS) | Transformation of each frequency bin to reference frequency | $O\left(M^2\right)$ |
| | DOA Estimation (by MUSIC) | Formation of noise subspace | $O\left(M^3\right)$ |
| | | Construction of $\mathbf{E}_W\mathbf{E}_W^H$ | $O\left(M^3\right)$ |
| | | Search process for each hypothesized angle | $O\left(M^2\right)$ |
| WAVES | Initial DOA Estimation (by Capon Beamformer) | Inversion of estimated correlation matrix | $O\left(M^3\right)$ |
| | | Search process for each hypothesized angle | $O\left(M^2\right)$ |
| | Focusing (by RSS) | Transformation of each frequency bin to reference frequency | $O\left(M^2\right)$ |
| | Signal Subspace (by SVD) | Formation of signal subspace for each frequency bin | $O\left(M^3\right)$ |
| | DOA Estimation (by MUSIC) | Formation of noise subspace | $O\left(M^3\right)$ |
| | | Construction of $\mathbf{E}_W\mathbf{E}_W^H$ | $O\left(M^3\right)$ |
| | | Search process for each hypothesized angle | $O\left(M^2\right)$ |
| TOPS | Focusing (by RSS) | Transformation of each frequency bin to reference frequency | $O\left(M^2\right)$ |
| | DOA Estimation (by MUSIC) | Formation of signal and noise subspaces for each frequency bin | $O\left(M^3\right)$ |
| | | Construction of $\mathbf{E}_W\mathbf{E}_W^H$ | $O\left(M^3\right)$ |
| | | Search Process for each hypothesized angle | $O\left(P^3\right)$ |

Table 5.1: Comparison of computational complexity of wideband algorithms

## 5.4 Detection of the Total Number of Multipaths

In this section, we discuss the problem of determining the total number of signals $P$ impinging at the array using our proposed combined correlation matrix in CFSSM. The value of $P$ is required in MUSIC algorithm for the separation of the signal and noise subspaces [2]. Estimation error in the value of $P$ will therefore result in the wrong estimation of these subspaces. Two popular methods are used for narrowband signal source detection: Akaike information criterion (AIC) and Rissanen minimum description length criterion (MDL) [2, 98, 99].

In [17], a coherent form of AIC, termed minimum Akaike information criterion estimate (MAICE), is derived for wideband signal sources detection using the combined correlation matrix in CSSM. Here, we adapt the algorithm in [17] by using the combined correlation matrix in our proposed CFSSM to determine the value of $P$. First we write the estimated combined frequency correlation matrix $\hat{\mathbf{R}}_y$ as:

$$\hat{\mathbf{R}}_y = \frac{1}{NQ} \sum_{n=1}^{N} \sum_{q=0}^{Q-1} \mathbf{Y}^{(n)}(q) \left[\mathbf{Y}^{(n)}(q)\right]^H \tag{5.31}$$

We denote the eigenvalues of the estimated combined frequency correlation matrix as $\hat{\lambda}_1 \geq \hat{\lambda}_2 \geq \ldots \geq \hat{\lambda}_M$. Following the derivation in [17], the total number of multipaths is estimated as $\hat{P}$ where:

$$\hat{P} = \arg\min_{P} \left\{ NQ(M-P) \log\left(\frac{a_0}{b_0}\right) + P(2M-P) \right\} \tag{5.32}$$

where

$$a_0 = \frac{1}{M-P} \sum_{i=P+1}^{M} \hat{\lambda}_i \tag{5.33}$$

$$b_0 = \left( \prod_{i=P+1}^{M} \hat{\lambda}_i \right)^{\frac{1}{M-P}} \tag{5.34}$$

In Section 5.6.2, we study the performance of the proposed detection in comparison with the coherent AIC detection in [17].

## 5.5 Asymptotic Performance

The asymptotic performance of MUSIC estimator with large number of snapshots has been derived previously in [100, 101] for the narrowband signals. Since the correlation matrix $\mathbf{R}_y$ and hence the estimated correlation matrix $\hat{\mathbf{R}}_y$ approximate to that of the narrowband signal source (with equality when fractional bandwidth is equal to zero), we can approximate the variance of asymptotic estimation error by [101]:

$$E\left[\left(\theta_p^{(k)}-\hat{\theta}_p^{(k)}\right)^2\right]=\frac{1}{2NQ}\frac{\mathbf{a}^H\left(\theta_p^{(k)}\right)\mathbf{L}\mathbf{a}\left(\theta_p^{(k)}\right)}{h\left(\theta_p^{(k)}\right)} \tag{5.35}$$

where

$$\mathbf{L}=\sigma\sum_{i=1}^{P}\frac{\lambda_i}{\left(\sigma-\lambda_i\right)^2}\mathbf{u}_i\mathbf{u}_i^H \tag{5.36}$$

and

$$h\left(\theta_p^{(k)}\right)=\sum_{i=P+1}^{M}\left\|\mathbf{d}^H\left(\theta_p^{(k)}\right)\mathbf{u}_i\right\|^2 \tag{5.37}$$

where $\mathbf{d}^H\left(\theta_p^{(k)}\right)=\frac{\partial}{\partial\theta_p^{(k)}}\mathbf{a}\left(\theta_p^{(k)}\right)$ and $\lambda_i$ and $\mathbf{u}_i$ are the $i^{\text{th}}$ largest eigenvalues and the corresponding eigenvector of $\mathbf{R}_y$.

## 5.6 Simulation Results

In this section, we provide some numerical results where the proposed CFSSM is compared with some existing methods. We consider the operating scenario of a future cellular system with large system bandwidth of $100$ MHz [102, 103]. The signal sources are modeled as zero-mean Gaussian processes with a carrier frequency of $2$ GHz and a bandwidth of $100$ MHz, and are assumed to be uncorrelated. The noise at the array is assumed to be AWGN. The antenna array is assumed to be a ULA of $11$ omni-directional antennas with inter-element spacing $\delta=\frac{1}{2}\lambda_c$ where $\lambda_c$ is the wavelength of

the carrier frequency. The Rayleigh angle resolution limit for the array is approximately $2/(M-1) \simeq 11.46^\circ$ (0.2 radians). Monte Carlo simulation of 2000 independent trials are conducted to obtain the statistical performance.

The received signal is down-converted to baseband and sampled at a frequency of 100 MHz. The total observation time is $T_0 = 20.48$ $\mu$s and are divided into 64 intervals with a duration of $\Delta T = 320$ ns each. Using DFT, the samples in each interval are converted into $Q = 32$ narrowband frequency bins.

### 5.6.1 Resolution of Signals

We consider $K = 2$ uncorrelated signal sources, each having two impinging wavefronts at the receiver (i.e. $P_1 = P_2 = 2$). The magnitudes of the complex gains for all the paths are assumed to be equal and the SNRs are set to 0 dB. For the first source, $\theta_1^{(1)} = 21^\circ$ and $\theta_2^{(1)} = 26^\circ$. The angle separation is $5^\circ$ which is less than half the Rayleigh angle resolution of $11.46^\circ$. The complex gains are set to $\alpha_1^{(1)} = \beta$ and $\alpha_2^{(1)} = \beta e^{j\frac{\pi}{5}}$ respectively, where $\beta$ is a constant such that the SNRs for both paths are equal to 0 dB. The time delays are expressed in terms of the sampling period $T$: $\tau_1^{(1)} = 0T$ and $\tau_2^{(1)} = 4.2T$. For the second source, the angle separation between the two arrival paths is set to $5^\circ$ with $\theta_1^{(2)} = 46^\circ$ and $\theta_2^{(2)} = 51^\circ$. The complex gains are set to $\alpha_1^{(2)} = \beta e^{-j\frac{\pi}{4}}$ and $\alpha_2^{(2)} = \beta e^{j\frac{\pi}{3}}$ while the time delays are $\tau_1^{(2)} = 0.1T$ and $\tau_2^{(2)} = 6T$.

For comparison, the spatial spectrums of the three different methods – the proposed CFSSM method, Wang and Kaveh's CSSM method [17] and the IMUSIC method [15] – are plotted in Figure 5.1, Figure 5.2 and Figure 5.3 respectively. In each method, the true number of signals $P = 4$ is used for processing. In each figure, the results from ten independents trials are plotted together. For ease of reference, the true DOAs are indicated by the vertical lines in the figures.

From Figure 5.1 and Figure 5.2, we see that our proposed CFSSM and CSSM estimation methods are able to resolve the different arrival paths from each source. The IMUSIC algorithm, however, is unable to resolve the different arrival paths from each

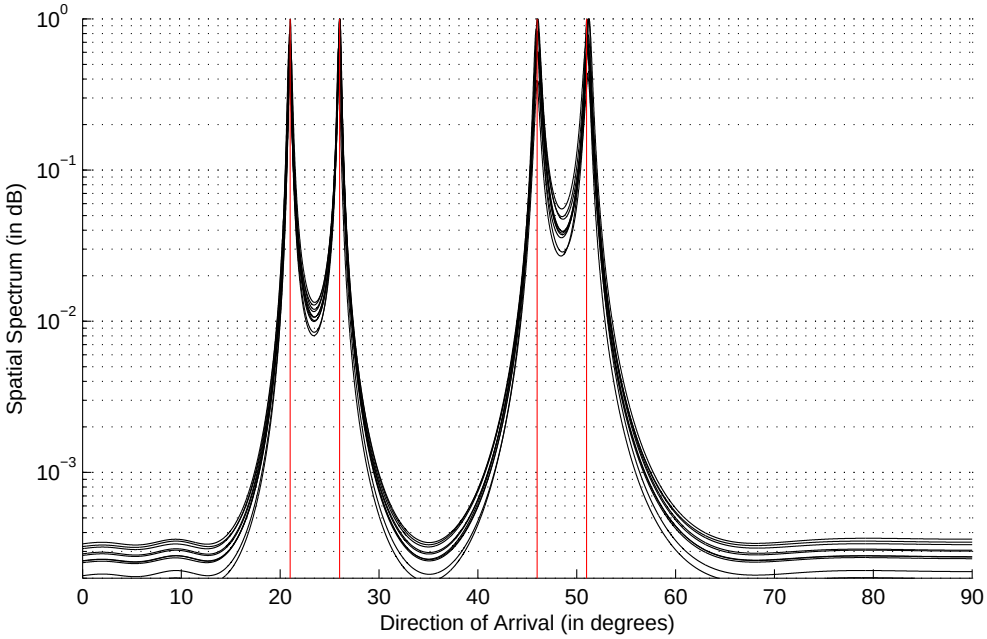


Figure 5.1: Spatial periodogram for two signal sources using CFSSM

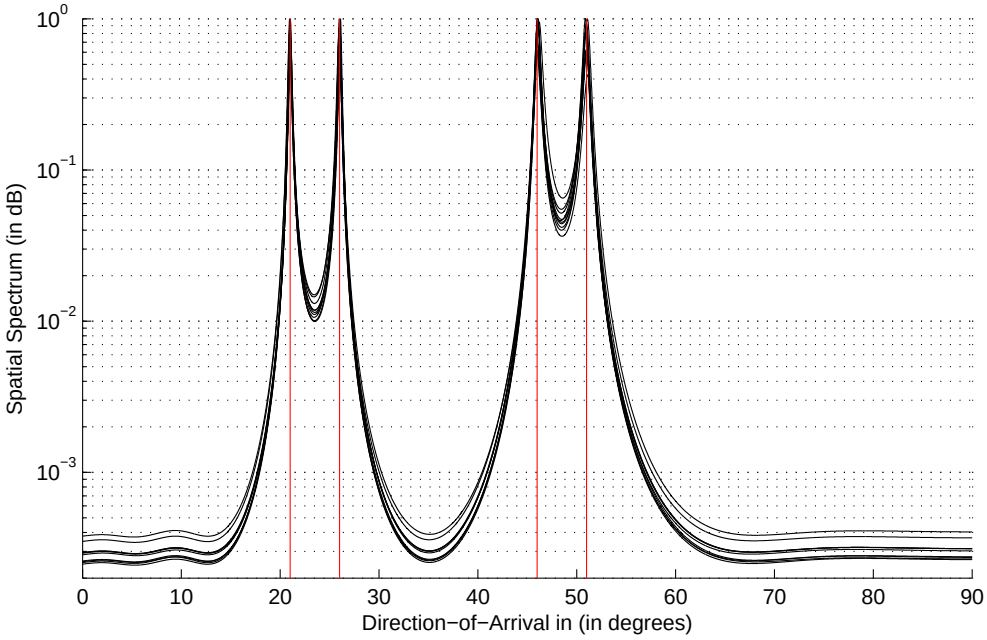


Figure 5.2: Spatial periodogram for two signal sources using CSSM

source despite knowing the true number of impinging wavefronts. Hence, we can conclude that both CFSSM and CSSM estimation methods, which are coherent methods, are superior to IMUSIC in terms of resolving correlated signals at the receiver.

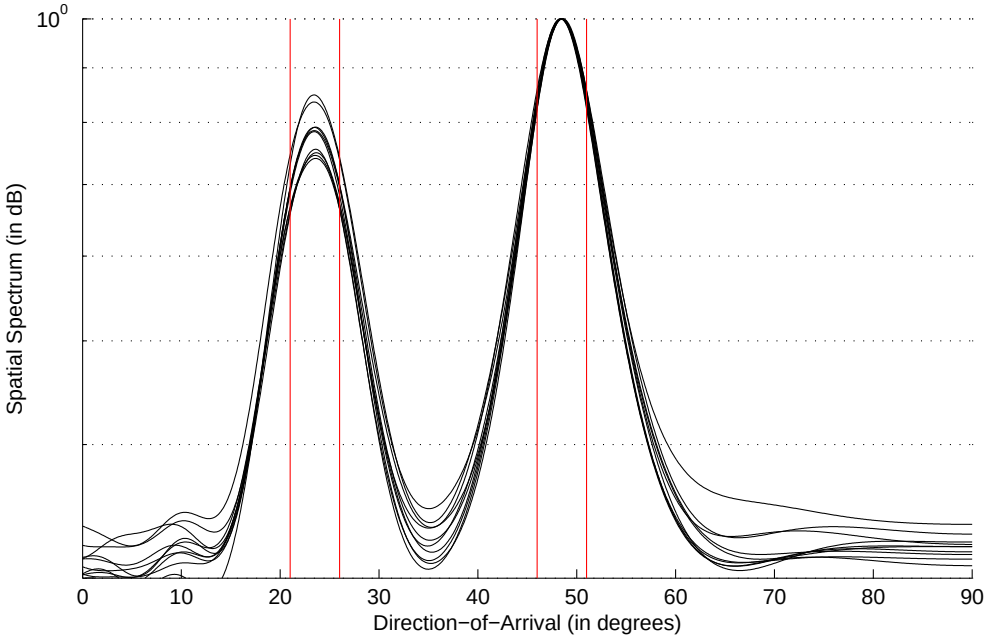


Figure 5.3: Spatial periodogram for two signal sources using IMUSIC

### 5.6.2 Detection Performance of Signals

In this section, we compare the statistical performance of the proposed detection algorithm described in Section 5.4 with the coherent AIC and incoherent AIC from [17,98]. First, we compare the detection performance for two uncorrelated signal sources each having a single path at the receiver. Both sources are assumed to have equal received power and the angle separation between the two sources is set to $7^\circ$.

In Figure 5.4, the detection performance against SNR for each method is plotted for comparison. The proposed detection algorithm and the coherent AIC [17] have similar performance, which are much better than that of incoherent AIC in low SNR conditions. For $100\%$ correct detection, the SNR threshold of our proposed detection algorithm and coherent AIC is $-13$ dB, while the SNR threshold of incoherent AIC is $-7$ dB, which is much higher than the former. In incoherent AIC, the detection is carried out at each frequency bin as compared to coherent AIC where the detection is carried out for the coherent signal subspace of all frequency bins. As such, a single outlier in one of the frequency bins can degrade the detection performance greatly in low SNRs.

Next, the detection performance of the proposed algorithm and coherent AIC for two correlated received signals (arising from two received signal paths from a single

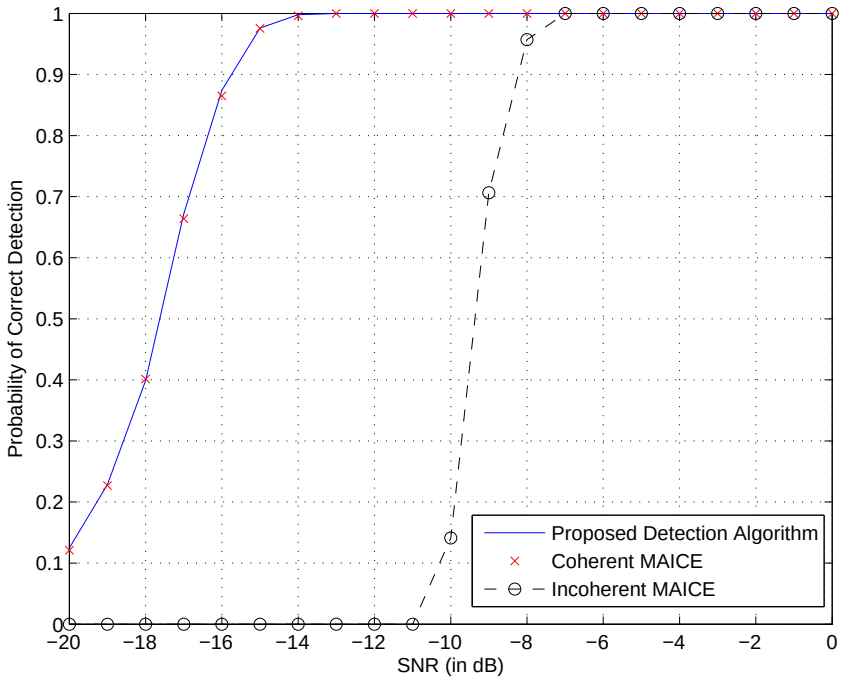


Figure 5.4: Detection performance against SNR for uncorrelated signals

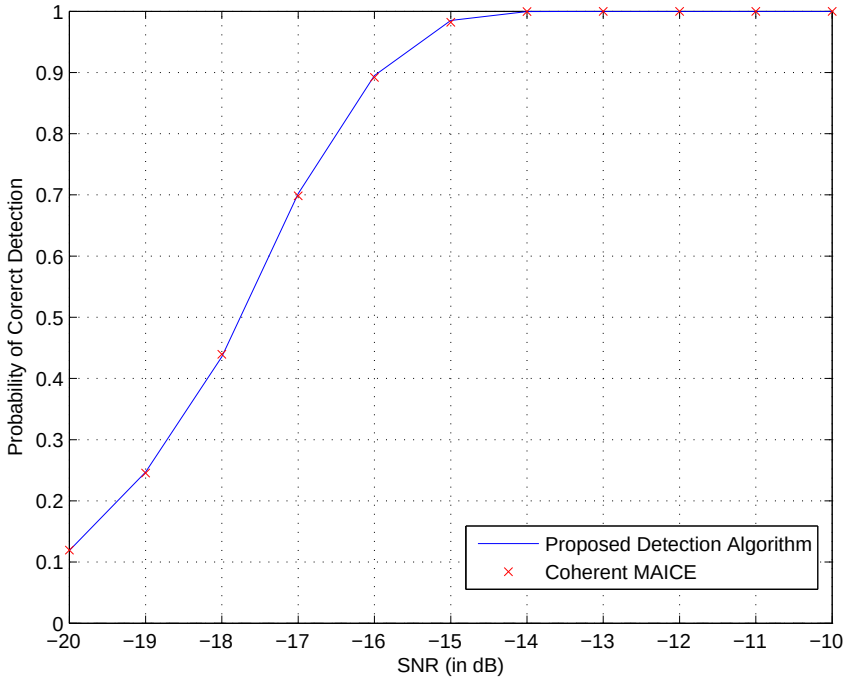


Figure 5.5: Detection performance against SNR for correlated signals

source) are compared. The signals from the two paths are assumed to arrive at the receiver with a relative delay of $4.2T$ and the angle separation for these correlated signals

is kept at $7^{\circ}$. The received power for each path is assumed to be equal as in the case for uncorrelated sources.

In Figure 5.5, the detection performance of the proposed detection algorithm and the coherent AIC for different SNRs are plotted for comparison. Once again the performances of the two schemes are identical, and have similar SNR thresholds. Note that the incoherent AIC cannot make the correct detection of the number of signals regardless of the SNR because of its inability to resolve correlated signals. As such, we omit the performance of incoherent AIC in Figure 5.5. Our proposed detection algorithm is better than that of coherent AIC as it does not require initial DOA estimates and has a lower computational complexity in the formation of the combined correlation matrix.

### 5.6.3 Performance of the DOA Estimators

The statistical estimation performance of our proposed method, in terms of estimation error deviation and estimation bias, is studied through Monte Carlo simulation in this section. The performances of coherent estimation methods like the CSSM [17], WAVES [38], TOPS [39], as well as the IMUSIC are also simulated for comparison. Monte Carlo simulation of $2000$ independent trials are conducted to obtain the statistical performance.

#### 5.6.3.1 Uncorrelated Signals

We investigate the estimation performance for two uncorrelated received signals using the various estimation methods. Two equal-power uncorrelated signal sources whose DOAs are randomly generated with a fixed angle separation of $7^{\circ}$ are simulated with the following parameters: $\alpha_1^{(1)} = \beta e^{j\frac{\pi}{5}}$, $\alpha_1^{(2)} = \beta e^{j\frac{\pi}{3}}$ and $\tau_1^{(1)} = \tau_1^{(2)} = 0T$. Note that the complex gains for the two sources have equivalent power so the received SNRs for both sources are the same. For CSSM and WAVES, the initial DOAs are estimated using the Capon's estimator which only provides a single DOA estimate, and the RSS focusing matrix [75] is chosen as the focusing matrix.

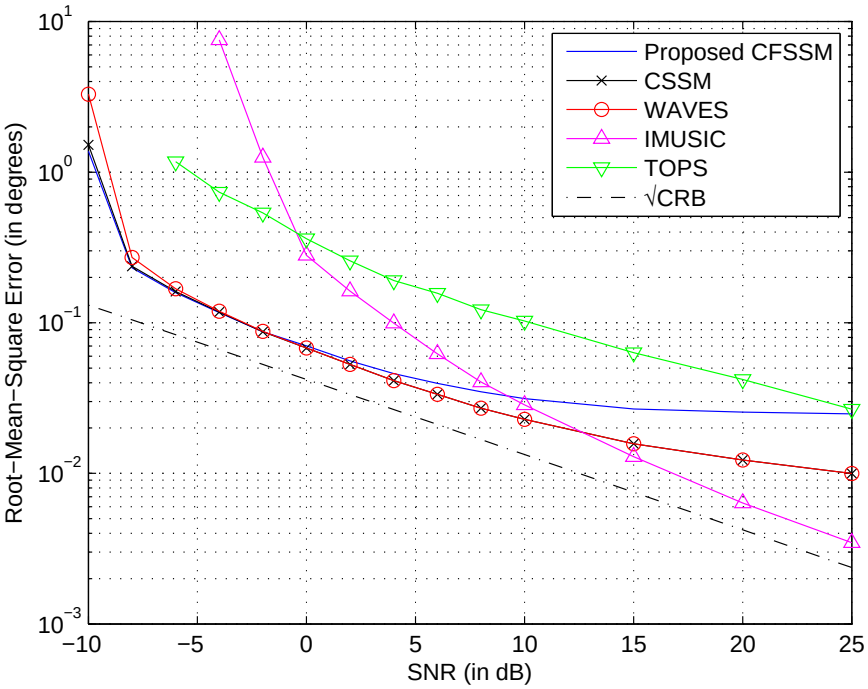


Figure 5.6: RMSE performance against SNR for uncorrelated signals

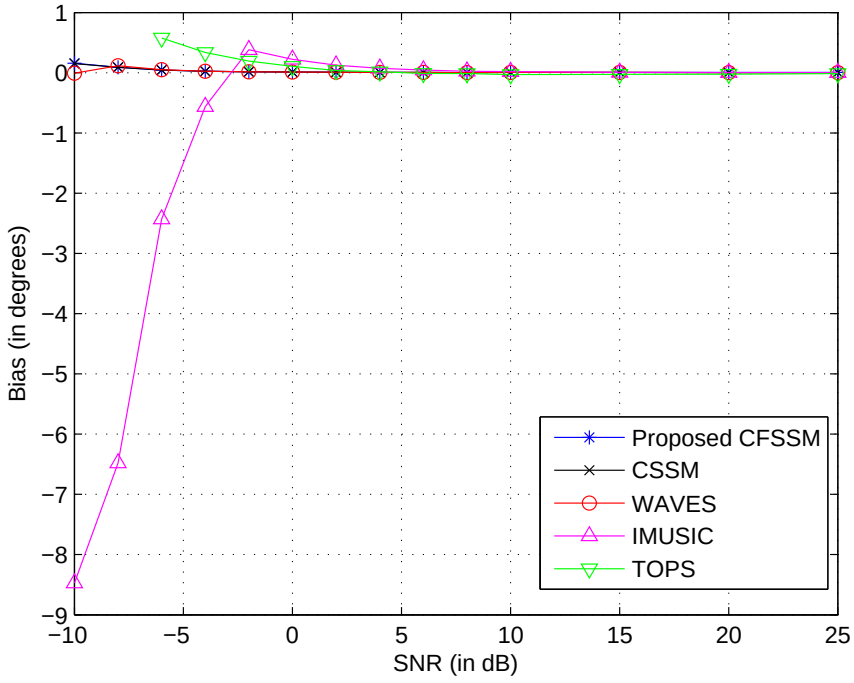


Figure 5.7: Bias performance against SNR for uncorrelated signals

In Figure 5.6, the RMSE performance for CFSSM, CSSM, WAVES, TOPS and IMUSIC is plotted against SNR. Here, the RMSE is averaged over the two multipaths.

The CRLB as calculated in [17] is also included for reference. In the low SNRs, the performances of proposed CFSSM, CSSM and WAVES are similar, and are significantly better than that of IMUSIC. The RMSE of the proposed CFSSM estimation method is also very near to the CRLB in the low SNRs. In high SNR region, IMUSIC performs better due to the bias in all the coherent methods [39, 96]. Note that the IMUSIC cannot resolve the two signals below the SNR detection threshold of $-7$ dB. Therefore the performance of IMUSIC below $-7$ dB (as seen from Figure 5.4) is not included in Figure 5.6 due to unreliable estimates.

In Figure 5.7, the bias performances for the different estimation methods are provided where the estimates from the different trials are averaged. Note that CFSSM, CSSM and WAVES exhibit an estimation bias even at high SNRs while the estimates from TOPS and IMUSIC tend to converge to the true DOAs with increasing SNR as reported in [39].

The proposed method is the best performing estimator which does not require initial DOA estimates (similar to IMUSIC and TOPS) in low SNR region. Either in terms of estimation variance or estimation bias, the performance of the proposed CFSSM estimation algorithm is comparable to existing coherent estimation methods such as CSSM and WAVES but is computationally less expensive. Moreover, the CFSSM estimation variance performance is close to the CRLB in low SNR region.

#### 5.6.3.2 Correlated Signals

We next investigate the estimation performance for two correlated received signals for each of the various estimation methods. We consider the case where two signals from the same source arrive at the receiver through two different paths with the following parameters: $\alpha_1^{(1)} = \beta e^{j\frac{\pi}{5}}$, $\alpha_2^{(1)} = \beta e^{j\frac{\pi}{4}}$ and $\tau_1^{(1)} = 0T$, $\tau_2^{(1)} = 6.2T$. Their DOAs are randomly generated with a fixed angle separation of $7^\circ$. Note that the complex gains for the two paths have equivalent power so the received SNRs for both paths are the same. As in the case for uncorrelated signals in Section 5.6.3.1, the initial DOA estimates for CSSM and WAVES are estimated by the Capon estimator which only provides a single

DOA estimate, and the RSS focusing matrix [75] is chosen as the focusing matrix.

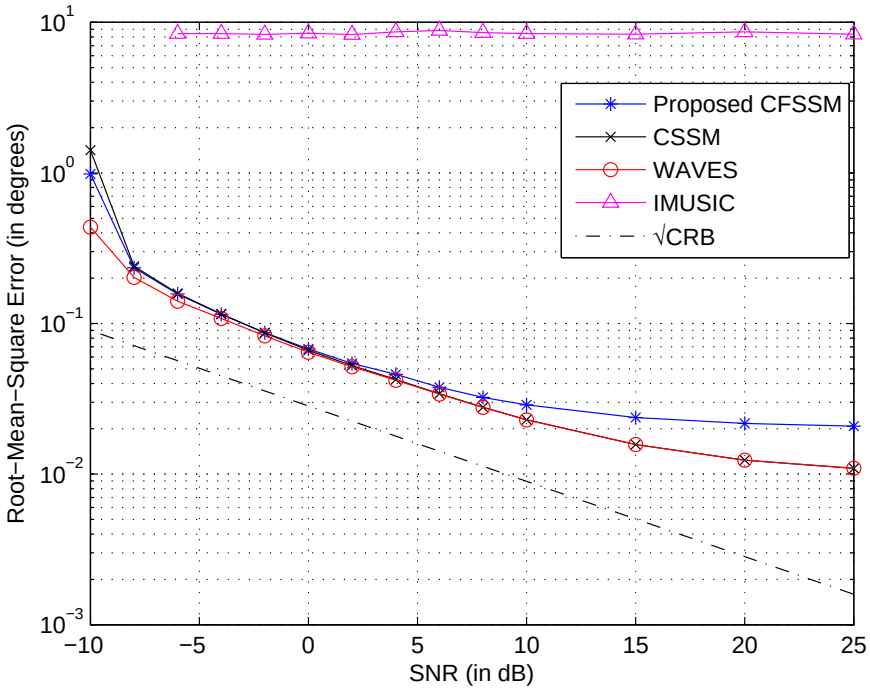


Figure 5.8: RMSE performance against SNR for correlated signals

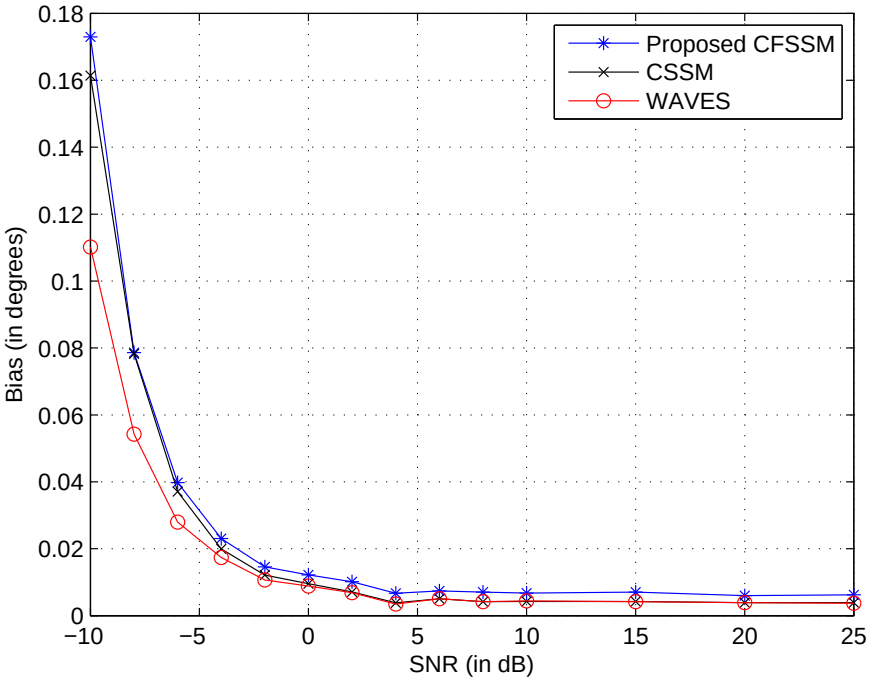


Figure 5.9: Bias performance against SNR for correlated signals

In Figure 5.8, the RMSE performance for CFSSM, CSSM, WAVES and IMUSIC

are plotted against SNR. Both TOPS and IMUSIC are not able to resolve correlated signals [17, 39]. The performance of IMUSIC is included for illustration only, demonstrating the incapability of incoherent methods to handle correlated signals. IMUSIC is only able to obtain a single DOA estimate instead of the required two estimates. The single estimates are always around the average of the two true DOAs, hence resulting in a constant estimation error as reflected in Figure 5.8. The performances of the remaining three coherent methods, namely the proposed CFSSM, CSSM and WAVES, are similar to that of uncorrelated signals. These three algorithms are able to resolve the correlated signals effectively due to the coherent combining of data from all frequency bins. In the low SNR region, the proposed CFSSM, CSSM and WAVES have similar performances and are very near to the CRLB. In the high SNR region, the error floor appears again for all three methods due to the bias, clearly illustrated in Figure 5.9.

## 5.7 Conclusion

We introduced a new, computationally attractive, coherent DOA estimation method for wideband sources, that does not require initial DOA estimates for focusing unlike conventional methods. The proposed method, termed CFSSM, has significantly lower computational requirements than existing estimation methods and can be used for both uncorrelated and correlated signals. We also demonstrated through simulation that the coherent detection performance using the combined correlation matrix in the proposed CFSSM is comparable to existing coherent AIC using the combined correlation matrix in CSSM. Moreover, as no initial DOA estimates are required for CFSSM, it can be used in tandem with some of the existing methods like CSSM and WAVES, replacing the initial low-resolution estimation process like the Capon estimator. The savings in computational load using the proposed method would make the necessary real-time estimation, in applications such as cellular mobile systems, more efficient.

# Chapter 6

# M-CFSSM: New Wideband DOA Estimator for Known Signals

In Chapter 5, we discussed the DOA estimation of wideband signals without a priori knowledge of the transmitted signals. Though this assumption makes the proposed CFSSM less restrictive in its application, it requires a significant number of snapshots so as to ensure the sample correlation matrix converges to the true correlation matrix [38]. Given short allocated estimation time, its detection and estimation performance may degrade significantly especially in low SNR region. In this chapter, we introduce an estimation algorithm that makes use of the knowledge of transmitted signals at the receiver to lower the requirement on the number of available snapshots. Transmission of short bursts of pre-determined preambles is a popular approach in cellular communications among other wireless systems [22]. Here, we consider the use of such known transmitted preambles for DOA estimation of wideband signals, as opposed to narrowband signals considered in [11,13]. The proposed algorithm, modified from the CFSSM introduced in Chapter 5, is termed modified CFSSM (M-CFSSM). We first formulate the estimation method and then use numerical results to illustrate the detection and estimation capabilities of the proposed method for a system with a small number of preambles.

## 6.1 Modified CFSSM

In this section, we modify the CFSSM algorithm in Chapter 5 to the case where the transmitted signals are known at the receiver. Note that the receiver only has the knowledge of transmitted signals, but not other parameters that characterize each signal path from each source. In other words, given the general expression in Section 2.4.2 for the received signal at the $m^{\text{th}}$ antenna with $K$ independent wideband sources:

$$y_m(t) = \sum_{k=1}^{K}\sum_{p=1}^{P_k} \alpha_p^{(k)} x^{(k)}\left(t - \tau_p^{(k)} - \kappa_{p,m}^{(k)}\right) + w_m(t) \tag{6.1}$$

the receiver only has the knowledge of transmitted signals $x^{(k)}(t)$ from the $k^{\text{th}}$ source, while the interpath delay $\tau_p^{(k)}$ and the complex gain $\alpha_p^{(k)}$ are unknown parameters at the receiver.

Recall from Section 5.1 that the received signal is down-converted to baseband and sampled at the Nyquist rate, producing $N$ intervals of $Q$ samples each. In each interval, a $Q$-point DFT is applied to the samples to obtain $Q$ frequency bins. We recall the $Q$-point DFT output at the $m^{\text{th}}$ antenna for $q = 0, 1, \ldots, Q-1$ from (5.4) is given by:

$$Y_m(q) = \sum_{k=1}^{K}\sum_{p=1}^{P_k} \alpha_p^{(k)} \tilde{X}^{(k)}(q)\, e^{-j2\pi\left(f_c + \frac{q}{Q}B\right)\tilde{\tau}_{p,m}^{(k)}} + W_m(q) \tag{6.2}$$

where $P_k$ is the total number of impinging plane waves at the receiver from the $k^{\text{th}}$ signal source, $W_m(q)$ is the additive white noise and $\tilde{\tau}_{p,m}^{(k)} = \tau_p^{(k)} + \kappa_{p,m}^{(k)}$. For a ULA with inter-element spacing $\delta$, the signal in each frequency bin can be written in the conventional matrix form:

$$\mathbf{Y}(q) = \mathbf{A}(q, \boldsymbol{\theta})\boldsymbol{\Lambda}\mathbf{X}(q) + \mathbf{W}(q) \tag{6.3}$$

where

$$\mathbf{Y}(q) = \left[ \begin{array}{cccc} Y_1(q) & Y_2(q) & \cdots & Y_M(q) \end{array} \right]^T \tag{6.4}$$

$$\mathbf{W}(q) = \left[ \begin{array}{cccc} W_1(q) & W_2(q) & \cdots & W_M(q) \end{array} \right]^T \tag{6.5}$$

$$\mathbf{X}(q) = \left[ \begin{array}{cccccccc} \tilde{X}^{(1)}(q) & \cdots & \tilde{X}^{(1)}(q) & \cdots & \tilde{X}^{(k)}(q) & \cdots & & \\ & & & & \cdots & \tilde{X}^{(K)}(q) & \cdots & \tilde{X}^{(K)}(q) \end{array} \right]^T \tag{6.6}$$

$$\mathbf{\Lambda} = \operatorname{diag}\left\{ \begin{array}{ccccccccc} \alpha_1^{(1)}, & \cdots & \alpha_{P_1}^{(1)}, & \cdots & \alpha_p^{(k)}, & \cdots & \alpha_1^{(K)}, & \cdots & \alpha_{P_K}^{(K)} \end{array} \right\} \tag{6.7}$$

$$\boldsymbol{\theta} = \left[ \begin{array}{cccccccc} \theta_1^{(1)} & \cdots & \theta_{P_1}^{(1)} & \cdots & \theta_p^{(k)} & \cdots & \theta_1^{(K)} & \cdots & \theta_{P_K}^{(K)} \end{array} \right]^T \tag{6.8}$$

$\mathbf{Y}(q)$ is the $M \times 1$ noisy received signal at the array, whereas $\mathbf{W}(q)$ is the $M \times 1$ additive white noise at the array. $\mathbf{X}(q)$ is the $P \times 1$ vector comprising of the repetitions of the $K$ signal sources according to the number of arrival paths for each source (i.e. $P_k$ repetitions for the $k^{\text{th}}$ source). $\mathbf{\Lambda}$ is the $P \times P$ diagonal matrix of the complex gains with entries equal to $\alpha_p^{(k)}$. $\boldsymbol{\theta}$ is the $P \times 1$ vector containing the DOAs of all impinging plane waves and the $M \times P$ frequency-dependent array response matrix $\mathbf{A}(q, \boldsymbol{\theta})$ is defined as:

$$\mathbf{A}(q, \boldsymbol{\theta}) = \left[ \begin{array}{cccccccc} \mathbf{a}\left(q, \theta_1^{(1)}\right) & \cdots & \mathbf{a}\left(q, \theta_{P_1}^{(1)}\right) & \cdots & \mathbf{a}\left(q, \theta_p^{(k)}\right) & \cdots & & \\ & & & & \cdots & \mathbf{a}\left(q, \theta_1^{(K)}\right) & \cdots & \mathbf{a}\left(q, \theta_{P_K}^{(K)}\right) \end{array} \right] \tag{6.9}$$

where

$$\mathbf{a}\left(q, \theta_p^{(k)}\right) = \left[ \begin{array}{cccc} e^{-j2\pi\left(f_c + \frac{q}{Q}B\right)\left(\tau_p^{(k)}\right)} & e^{-j2\pi\left(f_c + \frac{q}{Q}B\right)\left(\tau_p^{(k)} + \frac{\delta}{c}\sin\theta_p^{(k)}\right)} & \cdots & \\ & & \cdots & e^{-j2\pi\left(f_c + \frac{q}{Q}B\right)\left(\tau_p^{(k)} + \frac{(M-1)\delta}{c}\sin\theta_p^{(k)}\right)} \end{array} \right]^T \tag{6.10}$$

From this point onwards, we denote the received signal at different snapshots with a subscript $n$ for $n = 1, 2, \ldots, N$. Hence the received signal at the $n^{\text{th}}$ snapshot is given

by:

$$\mathbf{Y}_n(q) = \mathbf{A}(q, \boldsymbol{\theta}) \boldsymbol{\Lambda} \mathbf{X}_n(q) + \mathbf{W}_n(q) \tag{6.11}$$

Since we are transmitting deterministic known signals at the different sources, we can ensure that the signals from different sources are designed such that they are uncorrelated within the DOA estimation period. In other words, we want to design the preambles from the different sources ideally such that:

$$\frac{1}{N} \sum_{n=1}^{N} X_n^{(k_1)}(q) \left[X_n^{(k_2)}(q)\right]^* = \begin{cases} 1, & k_1 = k_2 \\ 0, & k_1 \neq k_2 \end{cases} \tag{6.12}$$

for all $q$. Other than using preambles, the receiver can acquire knowledge of the transmitted signals through receiver estimation. The receiver estimates the transmitted signals and then uses these estimated signals for DOA estimation as in decision-directed estimation [104]. Obviously for this case, the requirement in (6.12) will not be easily fulfilled if $N$ is small given that the transmitted signals from different sources are independent. In this scenario, the only requirement is that the transmitted signals from different sources are uncorrelated and for sufficiently large $N$, the following is satisfied:

$$\frac{1}{N} \sum_{n=1}^{N} X_n^{(k_1)}(q) \left[X_n^{(k_2)}(q)\right]^* \rightarrow \mathrm{E}\left\{X^{(k_1)}(q) \left[X^{(k_2)}(q)\right]^*\right\} = \begin{cases} 1, & k_1 = k_2 \\ 0, & k_1 \neq k_2 \end{cases} \tag{6.13}$$

However, since we are concerned with DOA estimation using small $N$, we assume that the transmitted signals satisfy (6.12) during the estimation period. We can form $K$ different data sets, one for each signal source, by correlating the received signals with each of the known transmitted signals. Each data set consists of $Q$ vectors denoted by

$\mathbf{Z}^{(k)}(q)$ for $q = 0, 1, \ldots, Q-1$, where $\mathbf{Z}^{(k)}(q)$ is defined as follows:

$$\begin{aligned}
\mathbf{Z}^{(k)}(q) &= \frac{1}{N}\begin{bmatrix} \mathbf{Y}_1(q) & \mathbf{Y}_2(q) & \cdots & \mathbf{Y}_N(q) \end{bmatrix}\begin{bmatrix} X_1^{(k)}(q) \\ X_2^{(k)}(q) \\ \vdots \\ X_N^{(k)}(q) \end{bmatrix}^* \\
&= \mathbf{A}\left(q, \boldsymbol{\theta}^{(k)}\right)\boldsymbol{\Lambda}^{(k)}\mathbf{1}_{P_k} + \mathbf{W}^{(k)}(q) \qquad (6.14)
\end{aligned}$$

where

$$\mathbf{A}\left(q, \boldsymbol{\theta}^{(k)}\right) = \begin{bmatrix} \mathbf{a}\left(q, \theta_1^{(k)}\right) & \mathbf{a}\left(q, \theta_2^{(k)}\right) & \cdots & \mathbf{a}\left(q, \theta_{P_k}^{(k)}\right) \end{bmatrix} \qquad (6.15)$$

$$\boldsymbol{\theta}^{(k)} = \begin{bmatrix} \theta_1^{(k)} & \theta_2^{(k)} & \cdots & \theta_{P_k}^{(k)} \end{bmatrix}^T \qquad (6.16)$$

$$\boldsymbol{\Lambda} = \operatorname{diag}\left\{ \begin{array}{cccc} \alpha_1^{(k)} & \alpha_2^{(k)} & \cdots & \alpha_{P_k}^{(k)} \end{array} \right\} \qquad (6.17)$$

$\mathbf{A}\left(q, \boldsymbol{\theta}^{(k)}\right)$ is the reduced size matrix consisting of the columns of $\mathbf{A}(q, \boldsymbol{\theta})$ with DOAs belonging to the $k^{\text{th}}$ source only, $\boldsymbol{\Lambda}^{(k)}$ is the $P_k \times P_k$ diagonal matrix of the complex gains of the $k^{\text{th}}$ source, $\boldsymbol{\theta}^{(k)}$ is the $P_k \times 1$ vector containing the DOAs of the $k^{\text{th}}$ source, $\mathbf{1}_{P_k}$ is a $P_k \times 1$ vector whose entries are all ones, and $\mathbf{W}^{(k)}(q)$ is the $M \times 1$ additive white noise at the array.

Hence, instead of estimating the DOAs of all the different sources simultaneously, we can estimate the DOAs of the individual sources separately by using $\mathbf{Z}_k(q)$ as defined in (6.14). For clarity, we drop the source index in the rest of the derivations since the DOA estimation is carried out for each source individually.

Like in CFSSM, we seek to combine the various frequency bins together to form a single combined frequency signal subspace. However, unlike the case of CFSSM, we do not combine the correlation matrix of each frequency bin. Instead, we first try to separate signals that arrive through different multipaths which are well-separated in

their arrival times (i.e. $B(\tau_{p_1} - \tau_{p_2}) > 1$). Define the following vector $\mathbf{H}(i)$ as follows:

$$\mathbf{H}(i) = \sum_{q=0}^{Q-1} \mathbf{Z}(q) e^{j2\pi \frac{iq}{Q}} \tag{6.18}$$

for $i = 0, 1, \ldots, Q-1$. The $m^{\text{th}}$ element in the noiseless vector $\mathbf{H}$ is thus:

$$\begin{aligned}
[\mathbf{H}(i)]_m &= \sum_{q=0}^{Q-1} \sum_{p=1}^{P} \alpha_p e^{-j2\pi\left(f_c + \frac{q}{Q}B\right)\left(\tau_p + \frac{(m-1)\delta}{c}\sin\theta_p\right)} e^{j2\pi\frac{iq}{Q}} \\
&= \sum_{p=1}^{P} \alpha_p e^{-j2\pi f_c\left(\tau_p + \frac{(m-1)\delta}{c} sin\theta_p\right)} \sum_{q=0}^{Q-1} e^{-j2\pi\frac{q}{Q}\left(B\tau_p - i + \frac{(m-1)\delta}{\lambda_c} B_f \sin\theta_p\right)} \\
&= \sum_{p=1}^{P} \alpha_p e^{-j\phi_p(i,m)} F(i,m,p)
\end{aligned} \tag{6.19}$$

where

$$\phi_p(i,m) = \pi\left\{2f_c\tau_p + \frac{Q-1}{Q}(B\tau_p - i) + 2(m-1)\frac{\delta}{\lambda_c}\left(1 + \frac{Q-1}{2Q}B_f\right)\sin\theta_p\right\} \tag{6.20}$$

and

$$F(i,m,p) = \frac{\sin\left[\pi\left(B\tau_p + \frac{\delta}{\lambda_c}(m-1)B_f\sin\theta_p - i\right)\right]}{\sin\left[\frac{\pi}{Q}\left(B\tau_p + \frac{\delta}{\lambda_c}(m-1)B_f\sin\theta_p - i\right)\right]} \tag{6.21}$$

The details in the simplification process from the second equality to the third equality in (6.19) can be found in Appendix B. Observe that when $B\tau_p \approx i$, $|F(i,m,p)| \approx 1$ and when $|B\tau_p - i| \geq 1$, $|F(i,m,p)| \approx 0$. Hence we can use the various $\mathbf{H}(i)$ to estimate the different DOAs individually. First, we have to determine which of the different vectors $\mathbf{H}(i)$, $i = 0, 1, \ldots, Q-1$, should be used for DOA estimation.

A possible way to determine the number of arrival paths (i.e. the number of impinging plane waves with significant powers) and the corresponding vectors to use for the DOA estimation is to search for peaks of $|\mathbf{H}(i)|^2$ across $i = 0, 1, \ldots, Q-1$ which are greater than a threshold, $\zeta$. If $|\mathbf{H}(i)|^2 \geq \zeta$, DOA estimation can be performed using

this particular vector; if $|\mathbf{H}(i)|^2 < \zeta$, no DOA estimation is carried out. For $P << Q$, a possible candidate for $\zeta$ is the arithmetic mean of $|\mathbf{H}(i)|^2$, $i = 0, 1, \ldots, Q-1$:

$$\zeta = \frac{1}{Q} \sum_{i=0}^{Q-1} |\mathbf{H}(i)|^2 \tag{6.22}$$

Without loss of generality, we assume that a peak is detected at $i = 0$ (i.e. $|\mathbf{H}(0)|^2 \geq \zeta$). We now discuss the estimation of $\theta_1$ using $\mathbf{H}(0)$ as an illustration of the DOA estimation algorithm. From (6.19), we can rewrite the vector noiseless $\mathbf{H}(0)$ as:

$$\mathbf{H}(0) = \tilde{\mathbf{A}}_{H(0)} \begin{bmatrix} \alpha_1 \\ \alpha_2 \\ \vdots \\ \alpha_P \end{bmatrix} \tag{6.23}$$

where the array response matrix $\tilde{\mathbf{A}}_{H(0)}$ is given by:

$$\tilde{\mathbf{A}}_{H(0)} = \begin{bmatrix} \left[\mathbf{a}_{H(0)}(\theta_1) e^{-j\pi\left[2f_c\tau_1 + \frac{Q-1}{Q}(B\tau_1)\right]}\right]^T \\ \left[\mathbf{a}_{H(0)}(\theta_2) e^{-j\pi\left[2f_c\tau_2 + \frac{Q-1}{Q}(B\tau_2)\right]}\right]^T \\ \vdots \\ \left[\mathbf{a}_{H(0)}(\theta_P) e^{-j\pi\left[2f_c\tau_P + \frac{Q-1}{Q}(B\tau_P)\right]}\right]^T \end{bmatrix}^T \tag{6.24}$$

with the steering vectors given by:

$$\mathbf{a}_{H(0)}(\theta_p) = \begin{bmatrix} F(0,1,p) e^{-j\tilde{\phi}_p(1)} \\ F(0,2,p) e^{-j\tilde{\phi}_p(2)} \\ \vdots \\ F(0,M,p) e^{-j\tilde{\phi}_p(M)} \end{bmatrix} \tag{6.25}$$

and $\tilde{\phi}_p(m)$ is a variation of $\phi_p(i,m)$ in (6.20) without the portion which is independent of $m$ (it will be canceled out during the correlation process at a later stage). More

formally:

$$\tilde{\phi}_p(m) = 2\pi \frac{\delta}{\lambda_c}(m-1)\left(1 + \frac{Q-1}{2Q}B_f\right)\sin\theta_p \tag{6.26}$$

We denote the correlation matrix of $\mathbf{H}(0)$ as $\mathbf{R}_H(0)$ where:

$$\begin{aligned}\mathbf{R}_H(0) &= \mathrm{E}\left[\mathbf{H}(0)\,\mathbf{H}^H(0)\right] \\ &= \mathbf{A}_{H(0)}\begin{bmatrix} |\alpha_1|^2 & \cdots & \alpha_1\alpha_p^* & \cdots & \alpha_1\alpha_P^* \\ \vdots & \ddots & \vdots & \ddots & \vdots \\ \alpha_p\alpha_1^* & \ldots & |\alpha_p|^2 & \cdots & \alpha_p\alpha_P^* \\ \vdots & \ddots & \vdots & \ddots & \vdots \\ \alpha_P\alpha_1^* & \cdots & \alpha_P\alpha_p^* & \cdots & |\alpha_P|^2 \end{bmatrix}\mathbf{A}_{H(0)}^H + \sigma^2\boldsymbol{I}\end{aligned} \tag{6.27}$$

where $\sigma^2$ is the noise variance and $\mathbf{A}_{H(0)}$ is the simplified form of the array response matrix in (6.24) and is given by:

$$\mathbf{A}_{H(0)} = \begin{bmatrix} \mathbf{a}_{H(0)}(\theta_1) & \mathbf{a}_{H(0)}(\theta_2) & \cdots & \mathbf{a}_{H(0)}(\theta_P) \end{bmatrix} \tag{6.28}$$

Using the fact that $|F(i,m,p)| \approx 1$ for $B\tau_p \approx i$ and $|F(i,m,p)| \approx 0$ for $|B\tau_p - i| \geq 1$, we can approximate $\mathbf{R}_H(0)$ as:

$$\mathbf{R}_H(0) \approx \mathbf{a}_{H(0)}(\theta_1)\,|\alpha_1|^2\left[\mathbf{a}_{H(0)}(\theta_1)\right]^H + \sigma^2\boldsymbol{I} \tag{6.29}$$

Note that the magnitude of each element in the steering vectors is no longer constant as in the classical MUSIC algorithm. Instead, the magnitude is not only dependent on the DOA $\theta_p$, it also depends on the interpath delay $\tau_p$. Another consequence of the varying magnitude is that the steering vectors for the different angles are no longer of the same form, resulting in another key difference as compared to the classical MUSIC algorithm. However, as mentioned previously, DOA estimation is performed separately for each source and we can see from (6.29) that $\mathbf{R}_H(0)$ is used to estimate for $\theta_1$ exclusively.

Considering $\mathbf{R}_H(0)$ in (6.29), we note that we have two unknowns: $\theta_1$ and $\tau_1$. We

can make use of an iterative process to estimate these two unknowns. First, using the fact that for $B\tau_1 \approx 0$, we can approximate $F(0, m, 1)$ by:

$$F(0, m, 1) \approx \frac{\sin\left[\pi\left(\frac{\delta}{\lambda_c}(m-1) B_f \sin\theta_1\right)\right]}{\sin\left[\frac{\pi}{Q}\left(\frac{\delta}{\lambda_c}(m-1) B_f \sin\theta_1\right)\right]} \tag{6.30}$$

and form an initial estimate $\hat{\theta}_1^{(0)}$ of $\theta_1$ using the MUSIC algorithm. With this initial estimate $\hat{\theta}_1^{(0)}$, we form an estimate $\hat{\tau}_1^{(0)}$ of $\tau_1$ by considering the cost function $L\left(u, \hat{\theta}_1^{(0)}\right)$:

$$\begin{aligned} L\left(u, \hat{\theta}_1^{(0)}\right) &= \sum_{m=1}^{M}\left|\sum_{q=0}^{Q-1}\left[\mathbf{Z}(q)\right]_m e^{j2\pi\frac{q}{Q}\left(u+\frac{(m-1)\delta}{\lambda_c}B_f\sin\hat{\theta}_1^{(0)}\right)}\right|^2 \\ &= \sum_{m=1}^{M}\left|e^{j\pi\frac{Q-1}{Q}\left(u+\frac{(m-1)\delta}{\lambda_c}B_f\sin\hat{\theta}_1^{(0)}\right)}\sum_{p=1}^{P}\alpha_p e^{-j\varphi_p(m)}F_1(u, m, p)\right|^2 \end{aligned} \tag{6.31}$$

where

$$\varphi_p(m) = 2\pi\left[\left(f_c + \frac{Q-1}{2Q}B\right)\tau_p + \frac{(m-1)\delta}{\lambda_c}\left(1 + \frac{Q-1}{2Q}B_f\right)\sin\theta_p\right] \tag{6.32}$$

and

$$F_1(u, m, p) = \frac{\sin\left[\pi\left(u - B\tau_p + \frac{(m-1)\delta}{\lambda_c}B_f\left(\sin\hat{\theta}_1^{(0)} - \sin\theta_p\right)\right)\right]}{\sin\left[\frac{\pi}{Q}\left(u - B\tau_p + \frac{(m-1)\delta}{\lambda_c}B_f\left(\sin\hat{\theta}_1^{(0)} - \sin\theta_p\right)\right)\right]} \tag{6.33}$$

$\tau_1$ is estimated by maximizing the cost function $L\left(u, \hat{\theta}_1^{(0)}\right)$ for $-1 < u < 1$. For single signal case, $u = B\tau_1$ maximizes the cost function $L\left(u, \hat{\theta}_1^{(0)}\right)$ provided that $\hat{\theta}_1^{(0)} \rightarrow \theta_1$. For multiple signals, $u \approx B\tau_1$ will be the maximization point with the offset limits dependent on the number of signals and their separation in arrival times. The discussion on the offset limits is given in Appendix C. With the initial estimate $\hat{\tau}_1^{(0)}$, we form $F(0, m, 1)$ to carry out the one-dimensional search process of the DOA $\theta_1$ again. The process can then be re-iterated several times to get DOA estimates of desired accuracy.

If we denote the iteration index as $l$ then the steps of the iterative process can be formally listed as below:

1. Using the approximation $F(0,m,1) \approx \frac{\sin\left[\pi\left(\frac{\delta}{\lambda_c}(m-1)B_f \sin\theta_1\right)\right]}{\sin\left[\frac{\pi}{Q}\left(\frac{\delta}{\lambda_c}(m-1)B_f \sin\theta_1\right)\right]}$, form an initial estimate $\hat{\theta}_1^{(0)}$ of $\theta_1$ by performing the MUSIC algorithm on $\mathbf{R}_H(0)$.

2. Using $\hat{\theta}_1^{(l-1)}$, $l = 1, 2, \ldots, L_{iter}$ (where $L_{iter}$ is the maximum number of iterations), form the estimate $\hat{\tau}_1^{(l-1)}$ of $\tau_1$ from the cost function $L\left(u, \hat{\theta}_1^{(l-1)}\right)$ where:

$$\hat{\tau}_1^{(l)} = \frac{1}{B} \arg\max_u L\left(u, \hat{\theta}_1^{(l-1)}\right) \tag{6.34}$$

3. Using $\hat{\tau}_1^{(l)}$, form $F^{(l)}(0,m,1)$

4. Using $F^{(l)}(0,m,1)$, estimate $\hat{\theta}_1^{(l)}$ by performing the MUSIC algorithm on $\mathbf{R}_H(0)$. Repeat Step 2 to Step 4 for $l < L_{iter}$.

The maximum number of iterations $L_{iter}$ is preset. For only a small number of iterations, the accuracy of DOA estimates is high, as shown in later sections. Alternatively, the stopping condition for the iterative procedure can be determined by the absolute difference between the current estimated DOA and the previous DOA estimate lesser than a pre-determined threshold whereby this threshold determines the resolution of the detected DOAs.

## 6.2 Proposed DOA Estimation Algorithm

From the discussion in Section 6.1, we now formulate the algorithm for DOA estimation of uncorrelated and correlated signals using the M-CFSSM together with the narrowband signal subspace estimation method, MUSIC. Note that we assume that the receiver has the knowledge of the total number of wideband signal sources. The signals from the sources are assumed to be uncorrelated which satisfy (6.12).

1. Down-convert the received signal at the array to baseband and sample the baseband signal at the Nyquist rate, $B$ Hz.

2. Divide the total number of sampled data into $N$ snapshots of $Q$ samples each.

3. For each snapshot, convert the sampled time domain data into frequency domain data of $Q$ frequency bins using $Q$-point DFT.

4. For each frequency bin, correlate the received signal with the different transmitted signals to form $\mathbf{Z}^{(k)}(q)$ in (6.14).

5. For each $\mathbf{Z}^{(k)}(q)$, form the corresponding $\mathbf{H}^{(k)}(i)$ using (6.18) and determine the number of received signals from the $k^{\text{th}}$ source by finding the number of peaks in the plot of $\left|\mathbf{H}^{(k)}(i)\right|^2$ for $i = 0, 1, \ldots, Q-1$ greater than a threshold $\zeta$ designed accordingly to (6.22).

6. Using each of the $\mathbf{H}^{(k)}(i)$ that corresponds to the peaks found in Step 5, form the correlation matrix $\mathbf{R}_H^{(k)}(i)$ as follows:

$$\mathbf{R}_H^{(k)}(i) = \mathrm{E}\left[\mathbf{H}^{(k)}(i)\left[\mathbf{H}^{(k)}(i)\right]^H\right] \tag{6.35}$$

7. The DOA estimation for each arrival path is carried out using the iterative process detailed at the end of Section 6.1.

Note that in the proposed estimation algorithm, the DOAs of all the impinging wavefronts from each source are estimated separately. In addition, the search through the hypothesized DOAs can be narrowed down after the initial estimate – only a single angle is expected and the initial estimate is near to the true DOA unlike the preliminary DOA estimates in CSSM [17] and WAVES [38].

## 6.3 Simulation Results

In this section, we provide some numerical results using the proposed M-CFSSM. We consider the same operating environment as that in Section 5.6 – a future cellular system with large system bandwidth of $100$ MHz [102, 103]. The signals from each source are

modeled in the frequency domain as random variables with constant amplitudes and uniformly distributed random phases. The sources have a carrier frequency of 2 GHz and a bandwidth of 100 MHz. They are designed accordingly to (6.12) so that they are uncorrelated within the observation window. The frequency domain signal from each source is generated randomly for a single snapshot. The signals are then repeated for $N = 4$ snapshots and are multiplied by different rows of the $4 \times 4$ Hadamard matrix for different signal sources to guarantee the signals from the sources satisfy (6.12). The signals are assumed to be known to the receiver. The noise at the array is assumed to be AWGN. The antenna array at the receiver is assumed to be a ULA of 11 omni-directional antennas with inter-element spacing $\delta = \frac{1}{2}\lambda_c$ where $\lambda_c$ is the wavelength of the carrier frequency. The Rayleigh angle resolution limit for the array is approximately $2/(M-1) \simeq 11.46^\circ$ (0.2 radians).

The received signal is down-converted to baseband and sampled at a frequency of 100 MHz. The total observation time is $T_0 = 1.28$ $\mu$s and are divided into 4 intervals each with duration $\Delta T = 320$ ns. Here, the number of intervals is chosen to be small so as to illustrate the capability of the proposed algorithm when small number of snapshots is available. The samples in each interval are converted into $Q = 32$ narrowband frequency bins using DFT. Note that the number of snapshots considered is much smaller than that used in Chapter 5 which is 64.

### 6.3.1 Detection Performance of Correlated Signals

Since the sources are designed to be uncorrelated and the number of sources is assumed to be known, we only need to determine the number of correlated signals at the receiver due to the different multipaths of each source. Without loss of generality, we consider the case of a single source with two impinging wavefronts at the receiver (i.e. $P_1 = 2$). The magnitudes of complex gains for all the paths are assumed to be equal and the SNRs are set to $-10$ dB. The two multipaths, with the DOAs randomly generated with an angle separation of 7°, have the following parameters: $\alpha_1^{(1)} = \beta e^{j\frac{\pi}{5}}$, $\alpha_2^{(1)} = \beta e^{j\frac{\pi}{4}}$ and

$\tau_1^{(1)} = 0T$, $\tau_2^{(1)} = 6.2T$. Note that the complex gains for the two paths have equivalent powers so that the received SNRs for both paths are the same. We plot the graph of $\left|\mathbf{H}^{(k)}(i)\right|^2$ against $i$, $i = 0, 1, \ldots, Q-1$ for ten independent trials in Figure 6.1. For ease of reference, the thresholds $\zeta$ as defined in (6.22) (indicated by the horizontal lines) are plotted as well.

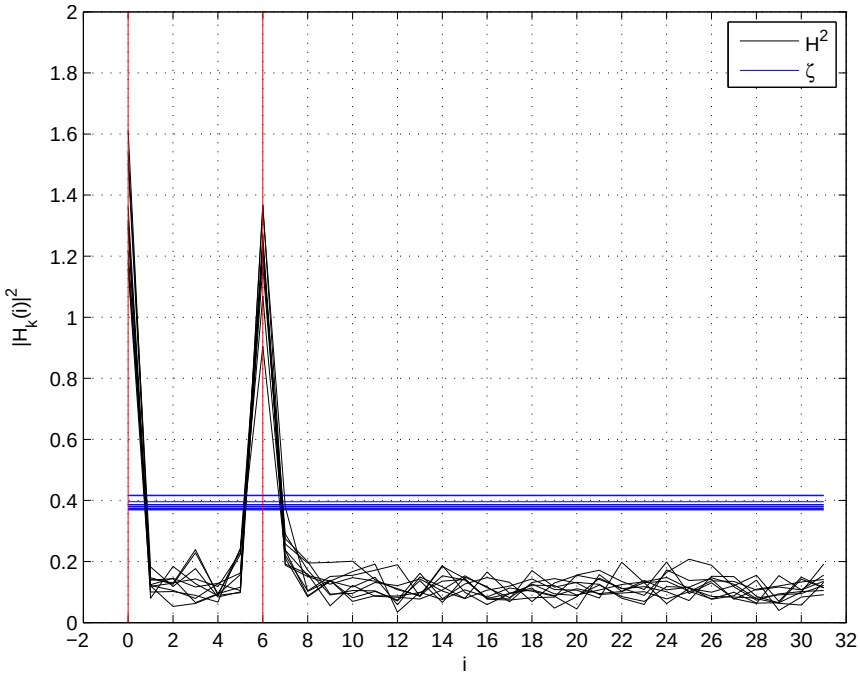


Figure 6.1: Plot of $|\mathbf{H}_k(i)|^2$ against $i$

As seen from Figure 6.1, we can correctly detect two peaks in the plot corresponding to the two arrival paths (indicated by the vertical lines) even at a low SNR of $-10$ dB. We compare the performance of the proposed detection method to that of the coherent AIC proposed in [17]. From Figure 6.2, our proposed detection algorithm performs better than the coherent AIC [17] at low SNRs. For $100\%$ correct detection, the SNR threshold of our proposed detection algorithm is around $-12$ dB while the SNR threshold of coherent AIC is $-8$ dB, which is higher than that of our proposed detection algorithm.

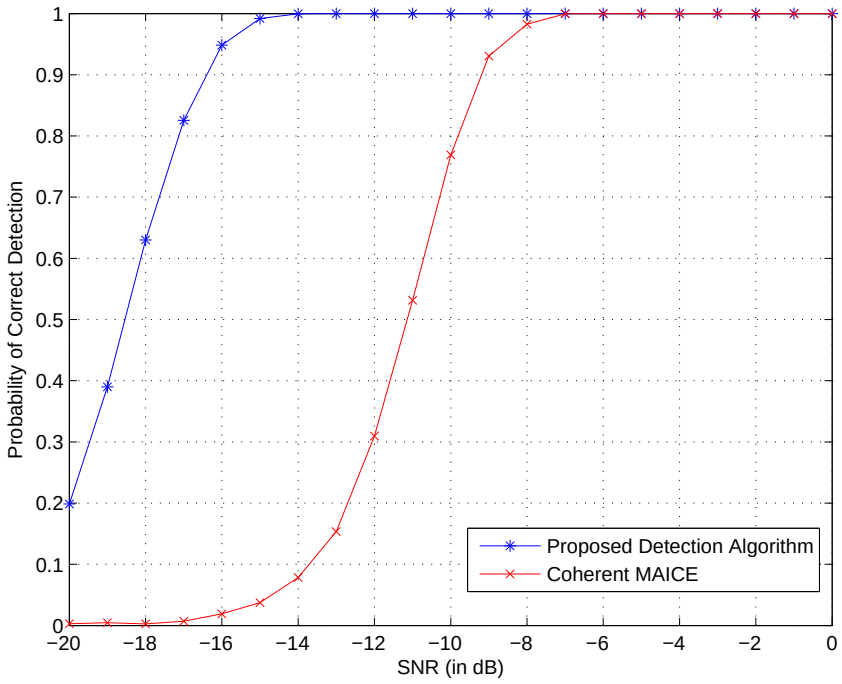


Figure 6.2: Detection performance against SNR for correlated signals

### 6.3.2 Performances of the DOA Estimators

In this section, we study the statistical estimation performance of the proposed M-CFSSM in terms of RMSE and estimation bias. The WAVES algorithm has similar performance to the CSSM algorithm as seen from the previous chapter. Hence the performance of proposed M-CFSSM is compared to that of the blind coherent estimation method CSSM [17] only. Monte Carlo simulation of 2000 independent trials are conducted to obtain the statistical performance.

#### 6.3.2.1 Correlated Signals

We investigate the estimation performance for two correlated received signals which arrive at the receiver simultaneously. The correlated signals are the result of two impinging wavefronts from the same source that arrive at the receiver through two independent multipaths. The DOAs of the two multipaths are randomly generated with an angle separation of $7^\circ$ with other parameters as follows: $\alpha_1^{(1)} = \beta e^{j\frac{\pi}{5}}$, $\alpha_2^{(1)} = \beta e^{j\frac{\pi}{4}}$

and $\tau_1^{(1)} = 0T$, $\tau_2^{(1)} = 6.2T$. Note that the complex gains for the two paths have equivalent powers so the received SNRs of both paths are the same. For the CSSM estimation method, the initial DOAs are estimated using the Capon's estimator which only provides a single DOA estimate, and the RSS focusing matrix is used as the focusing matrix. For our proposed M-CFSSM, the number of iterations is set to 1 (i.e. $L_{iter} = 1$).

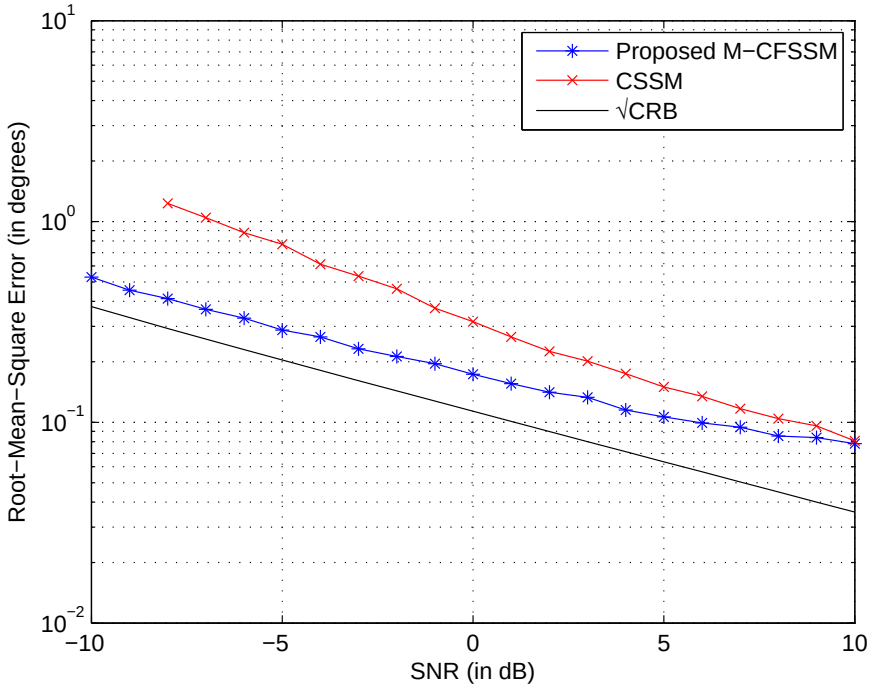


Figure 6.3: RMSE performance against SNR for correlated signals

In Figure 6.3, the RMSE for M-CFSSM and CSSM are plotted against SNR. We compare the performance of the algorithms with the CRLB derived for known waveforms given in [17]. Note that for CSSM, even though the coherent AIC is able to detect the number of correlated signals correctly from $-8$ dB onwards, the spatial plot of CSSM occasionally shows a single peak for SNRs below $0$ dB. Hence from Figure 6.4, we can see that CSSM has a large bias at $-8$ dB. This, in turn, affects the estimation performance in terms of RMSE. As seen from Figure 6.3, the performance of the CSSM is much worse than that of M-CFSSM in the low SNR region. On the other hand, the proposed M-CFSSM exhibits good estimation performance and has performance close to the CRLB at low SNRs. In Figure 6.5, the RMSE for the estimation of $B\tau_2^{(1)}$ is shown. Note that at high SNRs the plot exhibits an error floor, signifying a small offset

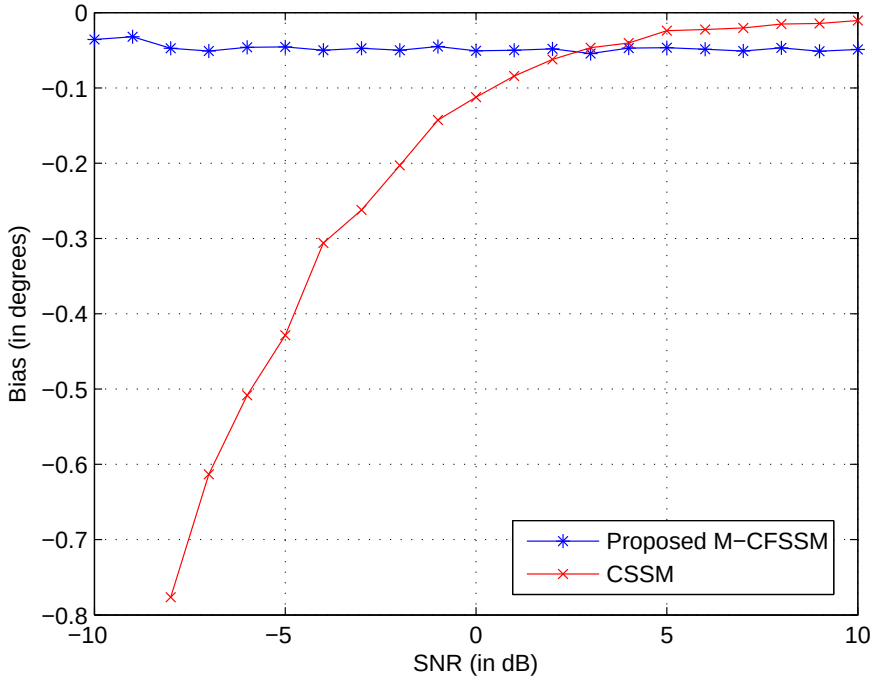


Figure 6.4: Bias performance against SNR for correlated signals

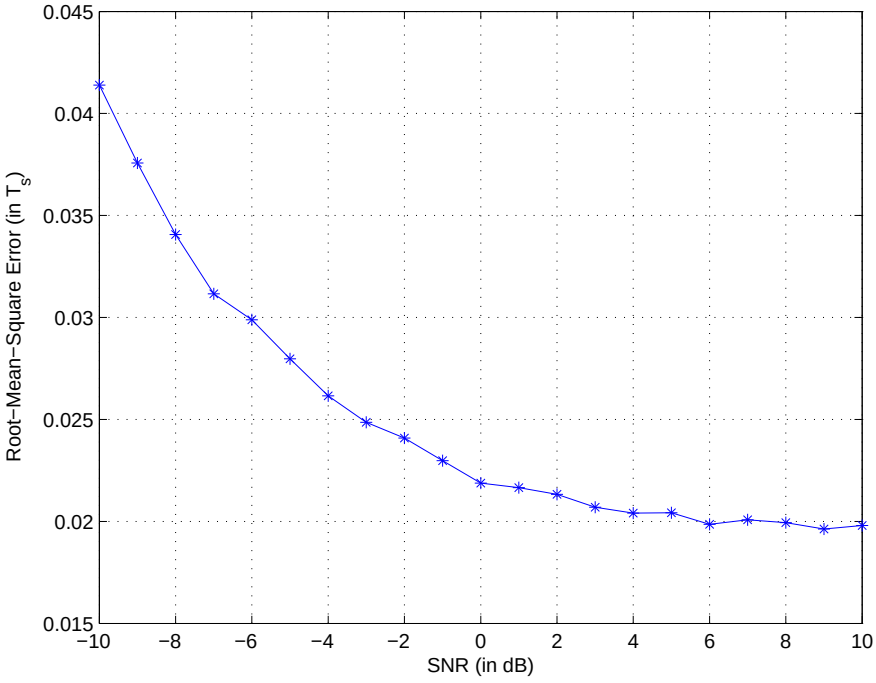


Figure 6.5: RMSE performance against SNR for $B\tau_2^{(1)} = 6.2T$

in the estimation.

#### 6.3.2.2 Uncorrelated Signals

We next investigate the estimation performance for two uncorrelated signals. The two signals are assumed to have equal power and their DOAs are randomly generated with an angle separation of $7^\circ$. They are simulated with the following parameters: $\alpha_1^{(1)} = \beta e^{j\frac{\pi}{5}}$, $\alpha_1^{(2)} = \beta e^{j\frac{\pi}{3}}$ and $\tau_1^{(1)} = \tau_1^{(2)} = 0T$. Note that the complex gains for the two signals have equivalent powers so the received SNRs of both signals are the same. We compare the performance of the proposed M-CFSSM to CSSM. Similar to Section 6.3.2.1, the initial DOAs for CSSM are estimated using the Capon's estimator which only provides a single DOA estimate. The RSS focusing matrix is used as the focusing matrix for CSSM .

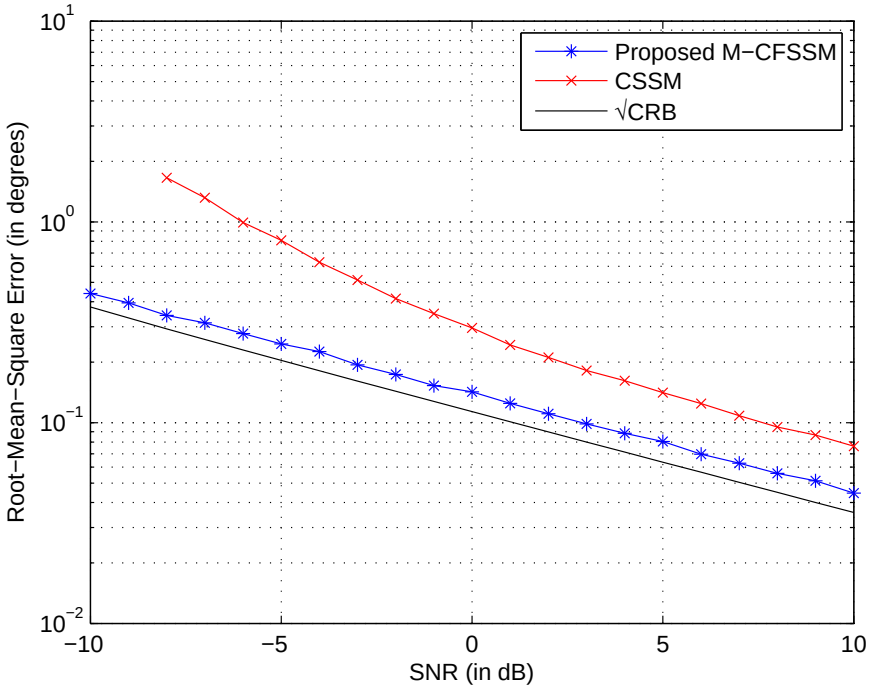


Figure 6.6: RMSE performance against SNR for uncorrelated signals

In Figure 6.6, the RMSE for M-CFSSM and CSSM are plotted against SNR. We compare the performance of the algorithms with the CRLB derived for known waveforms given in [17]. Similar to the case of correlated signals, the proposed M-CFSSM performs better than CSSM in the low SNR region. Moreover, there is no error floor in the RMSE plot unlike the case for correlated signals in the high SNR region. This is

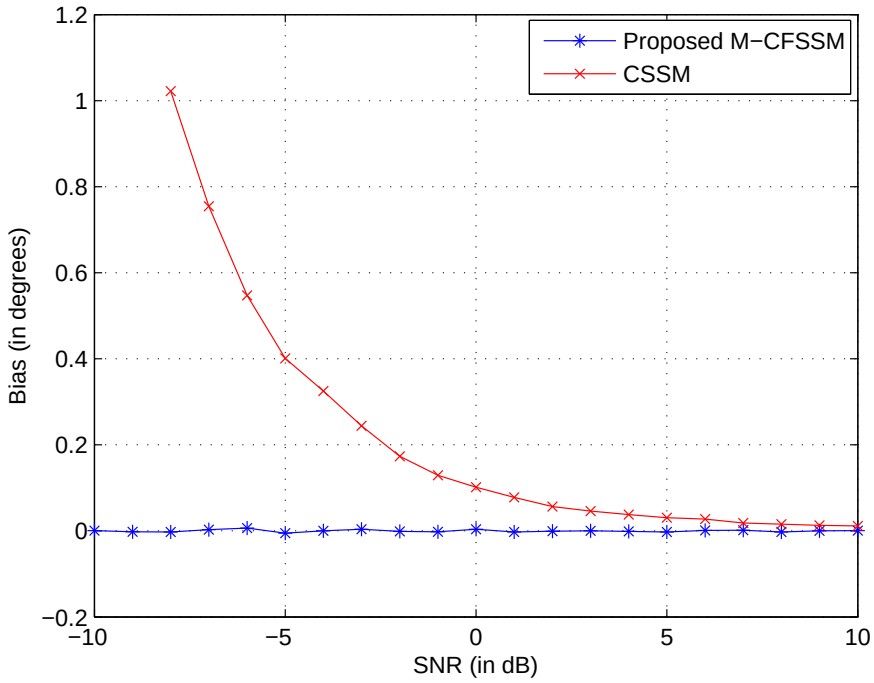


Figure 6.7: Bias performance against SNR for uncorrelated signals

shown more clearly in Figure 6.7.

The proposed M-CFSSM method proves to have good estimation performance at low SNRs even with only a small number of snapshots. Its estimation performance is close to the CRLB and it is able to resolve the signals correctly at low SNRs.

## 6.4 Conclusion

In this chapter, we modified the CFSSM introduced in Chapter 5 to the case when the receiver has the knowledge of transmitted signals. The modified CFSSM (M-CFSSM) method can be used for both uncorrelated and correlated signals and is useful for DOA estimation in systems with small amount of observation data provided the transmitted signals are designed appropriately. We demonstrated through simulation that the detection performance of the proposed M-CFSSM is robust at low SNRs for correlated signals. The estimation performance is also close to the CRLB at low SNRs. Moreover, the M-CFSSM exhibits small estimation bias for SNRs as low as $0$ dB. These charac-

teristics make the proposed M-CFSSM suitable for implementation in systems using preamble transmission such as cellular mobile systems.

# Chapter 7

# Direction-of-Arrival Estimation in Time-Varying Channels

In Chapters 4 and 6, we discussed the DOA estimation using known transmitted signals akin to the use of pilot symbols or preambles in conventional packet transmission in cellular communications among other wireless systems [22]. An underlying assumption made in those chapters is that the wireless multipath channel remains stationary during the course of the estimation process. This assumption is valid for stationary or slow-moving mobile transmitters and/or receivers. However, if any of them is fast-moving, the assumption breaks down and the channel can no longer be considered as time-invariant [23, 105, 106]. In this chapter, we extend the algorithms developed in Chapters 4 and 6 to the case of time-varying and investigate the effects of time-varying channels on the proposed algorithms.

## 7.1 Time-Varying Channels

We first modify the general expression (2.64) in Section 2.4 to reflect the time-varying characteristics of the complex gains of the multipaths, or equivalently the channel gains. Keeping to the same notations in Section 2.4, where $x^{(k)}(t)$ is the $k^{\text{th}}$ signal source, $\tau_p^{(k)}$ and $\alpha_p^{(k)}$ are the interpath delay and the complex gain of the $p^{\text{th}}$ multipath from the $k^{(k)}$ source respectively, $w_n(t)$ is the additive noise at the $m^{\text{th}}$ antenna, and $\kappa_{p,m}^{(k)}$ is the antenna delay of the $p^{\text{th}}$ multipath from the $k^{(k)}$ source at the $m^{\text{th}}$ antenna relative to the arrival time of the same path at the reference antenna, the received signal at the $m^{\text{th}}$

antenna is given by:

$$y_m(t) = \sum_{k=1}^{K} \sum_{p=1}^{P_k} \alpha_p^{(k)}(t)\, x^{(k)}\left(t - \tau_p^{(k)} - \kappa_{p,m}^{(k)}\right) + w_m(t) \tag{7.1}$$

The changes in the channel gain are brought about by the movement of mobile transmitters and/or receivers, which change the phases of the transmitted signals impinging on the local scatterers (see Figure 2.5) and result in a time-domain fading phenomena along the different dominant reflector paths [23]. The channel variations with time or the time selectivity of wireless multipath channels has been covered in details in Section 2.2. Suffice to repeat here that the rate of the variations is dependent on the speed of the mobile transmitters/receivers and the rate of transmission. Baring high mobility of more than $300$ km/h, we can safely assume that the channel is quasi-stationary during each observation period [23], or equivalently the period of pilot symbols or preamble transmission. However, the channel characteristics between different preamble transmission periods cannot be assumed to be the same as the time separation between consecutive preamble transmission periods is usually large to avoid too much overhead in the transmission. In this chapter, we assume that the time separation between consecutive preamble transmission periods (i.e. observation periods) is large enough that the channel characteristics among the different observation periods are independent and identically distributed (iid). We further assume the channel under consideration is non-frequency selective.

## 7.2 Narrowband Signals

Recall from Chapter 4 where we consider a single observation period with $N$ snapshots. We now extend the model to the case of multiple observation periods where the channel gains are assumed to be stationary within each observation period but are statistically independent among the different observation periods. We introduce the observation period index $o = 1, 2, \ldots, O$ where $O$ is the total number of observation periods. For

simplicity, we assume that the different sources transmit the same signals in all the observation periods. However, this is not a strict requirement. The minimum requirement is that the transmitted signals satisfy (4.18) for all the observation periods. For the $o^{\text{th}}$ observation period, the matrix in (4.14) is thus re-written as:

$$\mathbf{Y}_l^{(o)} = \mathbf{A}_1(\boldsymbol{\theta})\mathbf{D}^{l-1}\boldsymbol{\Lambda}^{(o)}\mathbf{S} + \mathbf{W}_l^{(o)} \tag{7.2}$$

where $\mathbf{Y}_l^{(o)}$ is the $M_0^{(k)} \times N$ matrix formed by the concatenation of all the $l^{\text{th}}$ subarray outputs at different snapshots and $\boldsymbol{\Lambda}^{(o)}$ is the $P \times P$ diagonal matrix of the complex gains with entries equal to $\alpha_p^{(o,k)}$.

For the $k^{\text{th}}$ source, we form the source signal dependent decision matrix in a similar fashion as in (4.25) by concatenating all the $L$ correlations between $\mathbf{Y}_l^{(o)}$ and the predetermined transmitted signals of the $k^{\text{th}}$ source. The noiseless decision matrix in the $o^{\text{th}}$ observation period is thus given by:

$$\mathbf{Z}^{(o,k)} = \mathbf{A}_2\left(\boldsymbol{\theta}^{(k)}\right)\boldsymbol{\Lambda}^{(o,k)}\mathbf{B}\left(\boldsymbol{\theta}^{(k)}\right) \tag{7.3}$$

where $\boldsymbol{\theta}^{(k)}$ is the $P_k \times 1$ vector containing all the DOAs of the $k^{\text{th}}$ source, and $\mathbf{A}_2\left(\boldsymbol{\theta}^{(k)}\right)$ is the $M_0 \times P_k$ submatrix of $\mathbf{A}_1(\boldsymbol{\theta})$, which consists of the $P_k$ steering vectors of the $k^{\text{th}}$ source. $\boldsymbol{\Lambda}_k = \text{diag}\left\{\alpha_1^{(o,k)},\ \alpha_2^{(o,k)},\ \cdots\ \alpha_{P_k}^{(o,k)}\right\}$ is a $P_k \times P_k$ diagonal matrix where $\alpha_p^{(o,k)}$ is the channel gain for the $o^{\text{th}}$ observation period. $\mathbf{B}\left(\boldsymbol{\theta}^{(k)}\right)$ is as defined in (4.27).

We consider the noiseless correlation matrix of the decision statistic matrix $\mathbf{Z}^{(o,k)}$:

$$\begin{aligned}
\mathbf{R}_{Z^{(o,k)}} &= \mathbf{Z}^{(o,k)}\left[\mathbf{Z}^{(o,k)}\right]^H \\
&= \mathbf{A}_2\left(\boldsymbol{\theta}^{(k)}\right)\boldsymbol{\Lambda}^{(o,k)}\mathbf{B}\left(\boldsymbol{\theta}^{(k)}\right)\left[\mathbf{B}\left(\boldsymbol{\theta}^{(k)}\right)\right]^H\left[\boldsymbol{\Lambda}^{(o,k)}\right]^H\left[\mathbf{A}_2\left(\boldsymbol{\theta}^{(k)}\right)\right]^H \\
&= \mathbf{A}_2\left(\boldsymbol{\theta}^{(k)}\right)\left[\mathbf{R}_{\Lambda^{(o,k)}} \odot \mathbf{R}_{B^{(k)}}\right]\left[\mathbf{A}_2\left(\boldsymbol{\theta}^{(k)}\right)\right]^H
\end{aligned} \tag{7.4}$$

where

$$\mathbf{R}_{\Lambda^{(o,k)}} = \begin{bmatrix} \left|\alpha_1^{(o,k)}\right|^2 & \alpha_1^{(o,k)}\left(\alpha_2^{(o,k)}\right)^* & \cdots & \alpha_1^{(o,k)}\left(\alpha_{P_k}^{(o,k)}\right)^* \\ \alpha_2^{(o,k)}\left(\alpha_1^{(o,k)}\right)^* & \left|\alpha_2^{(o,k)}\right|^2 & \cdots & \alpha_2^{(o,k)}\left(\alpha_{P_k}^{(o,k)}\right)^* \\ \vdots & \vdots & \ddots & \vdots \\ \alpha_{P_k}^{(o,k)}\left(\alpha_1^{(o,k)}\right)^* & \alpha_{P_k}^{(o,k)}\left(\alpha_2^{(o,k)}\right)^* & \cdots & \left|\alpha_{P_k}^{(o,k)}\right|^2 \end{bmatrix} \tag{7.5}$$

and

$$\begin{aligned} \mathbf{R}_{B^{(k)}} &= \mathbf{B}\left(\boldsymbol{\theta}^{(k)}\right)\left[\mathbf{B}\left(\boldsymbol{\theta}^{(k)}\right)\right]^H \\ &= \begin{bmatrix} 1 & F\left(\theta_1^{(k)}-\theta_2^{(k)}\right) & \cdots & F\left(\theta_1^{(k)}-\theta_{P_k}^{(k)}\right) \\ \left[F\left(\theta_1^{(k)}-\theta_2^{(k)}\right)\right]^* & 1 & \cdots & F\left(\theta_2^{(k)}-\theta_{P_k}^{(k)}\right) \\ \vdots & \vdots & \ddots & \vdots \\ \left[F\left(\theta_1^{(k)}-\theta_{P_k}^{(k)}\right)\right]^* & \left[F\left(\theta_2^{(k)}-\theta_{P_k}^{(k)}\right)\right]^* & \cdots & 1 \end{bmatrix} \end{aligned} \tag{7.6}$$

The function $F\left(\theta_{p1}-\theta_{p_2}\right)$ is the summation of a geometric series and is given by:

$$\begin{aligned} F\left(\theta_{p_1}-\theta_{p_2}\right) &= \sum_{i=0}^{L-1}\left[e^{-j\frac{2\pi\delta}{\lambda_c}\left(\sin\theta_{p_1}-\sin\theta_{p_2}\right)}\right]^i \\ &= \frac{\sin\left[\frac{\pi\delta L}{\lambda_c}\left(\sin\theta_{p_1}-\sin\theta_{p_2}\right)\right]}{\sin\left[\frac{\pi\delta}{\lambda_c}\left(\sin\theta_{p_1}-\sin\theta_{p_2}\right)\right]}e^{-j\frac{\pi\delta}{\lambda_c}(L-1)\left(\sin\theta_{p_1}-\sin\theta_{p_2}\right)} \end{aligned} \tag{7.7}$$

Now we sum up the different correlation matrices across the different observation periods and we get:

$$\begin{aligned} \mathbf{R}_{Z^{(k)}} &= \frac{1}{O}\sum_{o=1}^{O}\mathbf{R}_{Z^{(o,k)}} \\ &= \mathbf{A}_2\left(\boldsymbol{\theta}^{(k)}\right)\left\{\left[\frac{1}{O}\sum_{o=1}^{O}\mathbf{R}_{\Lambda^{(o,k)}}\right]\odot\mathbf{R}_{B^{(k)}}\right\}\left[\mathbf{A}_2\left(\boldsymbol{\theta}^{(k)}\right)\right]^H \end{aligned} \tag{7.8}$$

Assuming that the channel gains among the observation periods are independent and $O$

is sufficiently large, then:

$$\frac{1}{O}\sum_{o=1}^{O}\mathbf{R}_{\Lambda^{(o,k)}} \;\rightarrow\; \mathrm{E}\left[\mathbf{R}_{\Lambda^{(k)}}\right] = \begin{bmatrix} \mathrm{E}\left[\left|\alpha_1^{(o,k)}\right|^2\right] & 0 & \cdots & 0 \\ 0 & \mathrm{E}\left[\left|\alpha_2^{(o,k)}\right|^2\right] & \cdots & 0 \\ \vdots & \vdots & \ddots & \vdots \\ 0 & 0 & \cdots & \mathrm{E}\left[\left|\alpha_{P_k}^{(o,k)}\right|^2\right] \end{bmatrix} \tag{7.9}$$

Therefore, (7.8) simplifies to:

$$\mathbf{R}_{Z^{(k)}} = \mathbf{A}_2\left(\boldsymbol{\theta}^{(k)}\right) \begin{bmatrix} \mathrm{E}\left[\left|\alpha_1^{(o,k)}\right|^2\right] & 0 & \cdots & 0 \\ 0 & \mathrm{E}\left[\left|\alpha_2^{(o,k)}\right|^2\right] & \cdots & 0 \\ \vdots & \vdots & \ddots & \vdots \\ 0 & 0 & \cdots & \mathrm{E}\left[\left|\alpha_{P_k}^{(o,k)}\right|^2\right] \end{bmatrix} \left[\mathbf{A}_2\left(\boldsymbol{\theta}^{(k)}\right)\right]^H \tag{7.10}$$

Equation (7.10) has two important implications. Firstly, the use of independent observation data in time-varying channels decouple perfectly correlated signals without the need of spatial smoothing technique. Secondly, the received power of each path tends to a constant average power unlike the case for time-invariant channels where the received power is Rayleigh distributed. The availability of time diversity makes the DOA estimation more robust to the fading effects.

### 7.2.1 Proposed DOA Estimation Algorithm

We now formalize the DOA estimation algorithm for multiple observation periods by extending the iterative algorithm introduced in Section 4.2. For the $k^{\text{th}}$ source,

1. For each observation period, down-convert the received signal at the array to baseband and sample the baseband signal at the Nyquist rate, $T$ seconds.

2. Divide the $M$-element ULA into $L$ overlapping subarrays of size $M_0$, where $M_0 = M - L + 1$.

3. For each observation period, concatenate all the $l^{\text{th}}$ subarray outputs at different snapshots to form $\mathbf{Y}_l^{(o)}$ in (7.2) for $l = 1, 2, \ldots, L$.

4. Correlate each $\mathbf{Y}_l^{(o)}$ with the pilot signals for $l = 1, 2, \ldots, L$, and concatenate the resultant vectors to form $\mathbf{Z}^{(o,k)}$ in (7.3).

5. For each observation period, form the correlation matrix $\mathbf{R}_{Z^{(o,k)}}$ in (7.4).

6. Average all the correlation matrices $\mathbf{R}_{Z^{(o,k)}}$ to form $\mathbf{R}_{Z^{(k)}}$ in (7.8).

7. Obtain the initial DOA estimates $\hat{\boldsymbol{\theta}}^{(k)}$ from the left null space of $\mathbf{R}_{Z^{(k)}}$ using the MUSIC algorithm.

8. Refine the DOA estimates by the iterative procedure detailed in Section 4.2.

### 7.2.2 Simulation Results

We provide some numerical results for the case of a time-varying channel and highlight the differences between the performance of the proposed algorithm in time-varying and time-invariant channels. We consider a 7-element ULA with inter-element spacing $\delta = \frac{1}{2}\lambda_c$ where $\lambda_c$ is the wavelength of the carrier frequency. The noise at the array is assumed to be AWGN. The observation periods are assumed to be far apart from each other so that the complex gains in the different observation periods can be assumed to be independent complex random variables. The amplitudes of the random variables are Rayleigh distributed and the phases are uniformly distributed between $0$ and $2\pi$. The number of iterations is set to $2$ in the proposed PASI technique.

#### 7.2.2.1 Resolution of Correlated Signals

We first illustrate the use of different observation periods with independent channel gains to resolve different arrival paths from the same source without the use of spatial-smoothing technique in Chapter 4 (i.e. $L = 1$). We set the total number of observation periods to $O = 10$.

We consider two paths whose angle separation is less than $20°$: $\theta_1^{(1)} = 20°$ and $\theta_2^{(1)} = 30°$. We normalize the power of the two paths so that their averaged received SNRs are equal. The SNR of each path is set to $5$ dB. Figure 7.1 and Figure 7.2 show the spatial spectrums from ten independent trials for time-varying and time-invariant channels respectively. For ease of reference, the true DOAs are indicated by the vertical lines in the figures.

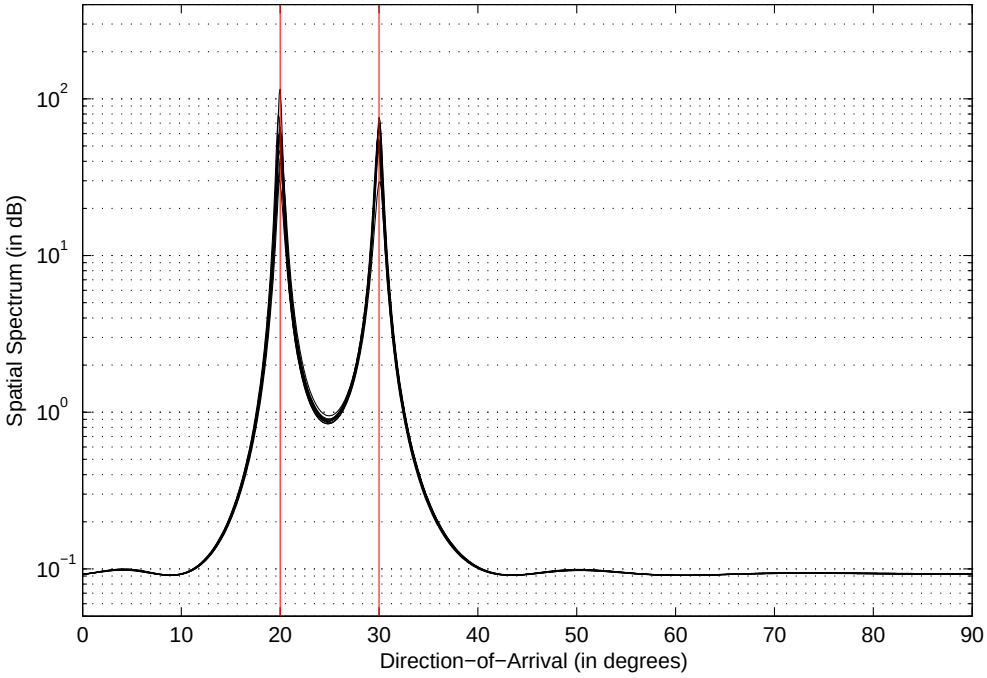


Figure 7.1: Spatial periodogram for time-varying channel

As shown in Figure 7.1, by combining independent observations of the time-varying channel, the correlated signals from the same source can be separated without any spatial smoothing technique. However, the correlated signals from the same source cannot be separated in the time-invariant channel as indicated in Figure 7.2 where no distinct peaks can be observed.

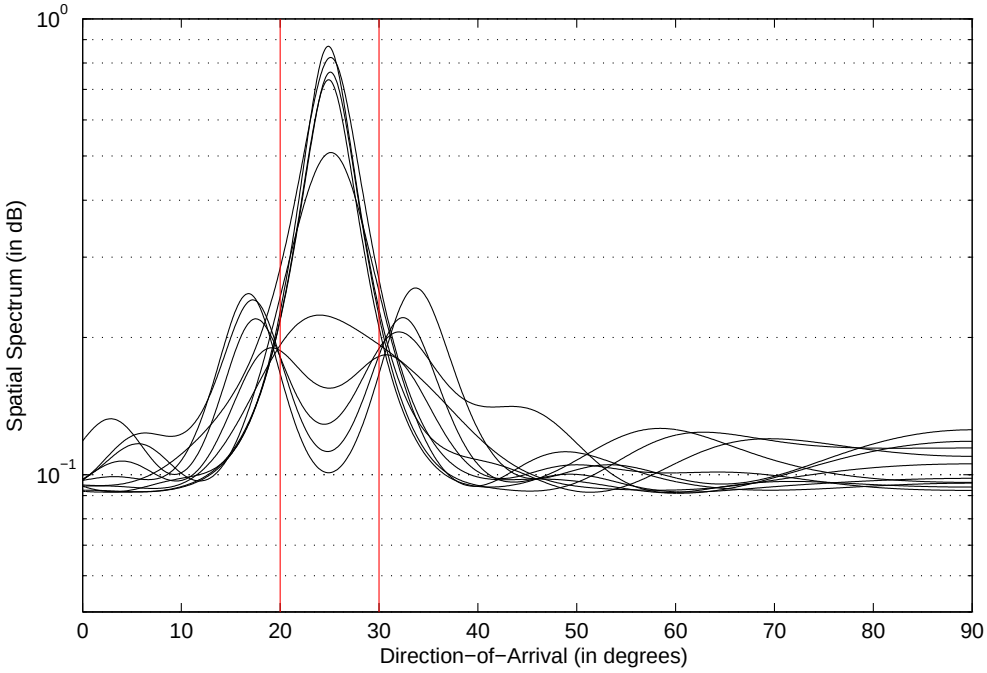


Figure 7.2: Spatial periodogram for time-invariant channel

In Figure 7.3, we plot the RMSEs of the proposed PAS and PASI techniques against number of observation periods and compare them to the CRLB. Here the RMSE is averaged over the two paths. The performance is plotted in Figure 7.3. The statistical performance is obtained through Monte Carlo simulation (for which the statistical performance converges) of $2000$ independent trials. We see that for small number of observation periods, there is a significant gain in the performance of the proposed PASI technique over that of the proposed PAS technique. The use of the iterative process eliminates the correlation between the two paths by canceling the interference path from the decision matrix. The signal subspace thus formed consists only of the desired signal path, resulting in a more accurate estimation. However, with the increase in the number of observation periods, the gain provided by the proposed PASI technique becomes less significant. The two signal paths become uncorrelated due to the independent fading over the different observation periods. Therefore, the benefit of the iterative process for reducing correlation becomes less significant. Note that for the special case of $O = 1$, which corresponds to the case of the time-invariant channel, the two paths cannot be separated as shown in Figure 7.2. Hence the performance of the both algorithms are significantly worse off.

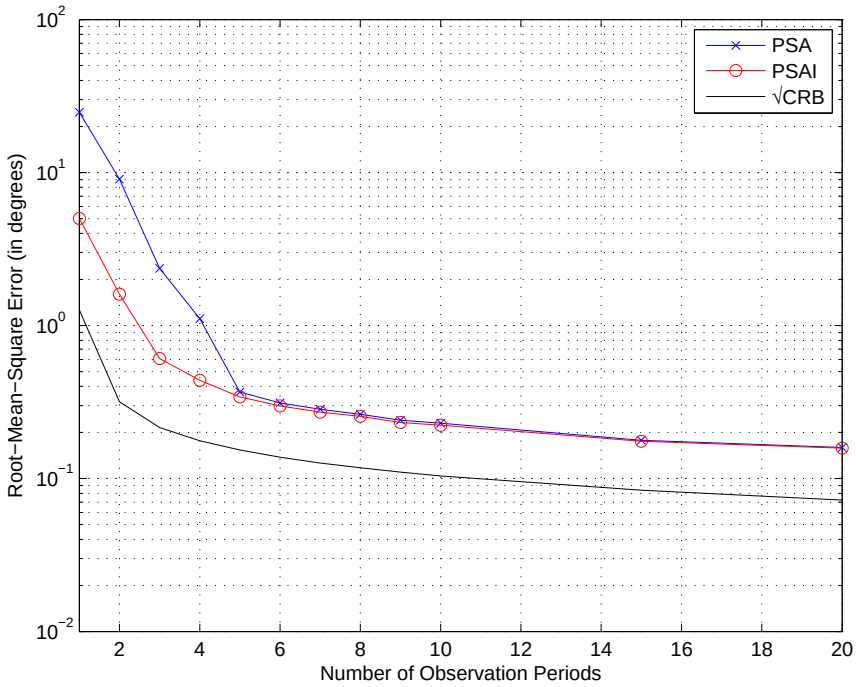


Figure 7.3: RMSE performance against number of observation periods in time-varying channel $(L = 1)$

#### 7.2.2.2 Statistical Performance in Time-Varying and Time-Invariant Channels

Next, we compare the estimation performance of the proposed algorithm against number of observation periods in the time-invariant and time-varying channels. We consider a source with two impinging plane waves at the receiver whose DOAs have an angle separation of $10°$. As shown in the previous section, the use of subarrays is required for accurate estimation in the time-invariant channel. Therefore, we use subarrays of size 3 (i.e. $M_0 = 3$, $L = 5$). Note that for fair comparison, we set the average received power in the time-varying channel to be equal to the received power in the time-invariant channel. The SNR is set to 5dB. The statistical performance is obtained through Monte Carlo simulation (for which the statistical performance converges) of $2000$ independent trials. We report the performance of the proposed algorithm in time-invariant and time-varying channels in Figure 7.4 and Figure 7.5 respectively where the RMSE is averaged over the two paths.

Comparing the CRLB in Figure 7.4 and Figure 7.5, we note that the achievable

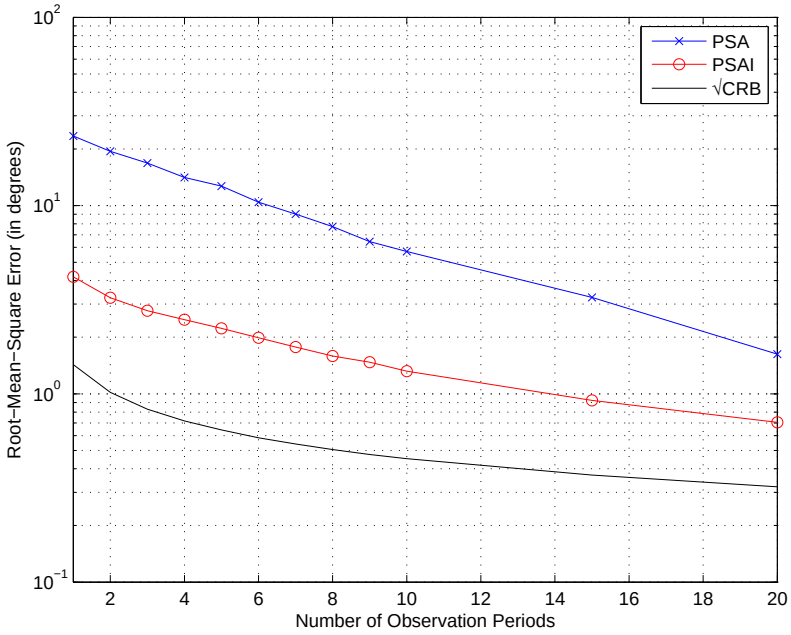


Figure 7.4: RMSE performance against number of observation periods in time-invariant channel $(L = 5)$

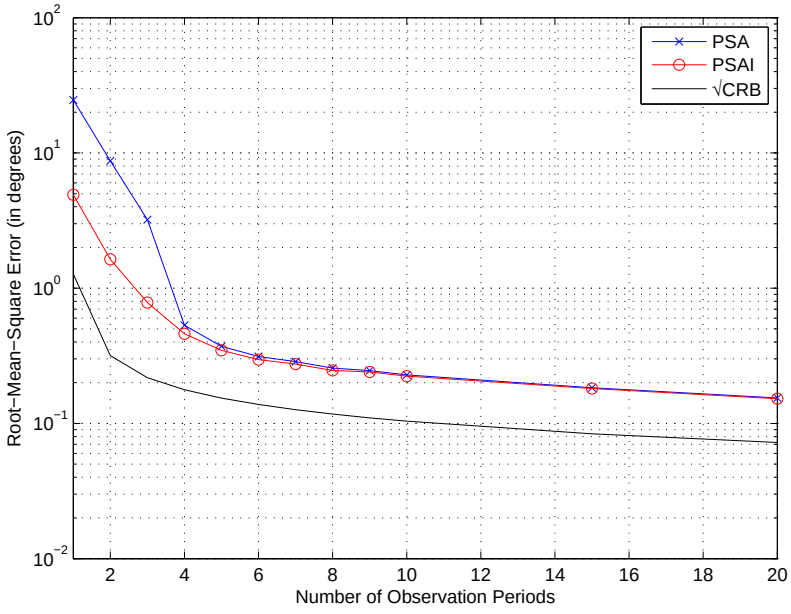


Figure 7.5: RMSE performance against number of observation periods in time-varying channel $(L = 5)$

estimation accuracy for the time-varying channel is higher than that of the time-invariant channel. This is the consequence of the inherent diversity of the time-varying channel. More importantly, Figure 7.4 and Figure 7.5 illustrate the importance of the iterative

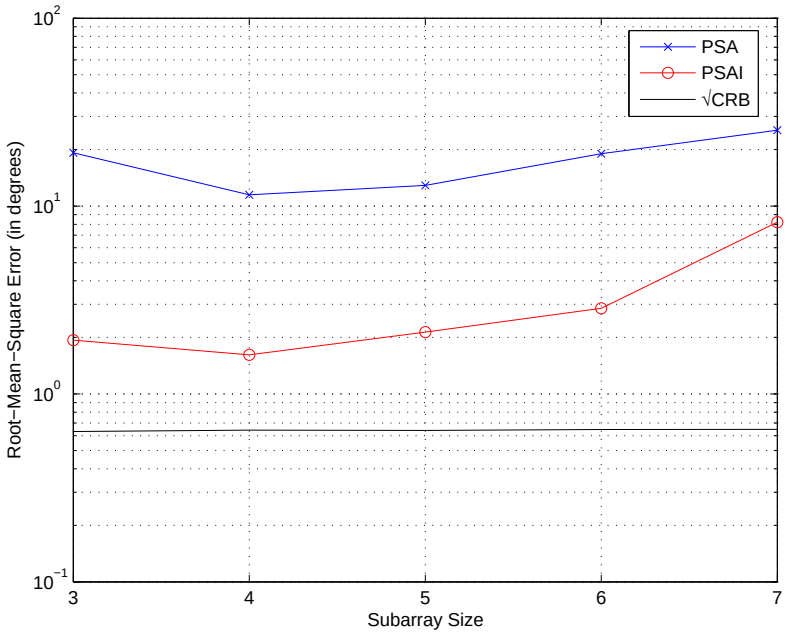


Figure 7.6: RMSE performance against subarray size in time-invariant channel

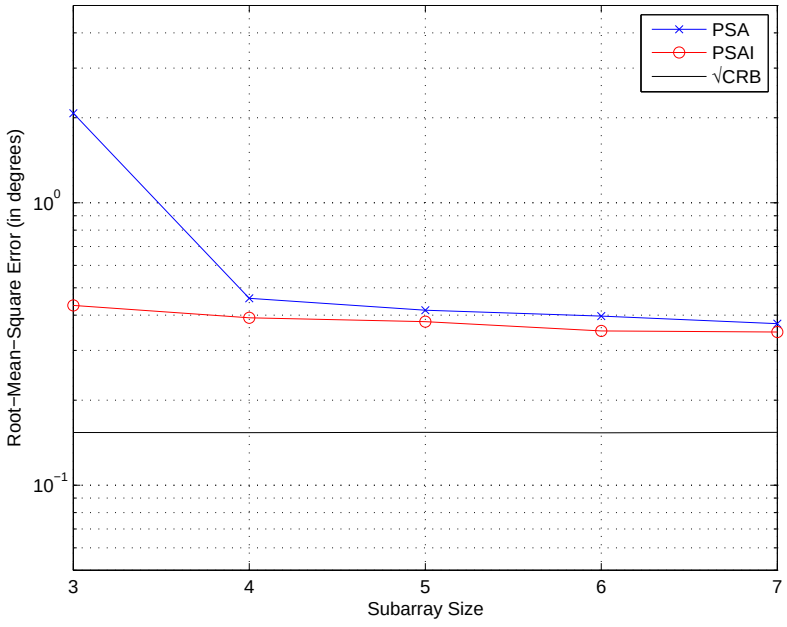


Figure 7.7: RMSE performance against subarray size in time-varying channel

process for improving the estimation performance in the time-invariant channel and for small number of observation periods in the time-varying channel.

In Figure 7.6 and Figure 7.7, we investigate the effect of subarray size (and correspondingly the number of subarrays given a fixed number of antenna elements in a

ULA) on the estimation performance. We set the number of observation periods to $O = 5$ and the SNR to $5$ dB. From Figure 7.6, we see that for the time-invariant channel, the size of the subarrays must be as small as possible limited by the constraints $M_0 > P_k$ and $L \geq P_k$ so that the corresponding increase in the number of subarrays can be used to decorrelate the correlated signals. The opposite is true for the time-varying channel as shown in Figure 7.7. Without the need for subarrays to decorrelate signals, the best performing arrangement is to use the data from the full array instead of splitting them into subarrays.

From the simulation results presented in Figure 7.4 to Figure 7.7, we can draw the conclusion that an adaptive algorithm would work best to cater for different channel time selectivity. In practical operating environment, the interdependency of the data in different observation periods are determined by the speed of mobile transmitter [23,107]. For observation periods not well-spaced apart or for slow moving transmitter/receiver, the best strategy is to maximize the number of subarrays used. On the other hand, if the observations periods are well-spaced out in time or the transmitter/receiver is moving at a relatively high speed, spatial smoothing technique need not be applied.

## 7.3 Wideband Signals

Given our assumption that the channel within each observation period is considered to be constant, we can reuse the matrix notations in Chapter 6 with a slight alternation. We introduce the observation period index $o = 1, 2, \ldots, O$ where $O$ is the total number of observation period in (6.11) to form:

$$\mathbf{Y}_n^{(o)}(q) = \mathbf{A}(q, \boldsymbol{\theta})\, \boldsymbol{\Lambda}^{(o)} \mathbf{X}_n(q) + \mathbf{W}_n^{(o)}(q) \tag{7.11}$$

Recall that we are transmitting deterministic known signals at the different sources

designed so that:

$$\frac{1}{N}\sum_{n=1}^{N} X_n^{(k_1)}(q)\left[X_n^{(k_2)}(q)\right]^* = \begin{cases} 1, & k_1 = k_2 \\ 0, & k_1 \neq k_2 \end{cases} \tag{7.12}$$

for all $q$. The $K$ different data sets in each observation period, one for each signal source, is formed by correlating the received signals with each of the known transmitted signals. The data sets in the $o^{\text{th}}$ observation period consists of $Q$ vectors denoted as $\mathbf{Z}^{(o,k)}(q)$, $q = 0, 1, \ldots, Q-1$, where:

$$\begin{aligned} \mathbf{Z}^{(o,k)}(q) &= \frac{1}{N}\begin{bmatrix} \mathbf{Y}_1^{(o)}(q) & \mathbf{Y}_2^{(o)}(q) & \cdots & \mathbf{Y}_N^{(o)}(q) \end{bmatrix} \begin{bmatrix} X_1^{(k)}(q) \\ X_2^{(k)}(q) \\ \vdots \\ X_N^{(k)}(q) \end{bmatrix}^* \\ &= \mathbf{A}\left(q, \boldsymbol{\theta}^{(k)}\right)\boldsymbol{\Lambda}^{(o,k)}\mathbf{1}_{P_k} + \mathbf{W}^{(o,k)}(q) \end{aligned} \tag{7.13}$$

where $\mathbf{A}(q, \boldsymbol{\theta}^{(k)})$ is the reduced size matrix consisting of the columns of $\mathbf{A}(q, \boldsymbol{\theta})$ with DOAs belonging to the $k^{\text{th}}$ source only. $\boldsymbol{\Lambda}_k = \text{diag}\left\{ \alpha_1^{(o,k)}, \ \alpha_2^{(o,k)}, \ \cdots \ \alpha_{P_k}^{(o,k)} \right\}$ is the $P_k \times P_k$ diagonal matrix where $\alpha_p^{(o,k)}$ is the channel gain for the $o^{\text{th}}$ observation period. $\mathbf{1}_{P_k}$ is the $P_k \times 1$ vector whose entries are all ones.

As mentioned in Chapter 6, the DOA estimation is carried out for each source separately. For clarity, we drop the source index $k$ in the rest of the derivations. In a time-varying channel, the combined frequency signal subspace vector $\mathbf{H}(i)$ in (6.18) for different arrival paths, which are also dependent on the channel gains, is rewritten as:

$$\mathbf{H}^{(o)}(i) = \sum_{q=0}^{Q-1} \mathbf{Z}^{(o)}(q)\, e^{j2\pi\frac{ig}{Q}} \tag{7.14}$$

with the $m^{\text{th}}$ element in the noiseless $\mathbf{H}^{(o)}$ vector given by

$$\left[\mathbf{H}^{(o)}(i)\right]_m = \sum_{p=1}^{P} \alpha_p^{(o)} e^{-j\phi_p(i,m)} F(i,m,p) \tag{7.15}$$

where $\phi_p(i,m)$ and $F(i,m,p)$ are defined in (6.20) and (6.21) respectively.

Recall that in Chapter 6, to determine which of the different $\mathbf{H}(i)$, $i = 0,\ldots,Q-1$, should be used for estimation, we search for peaks of $|\mathbf{H}(i)|^2$ across $i = 0,1,\ldots,Q-1$ which is greater than the arithmetic mean of $|\mathbf{H}(i)|^2$. Similarly, we can search for the peaks of $\frac{1}{O}\sum_{o=1}^{O}\mathbf{H}^{(o)}(i)$ and use it as the criterion to determine the number of arrival paths and which corresponding set of vectors $\mathbf{H}^{(o)}(i)$, $o = 1,\ldots,O$, to be used. The threshold $\zeta$ is changed from the arithmetic mean to the averaged arithmetic mean across the different observation periods. In other words,

$$\zeta = \frac{1}{O}\sum_{o=1}^{O}\frac{1}{Q}\sum_{i=0}^{Q-1}\left|\mathbf{H}^{(o)}(i)\right|^2 \tag{7.16}$$

Without loss of generality, we assume that a peak is detected at $i = 0$ and the set of vectors $\frac{1}{O}\sum_{o=1}^{O}\mathbf{H}^{(o)}(0) \geq \zeta$. The estimation of $\theta_1$ is thus made by using the set of vectors, $\mathbf{H}^{(o)}(0)$, $o = 1,2,\ldots,O$. We consider the summation of the correlation matrices of the different $\mathbf{H}^{(o)}(0)$ given by:

$$\begin{aligned}\mathbf{R}_H(0) &= \frac{1}{O}\mathrm{E}\left[\sum_{o=1}^{O}\mathbf{H}^{(o)}(0)\left[\mathbf{H}^{(o)}(0)\right]^H\right] \\ &= \mathbf{A}_{H(0)}\mathbf{E}_\alpha\mathbf{A}_{H(0)}^H + \sigma^2\boldsymbol{I}\end{aligned} \tag{7.17}$$

where

$$
\begin{aligned}
\mathbf{E}_{\alpha} &= \frac{1}{O}\mathrm{E}\left\{\sum_{o=1}^{O}\begin{bmatrix} \left|\alpha_1^{(o)}\right|^2 & \cdots & \alpha_1^{(o)}\left(\alpha_p^{(o)}\right)^* & \cdots & \alpha_1^{(o)}\left(\alpha_P^{(o)}\right)^* \\ \vdots & \ddots & \vdots & \ddots & \vdots \\ \alpha_p^{(o)}\left(\alpha_1^{(o)}\right)^* & \cdots & \left|\alpha_p^{(o)}\right|^2 & \cdots & \alpha_p^{(o)}\left(\alpha_P^{(o)}\right)^* \\ \vdots & \ddots & \vdots & \ddots & \vdots \\ \alpha_P^{(o)}\left(\alpha_1^{(o)}\right)^* & \cdots & \alpha_P^{(o)}\left(\alpha_p^{(o)}\right)^* & \cdots & \left|\alpha_P^{(o)}\right|^2 \end{bmatrix}\right\} \\
&= \frac{1}{O}\sum_{o=1}^{O}\begin{bmatrix} \mathrm{E}\left[\left|\alpha_1^{(o)}\right|^2\right] & \cdots & \mathrm{E}\left[\alpha_1^{(o)}\left(\alpha_p^{(o)}\right)^*\right] & \cdots & \mathrm{E}\left[\alpha_1^{(o)}\left(\alpha_P^{(o)}\right)^*\right] \\ \vdots & \ddots & \vdots & \ddots & \vdots \\ \mathrm{E}\left[\alpha_p^{(o)}\left(\alpha_1^{(o)}\right)^*\right] & \cdots & \mathrm{E}\left[\left|\alpha_p^{(o)}\right|^2\right] & \cdots & \left[\alpha_p^{(o)}\left(\alpha_P^{(o)}\right)^*\right] \\ \vdots & \ddots & \vdots & \ddots & \vdots \\ \mathrm{E}\left[\alpha_P^{(o)}\left(\alpha_1^{(o)}\right)^*\right] & \cdots & \mathrm{E}\left[\alpha_P^{(o)}\left(\alpha_p^{(o)}\right)^*\right] & \cdots & \mathrm{E}\left[\left|\alpha_P^{(o)}\right|^2\right] \end{bmatrix} \\
&= \begin{bmatrix} \mathrm{E}\left[\left|\alpha_1^{(o)}\right|^2\right] & \cdots & 0 & \cdots & 0 \\ \vdots & \ddots & \vdots & \ddots & \vdots \\ 0 & \cdots & \mathrm{E}\left[\left|\alpha_p^{(o)}\right|^2\right] & \cdots & 0 \\ \vdots & \ddots & \vdots & \ddots & \vdots \\ 0 & \cdots & 0 & \cdots & \mathrm{E}\left[|\alpha_P|^2\right] \end{bmatrix}
\end{aligned} \tag{7.18}
$$

since $\alpha_{p_1}^{(o)}$ and $\alpha_{p_2}^{(o)}$ are independent for $p_1 \neq p_2$ and $\alpha_p^{(o)}$ are zero-mean random variables for $p = 1, 2, \ldots, P$. The array response matrix $\mathbf{A}_{H(0)}$ and $\tilde{\phi}_p(m)$ are as defined in (6.28) and (6.26) respectively and $\sigma^2$ is the noise variance. In the case of time-invariant channels, (7.17) reduces to (6.27).

Comparing (7.17) to (6.27), we note two main differences for the signal subspaces between time-varying and time-invariant channels. Firstly, the time-varying channel adds a dimension of diversity in the received signal power. Secondly, it eliminates the correlations between signals from different arrival paths. In a time-invariant channel, we use the time separation between arrival paths to lower the correlation between different paths by combining the different frequency bins, and estimate the DOAs separately using data from different time instances. In a time-varying channel, however, the dif-

ferent paths are uncorrelated regardless of their separation in arrival times provided that the channel gains $\alpha_p^{(o)}$ are uncorrelated which is usually the case. This implies that the estimated correlation matrix $\hat{\mathbf{R}}_H(0)$ can thus be used to estimate DOAs of arrival paths whose arrival times are near to each other (i.e. $|B(\tau_{p_1} - \tau_{p_2})| < 1$). The condition for effective estimation is that the number of observation periods $O$ must be sufficiently large such that:

$$\frac{1}{O}\sum_{o=1}^{O} \alpha_{p_1}^{(o)} \left(\alpha_{p_2}^{(o)}\right)^* \quad \rightarrow \quad \mathrm{E}\left[\alpha_{p_1}^{(o)} \left(\alpha_{p_2}^{(o)}\right)^*\right] = \begin{cases} \mathrm{E}\left[\left|\alpha_{p_1}^{(o)}\right|^2\right] & , \quad p_1 = p_2 \\ 0 & , \quad p_1 \neq p_2 \end{cases} \tag{7.19}$$

In other words, in a time-varying channel, M-CFSSM can be applied to estimate the DOAs of different multipaths. However, if the channel is stationary across the different observation periods, the different arrival paths must be well separated in time (i.e. in frequency-selective channel) for accurate and distinct estimation of the different DOAs.

### 7.3.1 Proposed DOA Estimation Algorithm

We now extend the algorithm in Section 6.2 to the case of multiple observations. Note that the receiver does not need to have knowledge about the time selectivity of the channel because the algorithm is the same regardless of the channel time selectivity. For the $k^{\mathrm{th}}$ source:

1. In each observation period, down-convert the received signal at the array to baseband and sample the baseband signal at the Nyquist rate, $B$ Hz.

2. Divide the total number of sampled data into $N$ snapshots of $Q$ samples each.

3. For each snapshot, convert the sampled time domain data into frequency domain data of $Q$ frequency bins using $Q$-point DFT.

4. For each frequency bin, correlate the received signal with the different transmitted signals to form $\mathbf{Z}^{(o)}$ in (7.13) for $o = 1, 2, \ldots, O$.

5. For each $\mathbf{Z}^{(o)}$, form the corresponding $\mathbf{H}^{(o)}$ using (7.14).

6. Determine the number of received signals by finding the number of peaks in the plot of $\frac{1}{O}\sum_{o=1}^{O}\mathbf{H}^{(o)}(i)$ across $i = 0, 1, \ldots, Q-1$ greater than a threshold $\zeta$ designed accordingly to (7.16).

7. Using each set of vectors $\mathbf{H}^{(o)}(i)$, $o = 1, 2, \ldots, O$ that corresponds to the peaks found in Step 6, estimate the correlation matrix $\mathbf{R}_H(i)$:

$$\mathbf{R}_H(i) = \frac{1}{O}\mathrm{E}\left[\sum_{o=1}^{O}\mathbf{H}^{(o)}(i)\left[\mathbf{H}^{(o)}(i)\right]^H\right] \tag{7.20}$$

8. The DOA estimation for each arrival path is carried out by performing the MUSIC algorithm on the estimated correlation matrix.

Note that if there is more than one path within the specific $\mathbf{R}_H(i)$, the iterative process in Chapter 4 is not carried for estimation of $\tau_p$ because the offset may be too large to justify the iterative process.

### 7.3.2 Simulation Results

We provide some numerical results for the case of time-varying channels in the same operating scenario as that in Section 6.3. The sources have an identical carrier frequency of 2 GHz and bandwidth of 100 MHz and are designed accordingly to (6.12) so that they are uncorrelated within each observation window. The transmitted signals are generated in the same way as in Section 6.3. For each observation period, there are $N = 4$ snapshots. The signals are identical for all observation periods and are assumed to be known at the receiver. The noise at the array is assumed to be AWGN. The receiver is a 11-element ULA with inter-element spacing $\delta = \lambda_c/2$ where $\lambda_c$ is the wavelength of the carrier frequency. The received signal is converted into $Q = 32$ narrowband frequency bins using DFT.

#### 7.3.2.1 Resolution of Correlated Signals

We illustrate the ability of M-CFSSM to resolve different arrival paths that are not well-separated in time by using data collected from different observation periods in a time-varying channel. The complex gains in the different observation periods are assumed to be independent and are modeled as complex random variables. The amplitudes of the random variables are Rayleigh distributed and the phases are uniformly distributed between $0$ and $2\pi$. We set the total number of observation periods to $O = 10$.

We will consider two mulitpaths arising from the same source which are not well separated in time: $\theta_1^{(1)} = 21°$, $\theta_2^{(1)} = 28°$ and $\tau_1^{(1)} = 0T$, $\tau_2^{(1)} = 0.2T$. For fair comparison, we normalize the powers of the two paths so that the averaged received SNRs of the two paths are equal. The SNRs of the paths are set to $4$ dB. Figure 7.8 shows the spatial spectrum from ten independent trials of the time-varying channel. Figure 7.9 shows the spatial spectrum from ten independent trials of the time-invariant channel where the channel gains are constant for all observation periods. For ease of reference, the true DOAs are indicated by the vertical lines in both figures.

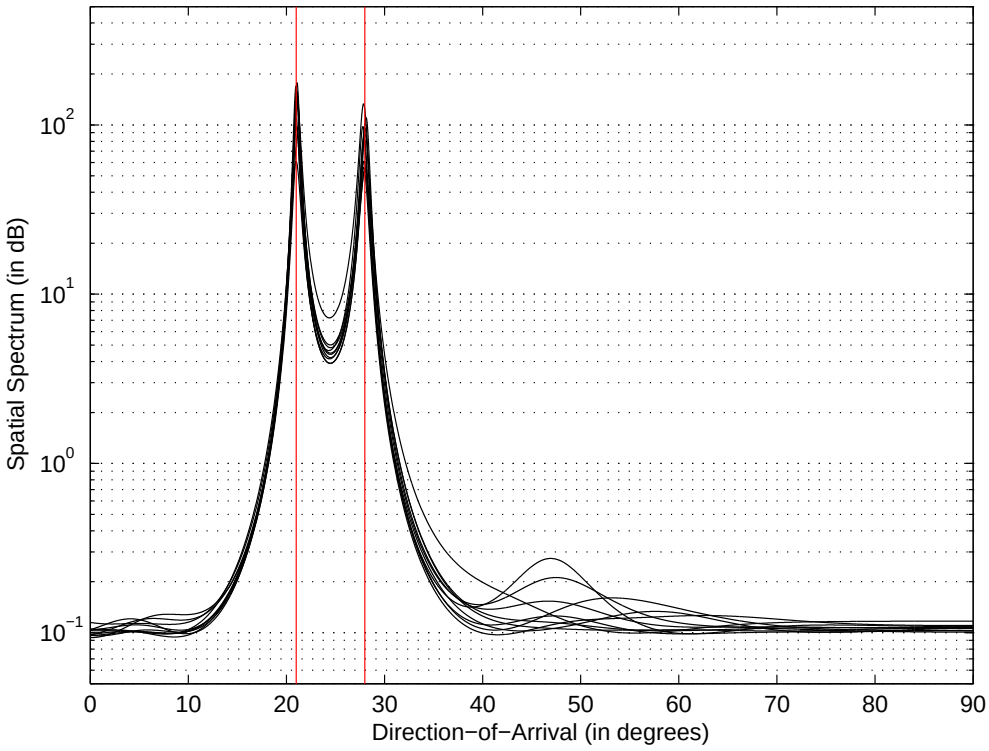


Figure 7.8: Spatial periodogram for time-varying channel

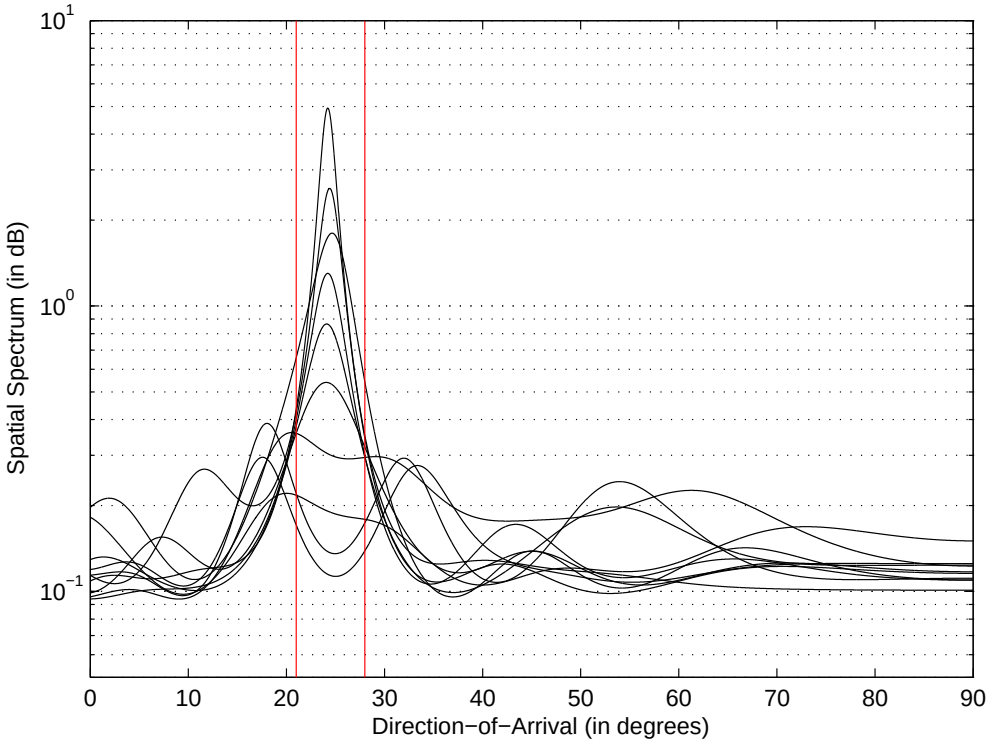


Figure 7.9: Spatial periodogram for time-invariant channel

By comparing Figure 7.8 and Figure 7.9, we can see that the two DOAs are separated and accurately estimated in the time-varying channel but not in the time-invariant channel. Note that the peaks in Figure 7.9 (if there are distinct peaks), are relatively smaller in magnitude and less distinct than those in Figure 7.8. This shows that in a time-invariant channel, the two DOAs cannot be accurately estimated without more pre-processing such as using spatial smoothing [108, 109]. The time-varying channel characteristics, introducing diversity gain, allows the separation of multipaths that are not well separated in time.

We plot the statistical estimation performance of the proposed method in Figure 7.10 for different number of observation periods. The results are obtained through Monte Carlo simulation of $2000$ independent trials. With an increase of number of observation periods, the RMSE performance becomes better across all SNRs.

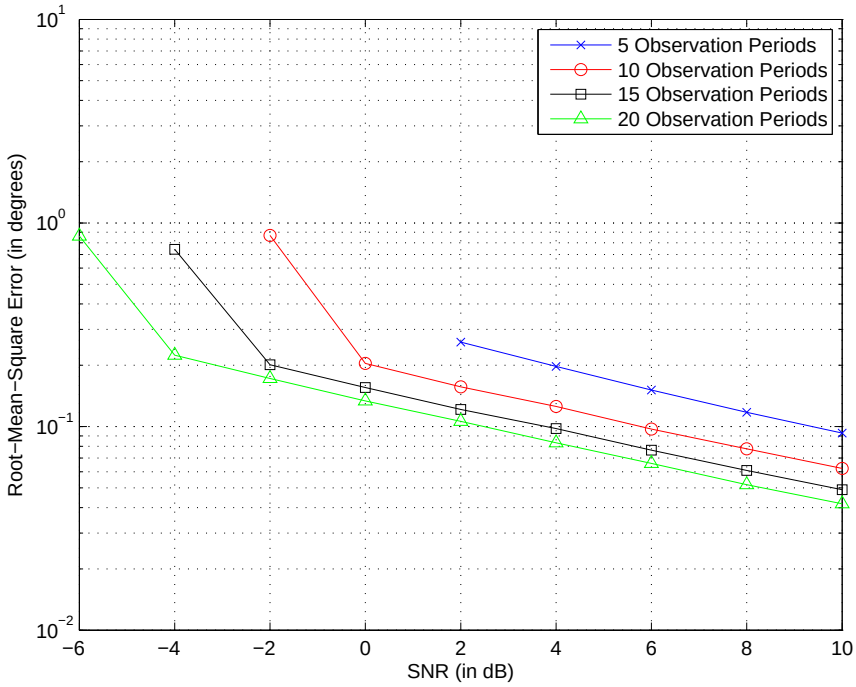


Figure 7.10: RMSE performance against SNR for varying number of observation periods

#### 7.3.2.2 Diversity Gains

Next we investigate the benefits of the diversity gains under time-varying channel characteristics. Diversity gain is defined as the ratio of the signal strength obtained by averaging over the multipaths to the signal strength obtained by a single path. We consider two arrival paths with a angle separation of $7^\circ$ from a single source that are well separated in time with the following parameters: $\tau_1^{(1)} = 0T$ and $\tau_2^{(1)} = 6.2T$. The number of observation periods is set to $O = 10$. Unlike previous simulation where we normalize the channel gain, we set the expected received SNR which in turn determines the expected variance of the complex gain. The expected variance is then used to generate the different complex gains randomly. The expected variances of the gains of both paths are set to be the same. We set the number of snapshots to $N = 4$.

In Figure 7.11, we compare the RMSE in both time-varying and time-invariant channels. The RMSE performance is averaged over two paths and is obtained through Monte Carlo simulation of $2000$ independent trials. From Figure 7.11, we can see that with the diversity gain from the time-varying channel, the RMSE is much lower compared to

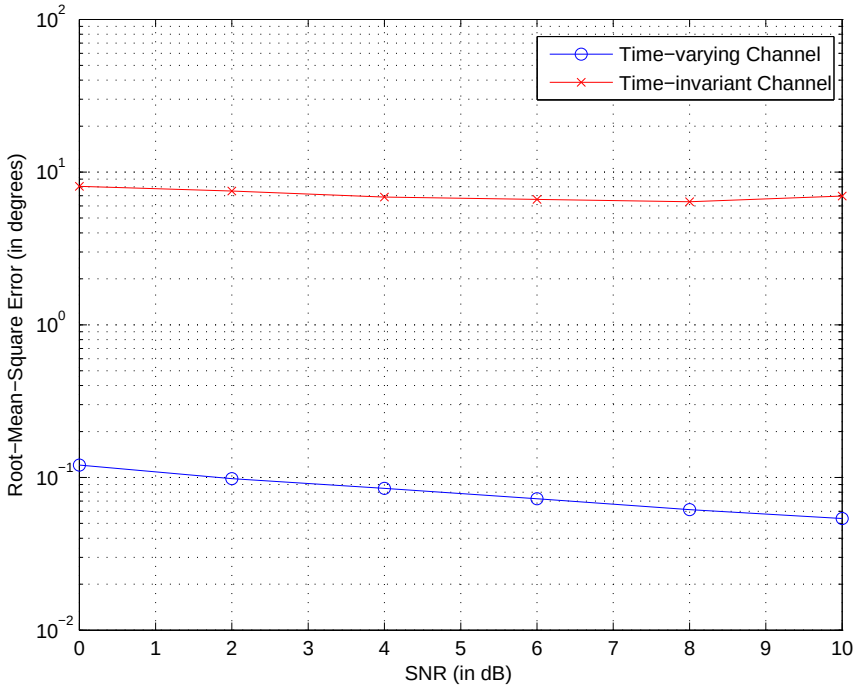


Figure 7.11: RMSE performance against SNR

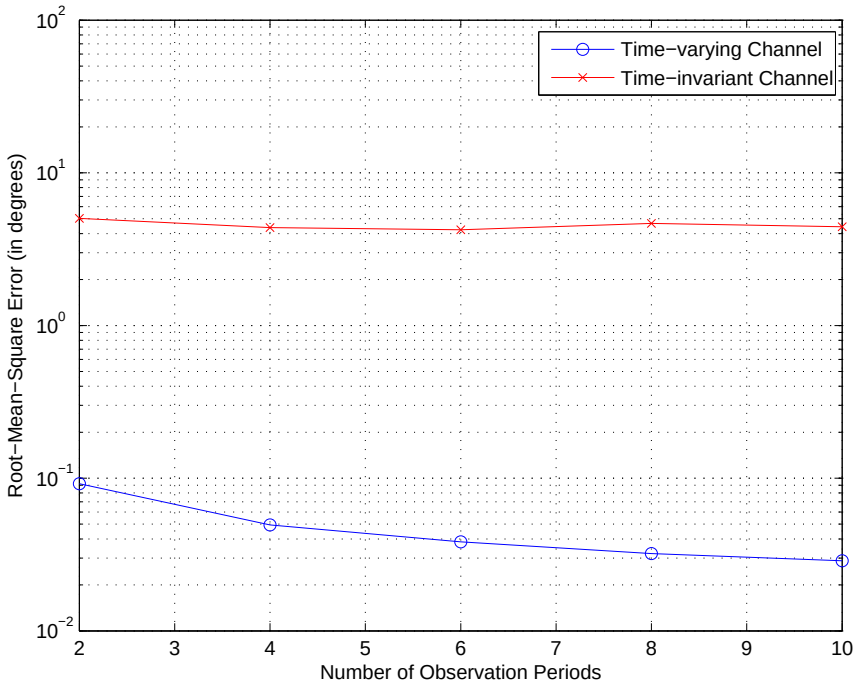


Figure 7.12: RMSE performance against number of observation periods

that of time-invariant channel.

In Figure 7.12, we investigate the effect of number of observation periods at the

expected SNR of $10$ dB. Note that with increasing number of observation periods, the RMSE decreases for the time-varying channel. This is because the diversity increases with the number of observation periods. Conversely, for the time-invariant channel, the increase in number of observation periods has little or no effect on the RMSE performance since there is no diversity gain.

## 7.4 Conclusion

From our preceding discussions, we identified two key differences affecting DOA estimation performance between time-invariant and time-varying channels. The first is the availability of time diversity which makes the estimation more robust against fading. The second is the decorrelation of correlated signals which is useful in the separation of the DOAs of these signals. The proposed algorithms when extended to multiple observation periods, were able to latch on to these two benefits to provide more robust DOA estimation as shown in the various simulation results.

# Chapter 8

# Conclusion

## 8.1 Contributions

In this thesis, two DOA estimation methods for narrowband signals using multiple sensors are presented. They are the PAS and the PASI techniques. In addition, two DOA estimation methods for wideband signals using multiple sensors are proposed. They are the CFSSM and the M-CFSSM.

The proposed PAS technique is developed to overcome the problem of multipath propagation. The technique characterizes each impinging plane wave at the array, where some of the plane waves may come from the same source. To decorrelate signal coherence among the impinging plane waves, the array is divided into overlapping subarrays and correlated with the pilot signals of the desired source. This process is equivalent to forward spatial smoothing. The proposed PAS technique has significant advantages over existing algorithms in terms of performance. In the case of uncorrelated signals, it is robust and has the ability to resolve closely-spaced DOAs of uncorrelated incident signals. It does not require large number of antennas to achieve performance close to the CRLB, hence the cost of hardware implementation is greatly reduced. In the case of correlated signals, the PAS technique exhibits performance close to the CRLB from $5$ dB onwards, regardless of array size. To further improve the performance of the PAS technique in the low SNR region for correlated signals, the proposed PASI technique is developed by including an additional iterative procedure to the PAS technique. With the iterative procedure, it is able to achieve RMSE much closer to the CRLB and is the

best performing algorithm among those algorithms being compared. Moreover, only a small number of iterations is required, without much increase in complexity. For both proposed techniques, the array size is no longer bounded by the total number of impinging plane waves at the array. Instead it is constrained by twice the maximum number of impinging wavefronts of the sources (see (4.34)). This greatly reduces the overall array size.

The proposed CFSSM takes a different approach from conventional coherent signal subspace methods to estimate the DOAs of wideband signals. It does not require the use of any focusing matrix which needs initial DOA estimates, usually provided by low-resolution estimators. Instead the proposed CFSSM exploits the structure of the combined correlation matrices of all frequencies bins. The resulting structure is of a similar form to the conventional narrowband model. The signal subspace and hence the DOAs can be estimated by existing narrowband techniques such as MUSIC and ESPRIT. The proposed CFSSM works well for both uncorrelated and correlated signals. It has significantly lower computational load compared to existing algorithms that use focusing matrices. Moreover, it can work in tandem with existing algorithms using focusing matrices by providing high-resolution initial DOA estimates. In the case where pilot signals are available, the proposed M-CFSSM is modified from the proposed CFSSM. The detection performance of the proposed M-CFSSM is robust at low SNRs for both uncorrelated and correlated signals. The estimation performance of the proposed M-CFSSM is also close to the CRLB at low SNRs. Moreover, the proposed M-CFSSM exhibits small estimation bias for SNRs as low as $0$ dB.

The proposed algorithms PAS, PASI and M-CFSSM are extended to time-varying channels. Numerical simulation shows that the proposed algorithms are able to utilize time diversity and gain diversity to provide robust DOA estimation.

## 8.2 Future Work

Several directions for future work are suggested. First, the performance of the proposed CFSSM is comparable to existing techniques. However, its performance is likely to be improved if spatial smoothing is applied for the case of correlated signals. Investigations can be carried out to study the effects of spatial smoothing to the proposed CFSSM.

Second, we assume that the multiple observations are independent to one another. However, in practice, this is generally not the case. The correlation between multiple observations are determined by the relative speed between the receiver and the transmitter [107]. We can study the performance of the proposed algorithms under real-time fading.

Third, pilot signals are used in the DOA estimation. In situations where pilot signals are not available, decision-directed estimation of DOAs can be performed using estimated transmitted signals. We can investigate the performance of the proposed algorithms with the use of estimated transmitted signals which are not entirely reliable as a result of noisy received signals. Possible extension of the proposed algorithms can be added to take into account the use of such unreliable reference signals.

# Appendix A

# Derivation of CFSSM Structure

Recall from Section 2.4.2, the received signal for the decomposed narrowband frequency $f_q$ can be written in the conventional matrix notation:

$$\mathbf{Y}(q) = \mathbf{A}(q)\,\mathbf{\Lambda X}(q) + \mathbf{W}(q) \tag{A.1}$$

and the corresponding correlation matrix is given by:

$$\begin{aligned}
\mathbf{R}_y(q) &= \mathrm{E}\left[\mathbf{Y}(q)\,\mathbf{Y}^H(q)\right] \\
&= \mathrm{E}\left[\mathbf{A}(q,\boldsymbol{\theta})\,\mathbf{\Lambda X}(q)\,\mathbf{X}^H(q)\,\mathbf{\Lambda}^H\mathbf{A}^H(q,\boldsymbol{\theta})\right] + \mathbf{\Sigma}(q) \\
&= \mathbf{A}(q,\boldsymbol{\theta})\,\mathbf{\Lambda}\mathrm{E}\left[\mathbf{X}(q)\,\mathbf{X}^H(q)\right]\mathbf{\Lambda}^H\mathbf{A}^H(q,\boldsymbol{\theta}) + \mathbf{\Sigma}(q) \\
&= \mathbf{A}(q,\boldsymbol{\theta})\,\mathbf{R}_x(q)\,\mathbf{A}^H(q,\boldsymbol{\theta}) + \mathbf{\Sigma}(q)
\end{aligned} \tag{A.2}$$

## Uncorrelated Signals

For $K$ uncorrelated signals (assuming each source has only $1$ impinging plane wave at the array),

$$\mathbf{R}_x(q) = \begin{bmatrix} \left|\alpha^{(1)}\right|^2 & 0 & \cdots & 0 \\ 0 & \left|\alpha^{(2)}\right|^2 & \cdots & 0 \\ \vdots & \vdots & \ddots & \vdots \\ 0 & 0 & \cdots & \left|\alpha^{(K)}\right|^2 \end{bmatrix} \tag{A.3}$$

Substituting into (A.2), we can write element in the $i^{\text{th}}$ row and $l^{\text{th}}$ column of $\mathbf{R}_y\left(q\right)$ as:

$$\begin{aligned}
\left[\mathbf{R}_y\left(q\right)\right]_{il} &= \sum_{k=1}^{K}\left|\alpha^{(k)}\right|^2 e^{-j2\pi\left(f_c+\frac{q}{Q}B\right)\left(\tau^{(k)}+\frac{(i-1)\delta}{c}\sin\theta^{(k)}\right)} e^{j2\pi\left(f_c+\frac{q}{Q}B\right)\left(\tau^{(k)}+\frac{(l-1)\delta}{c}\sin\theta^{(k)}\right)} \\
&= \sum_{k=1}^{K}\left|\alpha^{(k)}\right|^2 e^{-j2\pi\left(f_c+\frac{q}{Q}B\right)\left(\frac{(i-1)\delta}{c}\sin\theta^{(k)}-\frac{(l-1)\delta}{c}\sin\theta^{(k)}\right)} \\
&= \sum_{k=1}^{K}\left|\alpha^{(k)}\right|^2 e^{-j2\pi\left(f_c+\frac{q}{Q}B\right)\left(\frac{(i-l)\delta}{c}\sin\theta^{(k)}\right)} \\
&= \sum_{k=1}^{K}\left|\alpha^{(k)}\right|^2 e^{-j2\pi f_c\left(\frac{(i-l)\delta}{c}\sin\theta^{(k)}\right)} e^{-j2\pi\frac{q}{Q}B\left(\frac{(i-l)\delta}{c}\sin\theta^{(k)}\right)} \\
&= \sum_{k=1}^{K}\left|\alpha^{(k)}\right|^2 e^{-j2\pi\frac{(i-l)\delta}{\lambda_c}\sin\theta^{(k)}} e^{-j2\pi\frac{(i-l)\delta}{\lambda_c}\frac{q}{Q}B_f\sin\theta^{(k)}} \\
&= \sum_{k=1}^{K}\left|\alpha^{(k)}\right|^2 e^{-j2\pi\frac{(i-l)\delta}{\lambda_c}\left(1+\frac{q}{Q}B_f\right)\sin\theta^{(k)}}
\end{aligned} \tag{A.4}$$

Summing the elements across the different frequency bins, we get:

$$\begin{aligned}
\sum_{q=0}^{Q-1}\left[\mathbf{R}_y\left(q\right)\right]_{il} &= \sum_{q=0}^{Q-1}\sum_{k=1}^{K}\left|\alpha^{(k)}\right|^2 e^{-j2\pi\frac{(i-l)\delta}{\lambda_c}\left(1+\frac{q}{Q}B_f\right)\sin\theta^{(k)}} \\
&= \sum_{k=1}^{K}\left|\alpha^{(k)}\right|^2 e^{-j2\pi\frac{(i-l)\delta}{\lambda_c}\sin\theta^{(k)}}\sum_{q=0}^{Q-1} e^{-j2\pi\frac{(i-l)\delta}{\lambda_c}\frac{q}{Q}B_f\sin\theta^{(k)}} \\
&= \sum_{k=1}^{K}\left|\alpha^{(k)}\right|^2 e^{-j2\pi\frac{(i-l)\delta}{\lambda_c}\sin\theta^{(k)}}\mathrm{GP}_{sum}
\end{aligned} \tag{A.5}$$

The sum of geometric progression given as $\mathrm{GP}_{sum}$ can be evaluated as:

$$\begin{aligned}
\mathrm{GP}_{sum} &= \sum_{q=0}^{Q-1} e^{-j2\pi \frac{(i-l)\delta}{\lambda_c} \frac{q}{Q} B_f \sin\theta^{(k)}} \\
&= \frac{1 - \left[e^{-j2\pi \frac{(i-l)\delta}{\lambda_c} \frac{1}{Q} B_f \sin\theta^{(k)}}\right]^Q}{1 - e^{-j2\pi \frac{(i-l)\delta}{\lambda_c} \frac{1}{Q} B_f \sin\theta^{(k)}}} \\
&= \frac{1 - e^{-j2\pi \frac{(i-l)\delta}{\lambda_c} B_f \sin\theta^{(k)}}}{1 - e^{-j2\pi \frac{(i-l)\delta}{Q\lambda_c} B_f \sin\theta^{(k)}}} \\
&= \frac{e^{-j\pi \frac{(i-l)\delta}{\lambda_c} B_f \sin\theta^{(k)}} \left[e^{j\pi \frac{(i-l)\delta}{\lambda_c} B_f \sin\theta^{(k)}} - e^{-j\pi \frac{(i-l)\delta}{\lambda_c} B_f \sin\theta^{(k)}}\right]}{e^{-j\pi \frac{(i-l)\delta}{Q\lambda_c} B_f \sin\theta^{(k)}} \left[e^{j\pi \frac{(i-l)\delta}{Q\lambda_c} B_f \sin\theta^{(k)}} - e^{-j\pi \frac{(i-l)\delta}{Q\lambda_c} B_f \sin\theta^{(k)}}\right]} \\
&= e^{-j2\pi \frac{(i-l)\delta}{\lambda_c} \left(\frac{Q-1}{2Q}\right) B_f \sin\theta^{(k)}} \frac{\sin\left(\pi \frac{(i-l)\delta}{\lambda_c} B_f \sin\theta^{(k)}\right)}{\sin\left(j\pi \frac{(i-l)\delta}{Q\lambda_c} B_f \sin\theta^{(k)}\right)} \\
&= e^{-j2\pi \frac{(i-l)\delta}{\lambda_c} \left(\frac{Q-1}{2Q}\right) B_f \sin\theta^{(k)}} F_1\left(i-l, \theta^{(k)}\right) \qquad \text{(A.6)}
\end{aligned}$$

where

$$F_1\left(i-l, \theta^{(k)}\right) = \frac{\sin\left(\pi \frac{(i-l)\delta}{\lambda_c} B_f \sin\theta^{(k)}\right)}{\sin\left(j\pi \frac{(i-l)\delta}{Q\lambda_c} B_f \sin\theta^{(k)}\right)} \qquad \text{(A.7)}$$

For $\frac{\delta}{\lambda_c} B_f \sin\theta^{(k)} << 1$ ($\frac{\delta}{\lambda_c}$ is usually in the magnitude of $\approx 1/2$), $F_1\left(i-l, \theta^{(k)}\right) \approx 1$ for $i, l = 1, 2, \ldots, M$, thus the element in the $i^{\text{th}}$ row and $l^{\text{th}}$ column simplifies to:

$$\mathrm{GP}_{sum} \approx e^{-j2\pi \frac{(i-l)\delta}{\lambda_c} \left(\frac{Q-1}{2Q}\right) B_f \sin\theta^{(k)}} \qquad \text{(A.8)}$$

Consequently,

$$\begin{aligned}
[\mathbf{R}_y]_{il} &= \sum_{q=0}^{Q-1} [\mathbf{R}_y(q)]_{il} \\
&= \sum_{k=1}^{K} \left|\alpha^{(k)}\right|^2 e^{-j2\pi\frac{(i-l)\delta}{\lambda_c}\sin\theta^{(k)}} \mathrm{GP}_{sum} \\
&\approx \sum_{k=1}^{K} \left|\alpha^{(k)}\right|^2 e^{-j2\pi\frac{(i-l)\delta}{\lambda_c}\sin\theta^{(k)}} e^{-j2\pi\frac{(i-l)\delta}{\lambda_c}\left(\frac{Q-1}{2Q}\right)B_f\sin\theta^{(k)}} \\
&= \sum_{k=1}^{K} \left|\alpha^{(k)}\right|^2 e^{-j2\pi\frac{\delta}{\lambda_c}(i-l)\left(1+\frac{Q-1}{2Q}B_f\right)\sin\theta^{(k)}}
\end{aligned} \tag{A.9}$$

Hence the combined correlation matrix $\mathbf{R}_y$ can be written as:

$$\mathbf{R}_y = \mathbf{A}(\boldsymbol{\theta})\,\mathbf{R}_x\mathbf{A}^H(\boldsymbol{\theta}) + \boldsymbol{\Sigma} \tag{A.10}$$

where

$$\mathbf{A}(\boldsymbol{\theta}) = \left[\begin{array}{cccc} \mathbf{a}\left(\theta^{(1)}\right) & \mathbf{a}\left(\theta^{(2)}\right) & \cdots & \mathbf{a}\left(\theta^{(K)}\right) \end{array}\right] \tag{A.11}$$

with each column of (A.11) given by:

$$\mathbf{a}\left(\theta^{(k)}\right) = \left[\begin{array}{cccc} 1 & e^{-j\phi^{(k)}} & \cdots & e^{-j(M-1)\phi^{(k)}} \end{array}\right]^T \tag{A.12}$$

and

$$\phi^{(k)} = 2\pi\frac{\delta}{\lambda_c}\left(1+\frac{Q-1}{2Q}B_f\right)\sin\theta^{(k)} \tag{A.13}$$

# Correlated Signals

Considering $K = 1$ source with $P_1 = 2$ multipaths,

$$\mathbf{R}_x(q) = \begin{bmatrix} |\alpha_1|^2 & \alpha_1\alpha_2^* \\ \alpha_2\alpha_1^* & |\alpha_2|^2 \end{bmatrix} \tag{A.14}$$

The element in the $i^{\text{th}}$ row and $l^{\text{th}}$ column of the noiseless correlation matrix of the $q^{\text{th}}$ frequency bin is then given as:

$$\begin{aligned}
[\mathbf{R}_y(q)]_{il} &= |\alpha_1|^2 e^{-j2\pi(i-l)\frac{\delta}{\lambda_c}\sin\theta_1} e^{-j2\pi(i-l)\frac{\delta}{\lambda_c}\frac{q}{Q}B_f\sin\theta_1} \\
&\quad + \Big\{\alpha_1^*\alpha_2 e^{-j2\pi f_c(\tau_2-\tau_1)} e^{-j2\pi\frac{\delta}{\lambda_c}[(i-1)\sin\theta_2-(l-1)\sin\theta_1]} \\
&\quad \times e^{-j2\pi\frac{q}{Q}B(\tau_2-\tau_1)} e^{-j2\pi\frac{\delta}{\lambda_c}\frac{q}{Q}B_f[(i-1)\sin\theta_2-(l-1)\sin\theta_1]}\Big\} \\
&\quad + \Big\{\alpha_1\alpha_2^* e^{j2\pi f_c(\tau_2-\tau_1)} e^{j2\pi\frac{\delta}{\lambda_c}[(l-1)\sin\theta_2-(i-1)\sin\theta_1]} \\
&\quad \times e^{j2\pi\frac{q}{Q}B(\tau_2-\tau_1)} e^{j2\pi\frac{\delta}{\lambda_c}\frac{q}{Q}B_f[(l-1)\sin\theta_2-(i-1)\sin\theta_1]}\Big\} \\
&\quad + |\alpha_2|^2 e^{-j2\pi(i-l)\frac{\delta}{\lambda_c}\sin\theta_2} e^{-j2\pi(i-l)\frac{\delta}{\lambda_c}\frac{q}{Q}B_f\sin\theta_2} \\
&= |\alpha_1|^2 e^{-j2\pi(i-l)\frac{\delta}{\lambda_c}\left(1+\frac{q}{Q}B_f\right)\sin\theta_1} \\
&\quad + \alpha_1^*\alpha_2 e^{-j2\pi\left(f_c+\frac{q}{Q}B\right)(\tau_2-\tau_1)} e^{-j2\pi\frac{\delta}{\lambda_c}\left(1+\frac{q}{Q}B_f\right)[(i-1)\sin\theta_2-(l-1)\sin\theta_1]} \\
&\quad + \alpha_1\alpha_2^* e^{j2\pi\left(f_c+\frac{q}{Q}B\right)(\tau_2-\tau_1)} e^{j2\pi\frac{\delta}{\lambda_c}\left(1+\frac{q}{Q}B_f\right)[(l-1)\sin\theta_2-(i-1)\sin\theta_1]} \\
&\quad + |\alpha_2|^2 e^{-j2\pi(i-l)\frac{\delta}{\lambda_c}\left(1+\frac{q}{Q}B_f\right)\sin\theta_2}
\end{aligned} \tag{A.15}$$

Summing the various correlation matrices together as in (5.11) results in the summation of the individual elements across the different frequency bins. Hence,

$$\begin{aligned}
[\mathbf{R}_y]_{il} &= \sum_{q=0}^{Q-1} [\mathbf{R}_y(q)]_{il} \\
&= \underbrace{\sum_{q=0}^{Q-1} |\alpha_1|^2 e^{-j2\pi(i-l)\frac{\delta}{\lambda_c}\left(1+\frac{q}{Q}B_f\right)\sin\theta_1}}_{\text{Exp1}}
\end{aligned}$$

$$
\begin{aligned}
&+ \underbrace{\sum_{q=0}^{Q-1} \alpha_1^* \alpha_2 e^{-j2\pi\left(f_c+\frac{q}{Q}B\right)(\tau_2-\tau_1)} e^{-j2\pi\frac{\delta}{\lambda_c}\left(1+\frac{q}{Q}B_f\right)[(i-1)\sin\theta_2-(l-1)\sin\theta_1]}}_{\text{Exp2}} \\
&+ \underbrace{\sum_{q=0}^{Q-1} \alpha_1 \alpha_2^* e^{j2\pi\left(f_c+\frac{q}{Q}B\right)(\tau_2-\tau_1)} e^{j2\pi\frac{\delta}{\lambda_c}\left(1+\frac{q}{Q}B_f\right)[(l-1)\sin\theta_2-(i-1)\sin\theta_1]}}_{\text{Exp3}} \\
&+ \underbrace{\sum_{q=0}^{Q-1} |\alpha_2|^2 \, e^{-j2\pi(i-l)\frac{\delta}{\lambda_c}\left(1+\frac{q}{Q}B_f\right)\sin\theta_2}}_{\text{Exp4}}
\end{aligned}
\tag{A.16}
$$

Evaluating the first expression in (A.16), we get:

$$
\begin{aligned}
\text{Exp1} &= \sum_{q=0}^{Q-1} |\alpha_1|^2 \, e^{-j2\pi(i-l)\frac{\delta}{\lambda_c}\left(1+\frac{q}{Q}B_f\right)\sin\theta_1} \\
&= |\alpha_1|^2 \, e^{-j2\pi(i-l)\frac{\delta}{\lambda_c}\sin\theta_1} \sum_{q=0}^{Q-1} e^{-j2\pi(i-l)\frac{\delta}{\lambda_c}\frac{q}{Q}B_f\sin\theta_1} \\
&= |\alpha_1|^2 \, e^{-j2\pi(i-l)\frac{\delta}{\lambda_c}\sin\theta_1} \frac{1-\left[e^{-j2\pi(i-l)\frac{\delta}{\lambda_c}\frac{1}{Q}B_f\sin\theta_1}\right]^Q}{1-e^{-j2\pi(i-l)\frac{\delta}{\lambda_c}\frac{1}{Q}B_f\sin\theta_1}} \\
&= |\alpha_1|^2 \, e^{-j2\pi(i-l)\frac{\delta}{\lambda_c}\sin\theta_1} \frac{1-e^{-j2\pi(i-l)\frac{\delta}{\lambda_c}B_f\sin\theta_1}}{1-e^{-j2\pi(i-l)\frac{\delta}{\lambda_c}\frac{1}{Q}B_f\sin\theta_1}} \\
&= \Bigg\{ |\alpha_1|^2 \, e^{-j2\pi(i-l)\frac{\delta}{\lambda_c}\sin\theta_1} \\
&\quad \times \frac{e^{-j\pi(i-l)\frac{\delta}{\lambda_c}B_f\sin\theta_1}\left[e^{j\pi(i-l)\frac{\delta}{\lambda_c}B_f\sin\theta_1} - e^{-j\pi(i-l)\frac{\delta}{\lambda_c}B_f\sin\theta_1}\right]}{e^{-j\pi(i-l)\frac{\delta}{\lambda_c}\frac{1}{Q}B_f\sin\theta_1}\left[e^{j\pi(i-l)\frac{\delta}{\lambda_c}\frac{1}{Q}B_f\sin\theta_1} - e^{-j\pi(i-l)\frac{\delta}{\lambda_c}\frac{1}{Q}B_f\sin\theta_1}\right]} \Bigg\} \\
&= \Bigg\{ |\alpha_1|^2 \, e^{-j2\pi(i-l)\frac{\delta}{\lambda_c}\sin\theta_1} e^{-j\pi(i-l)\frac{\delta}{\lambda_c}\left(1-\frac{1}{Q}\right)B_f\sin\theta_1} \\
&\quad \times \frac{\sin\left(\pi\,(i-l)\,\frac{\delta}{\lambda_c}B_f\sin\theta_1\right)}{\sin\left(\pi\,(i-l)\,\frac{\delta}{\lambda_c}\frac{1}{Q}B_f\sin\theta_1\right)} \Bigg\} \\
&= |\alpha_1|^2 \, e^{-j2\pi(i-l)\frac{\delta}{\lambda_c}\left(1+\frac{Q-1}{2Q}\right)\sin\theta_1} \frac{\sin\left(\pi\,(i-l)\,\frac{\delta}{\lambda_c}B_f\sin\theta_1\right)}{\sin\left(\pi\,(i-l)\,\frac{\delta}{\lambda_c}\frac{1}{Q}B_f\sin\theta_1\right)}
\end{aligned}
\tag{A.17}
$$

The second expression is given by:

$$
\begin{aligned}
\text{Exp2} &= \sum_{q=0}^{Q-1} \alpha_1^* \alpha_2 e^{-j2\pi\left(f_c+\frac{q}{Q}B\right)(\tau_2-\tau_1)} e^{-j2\pi\frac{\delta}{\lambda_c}\left(1+\frac{q}{Q}B_f\right)[(i-1)\sin\theta_2-(l-1)\sin\theta_1]} \\
&= \alpha_1^* \alpha_2 e^{-j2\pi f_c(\tau_2-\tau_1)} e^{-j2\pi\frac{\delta}{\lambda_c}[(i-1)\sin\theta_2-(l-1)\sin\theta_1]} \sum_{q=0}^{Q-1} e^{-j2\pi\frac{q}{Q}B(\tau_2-\tau_1)} e^{-j2\pi\frac{\delta}{\lambda_c}\frac{q}{Q}B_f[(i-1)\sin\theta_2-(l-1)\sin\theta_1]} \\
&= \left\{ \alpha_1^* \alpha_2 e^{-j2\pi\left[f_c(\tau_2-\tau_1)+\frac{\delta}{\lambda_c}[(i-1)\sin\theta_2-(l-1)\sin\theta_1]\right]} e^{-j\pi\frac{(Q-1)}{Q}\left\{B(\tau_2-\tau_1)+\frac{\delta}{\lambda_c}B_f[(i-1)\sin\theta_2-(l-1)\sin\theta_1]\right\}} \right. \\
&\quad \left. \times \frac{\sin\left(\pi\left\{B\left(\tau_2-\tau_1\right)+\frac{\delta}{\lambda_c}B_f\left[(i-1)\sin\theta_2-(l-1)\sin\theta_1\right]\right\}\right)}{\sin\left(\frac{\pi}{Q}\left\{B\left(\tau_2-\tau_1\right)+\frac{\delta}{\lambda_c}B_f\left[(i-1)\sin\theta_2-(l-1)\sin\theta_1\right]\right\}\right)} \right\}
\end{aligned}
\tag{A.18}
$$

since

$$
\begin{aligned}
\sum_{q=0}^{Q-1} e^{-j2\pi\frac{q}{Q}B(\tau_2-\tau_1)} e^{-j2\pi\frac{\delta}{\lambda_c}\frac{q}{Q}B_f[(i-1)\sin\theta_2-(l-1)\sin\theta_1]} &= \frac{1-\left\{e^{-j2\pi\frac{1}{Q}B(\tau_2-\tau_1)} e^{-j2\pi\frac{\delta}{\lambda_c}\frac{1}{Q}B_f[(i-1)\sin\theta_2-(l-1)\sin\theta_1]}\right\}^Q}{1-e^{-j2\pi\frac{1}{Q}B(\tau_2-\tau_1)} e^{-j2\pi\frac{\delta}{\lambda_c}\frac{1}{Q}B_f[(i-1)\sin\theta_2-(l-1)\sin\theta_1]}} \\
&= \frac{1-e^{-j2\pi\left\{B(\tau_2-\tau_1)+\frac{\delta}{\lambda_c}B_f[(i-1)\sin\theta_2-(l-1)\sin\theta_1]\right\}}}{1-e^{-j\frac{2\pi}{Q}\left\{B(\tau_2-\tau_1)+\frac{\delta}{\lambda_c}B_f[(i-1)\sin\theta_2-(l-1)\sin\theta_1]\right\}}}
\end{aligned}
$$

$$
\begin{aligned}
&= \left\{ \frac{e^{-j\pi\left\{B(\tau_2-\tau_1)+\frac{\delta}{\lambda_c}B_f[(i-1)\sin\theta_2-(l-1)\sin\theta_1]\right\}}}{e^{-j\frac{\pi}{Q}\left\{B(\tau_2-\tau_1)+\frac{\delta}{\lambda_c}B_f[(i-1)\sin\theta_2-(l-1)\sin\theta_1]\right\}}} \times \right. \\
&\left. \frac{\left[e^{j\pi\left\{B(\tau_2-\tau_1)+\frac{\delta}{\lambda_c}B_f[(i-1)\sin\theta_2-(l-1)\sin\theta_1]\right\}} - e^{-j\pi\left\{B(\tau_2-\tau_1)+\frac{\delta}{\lambda_c}B_f[(i-1)\sin\theta_2-(l-1)\sin\theta_1]\right\}}\right]}{\left[e^{j\frac{\pi}{Q}\left\{B(\tau_2-\tau_1)+\frac{\delta}{\lambda_c}B_f[(i-1)\sin\theta_2-(l-1)\sin\theta_1]\right\}} - e^{-j\frac{\pi}{Q}\left\{B(\tau_2-\tau_1)+\frac{\delta}{\lambda_c}B_f[(i-1)\sin\theta_2-(l-1)\sin\theta_1]\right\}}\right]} \right\} \\
&= e^{-j\pi\left(1-\frac{1}{Q}\right)\left\{B(\tau_2-\tau_1)+\frac{\delta}{\lambda_c}B_f[(i-1)\sin\theta_2-(l-1)\sin\theta_1]\right\}} \frac{\sin\left(\pi\left\{B\left(\tau_2-\tau_1\right)+\frac{\delta}{\lambda_c}B_f\left[(i-1)\sin\theta_2-(l-1)\sin\theta_1\right]\right\}\right)}{\sin\left(\frac{\pi}{Q}\left\{B\left(\tau_2-\tau_1\right)+\frac{\delta}{\lambda_c}B_f\left[(i-1)\sin\theta_2-(l-1)\sin\theta_1\right]\right\}\right)} \\
&= e^{-j\pi\frac{(Q-1)}{Q}\left\{B(\tau_2-\tau_1)+\frac{\delta}{\lambda_c}B_f[(i-1)\sin\theta_2-(l-1)\sin\theta_1]\right\}} \frac{\sin\left(\pi\left\{B\left(\tau_2-\tau_1\right)+\frac{\delta}{\lambda_c}B_f\left[(i-1)\sin\theta_2-(l-1)\sin\theta_1\right]\right\}\right)}{\sin\left(\frac{\pi}{Q}\left\{B\left(\tau_2-\tau_1\right)+\frac{\delta}{\lambda_c}B_f\left[(i-1)\sin\theta_2-(l-1)\sin\theta_1\right]\right\}\right)}
\end{aligned}
\tag{A.19}
$$

Following the derivation for the second expression, the third expression can be evaluated as:

$$
\begin{aligned}
\text{Exp3} &= \sum_{q=0}^{Q-1} \alpha_1\alpha_2^* e^{j2\pi\left(f_c+\frac{q}{Q}B\right)(\tau_2-\tau_1)} e^{j2\pi\frac{\delta}{\lambda_c}\left(1+\frac{q}{Q}B_f\right)[(l-1)\sin\theta_2-(i-1)\sin\theta_1]} \\
&= \left\{ \alpha_1\alpha_2^* e^{j2\pi\left[f_c(\tau_2-\tau_1)+\frac{\delta}{\lambda_c}[(l-1)\sin\theta_2-(i-1)\sin\theta_1]\right]} e^{j\pi\frac{(Q-1)}{Q}\left\{B(\tau_2-\tau_1)+\frac{\delta}{\lambda_c}B_f[(l-1)\sin\theta_2-(i-1)\sin\theta_1]\right\}} \right. \\
&\quad \left. \times \frac{\sin\left(\pi\left\{B\left(\tau_2-\tau_1\right)+\frac{\delta}{\lambda_c}B_f\left[(l-1)\sin\theta_2-(i-1)\sin\theta_1\right]\right\}\right)}{\sin\left(\frac{\pi}{Q}\left\{B\left(\tau_2-\tau_1\right)+\frac{\delta}{\lambda_c}B_f\left[(l-1)\sin\theta_2-(i-1)\sin\theta_1\right]\right\}\right)} \right\}
\end{aligned}
\tag{A.20}
$$

The last expression is similar to the first equation and can be evaluated as:

$$\begin{aligned}\text{Exp4} &= \sum_{q=0}^{Q-1} |\alpha_2|^2 \, e^{-j2\pi(i-l)\frac{\delta}{\lambda_c}\left(1+\frac{q}{Q}B_f\right)\sin\theta_2} \\ &= |\alpha_2|^2 \, e^{-j2\pi(i-l)\frac{\delta}{\lambda_c}\left(1+\frac{Q-1}{2Q}\right)\sin\theta_2} \frac{\sin\left(\pi\,(i-l)\,\frac{\delta}{\lambda_c}B_f\sin\theta_2\right)}{\sin\left(\pi\,(i-l)\,\frac{\delta}{\lambda_c}\frac{1}{Q}B_f\sin\theta_2\right)} \end{aligned} \quad \text{(A.21)}$$

Combining the four expressions in (A.17), (A.18), (A.20) and (A.21), we get:

$$\begin{aligned}\left[\mathbf{R}_y\right]_{il} &= |\alpha_1|^2 F_1\left(i-l,\theta_1\right) e^{-j(i-l)\tilde{\psi}_1} + |\alpha_2|^2 F_1\left(i-l,\theta_2\right) e^{-j(i-l)\tilde{\psi}_2} \\ &\quad + \alpha_1^*\alpha_2 F_2\left(i,l,\theta_2,\theta_1\right) e^{-j2\pi\left[f_c\Delta\tau+\frac{\delta}{\lambda_c}\varphi_1\right]} e^{-j\pi\left(\frac{Q-1}{Q}\right)\left[B\Delta\tau+\frac{\delta}{\lambda_c}B_f\varphi_1\right]} \\ &\quad + \alpha_2^*\alpha_1 F_2\left(l,i,\theta_2,\theta_1\right) e^{j2\pi\left[f_c\Delta\tau+\frac{\delta}{\lambda_c}\varphi_2\right]} e^{j\pi\left(\frac{Q-1}{Q}\right)\left[B\Delta\tau+\frac{\delta}{\lambda_c}B_f\varphi_2\right]} \end{aligned} \quad \text{(A.22)}$$

where $\Delta\tau = \tau_2 - \tau_1$ , $\varphi_1 = (i-1)\sin\theta_2 - (l-1)\sin\theta_1$, $\varphi_2 = (l-1)\sin\theta_2 - (i-1)\sin\theta_1$, and $\tilde{\psi}_p$ is given by the following:

$$\tilde{\psi}_p = 2\pi\frac{\delta}{\lambda_c}\left(1+\frac{Q-1}{2Q}B_f\right)\sin\theta_p \quad \text{(A.23)}$$

$F_1\left(i-l,\theta\right)$ is defined as:

$$F_1\left(i-l,\theta\right) = \frac{\sin\left(\frac{\pi\delta}{\lambda_c}\left(i-l\right)B_f\sin\theta\right)}{\sin\left(\frac{\pi\delta}{Q\lambda_c}\left(i-l\right)B_f\sin\theta\right)} \quad \text{(A.24)}$$

and $F_2\left(i,l,\theta_{p_1},\theta_{p_2}\right)$ is defined as follows:

$$F_2\left(i,l,\theta_{p_1},\theta_{p_2}\right) = \frac{\sin\left[\pi\left\{B\Delta\tau+\frac{\delta}{\lambda_c}B_f\left((i-1)\sin\theta_{p_1}-(l-1)\sin\theta_{p_2}\right)\right\}\right]}{\sin\left[\frac{\pi}{Q}\left\{B\Delta\tau+\frac{\delta}{\lambda_c}B_f\left((i-1)\sin\theta_{p_1}-(l-1)\sin\theta_{p_2}\right)\right\}\right]} \quad \text{(A.25)}$$

For multipaths that are well separated in their arrival times at the receiver, (i.e. $B\Delta\tau > 1$), $F_2\left(i,l,\theta_2,\theta_1\right)$ and $F_2\left(l,i,\theta_2,\theta_1\right)$ are approximately zero. Hence the combined cor-

relation matrix reduces to:

$$\mathbf{R}_y = \mathbf{A}\left(\boldsymbol{\theta}\right) \begin{bmatrix} \left|\alpha_1\right|^2 & 0 \\ 0 & \left|\alpha_2\right|^2 \end{bmatrix} \mathbf{A}^H\left(\boldsymbol{\theta}\right) + \boldsymbol{\Sigma} \tag{A.26}$$

where

$$\mathbf{A}\left(\boldsymbol{\theta}\right) = \begin{bmatrix} \mathbf{a}\left(\theta_1\right) & \mathbf{a}\left(\theta_2\right) \end{bmatrix} \tag{A.27}$$

with each column of (A.27) given by:

$$\mathbf{a}\left(\theta_p\right) = \begin{bmatrix} 1 & e^{-j\tilde{\psi}_p} & \cdots & e^{-j(M-1)\tilde{\psi}_p} \end{bmatrix}^T \tag{A.28}$$

and $\tilde{\psi}_p$ is defined in (A.23)

# Appendix B

# Derivation of Vector $\mathbf{H}\left(i\right)$

In Chapter 6, we introduced the vector $\mathbf{H}\left(i\right)$ in (6.18) and is reproduced here for convenience:

$$\mathbf{H}\left(i\right) = \sum_{q=0}^{Q-1} \mathbf{Z}\left(q\right) e^{j2\pi \frac{iq}{Q}} \tag{B.1}$$

where $\mathbf{Z}\left(q\right)$ is given in (6.14). The $m^{\text{th}}$ element of vector $\mathbf{Z}\left(q\right)$ is given by:

$$\left[\mathbf{Z}\left(q\right)\right]_m = \sum_{p=1}^{P} \alpha_p e^{-j2\pi\left(f_c+\frac{q}{Q}B\right)\left(\tau_p+\frac{(m-1)\delta}{c}\sin\theta_p\right)} \tag{B.2}$$

Therefore the element in vector $\mathbf{H}\left(i\right)$ can be derived as:

$$\begin{aligned}
\left[\mathbf{H}\left(i\right)\right]_m &= \sum_{q=0}^{Q-1}\sum_{p=1}^{P} \alpha_p e^{-j2\pi\left(f_c+\frac{q}{Q}B\right)\left(\tau_p+\frac{(m-1)\delta}{c}\sin\theta_p\right)} e^{j2\pi\frac{iq}{Q}} \\
&= \sum_{p=1}^{P} \alpha_p e^{-j2\pi f_c\left(\tau_p+\frac{(m-1)\delta}{c}\sin\theta_p\right)} \sum_{q=0}^{Q-1} e^{-j2\pi\frac{q}{Q}\left(B\tau_p-i+\frac{B(m-1)\delta}{c}\sin\theta_p\right)} \\
&= \sum_{p=1}^{P} \alpha_p e^{-j2\pi f_c\left(\tau_p+\frac{(m-1)\delta}{c}\sin\theta_p\right)} \underbrace{\sum_{q=0}^{Q-1} e^{-j2\pi\frac{q}{Q}\left(B\tau_p-i+\frac{(m-1)\delta}{\lambda_c}B_f\sin\theta_p\right)}}_{GP} \\
&= \sum_{p=1}^{P} \alpha_p e^{-j2\pi f_c\left(\tau_p+\frac{(m-1)\delta}{c}\sin\theta_p\right)} \frac{1-\left[e^{-j\frac{2\pi}{Q}\left(B\tau_p-i+\frac{(m-1)\delta}{\lambda_c}B_f\sin\theta_p\right)}\right]^Q}{1-e^{-j\frac{2\pi}{Q}\left(B\tau_p-i+\frac{(m-1)\delta}{\lambda_c}B_f\sin\theta_p\right)}}
\end{aligned}$$

$$
\begin{aligned}
&= \sum_{p=1}^{P} \alpha_p e^{-j2\pi f_c\left(\tau_p+\frac{(m-1)\delta}{c}\sin\theta_p\right)} \frac{e^{-j\pi\left(B\tau_p-i+\frac{(m-1)\delta}{\lambda_c}B_f\sin\theta_p\right)}}{e^{-j\frac{\pi}{Q}\left(B\tau_p-i+\frac{(m-1)\delta}{\lambda_c}B_f\sin\theta_p\right)}} \\
&\qquad \times \frac{e^{j\pi\left(B\tau_p-i+\frac{(m-1)\delta}{\lambda_c}B_f\sin\theta_p\right)} - e^{-j\pi\left(B\tau_p-i+\frac{(m-1)\delta}{\lambda_c}B_f\sin\theta_p\right)}}{e^{j\frac{\pi}{Q}\left(B\tau_p-i+\frac{(m-1)\delta}{\lambda_c}B_f\sin\theta_p\right)} - e^{-j\frac{\pi}{Q}\left(B\tau_p-i+\frac{(m-1)\delta}{\lambda_c}B_f\sin\theta_p\right)}} \\
&= \sum_{p=1}^{P} \alpha_p e^{-j2\pi f_c\left(\tau_p+\frac{(m-1)\delta}{c}\sin\theta_p\right)} e^{-j\pi\left(B\tau_p-i+\frac{(m-1)\delta}{\lambda_c}B_f\sin\theta_p\right)} e^{j\frac{\pi}{Q}\left(B\tau_p-i+\frac{(m-1)\delta}{\lambda_c}B_f\sin\theta_p\right)} \\
&\qquad \times \frac{j2\sin\left[\pi\left(B\tau_p-i+\frac{(m-1)\delta}{\lambda_c}B_f\sin\theta_p\right)\right]}{j2\sin\left[\frac{\pi}{Q}\left(B\tau_p-i+\frac{(m-1)\delta}{\lambda_c}B_f\sin\theta_p\right)\right]} \\
&= \sum_{p=1}^{P} \alpha_p e^{-j2\pi f_c\tau_p} e^{-j\frac{2\pi\delta}{\lambda_c}(m-1)\sin\theta_p} e^{-j\pi\left[B\left(1-\frac{1}{Q}\right)\tau_p-i\left(1-\frac{1}{Q}\right)+\frac{(m-1)\delta}{\lambda_c}\left(1-\frac{1}{Q}\right)B_f\sin\theta_p\right]} \\
&\qquad \times \frac{\sin\left[\pi\left(B\tau_p-i+\frac{(m-1)\delta}{\lambda_c}B_f\sin\theta_p\right)\right]}{\sin\left[\frac{\pi}{Q}\left(B\tau_p-i+\frac{(m-1)\delta}{\lambda_c}B_f\sin\theta_p\right)\right]} \\
&= \sum_{p=1}^{P} \alpha_p e^{j\pi\left[2f_c\tau_p-i\left(\frac{Q-1}{Q}\right)+\frac{2\delta}{\lambda_c}(m-1)\sin\theta_p+B\left(\frac{Q-1}{Q}\right)\tau_p+\frac{(m-1)\delta}{\lambda_c}\left(\frac{Q-1}{Q}\right)B_f\sin\theta_p\right]} \\
&\qquad \times \frac{\sin\left[\pi\left(B\tau_p-i+\frac{(m-1)\delta}{\lambda_c}B_f\sin\theta_p\right)\right]}{\sin\left[\frac{\pi}{Q}\left(B\tau_p-i+\frac{(m-1)\delta}{\lambda_c}B_f\sin\theta_p\right)\right]} \\
&= \sum_{p=1}^{P} \alpha_p e^{j\pi\left[2f_c\tau_p+\frac{Q-1}{Q}(B\tau_p-i)+\frac{2\delta}{\lambda_c}(m-1)\left(1+\frac{Q-1}{2Q}B_f\right)\sin\theta_p\right]} \\
&\qquad \times \frac{\sin\left[\pi\left(B\tau_p-i+\frac{(m-1)\delta}{\lambda_c}B_f\sin\theta_p\right)\right]}{\sin\left[\frac{\pi}{Q}\left(B\tau_p-i+\frac{(m-1)\delta}{\lambda_c}B_f\sin\theta_p\right)\right]} \\
&= \sum_{p=1}^{P} \alpha_p e^{-j\phi_p(i,m)} F\left(i,m,p\right) \qquad \text{(B.3)}
\end{aligned}
$$

# Appendix C

# Offset Limits of Cost Function $L\left(u,\theta\right)$ for Multiple Signals

We rewrite the equation in (6.31) assuming that $\hat{\theta}_1^{(0)} = \theta_1$ as:

$$\begin{aligned} L\left(u,\theta_1\right) &= \sum_{m=1}^{M}\left|\sum_{p=1}^{P}\alpha_p e^{-j\varphi_p(m)}F_1\left(u,m,p\right)\right|^2 \\ &= \sum_{m=1}^{M}\left|\alpha_1 e^{-j\varphi_1(m)}\sum_{p=1}^{P}\frac{\alpha_p}{\alpha_1}e^{-j(\varphi_p(m)-\varphi_1(m))}F_1\left(u,m,p\right)\right|^2 \\ &= |\alpha_1|^2\sum_{m=1}^{M}\left|F_1\left(u,m,1\right)+\sum_{p=2}^{P}\frac{\alpha_p}{\alpha_1}e^{-j(\varphi_p(m)-\varphi_1(m))}F_1\left(u,m,p\right)\right|^2 \quad \text{(C.1)} \end{aligned}$$

We need to find the $u$ that maximize $L\left(u,\theta_1\right)$ under the condition of $-1 < u < 1$. To determine the offset limits due to the interference terms $\sum_{p=2}^{P}\alpha_p e^{-j\varphi_p(m)}F_1\left(u,m,p\right)$, we consider the worst case scenario when the interference terms are parallel to the desired signal path, $\alpha_1 e^{-j\varphi_1(m)}F_1\left(u,m,1\right)$ and the rate of change of the desired signal is opposite to that of the interference terms. This is the worst case scenario as the rate of change of individual interference terms affect the rate of change of $L\left(u,\theta\right)$ the greatest when this occur. Since we are assuming the worst case scenario, we ignore the contribution of the antenna index. In other words, the offset limits are independent of $m$.

Under these assumptions, the solution to the maximization of $L\left(u,\theta_1\right)$ with respect

to $u$ is given by:

$$\frac{\mathrm{d}F_1(u,m,1)}{\mathrm{d}u} + \sum_{p=2}^{P} \left|\frac{\alpha_p}{\alpha_1}\right| \frac{\mathrm{d}F_1(u,m,p)}{\mathrm{d}u} = 0 \tag{C.2}$$

where the $\frac{\mathrm{d}F_1(u,m,p)}{\mathrm{d}u}$ are of opposite signs to $\frac{\mathrm{d}F_1(u,m,1)}{\mathrm{d}u}$. If we let:

$$C_{p,m} = B\tau_p - \frac{(m-1)\,\delta}{\lambda_c} B_f \left(\sin\hat{\theta}_1^{(0)} - \sin\theta_p\right) \tag{C.3}$$

We can write $\frac{\mathrm{d}F_1(u,m,p)}{\mathrm{d}u}$ as:

$$\begin{aligned}
\frac{\mathrm{d}F_1(u,m,p)}{\mathrm{d}u} &= \frac{\pi}{\left(\sin\left[\frac{\pi}{Q}(u-C_{p,m})\right]\right)^2}\left\{\sin\left[\frac{\pi}{Q}(u-C_{p,m})\right]\cos\left[\pi(u-C_{p,m})\right]\right. \\
&\quad \left. - \frac{1}{Q}\sin\left[\pi(u-C_{p,m})\right]\cos\left[\frac{\pi}{Q}(u-C_{p,m})\right]\right\} \\
&= \pi\left\{\frac{\cos\left[\pi(u-C_{p,m})\right]}{\sin\left[\frac{\pi}{Q}(u-C_{p,m})\right]} - \frac{\cos\left[\frac{\pi}{Q}(u-C_{p,m})\right]}{Q\sin\left[\frac{\pi}{Q}(u-C_{p,m})\right]} F_1(u,m,p)\right\}
\end{aligned} \tag{C.4}$$

Without loss of generality, we plot $\left|\frac{\mathrm{d}F_1(u,m,p)}{\mathrm{d}u}\right|$ for the case $C_{p,m} = 0$ and $Q = 32$ in Figure C.1.

Note that the rate of changes corresponding to the desired signal is within the region of $-1 < u < 1$ (as indicated in Figure C.1) while those corresponding to the interference signals is outside this region. Since the maximum value of the rate of change of the interference signals are significantly smaller than those of the desired signal, the offset from the true $B\tau_1$ will be small provided that the signal-to-interference power ratio (SIR) is not too small. Moreover, note that there is a decrease in the maximum value of the rate of change as $u$ moves away from 0. This means that the offset limits reduces as the separation of different arrival path is increased.

For example, it is assumed that there is only one interference signal with equal power to the desired signal. We assume that the largest rate of change across all $m$ occurs when $C_{2,m} = 5$. The greatest rate of change is 2.121 and the corresponding

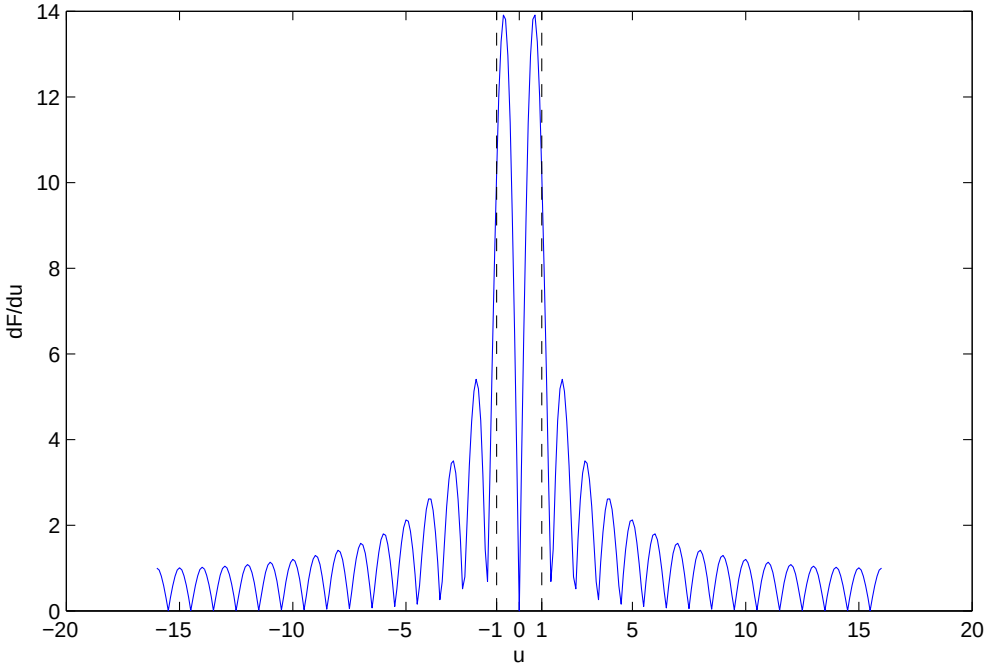


Figure C.1: $\left|\frac{\mathrm{d}F_1(u,m,p)}{\mathrm{d}u}\right|$ for the case $C_{p,m} = 0$ and $Q = 32$

offset is hence 0.065 from Figure C.1.

# Bibliography

[1] S. Haykin, J. P. Reilly, V. Kezys, and E. Vertatschitsch, "Some Aspects of Array Signal Processing," *IEE Proceedings F on Radar and Signal Processing*, vol. 139, no. 1, pp. 1–26, Feb 1992.

[2] H. Krim and M. Viberg, "Two Decades of Array Signal Processing Research — The Parametric Approach," *IEEE Signal Processing Magazine*, vol. 13, no. 4, pp. 67–94, Jul 1996.

[3] R. O. Schmidt, "Multiple Emitter Location and Signal Parameter Estimation," in *Proc. RADC Spectrum Estimation Workshop*, Rome, New York, USA, Oct. 3–5, 1979, pp. 234–258.

[4] R. O. Schmidt, "A Signal Subspace Approach to Multiple Emitter Location and Spectral Estimation," Ph.D. dissertation, Standford University, Standford, California, USA, 1981.

[5] R. O. Schmidt, "Multiple Emitter Location and Signal Parameter Estimation," *IEEE Transactions on Antennas and Propagation*, vol. 34, no. 3, pp. 276–280, Mar 1986.

[6] R. H. Roy, "ESPRIT — Estimation of Signal Parameters via Rotational Invariance Techniques," Ph.D. dissertation, Standford University, Standford, California, USA, 1987.

[7] R. Roy and T. Kailath, "ESPRIT — Estimation of Signal Parameters via Rotational Invariance Techniques," *IEEE Transactions on Acoustics, Speech, and Signal Processing*, vol. 37, no. 7, pp. 984–995, Jul 1989.

[8] J. Li, B. Halder, P. Stoica, and M. Viberg, "Computationally Efficient Angle Estimation for Signals with Known Waveforms," *IEEE Transactions on Signal Processing*, vol. 43, no. 9, pp. 2154–2163, Sep 1995.

[9] L. Huang, S. Wu, D. Feng, and L. Zhang, "Computationally Efficient Direction-of-Arrival Estimation Based on Partial A Priori Knowledge of Signal Sources," *EURASIP Journal on Applied Signal Processing*, pp. 1–7, 2006.

[10] B. Halder, M. Viberg, and T. Kailath, "An Efficient Non-Iterative Method for Estimating The Angles of Arrival of Known Signals," in *Conference Record of The Twenty-Seventh Asilomar on Signals, Systems & Computers*, vol. 2, Pacific Grove, California, USA, Nov. 1–3, 1993, pp. 1396–1400.

[11] J. Li and R. T. Compton, Jr., "Maximum Likelihood Angle Estimation for Signals with Known Waveforms," *IEEE Transactions on Signal Processing*, vol. 41, no. 9, pp. 2850–2862, Sep 1993.

[12] M. Cedervall and R. L. Moses, "Efficient Maximum Likelihood DOA Estimation for Signals with Known Waveforms in The Presence of Multipath," *IEEE Transactions on Signal Processing*, vol. 45, no. 3, pp. 808–811, Mar 1997.

[13] L. Najjar-Atallah and S. Marcos, "Subspace-Based Approach for DOA Estimation Using Pilot Symbol Channel Identification," *IEE Proceedings on Vision, Image and Signal Processing*, vol. 152, no. 1, pp. 20–28, Feb 2005.

[14] M. Z. Win and R. A. Scholtz, "Ultra-Wide Bandwidth Time-Hopping Spread-Sprectum Impulse Radio for Wireless Multiple-Access Communications," *IEEE Transactions on Communications*, vol. 48, pp. 679–691, Apr 2000.

[15] G. Su and M. Morf, "The Signal Subspace Approach for Multiple Wide-Band Emitter Location," *IEEE Transactions on Acoustics, Speech, and Signal Processing*, vol. 31, no. 6, pp. 1502–1522, Dec 1983.

[16] H. Wang and M. Kaveh, "Estimation of Angles-of-Arrival for Wideband Sources," in *Proc. IEEE International Conference on Acoustics, Speech and Signal Processing (ICASSP'84)*, vol. 9, San Diego, Calfornia, USA, Mar. 19–21, 1984, pp. 279–282.

[17] H. Wang and M. Kaveh, "Coherent Signal-Subspace Processing for Detection and Estimation of Angles of Arrival of Multiple Wide-Band Sources," *IEEE Transactions on Acoustics, Speech, and Signal Processing*, vol. 33, no. 4, pp. 823–831, Aug 1985.

[18] Y.-S. Soon, "Direction-of-Arrival Estimation of Wideband Sources Using Sensor Arrays," Ph.D. dissertation, Georgia Institute of Technology, Atlanta, Georgia, USA, 2004.

[19] M. N. O. Sadiku, *Elements of Electromagnetics*. New York, USA: Oxford University Press, 2001.

[20] J. D. Parsons, *The Mobile Radio Propagation Channel*. New York, USA: John Wiley & Sons, 2000.

[21] J. G. Proakis, *Digital Communications*. New York, USA: McGraw-Hill, 2001.

[22] T. S. Rappaport, *Wireless Communications: Principles and Practice*. New Jersey, USA: Pearson Education International, 2002.

[23] G. G. Raleigh and T. Boros, "Joint Space-Time Parameter Estimation for Wireless Communication Channels," *IEEE Transactions on Signal Processing*, vol. 46, no. 5, pp. 1333–1343, May 1998.

[24] S. R. Saunders, *Antennas and Propagation for Wireless Communication Systems*. New York, USA: John Wiley & Sons, 1999.

[25] P. S. Naidu, *Sensor Array Signal Processing*. Florida, USA: CRC Press, 2001.

[26] H. L. van Trees, *Optimum Array Processing - Part IV of Detection, Estimation and Modulation Theory*. New York, USA: John Wiley & Sons, 2002.

[27] A. J. Goldsmith and P. P. Varaiya, "Capacity of Fading Channels with Channel Side Information," *IEEE Transactions on Information Theory*, vol. 45, no. 6, pp. 2007–2019, Nov 1997.

[28] G. J. Foshini and M. J. Gans, "On Limits of Wireless Communications in A Fading Environment When Using Multiple Antennas," *Wireless Personal Communications*, vol. 6, pp. 311–335, Mar 1998.

[29] N. Chiurtu, B. Rimoldi, and E. Telatar, "On The Capacity of Multi-Antenna Gaussian Channels," in *Proc. IEEE International Symposium on Information Theory*, Washington, D.C., USA, Jun. 24–29, 2001, p. 53.

[30] J. A. Cadzow, "Multiple Source Location: The Signal Subspace Approach," *IEEE Transactions on Acoustics, Speech, and Signal Processing*, vol. 38, no. 10, pp. 1110–1125, Jul 1990.

[31] A. H. Tewfik and W. Hong, "On The Application of Uniform Linear Array Bearing Estimation Techniques to Uniform Circular Arrays," *IEEE Transactions on Signal Processing*, vol. 40, no. 4, pp. 1008–1011, Apr 1992.

[32] J.-J. Fuchs, "On The Application of The Global Matched Filter to DOA Estimation with Uniform Circular arrays," *IEEE Transactions on Signal Processing*, vol. 49, no. 4, pp. 702–708, Apr 2001.

[33] P. Ioannides and C. Balanis, "Uniform Circular Arrays for Smart Antennas," *IEEE Antennas and Propagation Magazine*, vol. 47, no. 4, pp. 192–206, Aug 2005.

[34] J.-I. Xie and Z.-S. He, "Beamforming of Coherent Signals for Weighted Two Concentric Ring Arrays," in *Proc. International Symposium on Intelligent Signal*

*Processing and Communication Systems (ISPACS 2007)*, Xiamen, China, Nov. 28 –Dec. 1, 2007, pp. 850–853.

[35] M. Zatman, "How Narrow Is Narrowband?" *IEE Proceedings on Radar, Sonar and Nagivation*, vol. 145, no. 2, pp. 85–91, Apr 1998.

[36] M. J. D. Rendas and J. M. F. Moura, "Cramér-Rao Bound for Location Systems in Multipath Environments," *IEEE Transactions on Signal Processing*, vol. 39, no. 12, pp. 2593–2610, Dec 1991.

[37] A. A. DAmico and U. Mengali, "DOA and Channel Parameter Estimation for Wideband CDMA Systems," *IEEE Transactions on Wireless Communications*, vol. 3, no. 6, pp. 1942–1947, Nov 2004.

[38] E. D. D. Claudio and R. Parisi, "WAVES: Weighted Average of Signal Subspaces for Robust Wideband Direction Finding," *IEEE Transactions on Signal Processing*, vol. 49, no. 10, pp. 2179–2191, Oct 2001.

[39] Y.-S. Yoon, L. M. Kaplan, and J. H. McClellan, "TOPS: New DOA Estimator for Wideband Signals," *IEEE Transactions on Signal Processing*, vol. 54, no. 6, pp. 1977–1989, Jun 2006.

[40] M. Agrawal and S. Prasad, "Broadband DOA Estimation Using Spatial-Only Modeling of Array Data," *IEEE Transactions on Acoustics, Speech, and Signal Processing*, vol. 48, no. 3, pp. 663–670, Mar 2000.

[41] W. Ng, J. P. Reilly, T. Kirubarajan, and J.-R. Larocque, "Wideband Array Signal Processing Using MCMC Methods," *IEEE Transactions on Signal Processing*, vol. 53, no. 2, pp. 411–426, Feb 2005.

[42] A. J. Barabell, J. Capon, D. F. Delong, J. R. Johnson, and K. Senne, "Performance Comparison of Superresolution Array Processing Algorithms," Massachusetts Institute of Technology Lincoln Lab, Lexington, Massachusetts, USA, Tech. Rep., May 9, 1984.

[43] N. Wang, P. Agathoklis, and A. Antoniou, "A New DOA Estimation Technique Based on Subarray Beamforming," *IEEE Transactions on Signal Processing*, vol. 54, no. 9, pp. 3279–3290, Sep 2006.

[44] N. L. Owsley, "Adaptive Data Orthogonalization," in *Proc. IEEE International Conference on Acoustics, Speech and Signal Procesing (ICASSP'78)*, vol. 3, Tulsa, Oklahoma, USA, Apr. 10–12, 1978, pp. 109–112.

[45] G. Bienvenu and L. Kopp, "Adaptivity to Background Noise Spatial Coherence for High Resolution Passive Methods," in *Proc. IEEE International Conference on Acoustics, Speech and Signal Procesing (ICASSP'80)*, vol. 5, Denver, Colorade, USA, Apr. 9–11, 1980, pp. 307–310.

[46] D. H. Johnson and S. R. DeGraff, "Improving The Resolution of Bearing in Passive Sonar Arrays by Eigenvalue Analysis," *IEEE Transactions on Acoustics, Speech, and Signal Processing*, vol. 30, no. 4, pp. 638–647, 30 1982.

[47] D. W. Tufts and R. Kumaresan, "Estimation of Frequencies of Multiple Sinusoids: Making Linear Prediction Perform Like Maximum Likelihood," *IEEE Proceedings*, vol. 70, no. 9, pp. 975–989, Sep 1982.

[48] R. Kumaresan and D. W. Tufts, "Estimating The Angles of Arrival of Multiple Plane Waves," *IEEE Transactions on Aerospace and Electronic Systems*, vol. 19, no. 1, pp. 134–139, Jan 1983.

[49] H. Wang and M. Kaveh, "On The Performance of Signal-Subspace Processing — Part I: Coherent Wide-Band Systems," *IEEE Transactions on Acoustics, Speech, and Signal Processing*, vol. 34, no. 5, pp. 1201–1209, Oct 1986.

[50] G. H. Golub and C. F. van Loan, *Matrix Computations*. Baltimore, Maryland, USA: Johns Hopkins University Press, 1984.

[51] L. N. Trefethen and D. Bau, III, *Numerical Linear Algebra*. Philadelphia, USA: Society for Industrial and Applied Mathematics, 1997.

[52] V. C. Soon and Y. F. Huang, "An Analysis of ESPRIT under Random Sensor Uncertainities," *IEEE Transactions on Signal Processing*, vol. 40, no. 9, pp. 2353–2358, Sep 1992.

[53] N. Tayem and H. M. Kwon, "Conjugate ESPRIT (C-SPRIT)," *IEEE Transactions on Antennas and Propagation*, vol. 52, no. 10, pp. 2618–2624, Oct 2004.

[54] J. Xin and A. Sano, "Direction Estimation of Coherent Narrowband Signals Using Spatial Signatures," in *Proc. IEEE Workshop on Sensor Array and Multichannel Signal Processing*, Rosslyn, Virginia, USA, Aug. 4–6, 2002, pp. 523–527.

[55] Y. Bresler, V. U. Reddy, and T. Kailath, "Optimum Beamforming for Coherent Signal and Interferences," *IEEE Transactions on Acoustics, Speech, and Signal Processing*, vol. 36, no. 6, pp. 833–843, Jun 1988.

[56] T.-T. Lin, "A Novel Beamforming for Coherent Signal Reception," in *Proc. 5th IEEE International Symposium on Antennas, Propagation and EM Theory (ISAPE 2000)*, Beijing, China, Aug. 15–18, 2000, pp. 599–602.

[57] L. Zhang, H. C. So, L. Ping, and G. Liao, "Effective Beamformer for Coherent Signal Reception," *IEE Electronic Letters*, vol. 39, no. 13, pp. 949–951, Jun 2003.

[58] S. Haykin, *Modern Filters*. New York, USA: Macmillan Publishing Company, 1989.

[59] J. M. Mendel, *Lessons in Estimation Theory for Signal Processing, Communications, and Control*. New Jersey, USA: Prentice Hall, 1995.

[60] J. S. Goldstein, I. S. Reed, and L. L. Scharf, "A Multistage Representation of The Wiener Filter Based on Orthogonal Projections," *IEEE Transactions on Information Theory*, vol. 44, no. 7, pp. 2943–2959, Nov 1998.

[61] L. Huang, S. Wu, D. Feng, and L. Zhang, "Low Complexity Method for Signal Subspace Fitting," *IEE Electronic Letters*, vol. 40, no. 14, pp. 847–848, Jul 2004.

[62] A. J. Barabell, "Improving The Resolution Performance of Eigenstructure-Based Direction-Finding Algorithm," in *Proc. IEEE International Conference on Acoustics, Speech and Signal Procesing (ICASSP'83)*, vol. 8, Boston, Massachusetts, USA, Apr. 14–16, 1983, pp. 336–339.

[63] J. Li, "Array Signal Processing for Polarized Signals and Signals with Known Waveforms," Ph.D. dissertation, Ohio State University, Columbus, Ohio, USA, 1991.

[64] G. H. Golub and V. Pereyra, "The Differentiation of Pseudo-Inverses and Non-Linear Least Squares Problems Whose Variables Separate," *SIAM Journal on Numerical Analysis*, vol. 10, no. 2, pp. 413–432, Apr 1973.

[65] Y. Bresler and A. Macovski, "Exact Maximum Likelihood Parameter Estimation of Superimposed Exponential Signals in Noise," *IEEE Transactions on Acoustics, Speech, and Signal Processing*, vol. 34, no. 5, pp. 1081–1089, Oct 1986.

[66] T. J. Ulrych and R. W. Clayton, "Time Series Modeling and Maximum Entropy," *Physics of the Earth and Planetary Interiors*, vol. 12, no. 2-3, pp. 188–200, Aug 1976.

[67] I. Ziskind and M. Wax, "Maximum Likelihood Localization of Multiple Sources by Alternating Projection," *IEEE Transactions on Acoustics, Speech, and Signal Processing*, vol. 36, no. 10, pp. 1553–1560, Oct 1988.

[68] M. Feder and E. Weinstein, "Parameter Estimation of Superimposed Signals Using The EM Algorithm," *IEEE Transactions on Acoustics, Speech, and Signal Processing*, vol. 36, no. 4, pp. 477–489, Apr 1988.

[69] K. Buckley and L. Griffiths, "Broad-Band Signal-Subspace Spatial-Spectrum (BASS-ALE) Estimation," *IEEE Transactions on Acoustics, Speech, and Signal Processing*, vol. 36, no. 7, pp. 953–964, Jul 1998.

[70] B. Friedlander and A. Weiss, "Direction Finding for Wideband Signals Using An Interpolated Array," *IEEE Transactions on Signal Processing*, vol. 41, no. 4, pp. 1618–1634, Apr 1993.

[71] M. A. Doron, A. J. Weiss, and H. Messer, "Maximum-Likelihood Direction Finding of Wideband Sources," *IEEE Transactions on Signal Processing*, vol. 41, no. 1, pp. 411–414, Jan 1993.

[72] D. Maiwald, D. V. Sidorovitch, and J. Bohme, "Broadband Maximum Likelihood Wave Parameter Estimation Using Polarization Sensitive Arrays," *IEEE Transactions on Acoustics, Speech, and Signal Processing*, vol. 4, pp. 356–359, Apr 1993.

[73] J. Chen, R. Hudson, and K. Yao, "Maximum-Likelihood Source Localization and Unknown Sensor Location Estimation for Wideband Signals in The Near-Field," *IEEE Transactions on Signal Processing*, vol. 50, no. 8, pp. 1843–1854, Aug 2002.

[74] K. Buckley and L. Griffiths, "Eigenstructure Based Broadband Source Location Estimation," in *Proc. IEEE International Conference on Acoustics, Speech and Signal Procesing (ICASSP'86)*, vol. 11, Tokyo, Japan, Apr. 8–11, 1986, pp. 1869–1872.

[75] H. Hung and M. Kaveh, "Focusing Matrices for Coherent Signal-Subspace Processing," *IEEE Transactions on Acoustics, Speech, and Signal Processing*, vol. 36, no. 8, pp. 1272–1282, Aug 1988.

[76] G. Bienvenu, "Eigensystem Properties of The Sampled Space Correlation Matrix," in *Proc. IEEE International Conference on Acoustics, Speech and Signal Procesing (ICASSP'83)*, vol. 8, Boston, Massachusetts, USA, Apr 1983, pp. 332–335.

[77] M. Wax, T.-J. Shan, and T. Kailath, "Spatio-Temporal Spectral Analysis by Eigenstructure Methods," *IEEE Transactions on Acoustics, Speech, and Signal Processing*, vol. 32, no. 4, pp. 817–827, Aug 1984.

[78] B. Ottersten and T. Kailath, "Direction-of-Arrival Estimation for Wide-Band Signals Using The ESPRIT Algorithm," *IEEE Transactions on Acoustics, Speech, and Signal Processing*, vol. 38, no. 2, pp. 317–327, Feb 1990.

[79] S. Valaee and P. Kabal, "Wideband Array Processing Using A Two-Sided Correlation Transformation," *IEEE Transactions on Signal Processing*, vol. 43, no. 1, pp. 160–172, Jan 1998.

[80] H. Wang and M. Kaveh, "On The Performance of Signal-Subspace Processing — Part II: Coherent Wide-Band Systems," *IEEE Transactions on Acoustics, Speech, and Signal Processing*, vol. 35, no. 11, pp. 1583–1591, Nov 1987.

[81] H. Hung and M. Kaveh, "Coherent Wide-Band ESPRIT Method for Directions-of-Arrival Estimation of Multiple Wide-Band Sources," *IEEE Transactions on Acoustics, Speech, and Signal Processing*, vol. 38, no. 2, pp. 354–356, Feb 1990.

[82] M. Doron and A. Weiss, "On Focusing Matrices for Wide-Band Array Processing," *IEEE Transactions on Signal Processing*, vol. 40, no. 6, pp. 1295–1302, Jun 1992.

[83] S. Valaee and P. Kabal, "The Optimal Focusing Subspace for Coherent Signal Subspace Processing," *IEEE Transactions on Signal Processing*, vol. 44, no. 3, pp. 752–756, Mar 1996.

[84] S. Valaee, B. Champagne, and P. Kabal, "Localization of Wideband Signals Using Least-Squares and Total Least-Squares Approaches," *IEEE Transactions on Signal Processing*, vol. 47, no. 5, pp. 1213–1222, May 1999.

[85] J. Krolik and D. Swingler, "Multiple Wide-Band Source Location Using Steered Covariance Matrices," *IEEE Transactions on Acoustics, Speech, and Signal Processing*, vol. 37, no. 10, pp. 1481–1494, Oct 1989.

[86] E. Doron and M. Doron, "Coherent Wideband Array Processing," in *Proc. IEEE International Conference on Acoustics, Speech and Signal Procesing (ICASSP'92)*, vol. 2, San Francisco, California, USA, Mar. 23–26, 1992, pp. 497–500.

[87] M. A. Doron and A. J. Weiss, "Coherent Wide-Band Processing for Arbitrary Array Geometry," *IEEE Transactions on Signal Processing*, vol. 41, no. 1, pp. 414–417, Jan 1993.

[88] T.-S. Lee, "Efficient Wideband Source Localization Using Beamforming Invariance Technique," *IEEE Transactions on Signal Processing*, vol. 42, no. 6, pp. 1376–1387, Jun 1994.

[89] G. Bienvenu, P. Fuerxer, G. Vezzosi, L. Kopp, and F. Florin, "Coherent Wide Band High Resolution Processing for Linear Array," *IEEE Transactions on Acoustics, Speech, and Signal Processing*, vol. 4, pp. 2799–2802, May 1989.

[90] H. Clergeot and O. Michel, "New Simple Implementation of The Coherent Signal Subspace Method for Wide Band Direction of Arrival Estimation," in *Proc. IEEE International Conference on Acoustics, Speech and Signal Procesing (ICASSP'89)*, vol. 4, Glasgow, Scotland, May 22–25, 1989, pp. 2764–2767.

[91] J. Krolik and D. Swingler, "Focused Wide-Band Array Processing by Spatial Resampling," *IEEE Transactions on Acoustics, Speech, and Signal Processing*, vol. 38, no. 2, pp. 356–360, Feb 1990.

[92] M. Viberg, B. Ottersten, and T. Kailath, "Detection and Estimation in Sensor Arrays Using Weighted Subspace Fitting," *IEEE Transactions on Signal Processing*, vol. 39, no. 11, pp. 2436–2449, Nov 1991.

[93] M. A. Doron and E. Doron, "Wavefield Modeling and Array Processing, Part I — Spatial Sampling," *IEEE Transactions on Signal Processing*, vol. 42, no. 10, pp. 2549–2559, Oct 1994.

[94] M. A. Doron and E. Doron, "Wavefield Modeling and Array Processing, Part II — Algorithms," *IEEE Transactions on Signal Processing*, vol. 42, no. 10, pp. 2560–2570, Oct 1994.

[95] J. Capon, "High-Resolution Frequnecy-Wavenumber Spectrum Analysis," *IEEE Proceedings*, vol. 57, no. 8, pp. 1408–1418, Aug 1969.

[96] D. N. Swingler and J. Krolik, "Source Location Bias in The Coherently Focused High-Resolution Broadband Beamformer," *IEEE Transactions on Acoustics, Speech, and Signal Processing*, vol. 37, no. 1, pp. 143–145, Jan 1989.

[97] M. R. Azimi-Sadjadi, A. Pezeshki, L. L. Scharf, and M. Hohil, "Wideband DOA Estimation Algorithms for Multiple Target Detection and Tracking Using Unattended Acoustic Sensors," in *Proc. SPIE Symposium on Defense & Security*, vol. 5417, no. 1, Orlando, Florida, USA, Apr. 12, 2004, pp. 1–11.

[98] M. Wax and T. Kailath, "Determining The Number of Signals by Information Theoretic Criteria," in *Proc. IEEE International Conference on Acoustics, Speech and Signal Procesing (ICASSP'84)*, vol. 9, San Diego, California, USA, Mar. 19–21, 1984, pp. 232–235.

[99] M. Wax and I. Ziskind, "Detection of The Number of Coherent Signals by The MDL Principle," *IEEE Transactions on Acoustics, Speech, and Signal Processing*, vol. 37, no. 8, pp. 1190–1196, Aug 1989.

[100] M. Kaveh and A. Barabell, "The Statistical Performance of The MUSIC and The Minimum-Norm Algorithms in Resolving Plane Waves in Noise," *IEEE Transactions on Acoustics, Speech, and Signal Processing*, vol. 34, no. 2, pp. 331–341, Apr 1986.

[101] P. Stocia and A. Nehorai, "MUSIC, Maximum Likelihood and Cramér-Rao Bound," *IEEE Transactions on Acoustics, Speech, and Signal Processing*, vol. 37, no. 5, pp. 720–741, May 1989.

[102] S. Ohmori, Y. Yamao, and N. Nakajima, "The Future Generations of Mobile Communications Based on Broadband Access Technologies," *IEEE Communications Magazine*, vol. 38, no. 12, pp. 134–142, Dec 2000.

[103] H. Taoka, K. Higuchi, and M. Sawahashi, "Field Experiment on Real-Time 1-Gbps High-Speed Packet Transmission in MIMO-OFDM Broadband Packet Radio Access," in *Proc. 63rd IEEE Vehicular Technology Conference (VTC 2006)*, vol. 4, Melbourne, Australia, May 7–10, 2006, pp. 1812–1816.

[104] A. L. Swindlehurst, S. Daas, and J. Yang, "Analysis of A Decision Directed Beamformer," *IEEE Transactions on Signal Processing*, vol. 43, no. 12, pp. 2920–2927, Dec 1995.

[105] Z. Gu and E. Gunawan, "Joint Space-Time Estimation for DS-CDMA System in Fast Fading Multipath Channel," *IEE Electronics Letters*, vol. 37, no. 23, pp. 1407–1408, Nov 2001.

[106] A. Dogandzic and A. Nehorai, "Space-Time Fading Channel Estimation and Symbol Detection in Unknown Spatially Correlated Noise," *IEEE Transactions on Signal Processing*, vol. 50, no. 3, pp. 457–474, Mar 2002.

[107] W. C. Jakes, *Microwave Mobile Communications*. New York, USA: Wiley, 1974.

[108] T. J. Shan, M. Wax, and T. Kailath, "On Spatial Smoothing for Direction-of-Arrival Estimation of Coherent Signals," *IEEE Transactions on Acoustics, Speech, and Signal Processing*, vol. 33, no. 4, pp. 806–811, Aug 1985.

[109] S. U. Pillai and B. H. Kwon, "Forward/Backward Spatial Smoothing Technique for Coherent Signal Identification," *IEEE Transactions on Acoustics, Speech, and Signal Processing*, vol. 37, no. 1, pp. 8–15, Jan 1989.